INEL-96/0040
May 1997

Idaho National Engineering Laboratory

Top-Down Scaling Analyses Methodology for AP600 Integral Tests

S. Banerjee, M. G. Ortiz,
T. K. Larson, D. L. Reeder

LOCKHEED MARTIN

INEL-96/0040

TOP-DOWN SCALING ANALYSES METHODOLOGY FOR AP600 INTEGRAL TESTS

S. Banerjee
University of California, Santa Barbara

M. G. Ortiz and T. K. Larson
Idaho National Engineering and Environmental Laboratory

D. L. Reeder
Consultant, Santa Barbara, CA

May 1997

Prepared for the
Division of Systems Technology
Office of Nuclear Regulatory Research
U.S. Nuclear Regulatory Commission
Washington, D.C. 20555

by
Idaho National Engineering and Environmental Laboratory
Nuclear Systems Analysis Technologies Department
Lockheed Martin Idaho Technologies Company
Idaho Falls, Idaho 83415

under
DOE Contract No. DE-AC07-94ID13223
NRC FIN J6008

ABSTRACT

A technique was developed to evaluate the applicability of data from small scale facilities for validation of codes for analysis of AP600 small break loss-of-coolant accidents (SBLOCA). The technique first divides the SBLOCA into phases based on the components that come into play as the postulated accident evolves. Conservation equations, resolved to the component level and their interconnections, are derived for the active components in each phase. The equations are then nondimensionalized and reference parameters are selected such that the dependent variables and their time derivatives, other than the system response of interest, are of order 1. Order of magnitude analysis is then performed for each equation and then between equations, based on the numerical values of the nondimensional coefficients for each term, with only the large order terms being retained. The resulting equations then contain terms whose impact on key system responses (e.g., reactor vessel level) are ordered in terms of the magnitude of the nondimensional groups multiplying the O[1] dependent variables. The reduced set of equations and nondimensional groups are validated with experimental data where possible. The validation process is meant to demonstrate that the important terms have been retained and enhance confidence in the system of equations used to capture the main processes occurring in each phase.

Based on the nondimensional equations, the dominant nondimensional groups, and hence the dominant physical mechanisms and their dependence on geometric and operational parameters, were identified for an AP600 1 inch cold leg break scenario starting from the initiating event through long term cooling. The important parameters entering the groups included elevation differences between the reactor vessel and other components, PRHR heat transfer rates, fluid thermophysical properties, liquid levels in tanks, and flow resistances in the CMT lines and IRWST lines. It was also shown that, after the beginning of CMT draining and accumulator injection, the dominant processes do not depend on break size provided they are small. The dominant processes were dependent on plant geometry and the operation of engineered safety features, such as the automatic depressurization system. The same transient events were evaluated for three experimental facilities and the same nondimensional groups, and hence mechanisms, were shown to be important. It was found that these nondimensional groups covered the range expected in the AP600, indicating that while there may be some distortions in scaling for a particular facility, between them, the important phenomena were captured.

Based on this analysis of for 1 inch cold leg breaks, it is concluded that the data appear to be applicable for assessment and validation of computer codes used for modeling small break LOCA scenarios in the AP600 system.

SUMMARY

In this study a method was developed and demonstrated for assessing the applicability of data, obtained in reduced-scale experimental facilities, to the validation of computer codes used in AP600 small break loss-of-coolant accident (SBLOCA) analysis.

In this procedure the SBLOCA transient was divided into several phases based on the process identification and ranking table (PIRT), in each of which different phenomena or components come in to play. Each phase was described in terms of a set of conservation equations resolved down to the relevant component and component interaction levels. These conservation equations were then nondimensionalized such that all dependent variables and their derivatives other than the key system response that was to be determined, were of O[1]. The magnitude of the nondimensional groups multiplying each term involving dependent variables (of O[1]), then gave a measure of the impact of each term on the system response of interest. To ascertain whether the hierarchy of nondimensionalized equations captured the dominant phenomena in each phase, each equation was checked against experimental data to the extent feasible.

The result of this process was a set of nondimensional groups for each phase whose magnitudes were a measure of their effect on a key system response such as reactor vessel mass inventory. These groups involved quantities like elevation differences, flow resistances of lines, component volumes, and thermophysical properties - all of which could be obtained from design information for each facility and the AP600. By comparing the dominant groups between facilities and with the AP600, conclusions were drawn as to whether the AP600 and the various facilities were in the same region of nondimensional parameter space from the viewpoint of their response in a SBLOCA. Variations in the ordering of the magnitudes of these groups and their relative magnitudes were noted. The effects of these differences in magnitude on key system responses were assessed to determine if distortions in response would be expected in any of the experimental facilities. Thus the method resulted in an assessment of how well a facility was scaled vis-à-vis the AP600 for each phase of a SBLOCA, and hence, how applicable the data from a given facility in a specific phase were to code validation.

The method was applied primarily to assessment of data for one-inch (equivalent) cold leg breaks, though for some phases, scaling with regard to other break sizes and locations, was also touched on.

In broad terms, the phases consisted of:

- subcooled depressurization until the pressurizer emptied
- an intermediate phase between the first phase and activation of ADS-4 (automatic depressurization system fourth stage), which included CMT (core makeup tank) and PRHR (passive residual heat removal system) recirculation, accumulator injection and partial draining of the CMTs as well as activation of ADS-1,-2, and -3

- ADS-4 discharge until the pressure dropped sufficiently to allow refilling by the IRWST (in-containment refueling water storage tank) system
- refilling by IRWST flow into the reactor vessel until the sump and IRWST tank levels equalized
- long term cooling.

In some cases, e.g. the intermediate phase, division into subphases was necessary to account for activation of different components like the ADS-1, -2, -3 systems. The results of analyzing these phases of the one inch cold leg break scenario in the AP600 system and the experimental facilities are presented below for each phase.

Subcooled Depressurization

For the 1 inch cold leg break, the system mass response during the initial portion of the subcooled blowdown phase were found to be dominated by the break flow rate. The break volumetric flow is the controlling term for the depressurization response as the net heat flows in and out of the system were nearly balanced. Order of magnitude analysis showed that effects due to convecting energy out the break and pressurizer heating were each an order of magnitude smaller than the break volumetric flow. Data from various facilities scaled with a time nondimensionalized by the break discharge rate and the initial coolant mass in the pressurizer.

Intermediate Phase

Following pressurizer draining and reactor scram, the balance of core, steam generator, and PRHR heat flows and break flow play an important role in the pressure response. The mass loss continues to depend on the break flow. Based on the values of the nondimensional groups, the same processes control the mass balance in the AP600 and the experimental facilities for all three subphases of the Intermediate Phase.

During the initial passive cooling phase, mass inventory changes depend on the break flow until the accumulator draining and CMT draining begin. In this interval the depressurization rate is related to the balance of core and PRHR heat flows and break volumetric flow. Following the initiation of accumulator injection and CMT draining, these flows govern the mass balance until ADS flow begins. The low temperatures of these flows determine the depressurization process primarily by decreasing the average specific volume of the system. From this point on, the depressurization transient is controlled by the actions of the engineered safety systems. All this can be phrased in terms of nondimensionalized equations, with nondimensional coefficients for the O[1] nondimensional variables that for the experimental facilities, lie in the same range as in the AP600 with some differences. For example, during this phase the heat in and out flows are distorted in SPES, though the overall effect on the subphase response does not appear to be significant as far as the ultimate outcome, coolant inventory before ADS-4 opens, is concerned. Also, the PRHR heat transfer appears to be oversized in the ROSA facility relative to the AP600 whereas it is somewhat undersized in the SPES and OSU facilities. These distortions appeared to have little effect on the overall transient response, however.

After the ADS-1,-2,-3 flows begin they, in addition to the accumulator and CMT flows, influence the system coolant inventory and depressurization rate. The ADS influence on the depressurization rate is accentuated by the discharge being of high quality. In the experimental facilities, essentially these same processes are dominant. In the full pressure facilities, the effect of the cooler accumulator and CMT fluid on depressurization occurred primarily by mixing with subcooled liquid. In the OSU APEX facility, the effect occurred more by mixing with saturated fluid. This difference does not appear to have a significant effect on the overall phase outcome.

A preliminary assessment of the presence of accumulator nitrogen in the primary system on the processes occurring during the intermediate phase was made. The two situations evaluated to provide a comparison included assuming the primary system vapor volume contained only steam and assuming the vapor space contained nitrogen. Results of this much simplified estimate indicate that the numeric values of the nondimensional groups for the two cases are different but the relative rankings for the groups for a given facility are the same. In both cases for all the facilities, the ADS-1,-2,-3 volumetric flow was the major factor affecting depressurization.

From the analysis of the Intermediate Phase, the conclusion is drawn that the nondimensional pressure and inventory are relatively independent of break size provided the break is small (<< ADS-1,-2,-3 area). These nondimensional parameters do depend on accumulator and CMT mass and to a lesser extent on the details of the net heating from core decay heat and steam generator and PRHR heat transfer. The experimental data tend to support this conclusion.

ADS-4 Blowdown

During the ADS-4 blowdown the vessel mass inventory is determined by the balance between CMT and ADS-4 flow rates. The CMT head relative to the vessel liquid level, CMT line resistance, and ADS-4 quality are important parameters during this phase. Temperature of the CMT liquid and mixing in the lower plenum affect the ADS-4 quality. In the full pressure facilities, the ratio of ADS-4 flow to CMT flow was greater than in AP600. This difference would cause these facilities to lose more mass during ADS-4 blowdown than the AP600. In OSU, the ratio of ADS-4 flow to CMT flow was less than in the AP600 which would cause OSU to lose less vessel inventory during ADS-4 blowdown than in the AP600.

IRWST Injection

During the initial vessel refill the vessel mass inventory is determined by the balance between IRWST, pressurizer surge line, and ADS-4 flow rates. The IRWST and pressurizer heads relative to the vessel level, IRWST line resistance, and ADS-4 quality are important parameters during this phase. Temperature of the IRWST liquid and mixing in the lower plenum affect the ADS-4 quality. The effects of oscillatory pressurizer draining were observed but did not significantly affect the vessel refill process. In the experimental facilities the same processes were dominant and the relative ordering of the flow magnitudes was the same. In OSU the ADS-4 flow appeared to be somewhat low relative to the other facilities. Conditions in the

experimental facilities cover the range, in nondimensional parameter space, expected in the AP600.

IRWST Drain(Long Term Cooling)

The OSU facility is the only experimental facility equipped to run transients through the IRWST draining phase. For this phase, the drain time for the IRWST is the relevant time scale and is much larger than the vessel residence time scale. The drain is essentially a series of steady-state points in which the flow rate through the DVI, core, and out the ADS-4 valves depends primarily on the IRWST water level and, to a lesser extent, the ratio of the hydraulic resistances in the DVI and ADS-4 trains. These ratios are well preserved in the OSU facility suggesting that similar performance should be observed in the plant.

IRWST/Sump Injection (Long Term Cooling)

Sump injection commences after the Sump level has increased to a point that causes check valves and eventually motor operated valves to open and allow communication between the IRWST and Sump. The head imposed on the primary system by the Sump level remains constant at that point and the system operation is basically steady-state wherein coolant from the IRWST/Sump enters the system via the DVI lines, flows through the vessel, and out the ADS-4 valves. The vessel collapsed level settles at an elevation near the DVI nozzle during this phase implying a relatively constant vessel mass since other experiment parameters are not changing. Based on test data, the vessel nondimensional mass (in OSU) is approximately 0.85. Experimental data suggests that significant phase separation occurs in the upper core region and upper plenum. In effect, a significant fraction of the liquid in the mixture flowing out the top of the heated region separates and/or de-entrains in the upper plenum. Scaling analysis results predicted a nondimensional vessel mass considerably lower than the experiment value. This result is a consequence of simplifying assumptions that were made in the analysis since the void profile above the core is not known The essence of the problem is that a more detailed, local effects description of the phase distribution is needed for the particular geometry in the upper plenum and various tee connections leading to the ADS-4 valves.

The magnitudes of the nondimensional coefficients in the reduced conservation equations were similar for the experimental facilities and the AP600 system. From this, the same important processes occurred in the experimental facilities as might be expected in the AP600. This similarity indicates that the experimental results are useful for understanding the response of the AP600 system. It further indicates that the data from the experimental facilities are in the same parameter range as the AP600, and hence are applicable to assessment of computer codes.

The important phenomena identified from the scaling analysis for the one inch cold leg break were in general agreement with those identified in the PIRT. Several phenomena were determined to play a primary role in the accident sequence that were not listed as high priority in the original PIRT (the rankings of these phenomena have been elevated in the current PIRT). These phenomena included:

- The CMT level and line resistance during the ADS-4 Blowdown and IRWST Phases

- The IRWST/DVI flow resistance during the IRWST Phase

- The initial pressurizer inventory at the start of the IRWST Phase

However the scaling of these in terms of the important nondimensional groups was such that significant distortions were not identified. The table below summarizes the important nondimensional groups for the transient phases.

Summary of Important Nondimensional Groups by Transient Phase.

Dimensionless group	Algebraic form	Physical meaning	AP600	ROSA	SPES	OSU
High Pressure Subcooled depressurization Phase						
Φ_4	$\frac{\dot{m}_0 t_0 v_0}{p_0 M_0} \frac{\mu_{fg0}}{v_{fg0}} \frac{\partial p}{\partial \mu}\Big\|_{v_0}$	Ratio of pressure change, due to volumetric outflow, to the reference pressure				
Φ_6	$\frac{\dot{m}_0 t_0}{M_0}$	Ratio of mass loss to total mass in volume				
Intermediate Phase Subphase I						
Ψ_3	$\frac{C_{1,1,0}\dot{q}_{SG,0} t_0}{P_0}$	Ratio of pressure change, due to change in specific energy of the subcooled field from heat transfer, to the reference pressure				
Ψ_{10}	$\frac{C_{2,0} v_{1,0} \dot{m}_0 t_0}{P_0}$	Ratio of pressure change, due to change in specific volume of the subcooled field, to the reference pressure				
π_{core}	$q_{core,0}/q_{SG,0}$	Ratio of heat addition by core to heat removal by steam generator				
Ψ_{13}	$\frac{\dot{m}_0 t_0}{M_0}$	Ratio of integrated mass flow to reference mass				

a, c

a, c

Summary of Important Nondimensional Groups by Transient Phase (continued).

Dimensionless group	Algebraic form	Physical meaning	AP600	ROSA	SPES	OSU
Intermediate Phase Subphase II						
Ψ_3	$\frac{C_{1,1,0}\dot{q}_{core,0}t_0}{P_0}$	Ratio of pressure change, due to change in specific energy of the subcooled field from heat transfer, to the reference pressure				
Ψ_4	$(C_{1,1}(h_f - u_l) - C_{1,m}(h_m - u_m))_0 \dot{m}_{0,sat} t_0 / P_0$	Ratio of pressure change, due to change in specific energy of the saturated field from mass inflows, to the reference pressure				
Ψ_{10}	$\frac{C_{2,0}v_{1,0}\dot{m}_0 t_0}{P_0}$	Ratio of pressure change, due to change in specific volume of the subcooled field, to the reference pressure				
π_{PRHR}	$q_{PRHR,0}/qc_{ore,0}$	Ratio of reference heat removal rate from PRHR and heat addition rate by core				
Ψ_{13}	$\frac{\dot{m}_0 t_0}{M_0}$	Ratio of integrated mass flow to reference mass				
Intermediate Phase Subphase III						
Ψ_1	$\frac{C_{1,1,0}\dot{m}_{0,ADS}(h_{in} - u_l)_0 t_0}{P_0}$	Ratio of pressure change, due to change in specific energy of the subcooled field from mass inflows, to the reference pressure				
Ψ_3	$\frac{C_{1,1,0}\dot{q}_0 t_0}{P_0}$	Ratio of pressure change, due to change in specific energy of the subcooled field from heat transfer, to the reference pressure				
Ψ_6	$\frac{C_{1,1,0}\dot{q}_0 t_0}{P_0}$	Ratio of pressure change, due to change in specific energy of the saturated field from heat transfer, to the reference pressure				
Ψ_{10}	$\frac{C_{2,1,0}v_0\dot{m}_{0,ADS}t_0}{P_0}$	Ratio of pressure change, due to change in specific volume of the subcooled field, to reference pressure				
Ψ_{11}	$\frac{C_{2,m,0}v_0\dot{m}_{0,ADS}t_0}{P_0}$	Ratio of pressure change, due to change in specific volume of the saturated field, to reference pressure				
Ψ_{13}	$\frac{\dot{m}_{0,ADS}t_0}{M_0}$	Ratio of integrated mass flow to reference mass				
M^*_{ACC}	M_{ACC}/M_0	Ratio of accumulator mass to reference mass				
M^*_{CMT}	M_{CMT}/M_0	Ratio of CMT mass to reference mass				
M^*_{PCS}	$M_{PCS,0}/M_0$	Ratio of PCS mass to reference mass				

a,c

Summary of Important Nondimensional Groups by Transient Phase (continued).

Dimensionless group	Algebraic form	Physical meaning	AP600	ROSA	SPES	OSU
Time ratio	$(t_0-\hat{t}_0)/t_0$	Equation (6.20c)				
π_{break}	$\dot{m}_{0,break}/\dot{m}_{0,ADS}$	Ratio of break and ADS-1,-2,-3 reference flows				
π_{ACC}	$\dot{m}_{0,ACC}/\dot{m}_{0,ADS}$	Ratio of accumulator and ADS-1,-2,-3 reference flows				
π_{CMT}	$\dot{m}_{0,CMT}/\dot{m}_{0,ADS}$	Ratio of CMT and ADS-1,-2,-3 reference flows				
ADS-4 Blowdown Phase						
Dimensionless group	Algebraic form	Physical meaning				
Term in Eq. (6.35)	$\frac{t_0}{V_0}\left(\frac{g_0 L_0}{R'_0}\right)^{1/2}$	Ratio of CMT flow to vessel volume				
Term in Eq. (6.35)	$\frac{G_0 A_0 t_0}{V_0 \rho_0}$	Ratio of ADS flow to vessel volume				
Term in Eq. (6.35)	$\frac{G_0 A_0}{\rho_0}\left(\frac{R'_0}{g_0 L_0}\right)^{1/2}$	Ratio of ADS flow to CMT flow				
IRWST Refill Phase						
Term in Eq. (6.55)	$\sqrt{\frac{g_0 L_0 t_0^2}{V_0^2 R'_0}}$	Ratio of IRWST flow to vessel volume				
Term in Eq. (6.55)	$\frac{G_{exit_0} A_0 t_0}{\rho_0 V_0}$	Ratio of ADS-4 flow to vessel volume				
Term in Eq. (6.55)	$\frac{0.1 t_0 A_0 \sqrt{g_0 D_0}}{V_0}$	Ratio of pressurizer surge line flow to vessel volume				
IRWST Drain Phase						
$Z^*_{dvi}+Z^*_{dc\text{-}dvi}$	$(Z_{dvi}+Z_{dc\text{-}dvi})/(Z_{dvi}+Z_{dc\text{-}dvi}+L_{IRWST,0})$	Nondimensional distance from bottom of IRWST to bottom of core				
$\Pi_{2\text{-}ads}/\Pi_{2\text{-}dvi}$	$\Delta Z_s/Y_0$	Ratio between ADS-4 height and IRWST initial level				
$\Pi_{3\text{-}dvi}/\Pi_{2\text{-}dvi}+\Pi_{3\text{-}ads}/\Pi_{2\text{-}dvi}$	See Equation (6.82)	Ratio between the sum of ADS-4 and IRWST injection line frictional losses and reference head				

a,c

Summary of Important Nondimensional Groups by Transient Phase (continued).

IRWST/Sump Injection Phase						
Dimensionless group	Algebraic form	Physical meaning	AP600	ROSA	SPES	OSU
$\Pi_{\rho_{dvi}}$	$\frac{v_{g_0}}{v_{f_0}}$	Vapor to liquid specific volume ratio				
$\Pi_{Z_{dvi}}$	$\frac{\rho_{H0}}{\rho_0}\frac{\Delta Z_{4_0}}{L_0}$	Ratio of head on the ADS side to the head on the IRWST side				
$\Pi_{\dot{R}_{dvi}}$	$\frac{\rho_0}{\rho_{H0}}\left(\frac{\dot{R}_{ads_0}}{\dot{R}_{dvi_0}}\right)$	Density weighted ratio of ADS-4 and DVI line resistances				
Π_{SUB}	$\frac{C_{p_0}\Delta T_0}{h_{fg_0}}$	Subcooling number				
$\Pi_{\dot{q}}$	$\frac{\dot{q}_0}{\dot{m}_{S_0} h_{fg_0}}$	Phase change number				

a, c

ACKNOWLEDGMENTS

The authors gratefully acknowledge the contributions through many discussions with Professors G. Kojasoy and M. DiMarzo, Drs. A. Ougouad, W. Terry, and J. Wolf; assistance with access and interpretation of the experimental data and facility's parameters as provided by R. Averill, R. Shaw, L. Stickler, J. Cozzuol and J. Fisher. The assistance with XMGR, data manipulation questions, and input deck parameter questions provided by S. Smith, C. Lenglade, R. Martin, S. Sloan, P. Roth, and P. Bayless is also gratefully acknowledged. The artwork in the form of facility schematics, topologies, and other sketches throughout the report is the contribution of Laura Teerlink, who also helped in the translation of text, figures, and equations from one word processor to another to make the document more consistent.

CONTENTS

ABSTRACT ii

SUMMARY iii

ACKNOWLEDGMENTS xi

CONTENTS xii

FIGURES xiv

TABLES xv

NOMENCLATURE xviii

1. INTRODUCTION 1

2. ROLE OF THE TOP-DOWN SCALING EFFORT 3

3. METHODOLOGY 5

4. AP600 DESIGN OVERVIEW 8

5. SMALL BREAK LOSS-OF-COOLANT SCENARIOS AND PHASE DESCRIPTIONS 11

5.1 AP600 SBLOCA Phase Description Summary 11
- 5.1.1 High Pressure Phase: Subcooled Depressurization 11
- 5.1.2 Intermediate Phase: Passive Cooling Phase (CMT/PRHR Recirculation and ADS-1,-2,-3 Blowdown) 13
- 5.1.3 ADS-4 Blowdown 13
- 5.1.4 IRWST Injection 14
- 5.1.5 IRWST Draining/Sump Injection (Long Term Cooling) Phase 14

6. DEMONSTRATIONS OF METHODOLOGY 15

6.1 High Pressure Subcooled Depressurization 15
- 6.1.1 Steps 1-3 - Subcooled Depressurization Definition and Topology 15
- 6.1.2 Steps 4 and 5 - Governing Equations and Nondimensionalization 15
- 6.1.3 Steps 6 and 7 - Reference Parameter Selection and Order of Magnitude Analysis 19
- 6.1.4 Step 8 - Validation of Results 22
- 6.1.5 Concluding Remarks 24

6.2 Intermediate Phase 25
- 6.2.1 Step 1: Intermediate Subphase I Description 25
- 6.2.2 Step 1: Intermediate Subphase II Description 28
- 6.2.3 Step 1: Intermediate Subphase III Description 31
- 6.2.4 Concluding Remarks 37

6.3 ADS-4 Blowdown 41
- 6.3.1 Step 1: ADS-4, Phase Description 41
- 6.3.2 Step 2: ADS-4, Identification Of Key Components Or Subsystems 41
- 6.3.3 Step 4: ADS-4, Governing Equations 41
- 6.3.4 Step 6: ADS-4, Selection Of Reference Parameters 43
- 6.3.5 Step 7: ADS-4, Order of Magnitude Analysis 46
- 6.3.6 Step 8: ADS-4 Blowdown, Verification with Data 49
- 6.3.7 Concluding Remarks 59

6.4 IRWST Injection Phase 60
- 6.4.1 Step 1: IRWST Injection Phase, Phase Description 60
- 6.4.2 Step 2: IRWST Injection Phase, Relevant Subsystems and Components 60

6.4.3 Step 4: IRWST Injection Phase, Governing Equations 60
6.4.4 Step 6: IRWST Injection Phase, Selection Of Reference Parameters 63
6.4.5 Step 7: IRWST Injection Phase, Order Of Magnitude Analysis 64
6.4.6 Step 8: IRWST Injection Phase, Verification with Data 65
6.4.7 Concluding Remarks 77

6.5 IRWST Drain (Long Term Cooling) Phase 79
6.5.1 Step 1: IRWST Drain (Long Term Cooling) Phase Description 79
6.5.2 Steps 2 and 3: IRWST Drain (Long Term Cooling) System Components and Topology 79
6.5.3 Step 4: IRWST Drain (Long Term Cooling) Governing Equations 80
6.5.4 Step 6: IRWST Drain (Long Term Cooling) Selection of Reference Parameters 81
6.5.5 Step 7: IRWST Drain (Long Term Cooling) Order Of Magnitude Analysis 83
6.5.6 Step 8: IRWST Drain (Long Term Cooling) Verification with Data 85
6.5.7 Concluding Remarks 86

6.6 IRWST/Sump Injection (Long Term Cooling) Phase 87
6.6.1 Step 1: IRWST/Sump Injection (Long Term Cooling) Phase Description 87
6.6.2 Steps 2 and 3: IRWST/Sump Injection (Long Term Cooling) System Components and Topology 87
6.6.3 Step 4: IRWST/Sump Injection (Long Term Cooling) Governing Equations 88
6.6.4 Step 5: IRWST/Sump Injection (Long Term Cooling) Nondimensionalization 90
6.6.5 Step 6: IRWST/Sump Injection (Long Term Cooling) Selection of Reference Parameters 92
6.6.6 Step 7: IRWST/Sump Injection (Long Term Cooling) Order of Magnitude Analysis 94
6.6.7 Step 8: IRWST/Sump Injection (Long Term Cooling) Verification with Data 94

7. CONCLUSIONS 95

8. REFERENCES 99

APPENDIX A–PRESSURE RATE EQUATION AND TANK LEVEL DERIVATION A-1

APPENDIX B–TABLES OF USEFUL AP600 FACILITY PARAMETERS B-1

APPENDIX C–TWO-FIELD PRESSURE RATE EQUATION DEVELOPMENT C-1

APPENDIX D–PRHR REFERENCE FLOW RATE AND HEAT TRANSFER D-1

APPENDIX E–DERIVATION OF GOVERNING EQUATIONS AND NONDIMENSIONAL GROUPS (Πs) FOR THE ADS-4 BLOWDOWN AND IRWST INJECTION PHASE E-1

APPENDIX F–DERIVATIONS OF ANALYTICAL EXPRESSIONS FOR VESSEL INVENTORY F-1

APPENDIX G–EQUATION DEVELOPMENT FOR IRWST DRAIN PHASE G-1

FIGURES

3.1. Sketch illustrating verification process to evaluate whether the dominant terms retained in each equation are sufficient to capture the experimental data 7

4.1. Sketch of AP600 design 9

5.1. Calculated pressure for AP600 one-inch cold leg break transient 12

6.1. Pressurizer connected to the primary system - schematic for subcooled depressurization phase 16

6.2. Pressurizer pressure comparison for different facilities and different break sizes 23

6.3. Pressurizer level comparison for different facilities and different break sizes 23

6.4. PCS pressure and liquid fraction at ADS-4 initiation in experimental facilities 40

6.5. ADS-4 Blowdown phase: schematics and important components 42

6.6. Vessel control volume for ADS-4 blowdown 49

6.7. ROSA, SPES, and OSU mass balances in nondimensional coordinates for the ADS-4 phase 50

6.8. ROSA, SPES, and OSU nondimensional flow integrals for ADS-4 phase 51

6.9. ROSA experiment AP-CL-03 ADS-4 mass flux 52

6.10. SPES experiment S00401 ADS-4 mass flux for ADS-4 blowdown 53

6.11. OSU experiment SB5 ADS-4 mass flux for ADS-4 blowdown 54

6.12. ROSA AP-CL-03 CMT line equation 55

6.13. SPES S00401 CMT line equation 56

6.14. OSU SB5 CMT line equation 56

6.15. Analytic solution for vessel level during ADS-4 blowdown 57

6.16. IRWST Injection schematic and important components 61

6.17. ROSA, SPES and OSU mass balances in nondimensional coordinates for the IRWST phase 66

6.18. ROSA experiment AP-CL-03 mass balance component integrals versus nondimensional time for the IRWST phase 67

6.19. SPES experiment S00401 mass balance component integrals versus nondimensional time for the IRWST phase 68

6.20. OSU experiment SB 5 mass balance component integrals versus nondimensional time for the IRWST phase 68

6.21. ROSA experiment AP-CL-03 ADS-4 integrated normalized mass flux ratio for IRWST phase and homogeneous equilibrium model 69

6.22. SPES experiment S00401 ADS-4 integrated normalized mass flux ratio for IRWST phase and homogeneous equilibrium model 70

6.23. OSU experiment SB5 ADS-4 integrated normalized mass flux ratio for IRWST phase and homogeneous equilibrium model 71

6.24. ROSA AP-CL-03 IRWST tank level - DVI line parameter relationship in nondimensional coordinates 72

6.25. SPES S00401 IRWST nondimensional coordinates 73
6.26. OSU SB5 IRWST tank level - DVI line parameter relationship in nondimensional coordinates 73
6.27. Analytic solution for vessel level with data from ROSA experiment AP-CL-03 75
6.28. Analytic solution for vessel level with data from SPES experiment S00401. 75
6.29. Analytic solution for vessel level with data from OSU experiment SB5. 76
6.30. System configuration during IRWST draining (prior to sump injection) 80
6.31. Left and right sides of Equation (6.87) SBLOCA scenarios in the OSU facility. 86
6.32. Schematic for Long Term Cooling Phase (after Sump injection) showing components involved 88
A-1. Simple control volume A-2
A-2. Control volume representing a tank A-7
C-1. Example of a volume containing two fields; the development is for a multifield system C-2
D-1. Closed loop with heat addition and heat removal D-2
E-1. Schematic for ADS-4 blowdown E-3
E-2. Schematic for IRWST refill E-7
G-1. System configuration during IRWST drain phase (prior to sump injection) G-2
G-2. Schematic of concrete penetration depth (thickness) to be determined according to duration of heating process G-3
G-3. Portion of concrete wall showing penetration depth (thickness) and variable definitions G-3

TABLES

6.1. Facility parameters and nondimensional Φ groups for one-inch cold leg break subcooled blowdown. 20
6.2. Facility parameters and nondimensional Φ groups for SPES two-inch breaks and DVI guillotine break 21
6.3. Dimensionless coefficients for Intermediate Subphase I 26
6.4. Reference parameters for Intermediate Subphase I. 26
6.5. Dimensionless coefficients for Intermediate Subphase I 27
6.6. Dimensionless coefficients for Intermediate Subphase II. 29
6.7. Reference parameters for Intermediate Subphase II 29
6.8. Dimensionless coefficients for Intermediate Subphase II. 30
6.9. Dimensionless coefficients for Intermediate Subphase III 34
6.10. Reference parameters for Intermediate Subphase III 35
6.11. Nondimensional coefficients for Intermediate Subphase III 36

6.12. Evaluated terms in dimensionless depressurization equation for Intermediate Subphase III. 38
6.13. Nondimensional coefficients at "end" Phase III (2-field model) 39
6.14. Nondimensional coefficients at "end" Phase III (3-field model) 39
6.15. Dimensionless coefficients for ADS-4 phase. 44
6.16. Reference parameters for plant and facilities during ADS-4 blowdown 45
6.17. Time scales for ADS-4 blowdown 46
6.18. Π values for the ADS-4 blowdown phase. 47
6.19. Π Ratios between facilities and AP600 for the ADS-4 Blowdown Phase. 47
6.20. Dimensionless groups for ADS-4 vessel mass balance. 48
6.21. Dimensionless coefficients in IRWST Injection Phase. 62
6.22. Reference parameters for plant and facilities during the IRWST Injection Phase 63
6.23. Π values for the IRWST Injection Phase 64
6.24. Π Ratios between facilities and AP600 for the IRWST Injection Phase 64
6.25. Dimensionless parameters for reactor vessel balance equation 65
6.26. Nondimensional coefficients (Πs) for the IRWST draining phase 81
6.27. Summary of relevant Π groups, Π ratios, and nondimensional reference quantities during the IRWST draining phase. 84
6.28. Nondimensional coefficients for the IRWST/Sump Injection Phase. 92
6.29. Reference parameters for IRWST/Sump Injection Phase 93
6.30. Reference parameter values for IRWST/Sump Injection Phase 93
6.31. Nondimensional coefficients for the IRWST/Sump Injection Phase. 94
B-1. Useful facility parameters B-3
B-2. ADS and break diameters B-5
B-3. ADS and break areas B-6
B-4. AP600 and facility component elevations relative to hot leg centerline B-7
B-5. Component volume distributions for AP600 and facilities B-8
B-6. Hydraulic resistance for AP600 and facilities B-9
B-7. CMT and vessel areas B-10
B-8. Levels at initiation of ADS-4 blowdown B-10
B-9. Levels from Table B-8 put on a common basis (bottom of core heated length) B-11
B-10. Elevation of bottom of CMT tank relative to hot leg centerline B-11
B-11. Conditions at start of ADS-4 blowdown B-11
B-12. Equation for Table B-11 ..... B-12
B-13. ADS-4 offtake diameters and ratios B-12
B-14. IRWST parameters B-12
C-1. Physical interpretation of Ψ groups for Intermediate Phase C-7

G-1. Nondimensional groups and description for IRWST drain phase G-8
G-2. Fluid properties for evaluation of overall heat transfer coefficient G-9
G-3. IRWST wall thermal properties G-10

NOMENCLATURE

c_p	specific heat
d	diameter
e	energy per unit mass
f	friction factor
g	gravitational acceleration
h	specific enthalpy
l	length or characteristic dimension
$\dot{m}$	mass flow
p	pressure
q	decay heat
r	radius
t	time
u or v	velocity
x	quality
A	area
C	coefficient for Intermediate Phase
C_p	specific heat
D	diameter or characteristic dimension
G	mass flux
H	height or elevation
K	loss coefficient
L	pipe length or level (tanks)
LHS	left hand side
M or m	mass
P	pressure
Q	volumetric flow
R	ideal gas constant or radius
R'	line resistance parameter
RHS	right hand side
T	temperature
V	volume
Y	elevation or elevation difference
Z	elevation difference

Greek symbols

α	void fraction
β	thermal expansion coefficient
γ	specific heat ratio
φ	nondimensional coefficient
Δ	difference (as in ΔT)
ρ	density
ν	specific volume
μ	viscosity or specific internal energy
π	ratio of reference values
Φ	nondimensional coefficient[a]
Π	nondimensional coefficient
Ψ	nondimensional coefficient

Subscripts

0	reference or initial value
acc	accumulator
ads	ADS system
ads123	stages 1, 2, and 3 automatic depressurization system
ads4	stage 4 automatic depressurization system
b	vessel upper head bubble
break	break value
cc	concrete
cmt	core makeup tank
cont	containment value
core	core value
crit	choked flow value
dc	downcomer
dvi	direct vessel injection
f	saturated liquid value
fg	saturated vapor - saturated liquid
g	gas or vapor value
head	manometric parameter
hl	hot leg parameter
i	ith component
in	control volume inlet
it	IRWST value
j	jth component
l	liquid parameter
lp	lower plenum
m	mixture
net	net value
out	control volume outlet
p	constant pressure
pzr	pressurizer
sat	saturation value
sl	surge line
tank	value for tank
uh	upper head
up	upper plenum
v	vessel or constant volume
w	wall

[a] For clarity, different Greek symbols are used to denote nondimensional coefficients for the different transient phases. For example, Φ is used for the Early Depressurization Phase, Ψ is used for the Intermediate Phase, and Π is used for other phases.

ACC	accumulator
ADS-1,2,3	stages 1, 2, and 3 automatic depressurization system
ADS-4	stage 4 automatic depressurization system
C	cold
CMT	core makeup tank
DC	downcomer
DVI	direct vessel injection
H	hot
HEM	homogeneous equilibrium
IRWST	in reactor refueling water storage tank
N	nitrogen/steam
PRHR	passive residual heat removal system
PZR	pressurizer
S	Sump
SG	steam generator
SL	pressurizer surge line
V	vessel

Superscripts

*	normalized value

TOP-DOWN SCALING ANALYSIS METHODOLOGY FOR AP600 INTEGRAL TESTS

1. INTRODUCTION

The Nuclear Regulatory Commission (NRC) Division of Systems Research is conducting a research program that has the ultimate goal of producing an assessed/validated computer code that can be used to analyze transient and off-normal operating conditions in advanced light water reactor designs. Such computer codes will eventually be used to independently evaluate the AP600[1] design and analyses associated with license submittals. The current research program centers around demonstrating the adequacy[2] of the RELAP5/MOD3[3] computer code for applications related to these advanced reactor designs.

The AP600 reactor design is unique relative to current light water reactor designs. It features passive safety systems that rely on gravity dominated heads and large volumes of water stored above the reactor vessel and automatic depressurization systems (relief valves) to provide core cooling during accident conditions. The passive safety system design results in numerous interconnected flow paths (loops) between fluid storage components and the reactor vessel. The unique features of this design suggests the potential for different types of response during off-normal conditions relative to current light water reactor designs. Any unique system behaviors are of interest and must be understood, to determine the significance for the plant design, and to provide assurance that current computer codes have the capability to properly predict the progression and end state of off-normal transients. One must therefore ensure that the experimental data base is applicable, ensure that analysis techniques have the inherent ability to calculate the observed response as appropriate, and identify any shortcomings in the experimental data or the analysis methods.

Several test facilities have been used to generate data for use in advanced reactor licensing activities. For the AP600, these include the SPES facility[4] in Italy, the Advanced Plant Experiment (APEX) facility[5] at Oregon State University, and the Rig of Safety Assessment (ROSA) facility[6] at the Japanese Atomic Energy Research Institute (JAERI). Relative to the AP600, SPES and ROSA are full-height, full-pressure, volume and power scaled facilities. Scale factors for SPES and ROSA are [ ]^{a,c} respectively, meaning that system fluid volumes, flow areas, and mass flow rates should be approximately in these ratios relative to AP600. As SPES and ROSA are full-height and full-pressure facilities, fluid velocities and transit times should be approximately the same as the AP600. The APEX facility is a reduced pressure, [ ]^{a,c} height system relative to the AP600. APEX scale factors are as follows: fluid velocity and transit times scale at [ ]^{a,c} relative elevation and lengths are scaled at [ ]^{a,c} flow areas are scaled at [ ]^{a,c} core power and mass flows are scaled at [ ]^{a,c} and fluid volumes are scaled at [ ]^{a,c}

The research program organized by the NRC includes evaluation of the test facilities being used to generate data for code verification of advanced reactor designs, evaluation of the data being produced by these facilities, RELAP5 thermal-hydraulics code applications for the plant and the test facilities similar to those discussed in References 7 and 8, and scaling analyses of the facility and code results. An objective of the NRC effort is to ensure that the data base generated with these facilities is applicable for evaluation of computer codes used to calculate advanced reactor response to off-normal conditions.

The NRC has assembled several working groups composed of NRC staff, contractors, and consultants to effect the elements of this program relative to the AP600. Each of these working groups is concentrating on a specific area of interest and has a different charter. The working groups are dealing with the general areas of AP600 test facility data analysis, facility bottom-up (or local) scaling[9], and facility top-down (or global) scaling. Each of these elements is a part of the overall effort required to ensure the applicability and adequacy of the experiment data base for application to AP600 licensing issues.

This report describes results from the top-down scaling group effort. The major objective of this work is to develop a methodology that can help provide information regarding the applicability of data taken in small-scale facilities for the full-scale system thereby supporting the overall code adequacy statement. The methodology is based on and complements the hierarchical two-tiered scaling methodology described in Reference 10. The approach involves decomposition of the system under consideration to identify characteristic geometries and processes, development of a system of dynamic lumped parameter equations from the conservation laws for these geometries and processes, nondimensionalization of these equations, identification of process scales, and the development of scaling groups from the equations that determine system and component response. Note that this approach is not intended to examine all of the components needed to perform facility design or scaled testing. The methodology is applied to test cases centered on facility results from one-inch cold leg break loss-of-coolant experiments including OSU APEX Test SB5[11], OSU Test NRC22[12], ROSA Test AP-CL-03[13], and SPES Test SB00401[14, 15].

Section 2 provides background information on scaling and the role of the top-down scaling effort and objectives. Section 3 outlines the development of the scaling analysis approach and discussion of the methodology for using the results. For the benefit of the reader, a brief overview of the AP600 design is given in Section 4. Transient scenario and phase descriptions are addressed in Section 5. Preliminary application of the methodology to a one-inch cold leg break scenario is discussed in Section 6. Conclusions and recommendations are presented in Section 7. Appendices provide additional information on development of the equations used in the analysis, facility parameter values, and other supporting material.

2. ROLE OF THE TOP-DOWN SCALING EFFORT

Detailed overviews of the NRC code adequacy demonstration procedure are given in References 2 and 8. Figure 2-1 of Reference 2 provides a graphical illustration of the various tasks and components of the overall demonstration process. In general, the procedure involves cycles of successively testing the code capabilities against experimental data applicable to the AP600 design, effecting model improvements (if necessary) to address identified deficiencies, and then conducting additional assessment to achieve specified performance criteria. Specifically, these tasks/components include: a) the definition of the relative importance of AP600 systems, components, processes, and phenomena, defining priorities in assessing code capability; b) detailed examination of the code structural components to assess separate effects models, correlations, and closure relationship capabilities; c) developmental assessment to determine code capabilities with respect to prediction of separate effects and integral experiment results; d) scaling studies to determine the applicability of the experimental data base; and e) an adequacy decision based on the results of the above tasks and the answers to questions such as "what are the accident scenarios required to ensure that the code is assessed over a sufficiently wide range of conditions?", "are the data applicable?", and "what phenomena are important?" for the code analysis/adequacy decision. Item a) above has been addressed by the AP600 PIRT (Phenomena Identification and Ranking Table)[16, 17] wherein the thermal-hydraulic phenomena, processes, and conditions that affect AP600 SBLOCA response have been identified and ranked according to their expected influence on a figure of merit considered to be the reactor vessel inventory. Items b) and c) are discussed in Reference 2. The top-down scaling effort discussed in this report along with other scaling and analysis efforts such as discussed in References 9 and 18 addresses Item d). In this regard, the goal of the top-down scaling effort is to develop a methodology that can help provide information regarding the applicability of data taken in small-scale facilities to the full-scale system. The primary emphasis is on scaling the system parameters influencing core cooling (such as reactor vessel liquid inventory) during the small break loss-of-coolant transient.

The top-down scaling effort is a component in the NRC Hierarchical Two Tiered Scaling[10] approach which also includes the bottom-up scaling effort described by Bessette et al. in Reference 9. The overall scaling effort is based on a similitude approach in which the governing equations are developed for the system being studied, the equations are nondimensionalized, and the coefficients are numerically evaluated to determine which processes are the most important. The present effort follows an approach well established for fluid mechanics problems, applied to pressurized water reactor LOCA assessments by Wulff[19] and Reyes[20]. In this study, the top-down scaling group applies the methodology to the conservation equations averaged down to the reactor system component level (e.g., tanks and interconnections).

The following objectives were defined to focus the effort:

1) Develop nondimensional groups in the averaged conservation equations that are resolved to preserve the main system level responses. Define reference scales to

calculate the values of these groups such that the dependent variables in each equation are O[1]. Note that these reference scales must be determined based on facility and AP600 design, therefore it is important to check by comparison with data that the choices are reasonable and give dependent variables ~O[1]. It is recognized that fine-scale information filtered out of these equations must be re-supplied via constitutive equations with their accompanying nondimensional groups via bottom-up scaling.

2) Conduct an order of magnitude analysis of the nondimensionalized equations to clarify the impact of the terms in each equation on the most important system responses in each phase of the transient. The analysis must be done for the AP600 reference system and for each experimental facility. This step will lead to a reduced set of dominant nondimensional groups.

3) Numerically evaluate and compare the reduced set of dimensionless groups from 2) above for the AP600 and for each of the experiment facilities. Based on these values clarify distortions in the experimental facilities vis-à-vis the AP600 and their impact on the main system responses(s) of interest. Hence, determine whether the data from the facilities are applicable to assessment of AP600 analysis methods, and whether the facility designs, taken together, give rise to ranges of important nondimensional groups that encompass those for the AP600.

3. METHODOLOGY

The AP600 PIRT[16, 17] indicates that the AP600 response for a given transient can be characterized by distinct chronological phases. Phase definitions are based on considerations such as the thermal-hydraulic processes that are expected to have an influence on the system response, geometric and operational characteristics, and system hardware components that are expected to be active and influential for the particular phase being considered. The PIRT results suggest that the active system components and the thermal-hydraulic processes of importance will change over the duration of a transient. Therefore details of the analysis will be different for each phase defined. The approach taken in this analysis involves a multi-step process that builds on the PIRT description of the accident scenario. The steps include:

1. Define the phenomenologically distinct phases of the transient identifying initiating and ending events, for example, when the CMT level drops to a specified value (i.e., 20%), ADS-4 is activated and the "ADS-4 Phase" is initiated.

2. Identify subsystems, components, and interactions of importance in each phase.

3. Develop a diagram of the system indicating subsystems, components, and interconnections identified in Step 2.

4. Define the governing equations for each component, in each phase and their interconnections as identified in Step 3 using a lumped parameter approach to develop integral forms of the conservation of mass, energy, and momentum equations.

5. Nondimensionalize the equations developed in Step 4.

6. Select reference scales such that the nondimensionalization process leads to the dependent variables and their time derivatives, except those characterizing the key system response in each equation, being ~O(1).

7. Order the terms in the nondimensional equations in terms of the magnitude of the nondimensional coefficients and retain only the dominant terms in each equation clarifying the impact of each remaining term on the system response of interest.

8. Evaluate the reduced nondimensional equations using data from experimental facilities to determine their validity in predicting the system responses of interest.

9. Compare the nondimensional groups that dominate the system response of interest, for the AP600 and experimental facilities, and thereby evaluate the applicability of the experimental data to assessments of AP600 analysis methods.

Section 5 presents the results of Step 3, Steps 4-7 are detailed in the Appendices. Section 6 summarizes Steps 1-7 and details Step 8. In general, more detail is given to higher priority phases - for example, those in which vessel inventory and therefore core cooling could be influenced.

The results of Steps 4-6 in the methodology provide a set of nondimensionalized equations that are used to predict a key system response such as vessel mass inventory. This closed set may contain certain requirements for closure relationships that eventually may be supplied by more detailed analysis. For example, the top-down nondimensionalized, equations for the IRWST refill phase contain a nondimensional group involving the pressurizer surge line density. This may not be specified accurately at this stage, but may be refined in future estimates. Characteristics of this top-down equation set which allows the calculation of a key system response, such as the reactor vessel mass inventory, are:

- All nondimensional variables and derivatives of variables except the key system response, are approximately O[1], with nondimensional coefficient groups which then determine the magnitude of each term
- Then groups can be evaluated so that their magnitudes can be compared to identify the dominant terms in each equation and their impact on the key system response. Based on this comparison, only the dominant groups in each equation are retained
- The dominant groups for each transient phase for each facility and the reference plant are then compared to help clarify distortions

Validation increases confidence that the dominant nondimensional groups, and correct reference scales, for each phase have been identified, that important phenomena have not been excluded, and helps identify the important closure relationships. After going through this process, if for a given facility, one or more of the dominant groups for a particular phase are significantly different from the reference plant, then the data for that phase must be carefully examined for applicability.

The sketch in Figure 3.1 illustrates the process of validation for each hierarchical level in the system of nondimensionalized equations resulting from the order of magnitude analysis. In essence for each equation, the integral of the left hand side of the equation can be plotted against the integral of the right hand side of the equation. If the result is near the $y = x$ line as indicated on the sketch, then there is reasonable assurance that the necessary terms have been accounted for in the equation and the retained nondimensional groups capture the main phenomena. This type of check ultimately should be done for each phase and for each equation in the hierarchy for that phase. For example, the equations starting with the vessel mass balance, then for the mass in flows and out flows, then for the head terms governing the flows, and so forth. This process also allows determination of the order of magnitude of the nondimensionalized dependent variable in each equation and ensures that the reference scales are selected such that they are ~O[1].

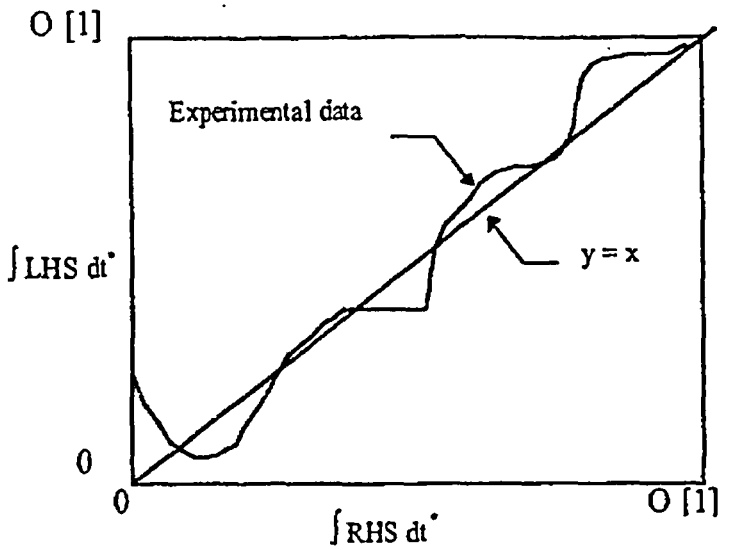

Figure 3.1. Sketch illustrating verification process to evaluate whether the dominant terms retained in each equation are sufficient to capture the experimental data.

4. AP600 DESIGN OVERVIEW

The AP600 reactor design is an advanced PWR concept that relies on a number of passive safety features. The design includes low core volumetric heat generation rates, low peak-to-average fuel heat flux ratio, reliance on gas pressurization and gravity heads for safety system operation, and dependence on natural circulation and condensation for safety system performance. All passive safety systems are an integral part of the reactor containment which incorporates heat exchange facilities for removing core decay heat from the reactor system and eventually from the containment to the environment.

Details of the AP600 design are contained in Reference 1. A brief overview of the plant operation will be given here. Figure 4.1 shows a sketch of the containment and reactor system. The AP600 design is a two-loop system consisting of two hot legs and four cold legs. The AP600 contains many components found in current generation pressurized water reactor designs (e.g., steam generators, pressurizer). A significant difference relative to current commercial systems is that passive emergency core cooling systems are included in the design. These systems are automatically activated in the event of loss of coolant from the primary system to replenish and maintain the reactor system inventory. An "S signal", which can be generated by off-normal plant operating conditions such as low pressurizer pressure, low cold leg temperature, low steam line pressure, or high containment pressure, generates a core scram signal, reactor coolant pump trip signal, main feedwater pump and turbine trip, and also activates many of the passive safety systems.

The passive systems consist of accumulators pressurized with nitrogen gas, core makeup tanks (CMTs) which contain cold water and are pressure balanced with the primary reactor system, and a large in-containment refueling water storage tank (IRWST) that is pressure balanced with the containment. The CMTs are activated (and thus can start recirculating by natural circulation) by pressurizer or steam generator low level setpoints or by receipt of the S signal which also activates the IRWST system valves. The bottoms of the CMTs and the IRWST are located at elevations above the reactor cold legs to provide the head necessary for coolant injection. Although the S signal activates the IRWST system, flow from the IRWST into the primary can not commence until the primary pressure decreases below the IRWST hydrostatic head. Once the IRWST tank inventory has been discharged, the containment liquid level will exceed the elevation of the coolant loops allowing liquid to be injected back into the primary system via sump valves. Steam in the containment (generated by flashing of primary coolant) is condensed on the interior walls of the containment, collected, and then returned to the IRWST. Gravity-driven evaporative cooling external to the containment provides passive containment cooling.

To help ensure the proper functioning of the gravity driven passive safety systems, an automatic depressurization system (ADS) is incorporated into the AP600 design to limit the primary system-to-containment differential pressure (i.e., depressurize the primary system). The ADS consists of four different stages of valves (ADS-1, ADS-2, ADS-3, and ADS-4) to provide

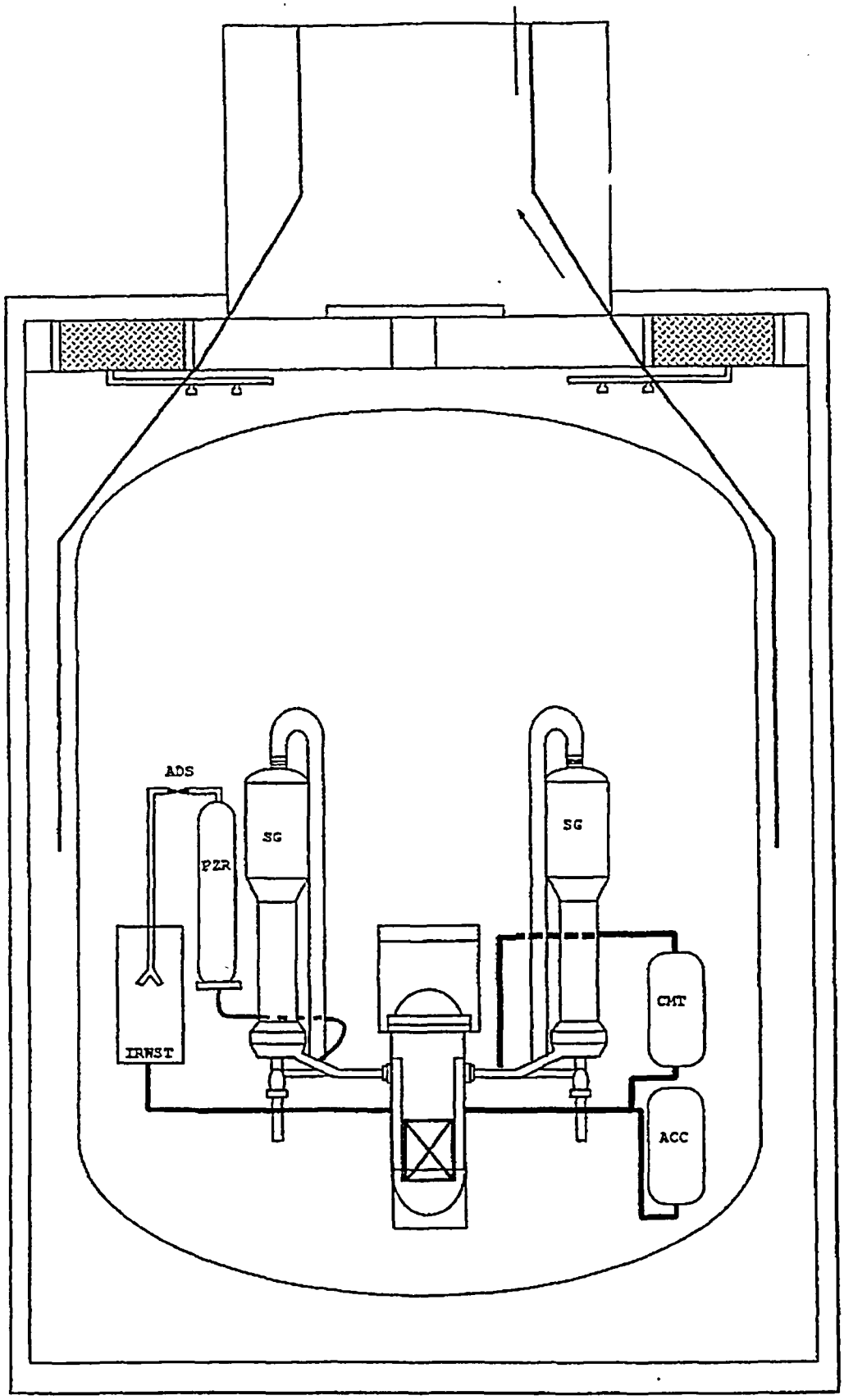

Figure 4.1. Sketch of AP600 design.

primary system pressure relief. ADS-1, ADS-2, and ADS-3 are connected to the top of the pressurizer and discharge through a sparger into the IRWST. The CMT actuation signal activates the ADS-1,-2,-3 valves. ADS-1 fires when the CMT level reaches 67% and the second and third ADS stages open based on elapsed time from the previous stage opening. ADS-4 valves are connected to the reactor hot legs and discharge directly to containment. ADS-4 valves are triggered by a CMT level setpoint of 20% in conjunction with an elapsed time from ADS-3 actuation. Core decay heat is rejected to the IRWST via a passive decay heat removal system (PRHR) which is capable of removing full decay heat and can operate at full system pressure.

Unlike existing operating reactors whose safety systems rely primarily on pump heads for operation, the AP600 design relies on gravity dominated forces for safety system operation. The current research program is focused on the evaluation of these systems and the processes that influence their operation.

5. SMALL BREAK LOSS-OF-COOLANT SCENARIOS AND PHASE DESCRIPTIONS

A cold leg small break loss-of-coolant transient scenario in the AP600 design is broken down into distinct chronological phases with the phase boundaries based on phenomenological considerations. Phases are characterized by an initiating time or event, an ending time or event, and the subsystems that play a significant role. Note that phase decomposition into well defined phases in this manner is important and requires knowledge of the systems in order to establish conditions needed for analysis of the phase. If care is not exercised, poorly defined phases and/or conditions may result. Phase definitions for the one-inch cold leg break scenario are defined in detail in the AP600 PIRT.

The one inch cold leg break scenario is summarized in the next section. An annotated pressure history for the calculated AP600 response to a one inch cold leg break is presented in Figure 5.1. The starting and ending points of the phases are shown in the figure and have been defined below with a summary of the important processes occurring in the system. Note that each of the phases has been given a priority rating of either high, medium, or low. This priority rating is based on the expectations regarding how the dominant processes and interactions occurring during the phase might influence the vessel inventory. Thus, the level of detail in the treatment in the following sections is related to the priority.

The analysis covers the accident in five phases: 1) Initial high pressure subcooled blowdown, 2) Intermediate passive cooling, CMT draining/accumulator injection, and ADS-1,-2,-3 blowdown, 3) ADS-4 blowdown to IRWST initiation, 4) IRWST injection through initial refill of the reactor vessel, and 5) IRWST draining/sump injection. With the exception of the OSU APEX facility, experiments generally were only conducted through the steady IRWST injection stage. The APEX facility does not simulate the initial high pressure subcooled blowdown.

5.1 AP600 SBLOCA Phase Description Summary

5.1.1 High Pressure Phase: Subcooled Depressurization

- Priority Low
- Beginning - Initiating event is the break opening
- Processes/events - pressurizer vapor bubble behavior, pressurizer heaters on initially and then are turned off, note that the core energy addition rate is balanced by the steam generator energy removal rate
- End - Pressurizer empties, knee in pressure-time curve - note that these events occur, within the order of magnitude analysis, at nearly the same times as the S-signal and "scram", hence core energy addition and steam generator energy removal balance through most of the phase.

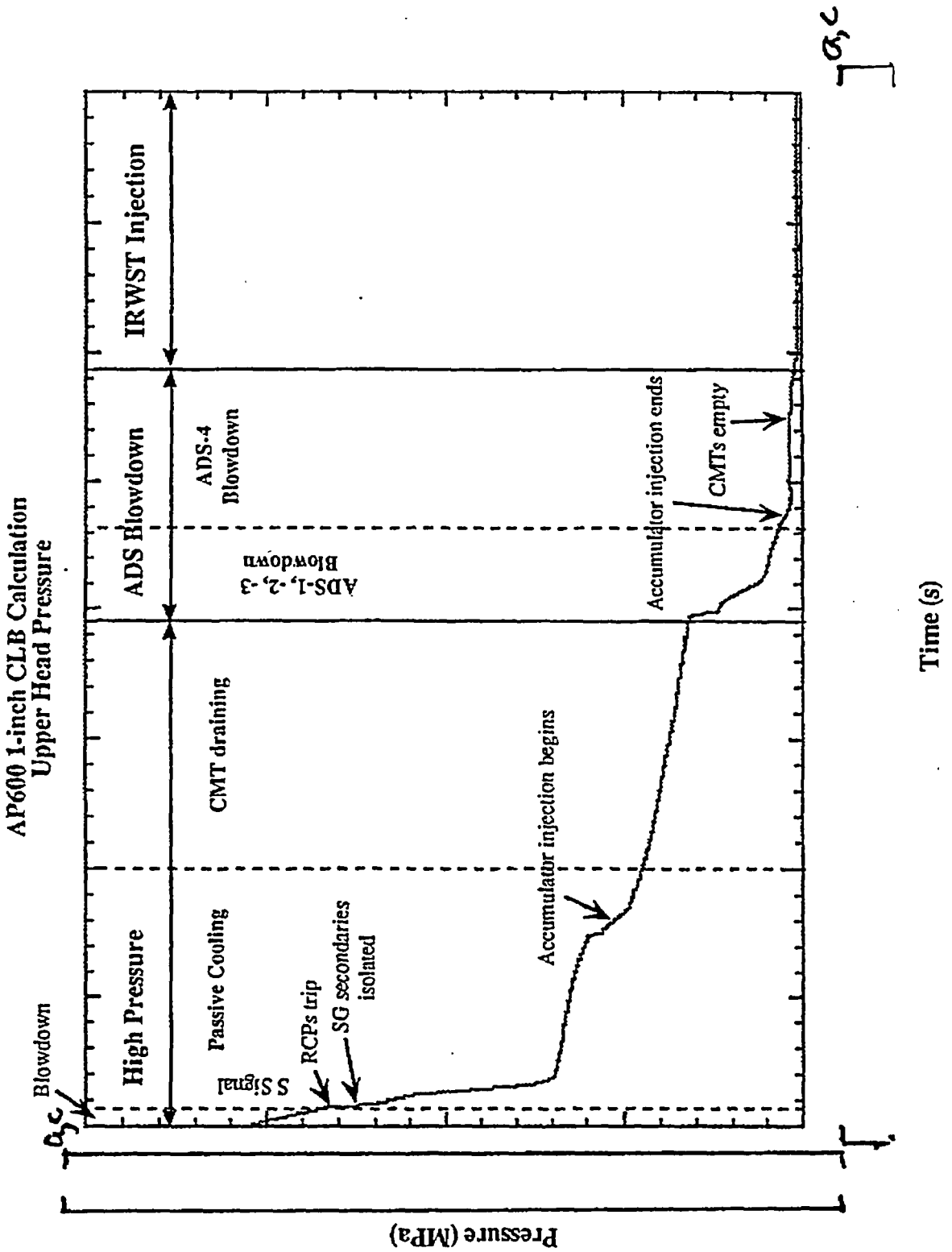

Figure 5.1. Calculated pressure for AP600 one-inch cold leg break transient.

5.1.2 Intermediate Phase: Passive Cooling Phase (CMT/PRHR Recirculation and ADS-1,-2,-3 Blowdown)

- Priority medium
- Beginning - pressurizer is empty or is nearly empty (10-12% level), "S" signal generated by low pressurizer pressure or high containment pressure condition at a time close to the pressurizer emptying, core scram (due to "S" signal, pressurizer overpressure or underpressure, steam generator level, etc. See Table H-2 of Reference 16 for complete list of setpoints).
- Processes/events
  - PRHR cooling
    - * heat transfer to IRWST
    - * recirculation in PRHR piping
  - CMT - recirculation and heat removal
  - System asymmetry caused by the differences in P-loop (loop containing pressurizer and PRHR connections) and C-loop (loop containing CMTs)
    - * Sub-phase 1 - Both steam generators are sinks
    - * Sub-phase 2 - P side steam generator voids (develops a steam bubble) and ceases to circulate. The P-loop steam generator along with the break flow determines the system dP/dt. The C-loop is still circulating.
    - * Sub-phase 3 - C-loop steam generator voids and circulation in the C-loop ceases.
    - * Sub-phase 4 - CMTs begin to drain
    - * Sub-phase 5 - Accumulators begin to inject
  - CMT level at 67% and ADS-1 opens
  - Pressurizer refills, mass loss through ADS
  - Flashing in pressurizer
  - Subcooling in vessel followed by return to boiling in core
  - CMT draining and flashing
    - * Sub-phase 6 - ADS-1 open, mostly vapor flow out ADS-1, level in pressurizer is increasing
    - * Sub-phase 7 - ADS-2 opens based on elapsed time signal from ADS-1 actuation point, ADS-1 and ADS-2 are open, two-phase flow out ADS-1 and ADS-2, pressurizer fill continues
    - * Sub-phase 8 - ADS-3 opens based on elapsed time signal from ADS-2 actuation point, ADS-1. ADS-2, and ADS-3 are open, pressurizer is full and low quality fluid is flowing out the ADS valves
- End - CMT level at 20% and ADS-4 opens

5.1.3 ADS-4 Blowdown

- Priority high

- Beginning - ADS-4 opens
- Processes/events - Pressurizer starts to drain (again), ADS-1,-2,-3 flows transitions from choked to friction dominated, choked and unchoked flow through ADS-4, core boiling is taking place, hot leg fluid is near saturation
  - Sub-phase 1 - Choked flow at ADS-4
  - Sub-phase 2 - Possibly unchoked flow at ADS-4
- End - Primary pressure decreases to a value below the IRWST pressure (hydrostatic head) and flow from the IRWST system commences.

5.1.4 IRWST Injection

- Priority high
- Beginning - Primary pressure decreases to a value below the IRWST pressure (hydrostatic head)
- Processes/events - DVI fluid is subcooled, pressurizer level oscillates as it drains, vessel level oscillations, ADS-4 oscillations are caused by pressurizer draining and plugging of ADS-4 inlet, core fluid is eventually subcooled by the IRWST flow
  - Sub-phase 1 - subcooled DVI injection (DVI with flow-level oscillations and vessel level oscillations in some facilities). IRWST head essentially constant
  - Sub-phase 2 - oscillations cease, pressurizer is empty
- End - Vessel level near hot leg elevation

5.1.5 IRWST Draining/Sump Injection (Long Term Cooling) Phase

- Priority medium
- Beginning - Vessel level near hot leg elevation IRWST and sump level are equal
- Processes/events - IRWST level decreases due to injection into primary. Sump filling, two-phase flow out ADS-4, core boiling, entrainment cooling. Heat removal from system due to external cooling of containment structure.
  - Sub-phase 1 - IRWST level decreasing, Sump filling, DVI fluid temperature slowly increasing
  - Sub-phase 2 - IRWST and Sump level are equal and constant at curb elevation, DVI fluid near saturation temperature, system in steady-state. Heat removal from containment balances heat generated in reactor.
- End -

6. DEMONSTRATIONS OF METHODOLOGY

The methodology was applied to all phases of the transient described in Section 5. The ADS-4 blowdown phase and the IRWST injection phase, are expected to be more complex and a significant test of the methodology as well as being the phases with the highest priorities from the viewpoint of the system response.

6.1 High Pressure Subcooled Depressurization

The high pressure subcooled depressurization phase was described in Section 5. The first three steps of the methodology are addressed there.

6.1.1 Steps 1-3 - Subcooled Depressurization Definition and Topology

During normal operating conditions the reactor system is running at rated power and at a pressure of approximately 15.5 MPa. Under these normal operating conditions, system pressure is controlled by the pressurizer which contains heaters that are operated to maintain the pressurizer fluid at saturation conditions corresponding to the desired system pressure. With the exception of the pressurizer, the primary coolant system contains subcooled fluid. If a small break is postulated to occur in the cold leg of the plant, system pressure will immediately start to decrease in response to the mass and energy loss out the break. The decrease in system pressure causes the highest temperature fluid in the system, that in the pressurizer, to flash to maintain equilibrium conditions. During this depressurization process, the flow out the break is subcooled and the majority of the reactor system remains subcooled until the pressure decreases far enough that other high temperature points in the system (such as the reactor upper head) reach saturation conditions. Other events may be occurring during this phase such as reactor scram and termination of pressurizer heater power. The major process occurring in the system is, however the break out flow.

The configuration of the system for this phase consists basically of a tank of saturated liquid and vapor (the pressurizer) that is connected to a large volume of subcooled liquid (the primary system) as shown in Figure 6.1. In effect, the pressurizer is connected to the break through the subcooled and largely incompressible primary system. As such, the pressurizer outflow is approximately equal to the break flow and the pressurizer level will respond accordingly. As shown in Figure 6.1, it is recognized that the core is adding energy to the system during this phase and that the steam generators are effective heat sinks that balance the core energy addition. At this point there are no inflows to the system.

6.1.2 Steps 4 and 5 - Governing Equations and Nondimensionalization

A pressure rate equation and level equation to describe the performance of a sub-component containing saturated fluid connected to a larger system containing subcooled liquid such as

depicted in Figure 6.1 are derived in Appendix A. These derivations are based on conservation of energy and mass for the control volume represented by the pressurizer (the top dashed line shown in Figure 6.1). For the present case, assumptions made include the following:

- thermodynamic equilibrium is assumed
- kinetic and potential energy are neglected
- the pressurizer contains saturated fluid and the rest of the primary system is subcooled
- the pressurizer outflow is essentially the break flow rate
- the core energy addition rate is balanced by steam generator heat removal rate
- pressurizer heaters add energy to the pressurizer fluid

In dimensionless form, these equations are

$$\begin{aligned}\frac{dp^*}{dt^*} &= \Phi_1 \sum \dot{m}_{in}^* \left(h_{in} - \left(\mu_f + x\mu_{fg}\right)\right)^* \left.\frac{\partial p}{\partial \mu}\right|_v^* \frac{1}{M^*} \\ &+ \Phi_2 \sum \dot{m}_{in}^* \left(v_f + x v_{fg}\right)^* \frac{\mu_{fg}^*}{v_{fg}^*} \left.\frac{\partial p}{\partial \mu}\right|_v^* \frac{1}{M^*} \\ &- \Phi_3 \sum \dot{m}_{out}^* \left(h_f + x h_{fg} - \left(\mu_f + x\mu_{fg}\right)\right)^* \left.\frac{\partial p}{\partial \mu}\right|_v^* \frac{1}{M^*} \\ &- \Phi_4 \sum \dot{m}_{out}^* \left(v_f + x v_{fg}\right)^* \frac{\mu_{fg}^*}{v_{fg}^*} \left.\frac{\partial p}{\partial \mu}\right|_v^* \frac{1}{M^*} \\ &+ \Phi_5 q_{net}^* \left.\frac{\partial p}{\partial \mu}\right|_v^* \frac{1}{M^*}\end{aligned} \tag{6.1}$$

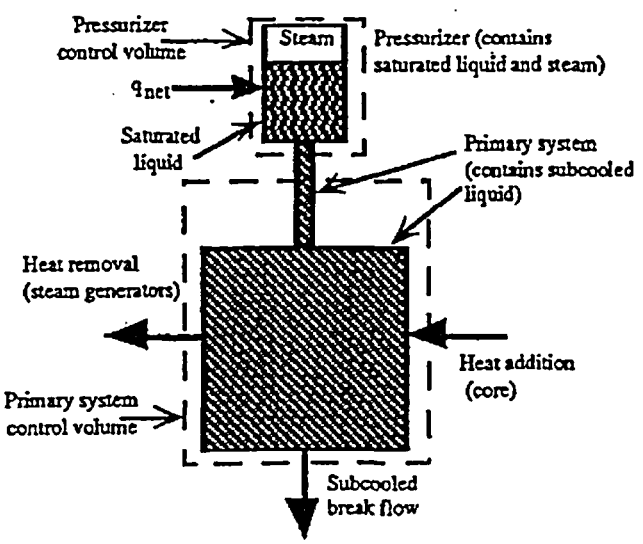

Figure 6.1. Pressurizer connected to the primary system - schematic for subcooled depressurization phase.

for the pressure rate equation and

$$\frac{dL^*}{dt^*} = \Phi_6 \frac{\left(\dot{m}_{in}^* - \dot{m}_{out}^*\right)}{\left(\rho_g^* - \rho_f^*\right)} - \frac{\left(1 - L^*\right)}{\left(\rho_g^* - \rho_f^*\right)} \frac{d\rho_g^*}{dp^*} \frac{dp^*}{dt^*} \tag{6.2}$$

for the level equation

where

- h_{in} - inlet liquid enthalpy
- h_f - saturated liquid enthalpy
- h_{fg} - latent heat of vaporization
- L - level
- $\dot{m}_{in}$ - inlet mass flow rate
- $\dot{m}_{out}$ - outlet mass flow rate
- p - pressure
- q_{net} - net energy addition
- t - time
- v - specific volume
- v_f - saturated liquid specific volume
- v_{fg} - specific volume on phase change
- x - static quality
- μ - specific internal energy
- μ_f - saturated liquid specific internal energy
- μ_{fg} - specific internal on phase change
- ρ_f - saturated liquid density
- ρ_g - saturated vapor density

and quantities with an asterisk represent normalized variables resulting from dividing a variable by a reference value.

Equations (6.1) and (6.2) represent a closed set of equations with unknowns p^* and L^*. The nondimensional groups appearing as multipliers in Equations (6.1) and (6.2) are defined as (see Appendix A)

$$\Phi_1 = \frac{t_0 \dot{m}_0 \left(h_{in} - \mu\right)_0}{p_0 M_0} \left.\frac{\partial p}{\partial \mu}\right|_{v_0} \tag{6.3}$$

$$\Phi_2 = \frac{t_0 \dot{m}_0 v_0}{p_0 M_0} \frac{\mu_{fg_0}}{v_{fg_0}} \left.\frac{\partial p}{\partial \mu}\right|_{v_0} \tag{6.4}$$

$$\Phi_3 = \frac{t_0 \dot{m}_0 (h-\mu)_0}{p_0 M_0} \left.\frac{\partial p}{\partial \mu}\right|_{v_0} \tag{6.5}$$

$$\Phi_4 = \frac{t_0 \dot{m}_0 v_0}{p_0 M_0} \frac{\mu_{fg_0}}{v_{fg_0}} \left.\frac{\partial p}{\partial \mu}\right|_{v_0} \tag{6.6}$$

$$\Phi_5 = \frac{t_0 q_0}{p_0 M_0} \left.\frac{\partial p}{\partial \mu}\right|_{v_0} \tag{6.7}$$

$$\Phi_6 = \frac{t_0 \dot{m}_0}{M_0} \tag{6.8}$$

where

$(h_{in} - \mu)_0$ - reference value of inlet fluid enthalpy minus pressurizer specific internal energy
$(h - \mu)_0$ - reference value of fluid enthalpy minus specific internal energy
$\dot{m}_0$ - reference flow rate
M_0 - reference mass
p_0 - reference pressure
q_0 - reference net energy addition
t_0 - reference time
μ_{fg_0} - reference value of $\mu_g - \mu_f$
v_0 - reference specific volume
v_{fg_0} - reference value of $v_g - v_f$

The dimensionless Φ groups listed in (6.3) to (6.8) are parameters that help characterize the system response. Φ_1 is the ratio of pressure change, due to the net energy added by inflow, to the reference pressure; Φ_2 represents the ratio of pressure change, due to volumetric inflow, to the reference pressure; Φ_3 is the ratio of pressure change, due to the net energy removed by outflow, to the reference pressure; Φ_4 represents the ratio of pressure change, due to volumetric outflow, to the reference pressure; Φ_5 is the ratio of pressure change, due to generation rate of the pressurizer heaters, to the reference pressure; and Φ_6 represents a ratio of the mass loss from a volume in time t_0 to the total mass in the volume, in effect a nondimensional transit time.

With reference to Figure 6.1, Equation (6.1), and the discussion above, it is clear that for the system under consideration, there is no net mass flow into the system. The pressure and level equations (Equations (6.1) and (6.2)) then reduce to the following

$$\frac{dp^*}{dt^*} = -\Phi_3 \sum \dot{m}^*_{out}\left(h_f + xh_{fg} - \left(\mu_f + x\mu_{fg}\right)\right)^* \left.\frac{\partial p}{\partial \mu}\right|^*_v \frac{1}{M^*}$$

$$-\Phi_4 \sum \dot{m}^*_{out}\left(v_f + xv_{fg}\right)^* \frac{\mu^*_{fg}}{v^*_{fg}} \left.\frac{\partial p}{\partial \mu}\right|^*_v \frac{1}{M^*} \qquad (6.9)$$

$$+\Phi_5 q^*_{net} \left.\frac{\partial p}{\partial \mu}\right|^*_v \frac{1}{M^*}$$

$$\frac{dL^*}{dt^*} = \Phi_6 \frac{-\dot{m}^*_{out}}{(\rho^*_f - \rho^*_g)} - \frac{(1-L^*)}{(\rho^*_f - \rho^*_g)} \frac{d\rho^*_g}{dp^*} \frac{dp^*}{dt^*}. \qquad (6.10)$$

6.1.3 Steps 6 and 7 - Reference Parameter Selection and Order of Magnitude Analysis

Equation (6.10) is coupled to Equation (6.9) through the occurrence of dp^*/dt^* in the second term on the right hand side. Note that by examination, the term

$$\frac{(1-L^*)}{(\rho^*_f - \rho^*_g)} \frac{d\rho^*_g}{dp^*}$$

multiplying dp^*/dt^* is of order unity. The gas density derivative with pressure is O[1], the numerator can vary from 0 to 1 depending on L^* and the denominator will be of order unity since the normalized saturated liquid density is always much larger than the saturated vapor density. If Equation (6.9) is substituted into (6.10) it is seen that the level depends on Φ_6 and the terms this coefficient multiplies and the terms in Equation (6.9).

We can arbitrarily set Φ_6 to unity to define t_0 or

$$\Phi_6 = \frac{t_0 \dot{m}_0}{M_0} = \frac{t_0 G_{crit,0} A_{break}}{\rho_0 V_0} = 1 \text{ or } t_0 = \frac{M_0}{\dot{m}_0} = \frac{\rho_0 V_0}{G_{crit,0} A_{break}} \qquad (6.11)$$

Since we are dealing with the pressurizer, the following are reasonable choices for scaling parameters:

$(h - \mu)_0$ - pressurizer initial liquid specific enthalpy minus specific internal energy

$\dot{m}_0$ - initial break critical flow rate

M_0 - pressurizer initial liquid mass

p_0 - pressurizer initial pressure

v_0 - pressurizer initial specific volume

Table 6.1 lists the reference parameters above and the computed Φ values for the AP600 one-inch cold leg break calculation and one-inch cold leg break experiments in the ROSA and SPES facilities. The initial critical flow rate was computed using the reference pressure and system

Table 6.1. Facility parameters and nondimensional Φ groups for one-inch cold leg break subcooled blowdown.

Parameters	AP600	ROSA	SPES
Break diameter (mm)			
Break area (mm^2)			
System pressure-P_0 (MPa)			
T_{sat}-T_0 (K)			
Liquid enthalpy (kJ/kg)			
Liquid density (kg/m^3)			
Cold leg fluid temperature (K)			
Critical mass flux-G^* (Mg/m^2-s)[a]			
Nominal break flow (kg/s)			
Pressurizer volume (m^3)			
Pressurizer length (m)			
Pressurizer area (m^2)			
Initial pzr. level (%)			
Initial liquid mass (kg)			
Initial liquid volume (m^3)			
Pressurizer heater power (kW)			
$\left.\frac{\partial P}{\partial \mu}\right\|_{v,0}$ (kg/m^3)			
μ_{fg_0} (kJ/kg)			
v_0 (m^3/kg)			
v_{fg_0} (m^3/kg)			
$(h-\mu)_0$ (kJ/kg)			
t_0			
Φ_3			
Φ_4			
Φ_5			
Φ_6			
Φ_4/Φ_3			
Φ_4/Φ_5			

a. G^* computed using Henry-Fauske model with system cold leg temperature.

cold leg fluid temperature with the Henry-Fauske[21] subcooled break flow model and multiplying the resulting critical mass flux by the break area. The last four rows in the table show the ratio of the Φ groups between the plant calculation and the facility. Table 6.2 shows similar information for larger break sizes including the SPES two-inch cold leg break, the SPES two-inch downcomer vessel injection (DVI) line break, and the SPES double-ended guillotine break in the DVI line.

Table 6.2. Facility parameters and nondimensional Φ groups for SPES two-inch breaks and DVI guillotine break.

Parameters	SPES_2inCLB	SPES_2inDVI	SPES_DEGB_DVI
Break diameter (mm)			
Break area (mm^2)			
System pressure-P_0 (MPa)			
T_{sat}-T_0 (K)			
Liquid enthalpy (kJ/kg)			
Liquid density (kg/m^3)			
Cold leg fluid temperature (K)			
Critical mass flux-G^* (Mg/m^2-s)[a]			
Nominal break flow (kg/s)			
Pressurizer volume (m^3)			
Pressurizer length (m)			
Pressurizer area (m^2)			
Initial pzr. level (%)			
Initial liquid mass (kg)			
Initial liquid volume (m^3)			
Pressurizer heater power (kW)			
$\left.\frac{\partial P}{\partial \mu}\right\|_{v,0}$ (kg/m^3)			
μ_{fg_0} (kJ/kg)			
v_0 (m3/kg)			
v_{fg_0} (m3/kg)			
$(h-\mu)_0$ (kJ/kg)			
t_0			
Φ_3			
Φ_4			
Φ_5			
Φ_6			
Φ_4/Φ_3			
Φ_4/Φ_5			

a. G^* computed using Henry-Fauske model with system cold leg temperature.

Values in these tables show that Φ_4 is the dominant group in all cases. This dominance indicates that volumetric flow out the break is more important in controlling pressure than the enthalpy/energy difference convected out the break or the pressurizer heaters. The increase in the ratio of Φ_4 to Φ_5, which represents the relative effect of volumetric flow out the break to the pressurizer heaters, between the one inch breaks and the two inch and DVI breaks indicates the

decreasing importance of the pressurizer heaters as break size increases. The quality in Equation (6.9) increases from an initial value of ~6% to 100% when the pressurizer empties. Note that the values in Tables 6.1 and 6.2 are evaluated at a quality of 6%. The ratio of Φ_4 to Φ_3 does not change with quality. For the 1" breaks, the ratio of Φ_4 to Φ_5 increases by a factor ~6 as the quality increases to 1.0. Thus, the value of Φ_4/Φ_5 in Tables 6.1 and 6.2 represents the maximum effect the pressurizer heaters can have on the depressurization process. These values suggest that the pressurizer heaters have between a 1% and 10% effect.

In the tables the values of Φ_4 agree very well between the facilities and the plant. This agreement is expected since Φ_4 represents the effect of break volumetric flow on depressurization and the facilities were all designed to maintain the ratios of break area to PCS volume and the pressurizer volume to PCS volume. By operating the facilities at the same conditions as AP600 and using the same fluid, the properties and property derivatives are maintained.

6.1.4 Step 8 - Validation of Results

The order of magnitude results indicate that Φ_4 and Φ_6 are the groups controlling the level and the pressure change. Furthermore, it is seen that Φ_4 contains the parameters that constitute Φ_6. This suggests that we can use the computed reference value for t_0 to scale the data from the test facilities. In other words, if L^* and p^* are plotted against t^* where t^* is defined as t/t_0 where t_0 is specified by Equation (6.11) the data would be expected to collapse to the same region (within reason) and, in the ultimate, collapse to a single curve.

To demonstrate this expectation, pressurizer pressure and level data from several different facilities and experiments were normalized and plotted against t^*. These data are shown in Figures 6.2 and 6.3. In Figure 6.2, test data are shown for the ROSA and SPES one-inch cold leg breaks, for the SPES two-inch cold leg and two-inch DVI line break, and for the SPES double-ended guillotine DVI break (approximately a four-inch break). Pressurizer level data from the same ROSA and SPES experiments are shown in Figure 6.3.

Examination of the data in Figure 6.2 indicates that the process of scaling the depressurization data with the appropriate nondimensional transit time as indicated by the Φ_6 group does collapse the data to a large extent up to a nondimensional time of 1. At t^* of about 1 the PRHR system has been activated and will eventually influence the energy balance in the system (recall that the q_{net} term to the subcooled part of the system was assumed to be zero).

It is important to note that data in Figure 6.2 come from one-inch, two-inch, and larger breaks. These data collapse reasonably well for the 0 - 1 nondimensional time frame.

The OSU one-inch cold leg break data are not included in Figures 6.2 and 6.3. The OSU system is a low pressure system that is largely saturated at the initiation of the transient and a large fraction of the system starts to flash when the break is opened. The OSU system was not designed with operation in the subcooled depressurization phase as an objective.

Figure 6.2. Pressurizer pressure comparison for different facilities and different break sizes.

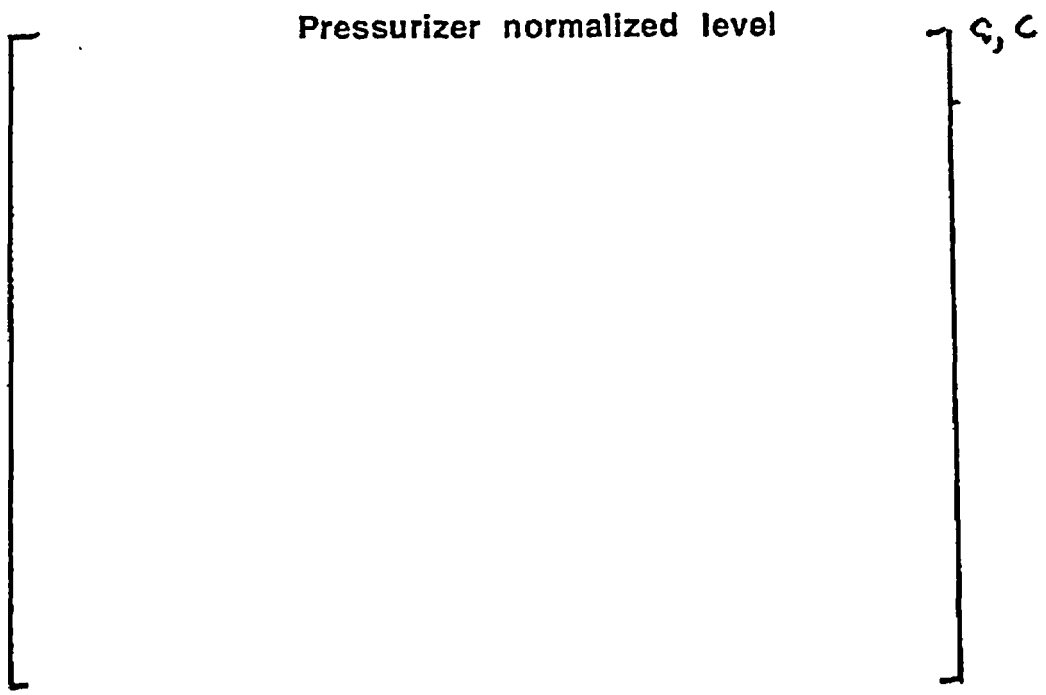

Figure 6.3. Pressurizer level comparison for different facilities and different break sizes.

Breaks larger than one-inch were included as a test of the process and methodology. It was expected that (and demonstrated in Reference 18) data from different break sizes should collapse using this approach as long as the dominant processes occurring are the ones assumed in the development. Clearly at some break size, the processes influencing the initial depressurization could depend on factors in addition to the break mass/energy. The SPES double ended guillotine

break illustrates this. This particular break represents a size that is somewhere between a four-inch and an eight-inch break in the plant (the break is actually in an eight-inch line but the DVI nozzle and flow restrictors in the CMT line limit the break flow). This particular break depressurizes more quickly than smaller breaks and in fact the PRHR activates early in the transient suggesting that q_{net} may be a factor in the depressurization.

Figure 6.3 shows the pressurizer level response for the same experiments as shown in Figure 6.2. It is obvious that the data collapse well and the pressurizer is empty shortly after t^* reaches 1. The pressurizer emptying effectively ends Phase 1 as discussed above.

6.1.5 Concluding Remarks

The analysis showed that two nondimensional groups characterize the system response for the subcooled blowdown. In the mass balance the break mass flow rate is the dominant term. The dimensionless group multiplying the break flow, Φ_6, contains the ratio of break area to PCS volume. This ratio was maintained in the experimental facilities and data from the facilities were collapsed using the dimensionless form of the mass balance.

In the depressurization equation the break volumetric flow is the dominant term. The dimensionless group multiplying the break volumetric flow, Φ_4, contains the same area to volume ratio as the Φ_6 term and some fluid property values. Since the facilities are operated at the same conditions as AP600 and use the same fluid, water, there is very good agreement for the Φ_4 term between the facilities and AP600. Order of magnitude analysis showed that the effects of convecting (h-u) out the break and of the pressurizer heaters were each an order of magnitude smaller than break volumetric flow. Using the reduced form of the depressurization equation, data from 1", 2", and DVI breaks in ROSA and SPES were collapsed.

6.2 Intermediate Phase

This phase includes the events from pressurizer emptying up to the opening of the ADS-4 valves as described in Sections 5.1.2 and 5.1.3. There were no critical events identified for this phase of the transient in the PIRT. The primary motivation for analyzing this portion of the transient was to identify the dominant phenomena and compare them between the facilities to determine if there was any evidence suggesting that significant differences in system pressure and vessel inventory would exist at ADS-4 initiation in the facilities. In other words, the primary objective was to determine the effect of break size and location on the initial conditions obtaining when ADS-4 was opened, and to determine the differences between facilities, if any, with respect to these initial conditions.

The intermediate phase was divided into three subphases for purposes of the analysis. The subphase boundaries were chosen to separate phenomena, component actions, and responses.

6.2.1 Step 1: Intermediate Subphase I Description

This subphase extends from the pressurizer draining to the hot legs, upper head, and steam generator primary side reaching saturation pressure. Specifically, the phase ends when significant void occurs in the hot leg due to surge line draining. Initially, the only vapor in the system is in the pressurizer, there are no inflows to the primary coolant system (PCS), subcooled mass loss is occurring through the break, and reactor scram and steam generator secondary side isolation occur. During isolation of the steam generator secondary side and the core power reduction following scram, large imbalances can occur in the PCS energy balance.

6.2.1.1 Step 2: Intermediate Subphase I Key Components and Subsystems

The subsystems involved in this phase includes the entire PCS. The break flow is subcooled, the pressurizer is filled with saturated vapor and the hot legs and steam generators contain a volume of saturated liquid equal to [redacted] of the pressurizer volume. The remainder of the PCS contains subcooled liquid. The steam generator secondary side participates as a heat sink. As the phase progresses the thermal driving force between the primary and secondary side decreases and this heat transfer mode becomes less important.

6.2.1.2 Steps 3-5: Intermediate Subphase I Equations

The governing equations for this subphase are derived in Appendix C. Since there are no mass flows into the PCS during this subphase only the break flow occurs on the RHS in the mass balance. The lack of mass flows into the PCS also makes the terms multiplied by Ψ_1 and Ψ_3 equal to zero. Since the PCS is liquid filled outside the pressurizer and the thermophysical properties of saturated liquid are closer to those of subcooled liquid than to two phase mixtures, the q_{net} term in the saturated fluid is taken to be equal to zero. With these modifications, the mass balance is given as

$$\frac{dM^*}{dt^*} = \Psi_{13}\dot{m}^*_{break} \tag{6.12}$$

and the dimensionless depressurization equation is

$$\frac{dP^*}{dt^*} = -\Psi_2 C^*_{1,1}\dot{m}^*_{break}(h_l - u_l)^* + \Psi_3 C^*_{1,1}\left[\pi_{core}q^*_{core} - q^*_{SG}\right] + \Psi_{10}C^*_2 v^*_l \dot{m}^*_{break} \tag{6.13}$$

The Ψ groups and π_{core} are described in Table 6.3.

Table 6.3. Dimensionless coefficients for Intermediate Subphase I.

Dimensionless Coefficient	Algebraic Description	Physical Interpretation
Ψ_2	$\frac{C_{1,1,0}(h_l - u_l)_0 \dot{m}_0 t_0}{P_0}$	Ratio of pressure change, due to subcooled outflow of (h-u), to the reference pressure
Ψ_3	$\frac{C_{1,1,0}\dot{q}_{SG,0}t_0}{P_0}$	Ratio of pressure change, due to change in specific energy of the subcooled field from heat transfer, to the reference pressure
Ψ_{10}	$\frac{C_{2,0}v_{l,0}\dot{m}_0 t_0}{P_0}$	Ratio of pressure change, due to change in specific volume of the subcooled field, to reference pressure
Ψ_{13}	$\frac{\dot{m}_0 t_0}{M_0}$	Ratio of integrated mass flow to reference mass
π_{core}	$q_{core,0}/q_{SG,0}$	Ratio of heat addition by core to heat removal by steam generator

6.2.1.3 Step 6: Intermediate Subphase I Reference Conditions

The reference conditions used to evaluate the Ψ groups in subphase I are given in Table 6.4.

Table 6.4. Reference parameters for Intermediate Subphase I.

Reference Parameter	AP600 Value	ROSA Value	SPES Value	Description
t_0 (s)				Time for pressurizer surge line mass to be lost through break
$\dot{m}_0$ (kg/s)				Break flow assuming Henry-Fauske critical flow at 12 MPa and 5 K subcooling
M_0 (kg)				Mass of liquid in surge line
$q_{core,0}$ (MW)				Reference heat addition by core
$q_{SG,0}$ (MW)				Reference heat removal by steam generators at steady operation
P_0 (MPa)				System Pressure
v_0 (m^3/kg)				Average specific volume of saturated field
$(h_l\text{-}u_l)_0$ (kJ/kg)				Difference between enthalpy and internal energy for the subcooled field
$C_{1,1_0}$ (m^{-3})				Weighted value of partial derivative of pressure wrt specific energy at constant specific volume for the subcoooled field (see Appendix C)

Table 6.4. Reference parameters for Intermediate Subphase I (continued).

$C_{2_0}v_{l_0}$ (J/m^3-kg)		See Appendix C
$C_{2_g}v_{m_0}$ (J/m^3-kg)		See Appendix C

6.2.1.4 Step 9: Intermediate Subphase I Dimensionless Groups

The numerical values for the Ψ groups in this subphase are given in Table 6.5.

Table 6.5. Dimensionless coefficients for Intermediate Subphase I.

Facility	Ψ_2	Ψ_3	Ψ_{10}	Ψ_{13}	π_{core}
AP600					
ROSA					
SPES					

The q_{net} term in the subcooled liquid is the dominant term in the AP600 and in the experimental facilities. The Ψ_2 term is several orders of magnitude smaller and will not be important to this phase of the transient. The break volumetric flow term (Ψ_{10}) is roughly an order of magnitude smaller. The magnitude of the Ψ_3 terms is similar for AP600 and the experimental facilities. Note that π_{core} is considerably less than unity indicating that the steam generator heat removal rate has a larger effect on the depressurization (note that the sign on q^*_{SG} in Equation (6.13) is negative) relative to the core power.

6.2.1.5 Step 7: Intermediate Subphase I Reduced Equation Set

The reduced set of equations for this subphase is

$$\frac{dM^*}{dt^*} = \Psi_{13}\dot{m}^*_{break} \tag{6.14a}$$

or in integrated form

$$\Delta M^* \approx \Psi_{13} \tag{6.14b}$$

for the mass balance and

$$\frac{dP^*}{dt^*} = \Psi_3 C^*_{1,1}\left[\pi_{core}q^*_{core} - q^*_{SG}\right] + \Psi_{10}C^*_{2,1}v^*_1\dot{m}^*_{break} \tag{6.15a}$$

or in integrated form, assuming that the quantity in the square brackets on the RHS is O[1]

$$\Delta P^* \approx \Psi_3 + \Psi_{10} \tag{6.15a}$$

The system mass inventory is affected only by the break flow. The PCS depressurization is dependent on the effects of shrinkage or expansion of the subcooled liquid due to imbalances in the core and steam generator heat transfer rates and, to a lesser extent, the break volumetric flow rate. Based on the values in Table 6.5, the steam generator heat removal rate dominates.

6.2.2 Step 1: Intermediate Subphase II Description

This subphase extends from the system reaching saturation pressure of the hot legs, upper head, and steam generator primary sides to the initiation of net inflows to the PCS from the accumulators or CMTs. Initially only the pressurizer, surgeline, and a small portion of the hot legs contains vapor. The PRHR and CMTs have been activated by the S-signal, the primary coolant pumps have coasted down, and the steam generator secondary sides are isolated.

6.2.2.1 Step 2: Intermediate Subphase II Key Components and Subsystems

The subsystems involved include the entire PCS, the PRHR, and the CMTs. The PRHR is active, the steam generator primary coolant is saturated and voiding, there is a small thermal driving force from primary to secondary that transitions to a small thermal driving force from the secondary to the primary side of the steam generators. The small thermal driving force and increased voiding in the steam generator primary side are assumed to make heat transfer through the steam generator tubes unimportant during this subphase. It is assumed that the pressurizer is filled with saturated vapor, the steam generators, hot legs, and upper head are initially filled with saturated liquid, and the remainder of the PCS is filled with subcooled liquid. The break flow is subcooled and the q_{net} effects are all in the subcooled liquid.

6.2.2.2 Steps 3-5: Intermediate Subphase II Equations

The governing equations for this subphase are derived in Appendix C. Since there are no mass flows into the PCS during this subphase only the break flow occurs on the RHS in the mass balance. The lack of mass flows into the PCS also makes the term multiplied by Ψ_1 equal to zero. Since there is no effective thermal driving force across the steam generator tubes, q_{net} in the saturated fluid is assumed to be equal to zero. The resulting equation for the mass balance is

$$\frac{dM^*}{dt^*} = \Psi_{13}\dot{m}^*_{break} \tag{6.16}$$

and the dimensionless depressurization equation is

$$\frac{dP^*}{dt^*} = -\Psi_2 C^*_{1,1}\dot{m}^*_{break}(h_l - u_l)^* + \Psi_3 C^*_{1,1}\left[q^*_{core} - \pi_{PRHR}q^*_{PRHR}\right] + \Psi_{10}C^*_2 v^*_l \dot{m}^*_{break} \tag{6.17}$$

The Ψ groups are described in Table 6.6.

6.2.2.3 Step 6: Intermediate Subphase II Reference Conditions

The reference conditions used to evaluate the Ψ groups are given in Table 6.7.

Table 6.6. Dimensionless coefficients for Intermediate Subphase II.

Dimensionless Coefficient	Algebraic Description	Physical Interpretation
Ψ_2	$\frac{C_{1,1,0}(h_1 - u_1)_0 \dot{m}_0 t_0}{P_0}$	Ratio of pressure change, due to subcooled outflow of (h-u), to the reference pressure
Ψ_3	$\frac{C_{1,1,0}\dot{q}_{core,0} t_0}{P_0}$	Ratio of pressure change, due to change in specific energy of the subcooled field from heat transfer, to the reference pressure
Ψ_{10}	$\frac{C_{2,0} v_{1,0} \dot{m}_0 t_0}{P_0}$	Ratio of pressure change, due to change in specific volume of the subcooled field, to reference pressure
Ψ_{13}	$\dot{m}_0 t_0 / M_0$	Ratio of integrated mass flow to reference mass
π_{PRHR}	$\dot{q}_{PRHR,0} / \dot{q}_{core,0}$	Ratio of reference heat removal rate from PRHR and heat addition rate by core

Table 6.7. Reference parameters for Intermediate Subphase II.

Reference Parameter	AP600 Value	ROSA Value	SPES Value	OSU Value a, c	Description
t_0					Time for mass in and above hot legs to be lost through break
$\dot{m}_0$ (kg/s)					Henry-Fauske critical flow at 7 MPa and 5 K subcooling
M_0 (kg)					Mass of liquid in and above hot legs
$q_{core,0}$ (MW)					Reference heat addition by core
$q_{PRHR,0}$ (MW)					Reference heat removal by PRHR using Equation (D-10) and reference conditions given below
P_0 (MPa)					System Pressure
$(v_m - v_l)_0$ (m^3/kg)					Difference between specific volume of saturated field and subcooled field
$(h_l - u_l)_0$ (kJ/kg)					Difference between enthalpy and internal energy for the subcooled field
C_{1,l_0} (m^3)					Weighted value of partial derivative of pressure wrt specific energy at constant specific volume for the subcoooled field (See Appendix C)
C_{1,m_0} (m^3)					Weighted value of partial derivative of pressure wrt specific energy at constant specific volume for the saturated field (See Appendix C)
$C_{2,0}v_{l,0}$ (J/m^3-kg)					See Appendix C
$C_{2,0}v_{m,0}$ (J/m^3-kg)					See Appendix C
$(C_{1,l}(h_l - u_l) - C_{1,m}(h_m - u_m))_0$					Change in pressure due to interfield mass flows per unit mass (App. C)
$T_{in,PRHR}$ (K)					PRHR inlet fluid temperature
$T_{out,PRHR}$ (K)					PRHR outlet fluid temperature
ρ_f (kg/m^3)					Fluid density based on average PRHR fluid temperature
β (1/K)					Thermal expansion coef. based on average PRHR fluid temperature

Table 6.7. Reference parameters for Intermediate Subphase II (continued).

c_p (J/kg-K)	[	Specific heat based on average PRHR fluid temperature
ΔZ (m)		PRHR to core thermal center difference based on Equation (D-3)
R' (m^{-4})		PRHR hydraulic resistance
$\dot{m}_{0,PRHR}$	]	PRHR reference flow rate from Equation (D-8)

6.2.2.4 Step 9: Intermediate Subphase II Dimensionless Groups

The numerical values of the Ψ groups and π_{PRHR} for this phase are given in Table 6.8.

Table 6.8. Dimensionless coefficients for Intermediate Subphase II.

Facility	Ψ_2	Ψ_3	Ψ_{10}	Ψ_{13}	π_{PRHR}	$\Psi_3(1-\pi_{PRHR})$
AP600	[					]
ROSA						
SPES						
OSU						

a. Second number is based on volume scaled core power.

The q_{net} term in the subcooled liquid and the break volumetric flow are the dominant terms in the depressurization equation in AP600 and the experimental facilities. The Ψ_2 term is 2 to 3 orders of magnitude smaller and will not be important to this phase of the transient. The magnitude of the Ψ_3 term is similar for AP600 and the experimental facilities although the value for SPES is a factor of 4-5 larger and the value for OSU is a factor of 2 smaller. The reason for the SPES value being larger is that the q_0 term used in evaluating Ψ_3 is the total core power, which in SPES is larger than the volume scaled power to account for PCS heat losses. If the volume scaled core power is used to evaluate Ψ_3 the value for SPES becomes [ ] which agrees better with the AP600 and ROSA values. The OSU values are lower primarily because of differences in the partial derivatives of pressure at the reduced pressure in OSU.

The π_{PRHR} values shown in Table 6.8 are based on reference conditions listed in Table 6.7. These values suggest that the AP600 PRHR system can remove up to approximately two times the reference decay heat value and that the ROSA PRHR system can remove about [ ] times decay heat. In the SPES facility, on the other hand, the PRHR system can remove less than half the decay heat value and in the OSU system, the PRHR reference heat removal rate is about equal to the decay heat. Note that the SPES value is based on the total core power. If the π_{PRHR} value for SPES is based on the volume scaled core power, the result is [ ] suggesting that the SPES PRHR can approximately remove decay heat. Note that the π values shown in Table 6.8 for the facilities are in fair agreement with the one-inch cold leg break experiment data. For example, the π_{PRHR} values based on the data are [ ] for the ROSA, SPES, and OSU experiments, respectively.

Several reasons for the differences in experiment facility π_{PRHR} values relative to the values calculated for the plant case are evident. For ROSA, the PRHR resistance is about 40% less than

the ideal scaled value which, for a given set of reference conditions, gives a PRHR mass flow rate and, thus heat transfer rate, that is high relative to the ideal scaled value. In the SPES experiment, the actual IRWST temperature was somewhat higher (about [+2,-2]) than assumed for the reference which gives a lower overall temperature differential for PRHR heat transfer and thus a lower heat transfer rate. Even if the reference core power is corrected by the amount added to compensate heat losses as discussed above, the SPES PRHR π value is low relative to the plant suggesting that the SPES PRHR may be somewhat undersized. The OSU π_{PRHR} value is lower than the plant value primarily because of the lower hot leg saturation temperature (because of reduced pressure operation) which affects the temperature differential for PRHR heat transfer. The net effect of the core and PRHR heat transfer is shown by the last column of Table 6.8 where the term $\Psi_3(1 - \pi_{PRHR})$ is listed for each of the facilities under the assumption that q^*_{core} and q^*_{PRHR} are O[1]. This term describes the net effect of the core and PRHR heat transfer on the pressure behavior. These values suggest that in the plant and the ROSA facility, the q_{net} effect causes depressurization whereas in SPES (using a volume scaled reference core power) and OSU, the two heat transfer effects tend to cancel out.

6.2.2.5 Step 7: Intermediate Subphase II Reduced Equation Set

The reduced set of equations for this subphase is

$$\frac{dM^*}{dt^*} = \Psi_{13}\dot{m}^*_{break} \tag{6.18a}$$

or in integrated form

$$\Delta M^* = \Psi_{13} \tag{6.18b}$$

for the mass balance and

$$\frac{dP^*}{dt^*} = \Psi_3 C^*_{1,1}\left[q^*_{core} - \pi_{PRHR} q^*_{PRHR}\right] + \Psi_{10} C^*_2 v^*_1 \dot{m}^*_{break} \tag{6.19a}$$

or in integrated form

$$\Delta P^* = \Psi_3(1-\pi_{PRHR}) + \Psi_{10} \tag{6.19b}$$

for the depressurization since Ψ_2 is two orders of magnitude smaller than Ψ_3 or Ψ_{10}. The system mass inventory is affected only by the break flow. The PCS depressurization is primarily dependent on the break volumetric flow and the effects of PCS shrinkage due to the PRHR cooling exceeding core decay heat levels.

6.2.3 Step 1: Intermediate Subphase III Description

This subphase extends from the initiation of accumulator injection or CMT draining to the opening of the ADS-4 valves. During this phase the accumulators are assumed to inject their liquid inventory and 80% of the CMT inventory is assumed to enter the PCS. The ADS-1,-2,-3 systems are assumed to open and vent high quality fluid once CMT levels reach 67%. Core

power continues at decay heat levels and the PRHR continues to operate, however, its performance is assumed to degrade after the ADS-1,-2,-3 systems actuate.

Note that there are two distinct parts to this subphase. In the first, the accumulators and CMTs inject into the PCS with the only mass losses being through the break. Once the CMT level is at 67%, the ADS-1 and then ADS-2 and -3 systems activate, significantly enhancing mass outflows and the depressurization rate.

6.2.3.1 Step 2: Intermediate Subphase III Key Components and Subsystems

The subsystems involved include the entire PCS, the accumulators, the CMTs, the ADS-1,-2,-3 system, the PRHR, and the break. The steam generator is assumed not to play an important role because the tubes are full of vapor, the thermal driving force is small, and the steam generator tubes are a high point in the PCS. Having the heat source at the high point impedes the development of natural circulation heat transfer. The pressurizer, steam generator primary side, hot legs, and reactor vessel upper head are assumed to be filled with vapor at the start of the subphase. The upper plenum and upper half of the core are assumed to be filled with saturated liquid and the remainder of the PCS is assumed to be filled with subcooled liquid. The inflows from the accumulators and CMTs are assumed to be at containment ambient conditions (298 K).

6.2.3.2 Steps 3-5: Intermediate Subphase III Equations

As pointed out earlier while we consider this subphase all together, there are actually two distinct time increments – in the first, the mass outflow is through the break and this proceeds till the CMT levels are at 67%. In the second, the ADS systems add to the mass outflow and depressurization rate. The governing equations were derived in differential form for this subphase in Appendix C. However, because of the two distinct portions to this subphase, and because we are primarily interested in system mass inventory and pressure at the end of the subphase (i.e. at the beginning of the ADS-4 discharge phase), it is also useful to express the results in terms of the integrated equations. This, then gives the change in system mass inventory and system pressure over the whole subphase.

To this end, we divide the characteristic time for this subphase, t_0 into $\hat{t}_0$, which gives the time elapsed from the beginning of the subphase to CMTs at 67%, and $t_0 - \hat{t}_0$ which gives the time over which ADS-1,-2,-3 discharge until CMT levels drop to 20 % and ADS-4 starts to discharge.

The form of the differential equations are as in Appendix C, where the derivation is done without q_{net} into the saturated mixture field. We present here the "two-field" form of the multifield equations in Appendix C, noting that the three-field form for the depressurization rate is presented in Appendix C as Equation (C-17). The two-fields here are subcooled liquid, subscripted l, and a homogeneous-equilibrium vapor-liquid mixture field, subscripted m. The form with the third field being steam/nitrogen is given in Appendix C.

To proceed, the dimensionless mass balance (for PCS mass) in differential form is

$$\frac{dM^*}{dt^*} = \Psi_{13}\left[\pi_{ACC}\dot{m}^*_{ACC} + \pi_{CMT}\dot{m}^*_{CMT} - \pi_{break}\dot{m}^*_{break} - \dot{m}^*_{ADS-1,2,3}\right] \quad (6.20a)$$

where

$\dot{m}^*_{ACC} = \dot{m}_{ACC}/\dot{m}_{0,ACC}$; $\dot{m}^*_{CMT} = \dot{m}_{CMT}/\dot{m}_{0,CMT}$; $\dot{m}^*_{break} = \dot{m}_{break}/\dot{m}_{0,break}$, and

$\dot{m}^*_{ADS-1,2,3} = \dot{m}_{ADS-1,2,3}/\dot{m}_{0,ADS-1,2,3}$

To ensure that the starred variables are O[1] on the RHS, it is necessary to introduce the πs on the RHS, which are ratios of the reference flow rates for each component to the reference flow rate for the ADS-1,-2,-3. Note also that $\dot{m}^*_{ADS-1,2,3}$ is zero for the period $\hat{t}_0$ and is O[1} for t_0 -$\hat{t}_0$. This leads to the integral form of Equation (6.20a) being

$$\Delta M^* = M^*_{ACC} + 0.8M^*_{CMT} - \Psi_{13}\left[\pi_{break} + \frac{t_0 - \hat{t}_0}{t_0}\right] \quad (6.20b)$$

where ΔM^* is the nondimensional change in PCS mass inventory, and M^*_{ACC} and M^*_{CMT} are the nondimensional masses in the accumulator and CMT. (Recall that ADS-4 starts to discharge when CMT levels decrease to 20%, so only $0.8M^*_{CMT}$ enters the PCS during this subphase). To obtain the fractional change in mass in the PCS we note that this is $\Delta M^*/M^*_{PCS}$, where M^*_{PCS} is M_{PCS}/M_0.

To proceed, it is necessary to define t_0 in order to give the nondimensional period for this subphase O[1]. To first order,

$$t_0 = \frac{0.33M_{CMT} + (0.33/0.88)M_{ACC}}{\dot{m}_{0,break}} + \frac{0.47M_{CMT} + 0.6M_{ACC}}{\dot{m}_{0,break} + \dot{m}_{0,ADS-1,2,3}} = \hat{t}_0 + (t_0 - \hat{t}_0) \quad (6.20c)$$

achieves this – though the implicit assumption that $\hat{t}_0$is given by the first term requires validation against data, as does the whole expression for t_0 to ensure $t^* \sim$ O[1] for this subphase.

Turning now to the nondimensional depressurization rate in differential form

$$\begin{aligned}\frac{dP^*}{dt^*} = {} & \Psi_1 C^*_{1,1}\left[\pi_{ACC}\dot{m}^*_{ACC}(h_{ACC} - u_1)^* + \pi_{CMT}\dot{m}^*_{CMT}(h_{CMT} - u_1)^*\right] - \Psi_2 C^*_{1,1}\left[\dot{m}^*_{break}(h_1 - u_1)^*\right] \\ & + \Psi_3 C^*_{1,1}\left[\pi_{core,1}q^*_{core,1} - \pi_{PRHR,1}q^*_{PRHR}\right] - \Psi_5 C^*_{1,m}\left[\dot{m}^*_{ADS}(h_m - u_m)^*\right] \\ & + \Psi_6 C^*_{1,m}\left[\pi_{core,m}q^*_{core,m} - \pi_{PRHR,m}q^*_{PRHR}\right] \\ & + \Psi_{10} C^*_2 v^*_1\left[-\pi_{ACC}\dot{m}^*_{ACC} - \pi_{CMT}\dot{m}^*_{CMT} + \pi_{break}\dot{m}^*_{break}\right] + \Psi_{11} C^*_2 v^*_m \dot{m}^*_{ADS}\end{aligned} \quad (6.21a)$$

where the Ψ, π, and M^* groups are defined in Table 6.9.

It is reasonable to assume that the quantities in square brackets multiplying Ψ_3 and Ψ_6 are ~ O[1]. Integrating gives

$$\Delta P^* \approx \frac{M^*_{ACC}}{\Psi_{13}}[\Psi_1 - \Psi_{10}] + \frac{0.8M^*_{CMT}}{\Psi_{13}}[\Psi_1 - \Psi_{10}] - [\Psi_2 - \pi_{break}\Psi_{10}] + [\Psi_3 + \Psi_6] + \frac{t_0 - \hat{t}}{t_0}\Psi_{11} \qquad (6.21b)$$

where the time scale ratio multiplying Ψ_{11} is obtainable from Equation (6-20c), and is a function of M^*_{ACC}, M^*_{CMT}, and π_{break}. The first term gives the effect of accumulator inflow, the second of CMT draining, the third of subcooled break discharge, the fourth of heat input (or removal) and the fifth of ADS-1,-2,-3 discharge, on pressure change.

6.2.3.3 Step 6: Intermediate Subphase III Reference Conditions

The reference conditions used to evaluate the Ψ groups in subphase III are given in Table 6.10.

Table 6.9. Dimensionless coefficients for Intermediate Subphase III.

Dimensionless Coefficient	Algebraic Description	Physical Interpretation
Ψ_1	$\frac{C_{1,1,0}\dot{m}_{0,ADS}(h_{in} - u_l)_0 t_0}{P_0}$	Ratio of pressure change, due to change in specific energy of the subcooled field from mass inflows, to the reference pressure
Ψ_2	$\frac{C_{1,1,0}\dot{m}_{0,break}(h_l - u_l)_0 t_0}{P_0}$	Ratio of pressure change due to subcooled outflow of (h-u) to the reference pressure
Ψ_3	$\frac{C_{1,1,0}\dot{q}_0 t_0}{P_0}$	Ratio of pressure change, due to change in specific energy of the subcooled field from heat transfer, to the reference pressure
Ψ_5	$\frac{C_{1,m,0}\dot{m}_{0,ADS}(h_m - u_m)_0 t_0}{P_0}$	Ratio of pressure change due to saturated outflow of (h-u) to the reference pressure
Ψ_6	$\frac{C_{1,1,0}\dot{q}_0 t_0}{P_0}$	Ratio of pressure change, due to change in specific energy of the saturated field from heat transfer, to the reference pressure
Ψ_{10}	$C_{2,0}v_{1,0}\dot{m}_{0,ADS}t_0/P_0$	Ratio of pressure change, due to change in specific volume of the subcooled field, to reference pressure
Ψ_{11}	$C_{2,0}v_{m,0}\dot{m}_{0,ADS}t_0/P_0$	Ratio of pressure change, due to change in specific volume of the saturated field, to reference pressure
Ψ_{13}	$\dot{m}_{0,ADS}t_0/M_0$	Ratio of integrated mass flow to reference mass
π_{ACC}	$\dot{m}_{0,ACC}/\dot{m}_{0,ADS}$	Ratio of accumulator and ADS-1,2,3 reference flows
π_{CMT}	$\dot{m}_{0,CMT}/\dot{m}_{0,ADS}$	Ratio of CMT and ADS-1,2,3 reference flows
π_{break}	$\dot{m}_{0,break}/\dot{m}_{0,ADS}$	Ratio of break and ADS-1,2,3 reference flows
M^*_{ACC}	M_{ACC}/M_0	Ratio of accumulator mass to reference mass
M^*_{CMT}	M_{CMT}/M_0	Ratio of CMT mass to reference mass
M^*_{PCS}	M_{PCS}/M_0	Ratio of PCS mass to reference mass

Table 6.10. Reference parameters for Intermediate Subphase III.

Reference Parameter	AP600 Value	ROSA Value	SPES Value	OSU Value	Description
t_0 (s)					Reference time based on Equation (6.20c)
$\dot{m}_{0,ADS}$ (kg/s)					ADS-1,-2,-3 flow assuming HEM critical flow at P_0, quality of 1
$\dot{m}_{0,break}$ (kg/s)					Break flow assuming Henry Fauske model at P_0 and 5 K subcooling
$\dot{m}_{0,ACC}$ (kg/s)					Reference accumulator flow (both)
$\dot{m}_{0,CMT}$ (kg/s)					Reference CMT flow (both)
M_0 (kg)					Mass of liquid in accumulators and 80% of CMT volume
$M_{0,ACC}$ (kg)					Accumulator reference mass
$M_{0,CMT}$ (kg)					CMT reference mass
$M_{0,PCS}$ (kg)					PCS reference mass (primary system volume with density evaluated at T_{AVE}, ACC and CMT not included)
q_0 (MW)					Core power divided by 2 since half goes into the subcooled and half goes into the saturated
P_0 (MPa)					System pressure
$(h_m-u_l)_0$ (kJ/kg)					Difference between average energy in subcooled field and the enthalpy in the CMTs and accumulators
$(h_m-u_m)_0$ (kJ/kg)					Difference between average energy in saturated field and saturated liquid enthalpy ($\sim x^*h_{fg}$)
$(h_l-u_l)_0$ (kJ/kg)					(h-u) for subcooled field
$(h_m-u_m)_0$ (kJ/kg)					(h-u) for saturated field
C_{1,J_0} (m^{-3})					Weighted value of partial derivative of pressure wrt specific energy at constant specific volume for the subcoooled field (See Appendix C)
C_{1,m_0} (m^{-3})					Weighted value of partial derivative of pressure wrt specific energy at constant specific volume for the saturated field (See Appendix C)
$C_{2,0}v_{l,0}$ (J/m^3-kg)					Weighted value of partial derivative of pressure wrt specific volume at constant specific energy for the subcoooled field (See Appendix C)
$C_{2,0}v_{m,0}$ (J/m^3-kg)					Weighted value of partial derivative of pressure wrt specific volume at constant specific energy for the saturated field (See Appendix C)
$(C_{1,m}(h_f-u_m))-C_{1,l}(h_l-u_l))_0$					Change in pressure due to interfield mass flows per unit mass (App. C)

6.2.3.4 Step 9: Intermediate Subphase III Dimensionless Groups

The numerical values of the Ψ groups, π_{break}, M^*_{ACC}, and M^*_{CMT} for this phase are given in Table 6.11.

Table 6.11. Nondimensional coefficients for Intermediate Subphase III.

Facility	Ψ_1	Ψ_2	Ψ_3	Ψ_4	Ψ_5	Ψ_6	Ψ_{10}	Ψ_{11}	Ψ_{13}
AP600									
ROSA									
SPES									
OSU									

c, c

Facility	M^*_{ACC}	M^*_{CMT}	$M_{0,PCS}/M_0$	$(t_0-\hat{t}_0)/t_0$	π_{break}	π_{ACC}	π_{CMT}
AP600							
ROSA							
SPES							
OSU							

a, c

It is clear from Table 6.11 that the mass discharged over the subphase is related to $[t_0 - \hat{t}_0/t_0]\Psi_{13}$, M^*_{ACC}, and M^*_{CMT} since $\pi_{break}\Psi_{13}$ is small in comparison to the other terms in Equation (6.20b). Furthermore, the change in pressure is also dominated by groups that do not involve π_{break}, i.e. the break effect is small compared to ADS-1,-2,-3. The ADS-1,-2,-3 discharge in fact dominated, as suggested by the relatively large value of the Ψ_{11} group.

6.2.3.5 Step 7: Intermediate Subphase III Reduced Equation Set

The mass inventory change over the subphase period is immediately derivable from Equations (6.20b) and (6.20c), since $\pi_{break} << 1$ as

$$\Delta M^* \approx 0.4M^*_{ACC} + 0.33M^*_{CMT} \tag{6.22}$$

where the numerical values of the nondimensional groups will depend on the choice of M_0, but this is a matter of taste and does not affect the dimensional values. Note that break size and location does not enter Equation (6.22).

Similarly the change in pressure over the subphase can be written, eliminating $(t_0-\hat{t}_0)/t_0$ as

$$\Delta P^* \approx \left[\left((\Psi_1 - \Psi_{10})/\Psi_{13}\right)\right]\left[M^*_{ACC} + 0.8M^*_{CMT}\right] + \left[\Psi_3 + \Psi_6\right] + \frac{\Psi_{11}}{\Psi_{13}}\left[0.6M^*_{ACC} + 0.47M^*_{CMT}\right] \tag{6.23}$$

assuming $\pi_{break} << 1$ to obtain the last term.

Note that $[\Psi_2 - \pi_{break}\Psi_{10}]$ is also small in comparison with the other terms.

This suggests that the break size and location - provided it is a small break, and since $\pi_{break} << 1$ - affects the pressure change in this subphase by about an order of magnitude less than the other effects, e.g. ADS-1,-2,-3 discharge.

6.2.3.6 Investigation of End-Phase, Three-Field, and Nitrogen Effects

The results presented in this subsection are aimed at clarifying the importance of three effects: a) change in nondimensional groups if the scaling was based on the values of properties at the end of the subphase; b) the impact of a three-field rather than a two-field description of the subphase, and; c) the effect of nitrogen if mixed with the steam in the three-field description - to later account for accumulator nitrogen at the end of the phase. The focus was on c) for the assessment.

Conditions were chosen with the same liquid and vapor distribution that existed at the start of Intermediate Subphase III with the exception that the pressurizer was assumed to be full of saturated liquid. A reference pressure was chosen at which the nitrogen would fill the accumulators and the vapor volume of the PCS. The reference conditions summarized in Table 6.12 were used to evaluate two cases. In the first case the PCS vapor volume contained only vapor while in the second case nitrogen in the PCS vapor volume was used to evaluate partial derivatives of pressure with respect to specific energy and volume. Differences in system response based on the dimensionless groups can be used to assess the effects of nitrogen on intermediate phase processes. The resulting dimensionless groups are presented in Tables 6.13 and 6.14. Note that, as shown in Appendix C, the C coefficients are the same for nitrogen and steam, so there is no effect if the "static" situation, with no inflows and outflows is considered. While the numeric values are different for corresponding Ψ groups in the tables, the relative rankings of the groups for a given facility are identical. In all facilities the volumetric flow through ADS-1,-2,-3 is the dominant process affecting depressurization. The differences in numeric values for corresponding Ψ groups for the two cases do not change the relative rankings of the mechanisms. A more detailed analysis of nitrogen effects does not appear to be warranted.

6.2.4 Concluding Remarks

To understand the conditions that obtain at the end of the Intermediate Phase, it is necessary to review the results for Subphases I, II, and III. Consider that the Intermediate Phase starts with the PCS full of liquid except for the pressurizer.

The change in inventory in Subphases I and II are given by Equations (6.14b) and (6.18b), and based on the reference mass used for each subphase, $\Delta M^* \sim 1$.

For Subphase III, the mass change is given by Equation (6.22). Each of these subphases have their own reference masses, as given in Tables 6.4, 6.9, and 6.10. If one puts everything on a consistent basis i.e. mass lost in each subphase relative to PCS mass, $M_{PCS,0}$, then the mass loss in the first subphase is negligible. Thus the total mass loss in dimensional terms is

$$\Delta M_{PCS,II} + \Delta M_{PCS,III} = M_{0,II}\Delta M^*_{II} + M_{0,III}\Delta M^*_{III}$$
$$= M_{O,II} + M_{0,III}\left[0.4M^*_{ACC} + 0.33M^*_{CMT}\right]$$

since $\Delta M^*_{II} \approx \Psi_{13,II} = 1$.

Table 6.12. Evaluated terms in dimensionless depressurization equation for Intermediate Subphase IIL

Refcrence Parameter	AP600 Value	ROSA Value	SPES Value	OSU Value	Description a,c
t_0 (s)					Time for accumulator and CMT mass to be lost through ADS-1,-2,-3
$\dot{m}_{0,ADS}$ (kg/s)					ADS-1,-2,-3 flow assuming HEM critical flow at P_0 with quality of 1
$\dot{m}_{0,break}$(kg/s)					Break flow assuming HEM model at P_0 with quality of 1
$\dot{m}_{0,sat}$ (kg/s)					Rate of subcooled liquid being raised to saturation using half of core power
M_0 (kg)					Mass of liquid in accumulators and 80% of CMT volume
q_0 (MW)					Core power divided by 2 since half goes into the subcooled and half goes into the saturated
P_0 (MPa)					System Pressure
$v_{l,0}$ (m^3/kg)					Specific volume of liquid field
$v_{m,0}$ (m^3/kg)[a]					Specific volume of mixture w/o N_2 Specific volume of mixture w N_2
v_{N_2} (m^3/kg)					Specific volume of N_2
$(h_m-u_l)_0$ (kJ/kg)					Difference between average energy in subcooled field and the enthalpy in the CMTs and accumulators
$(h_m-u_m)_0$ (kJ/kg)					Difference between average energy in saturated field and saturated liquid enthalpy (~x^*h_{fg})
$(h_l-u_l)_0$ (kJ/kg)					(h-u) for subcooled field
$(h_m-u_m)_0$ (kJ/kg)[a]					(h-u) for saturated field w/o nitrogen (h-u) for saturated field with nitrogen
C_{1,l_0} (MPa/kJ/kg)[a]					Weighted value of partial derivative of pressure wrt specific energy at constant specific volume for the subcoooled field (See Appendix C)
C_{1,m_0} (MPa/kJ/kg)[a]					Weighted value of partial derivative of pressure wrt specific energy at constant specific volume for the saturated field (See Appendix C)
$C_{2,0}$ (MPa/m^3/kg)[a]					Weighted value of partial derivative of pressure wrt specific volume at constant specific energy for the subcoooled field (See Appendix C)

a. First row is case without nitrogen. Second row is case with nitrogen.

Thus the change in PCS inventory is independent of break size and location. In fact, based on the values of the reference masses it is clear that

$\Delta M_{PCS}/M_{PCS,0} \approx$ [redacted] a,c

There are clearly some secondary effects, but the above expression is accurate to an order of magnitude – and is break size independent, though dependent on accumulator and CMT sizes.

Table 6.13. Nondimensional coefficients at "end" Phase III (2-field model).

Facility	Ψ_1	Ψ_2	Ψ_3	Ψ_4	Ψ_5	Ψ_6	Ψ_{10}	Ψ_{11}	Ψ_{13}
AP600									
ROSA									
SPES									
OSU									

a, c

Table 6.14. Nondimensional coefficients at "end" Phase III (3-field model).

Facility	Ψ_1	Ψ_2	Ψ_3	Ψ_4	Ψ_5	Ψ_6	Ψ_{10}	Ψ_{11}	Ψ_{13}
AP600									
ROSA									
SPES									
OSU									

a, c

Turning now to the depressurization, the magnitudes of the pressure changes shown in Equations (6.15b) and (6.19b) are similar in Subphases I and II, and while the depressurization rate clearly depends on break size, the magnitude of the pressure change does not. This is also true for Subphase III for $\dot{m}_{break,0} << \dot{m}_{ADS\text{-}1,\text{-}2,\text{-}3}$ as shown in Equation (6.23). Note that accumulator and CMT volume can enter the pressure change equation, but the change is then facility dependent – but break size independent.

From this we conclude that the pressures and system inventories (in terms of nondimensional pressure P^* and $M^*_{PCS} = M_{PCS}/M_{PCS,0}$) are independent of break size, but depend on M^*_{ACC} and M^*_{CMT}, as well as, to a lesser extent, on the details of heat input and heat removal by the steam generators and PRHR, and on core heating.

If the analysis is correct in overall terms, ΔM^*_{PCS} vs. P^* at the end of the Intermediate Phase should be break size independent, but could be facility dependent because of the masses in accumulators and CMTs relative to PCS at the beginning of the transient. This conclusion is tested in Figure 6.4 and found to be correct – supporting the main findings presented here.

Based on the values of the Ψ groups the same processes control the mass balance in the AP600 and the experimental facilities for all three subphases of the Intermediate Phase. The agreement in Ψ groups between the experimental facilities and AP600 indicates that the mass inventory in the experiments should be representative of the AP600 mass inventory at the initiation of ADS-4.

In the depressurization equation, the same processes are dominant in AP600 and the experimental facilities with the exception of SPES during Subphase II. In SPES, the effects of q_{net} (Ψ_3) dominate the break volumetric flow (Ψ_{10}). This reversal of dominant mechanisms relative to the other facilities is due to the additional core power added in SPES to account for heat losses. Other than the difference in SPES for the two dominant terms in Subphase II, the relative ranking of terms in the depressurization equation is the same for AP600 and the full pressure facilities. In Subphase II, the relative rankings in OSU are identical to those in AP600. In Subphase III, the

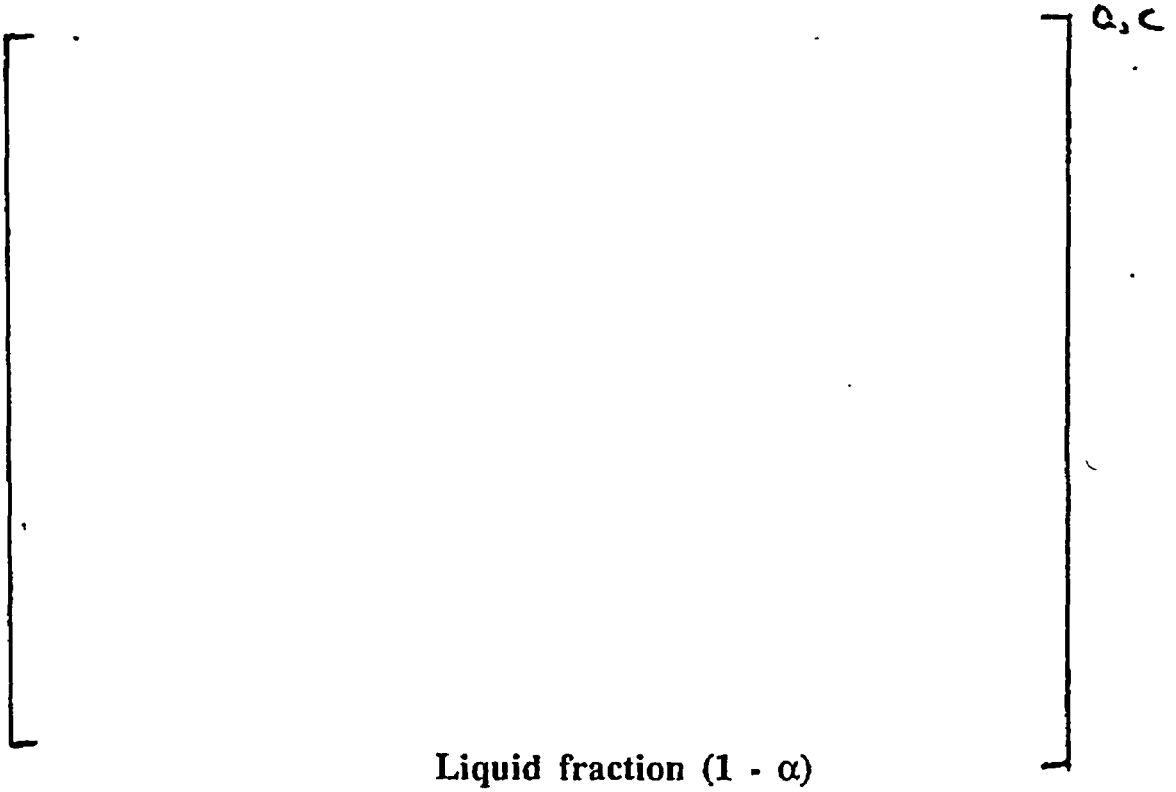

Figure 6.4. PCS pressure and liquid fraction at ADS-4 initiation in experimental facilities.

relative rankings of the non dominant phenomena differ relative to the AP600. The differences are due primarily to variations in fluid properties relative to the high pressure facilities. The differences in OSU and SPES do not seem to be significant relative to the overall system response. In terms of detailed analyses of component and subsystem responses, the differences could be important and should be considered when using the data.

In the intermediate phase CMT circulation begins near the beginning of Subphase I and continues to the beginning of Subphase III when CMT draining is assumed to begin. In this analysis the effect of CMT recirculation and the associated net heat transfer from the PCS to the CMTs was not accounted for in Subphases II and III. This approach was taken primarily to enable the analysis to be done in a straight forward manner and avoid estimating the rate of CMT circulation. A sensitivity analysis was performed in which the fraction of total PCS to CMT heat transfer occurring before Subphase III was varied from 0 to 50 %. Based on this analysis the dominant phenomena were unchanged in all 3 subphases. Changes in the relative magnitudes of the terms in the reduced equations were small.

6.3 ADS-4 Blowdown

This phase corresponds to the ADS-4 Blowdown Phase described in the PIRT. Appendix E describes the application of steps 1 through 5 of the methodology for this phase.

6.3.1 Step 1: ADS-4, Phase Description

The ADS-4 blowdown is defined to begin with the opening of the ADS-4 valves and ends with the initiation of IRWST flow. The CMTs are the active source of coolant for the core and, at the ADS-4 actuation signal, the CMTs will contain approximately 20% of their initial inventory.

The pressurizer has a significant liquid inventory due to accumulation of water entrained into it by the blowdown through ADS-1-3 valves in the previous phase. When the ADS-4 valves open the system depressurization rate increases, and flow through ADS-1,-2,-3 transitions from choked to friction dominated. Flow through the pressurizer and ADS-1-3 decreases to a negligible quantity when compared to the ADS-4 flows. The system is mostly saturated, except perhaps for the liquid in the CMTs. The CMTs deliver this liquid to the vessel downcomer through the CMT/DVI lines.

6.3.2 Step 2: ADS-4, Identification Of Key Components Or Subsystems

As depicted in Figure 6.5, the participating components are the CMTs, the vessel, the pressurizer, the ADS-4 Valves, the CMT injection line, the pressurizer surge line, and the hot legs. There are two steam bubbles in the system: one in the vessel upper head and one in the steam space of the pressurizer. The upper head bubble is part of a larger steam space that includes the steam generators, hot legs, etc. but is assumed not to participate in this subphase of the transient. After the ADS-1,-2,-3 flow transitions from choked to friction dominated flow the steam space above the pressurizer liquid is affected by the level of immersion of the sparger in the IRWST. It is assumed that the steam space in the pressurizer is at constant pressure related to the head of water above the sparger in the IRWST. Furthermore, the CMTs and the upper head are at the same pressure as they communicate via the downcomer bypass, the loops, and PBLs. Other assumptions made include; the accumulators are empty; break flow can be ignored as the beak area is much less than the ADS-4 area; there is no significant pressurizer draining; there is no flow between the hot legs and steam generators; and injected CMT fluid does not get to the cold legs since the downcomer level is beneath the cold leg nozzle elevation.

6.3.3 Step 4: ADS-4, Governing Equations

The system of equations for the configuration shown in Figure 6.5 were derived from basic conservation laws of mass, energy, and momentum, in Appendix E. The resulting nondimensionalized equations are presented below. Quantities with an asterisk in these equations denote division by a reference value.

The vessel mass balance is

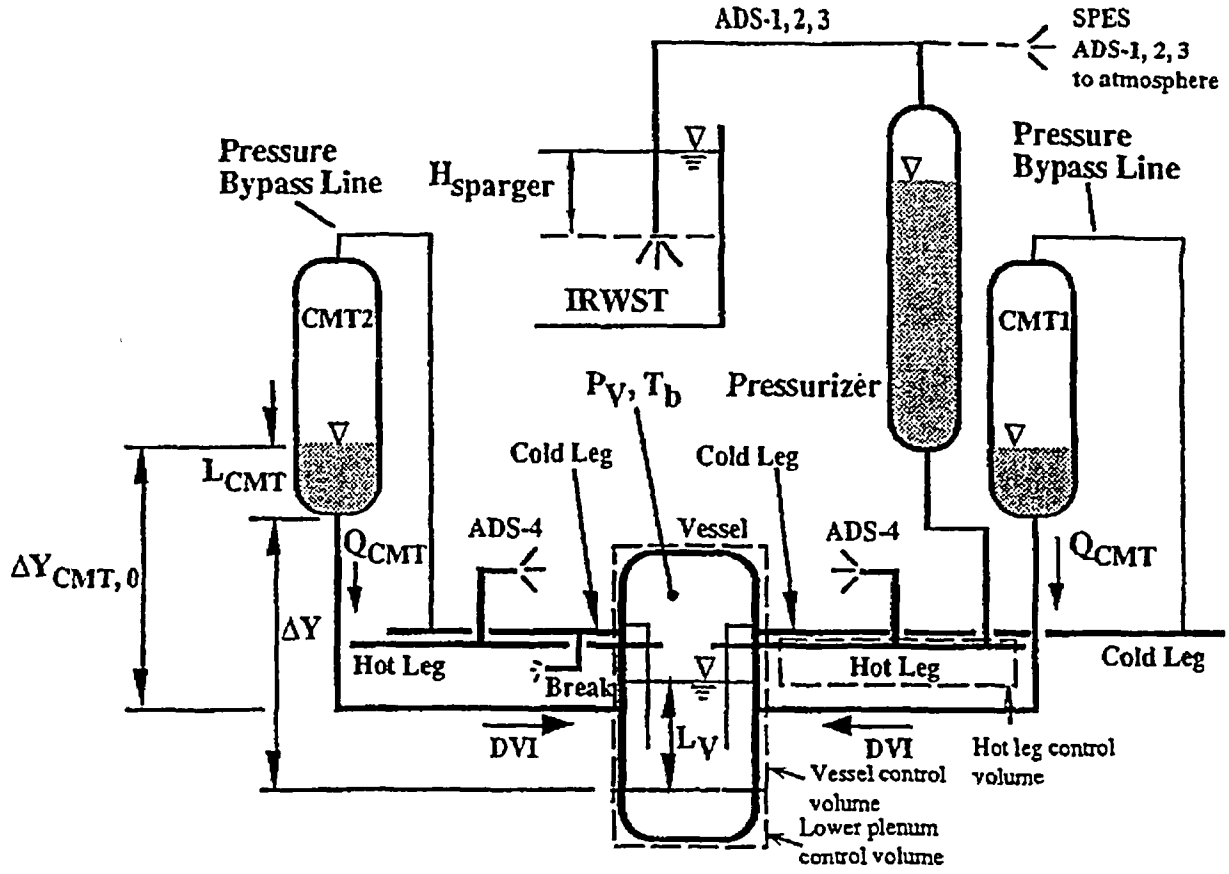

Figure 6.5. ADS-4 Blowdown phase: schematics and important components.

$$\frac{dV_l^*}{dt^*} = \frac{dL_V^*}{dt^*} = \Pi_{7-V}(\Pi_{16}Q_{CMT}^* - \dot{m}_{ADS-4}^*) \tag{6.24}$$

where the CMT mass flow rate is defined as

$$\dot{m}_{CMT}^* = \Pi_{16}Q_{CMT}^* \tag{6.25}$$

and it is assumed that the pressurizer flow is negligible and that there is no flow from the hot legs into the steam generators (or vice versa) so that the hot leg flow is equal to the ADS-4 flow.

The CMT mass balance in terms of the nondimensionalized CMT level and volumetric flow rate is given by

$$\frac{dL_{CMT}^*}{dt^*} = -\Pi_{15-CMT}Q_{CMT}^* \tag{6.26}$$

The CMT discharge line flow is given by

$$\frac{dQ_{CMT}^*}{dt^*} = -\Pi_{2-CMT}\left[\Pi_{17}L^* - \Pi_{18}L_{CMT}^* - \Delta Y^*\right] - \Pi_{3-CMT}Q_{CMT}^{*2} \tag{6.27}$$

where L^* is the vessel level and is constrained by the DVI nozzle elevation (L_{DVI}^*) as follows:

$$L^* = L_V^* \text{ for } L_V^* \geq L_{DVI}^*$$
$$= L_{DVI}^* \text{ for } L_V^* < L_{DVI}^* \tag{6.28}$$

An energy balance on the lower plenum fluid assuming that the CMT temperature is approximately constant (fluid temperature stratification and change may occur in the CMTs due to circulation. However, this assumption is valid when the CMTs are 20% full) yields the following expression for the mixing

$$\frac{d(T_{CMT} - T_{lp})^*}{dt^*} = -\Pi_{9-lp} Q_{CMT}^* (T_{CMT} - T_{lp})^* \tag{6.29}$$

The variables with asterisks in the above equations are specified as

$$V_l^* = \frac{V_l}{V_0}; t^* = \frac{t}{t_0}; L_V^* = \frac{L_V}{V_0/A_0}; \dot{m}_{ADS-4}^* = \frac{\dot{m}_{ADS-4}}{\dot{m}_0}; Q_{CMT}^* = \frac{Q_{CMT}}{Q_{CMT,0}}; L_{CMT}^* = \frac{L_{CMT}}{L_{CMT,0}}$$
$$\Delta Y^* = \frac{\Delta Y}{\Delta Y_{CMT,0}}; (T_{CMT} - T_{lp})^* = \frac{(T_{CMT} - T_{lp})}{\Delta T_0} \tag{6.30}$$

where the terms with subscript "0" denote reference values.

It was shown in Appendix E that these equations require additional relationships in order to constitute a closed system. To complete the analysis from a top-down perspective, the following assumptions were made about the form of these relationships.

As stated above, the ADS-4 flowrate is assumed to be equal to the hot leg flow rate and the ADS-4 discharge is given by the homogeneous equilibrium model[22] (HEM) evaluated at the ADS-4 quality or

$$\dot{m}_{hl}^* = \dot{m}_{ADS-4}^* = G_{HEM}(x_{ADS-4}) A_{ADS-4} / \dot{m}_0 \tag{6.31}$$

where the ADS-4 quality is specified by an energy balance across the core

$$x_{ADS-4} = \frac{\dot{q}_f - Q_{CMT} \rho_l C_p (T_{sat} - T_{lp})}{\rho_l Q_{CMT} h_{fg}} \tag{6.32}$$

The nondimensional groups in the above equations are summarized in Table 6.13.

6.3.4 Step 6: ADS-4, Selection Of Reference Parameters

The reference values were chosen to obtain numerical values of the Π s that can be used to compare the facilities and their behavior with that of the plant and with each other. Reference parameters are selected such that the normalized variables in each equation are of O[1] and the time scale of the system is selected as the residence time of the mass inventory in the vessel above the bottom of the heated length (e.g. $\Pi_{7\text{-}V}$ is taken as unity). Choosing the coefficient of the vessel mass inventory equation, Π_7, to define the reference time focuses the analysis on the dynamic processes that participate in the emptying and filling of the vessel. The details of

Table 6.15. Dimensionless coefficients for ADS-4 phase.

Dimensionless Coefficient	Algebraic Description	Physical interpretation
$\Pi_{2\text{-CMT}}$	$\frac{g\Delta Y_{CMT,0}t_0}{Q_{CMT,0}L/A)_{CMT,0}}$	Ratio of hydrostatic and acceleration forces
$\Pi_{3\text{-CMT}}$	$\frac{Q_{CMT,0}t_0R'_{CMT,0}}{L/A)_{CMT,0}}$	Ratio of friction and acceleration forces
$\Pi_{7\text{-V}}$	$\frac{\dot{m}_0t_0}{\rho_1V_0}$	Vessel nondimensional residence time
$\Pi_{9\text{-lp}}$	$\frac{Q_{CMT,0}t_0}{V_{lp+dc,0}}$	Lower plenum mixing time
$\Pi_{15\text{-CMT}}$	$\frac{Q_{CMT,0}t_0}{A_{CMT,0}L_{CMT,0}}$	Ratio of vessel and CMT emptying times
Cross groups		
Π_{16}	$\frac{\rho_1}{\dot{m}_0}\left(\frac{g\Delta Y_{CMT,0}}{R'_{CMT,0}}\right)^{1/2}$	Ratio of CMT flow to reference flow
Π_{17}	$\frac{V_0}{A_0\Delta Y_{CMT,0}}$	Ratio of head in vessel to CMT line head
Π_{18}	$\frac{L_{CMT,0}}{\Delta Y_{CMT,0}}$	Ratio of CMT level to CMT line head

reference parameter selection are described in Appendix E. Table 6.16 lists the reference parameters selected. Note that in this table, the reference pressure is taken to be the pressurizer pressure plus the hydrostatic head due to the pressurizer level (assumed to be half full). The pressurizer pressure is assumed to be atmospheric pressure plus the hydrostatic head due to the sparger submergence in the IRWST. Also note that the reference CMT flow is defined as

$$Q_{cmt,0} = \sqrt{\frac{g\Delta Y_{cmt,0}}{(K/2A^2)_{cmt,0}}} \tag{6.33}$$

and the reference mass flow rate ($\dot{m}_0$) is based on the HEM model evaluated using the quality from Equation (6.31) and the ADS-4 area (SPES is an exception as discussed below). As mentioned above, setting $\Pi_{7\text{-V}}$ to unity and solving for t_0 using values from Table 6.16 produces a time scale. Table 6.17 shows the resulting values for t_0. Also shown in this table are reference mass flow rates obtained from experimental data and the time scales that result from using these

Table 6.16. Reference parameters for plant and facilities during ADS-4 blowdown.

Reference Parameters[a]	AP600	ROSA	SPES	OSU
P_0 (kPa)				
$K/(2A^2)_{cmt}$ (both) (m^{-4})				
$L/A)_{cmt}$ (both) (m^{-1})				
ΔY_{CMT-0} (m)				
L_{cmt-0} (m)				
A_{cmt} (m^2)				
$V_{vessel-0}$ (m^3)				
$L_{vessel-0}$ (m)				
V_{dc+lp} (m^3)				
A_{ads-4} (m^2)				
$\dot{q}_{core,0}$ (kW)				
$Q_{cmt,0}$ (both) (m^3/s)				
$\dot{m}_{cmt,0}$ (both) (kg/s)				
T_{sat} (K)				
ρ_f (kg/m^3)				
h_{fg} (kJ/kg)				
ρ_{cmt} (kg/m^3)				
T_{cmt} (K)				
c_p (j/kg)				
x_{core}				
$G_{critical-HEM}$ at x_{core} (kg/m^2 s)				
$\dot{m}_0$ (kg/s) ($=G_{HEM}A_{ads-4}$)				

a, c

a. Note that some of the reference parameters from facility to facility are different. This is due to the fact that the facilities are of significantly different scale size. See page 1 of this report.

values to compute t_0. Note that for the ROSA and OSU data, there is quite good agreement between the external (based on experiment) and internal (HEM model) values.

Table 6.17. Time scales for ADS-4 blowdown.

Parameter	AP600	ROSA	SPES	OSU
$V_{v,0}$ (m^3)				
ρ_l (kg/m^3)				
$\dot{m}_0$ (kg/s)				
t_0 (s)				

In Table 6.17 multiple values are listed for the SPES experiment. This stems from the manner in which the experiment was conducted. Due to mechanical malfunction on this experiment, the ADS-4 valves opened approximately 300 s after the 20% CMT level set point was reached. Due to the fact that the ADS-1-3 train in the SPES facility discharges to atmosphere (rather than to the IRWST sparger as in the other experimental facilities), the ADS1-3 train is assumed to be a part of ADS-4 blowdown for the purpose of this analysis. Thus it was assumed that the when 20% CMT level was reached, flow out the ADS1-3 train is included as part of ADS-4 flow. The experimental data value for SPES is an average of both flows over the time frame between 20% CMT level and the end of ADS-4 blowdown. The time scales shown in Table 6.17 appear reasonable in that ROSA is reasonably close to the plant value and OSU is on the order of half the plant value as expected based on the reduced height scaling for APEX. The SPES time scales are as expected in light of the fact that the ADS-4 train is oversized by a factor of approximately 2.5 and the ADS1-3 train discharges to atmosphere rather than to the IRWST.

6.3.5 Step 7: ADS-4, Order of Magnitude Analysis

Table 6.18 lists numerical values for the groups listed in Table 6.15 using values from Tables 6.14 and 6.15. In this table two values are listed for the SPES facility as appropriate for the different time scales noted above.

Note from Table 6.18 that the values of the $\Pi_{2\text{-cmt}}$ and $\Pi_{3\text{-cmt}}$ groups are large and with the definition used in Equation (6.33), they are numerically equal. Because the values are much larger than the other groups, Equation (6.27) can therefore be divided through by $\Pi_{2\text{-cmt}}$ making the LHS of the equation much smaller than the RHS. The equation describing the CMT flow then becomes

$$Q^*_{cmt} = \left[\Pi_{18} L^*_{CMT} - \Pi_{17} L^* + \Delta Y^*\right]^{1/2} \tag{6.34}$$

This result indicates that the line inertias are not a dominant factor in the CMT flow determination. Observation of the remaining Π values in Table 6.18 indicates that the experimental facility values tend to bound the value calculated for the plant and for the large part are reasonably close to the plant value. To further illustrate this, Table 6.19 gives the ratios of

Table 6.18. Π values for the ADS-4 blowdown phase.

Π	AP600	ROSA	SPES	OSU
$\Pi_{2\text{-cmt}}$				
$\Pi_{3\text{-cmt}}$				
$\Pi_{7\text{-v}}$				
$\Pi_{9\text{-lp-dc}}$				
$\Pi_{15\text{-cmt}}$				
Π_{16}				
Π_{17}				
Π_{18}				

a, c

a. SPES based on time scale of 714 s.
b. SPES based on time scale of 300 s.

the Π groups for the facilities to that of the plant. With the exception of the $\Pi_{2\text{-cmt}}$ and $\Pi_{3\text{-cmt}}$ groups which are of little consequence on the CMT flow rate as noted above, the ratios are reasonably close to unity.

Table 6.19. Π Ratios between facilities and AP600 for the ADS-4 Blowdown Phase.

Ratio	ROSA/AP600	SPES/AP600	OSU/AP600
$\Pi_{7\text{-v}}$			
$\Pi_{2\text{-cmt}}$			
$\Pi_{3\text{-cmt}}$			
$\Pi_{9\text{-lp}}$			
$\Pi_{15\text{-cmt}}$			
Π_{16}			
Π_{17}			
Π_{18}			

a, c

a. SPES based on time scale of 714 s.
b. SPES based on time scale of 300 s.

Based on Table 6.19, the three facilities should do a reasonable job at either individually representing or, as a group, enveloping AP600 behavior for the ADS 4 phase. The biggest consideration is the time scale for the SPES facility due to the oversized nature of the ADS-4 valves and the manner in which this particular experiment was conducted. It is clear from this analysis that the line resistance of the CMT line is an important parameter, for it defines the rate and duration of water delivery to the vessel. In general, the groups that influence the vessel mass directly (Π_{16} Π_{17}, and Π_{18} from Equations (6.24) and (6.34)) are fairly well preserved in the facilities.

The equations for the CMT and ADS-4 flows can be substituted into the vessel mass balance to provide the following expression

$$\frac{dV^*}{dt^*} = \frac{t_0}{V_0}\left(\frac{g_0 L_0}{R_0'}\right)^{1/2}\left[\frac{g^*}{R'^*}\left(L^*_{CMT} - L^*_{DC} + \Delta Y^*\right)\right]^{1/2} - \frac{G_0 A_0 t_0}{V_0 \rho_0}\frac{G^* A^*}{\rho^*} \qquad (6.35)$$

These dimensionless groups were evaluated using the reference parameters in Table 6.16 and the time scales in Table 6.17. For the experimental facilities the data values of the time were used. The numerical values of the dimensionless groups are summarized in Table 6.20 with the ratio of ADS-4 flow to CMT flow. The ratio of ADS flow to CMT flow is greater than 1 in the full pressure facilities and less than 1 in OSU. The ratio in ROSA is ~30 % large relative to AP600 while in SPES the value is ~220 % larger than in AP600. These differences are consistent with the differences in the ratios of ADS-4 flow area to vessel volume in the full pressure facilities. The reason for the ratio of ADS-4 flow to CMT flow being less than 1 in OSU is less clear. It may be due to the flow in OSU not being choked. The effect of the differences in the ratios of ADS-4 flow to CMT flow can be expected to affect the amount of vessel mass loss occurring during ADS-4 blowdown. Based on these values the full pressure experimental facilities would be expected to lose a larger fraction of vessel inventory than the AP600 while OSU would be expected to lose less. Note that the last row in Table 6.20 is a ratio of values from the second and first rows.

Table 6.20. Dimensionless groups for ADS-4 vessel mass balance.

Dimensionless Group	Physical Meaning	AP600	ROSA	SPES	OSU
$\frac{t_0}{V_0}\left(\frac{g_0 L_0}{R_0'}\right)^{1/2}$	Ratio of CMT flow to vessel volume	[			] a,c
$\frac{G_0 A_0 t_0}{V_0 \rho_0}$	Ratio of ADS flow to vessel volume	[			]
$\frac{G_0 A_0}{\rho_0}\left(\frac{R_0'}{g_0 L_0}\right)^{1/2}$	Ratio of ADS flow to CMT flow	[			]

6.3.6 Step 8: ADS-4 Blowdown, Verification with Data

Using the methodology described in Section 3 each of the important equations is verified with data to show that the equations and nondimensional groups are correct. We now proceed to demonstrate this process starting with the vessel mass inventory balance and then work outward to the flows that influence the vessel inventory. Liquid inventory in the vessel is the primary consideration as this inventory is the controlling factor for core cooling.

Vessel Mass Balance

With respect to the vessel (see schematic in Figure 6.6), Equations (6.24) and (6.25) can be combined to get the following nondimensional mass balance

$$\Pi_7^{-1} \frac{dV_l^*}{dt^*} = \dot{m}_{cmt}^* - \dot{m}_{ads4}^* \tag{6.36}$$

where

$$\Pi_7 = \frac{t_0 \dot{m}_0}{\rho_0 V_0} \tag{6.37}$$

and is unity for the time scale used and variables with an asterisk are defined in Equation (6.30).

Equation (6.36) can be integrated with respect to the dimensionless time variable to provide an expression for the vessel dimensionless liquid volume.

$$\int_{t_0^*}^{t^*} \frac{dV_l^*}{dt^*} dt^* = \int_{t_0^*}^{t^*} \dot{m}_{cmt}^* dt^* - \int_{t_0^*}^{t^*} \dot{m}_{ads4}^* dt^* \tag{6.38}$$

or

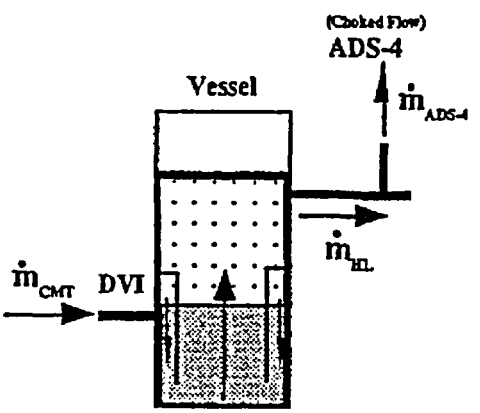

Figure 6.6. Vessel control volume for ADS-4 blowdown.

$$V_l^*(t^*) - V_l^*(t_0^*) - \int_{t_0}^{t^*} \dot{m}_{cmt}^* \, dt^* = - \int_{t_0}^{t^*} \dot{m}_{ads4}^* \, dt^* \tag{6.39}$$

where $V_l^*(t_0^*)$ is a constant of integration. Equation (6.39) can be applied to the experimental data from each facility to calculate the nondimensional vessel liquid volume change with dimensionless time for the ADS-4 phase. This equation will balance if the mass inflows and outflows have been correctly accounted for. Furthermore, if reasonable reference scales have been chosen, the variables will be O[1] and plotting the LHS of the equation against the RHS should produce a slope near unity.

Figure 6.7 shows the result of evaluating Equation (6.39) with the ROSA, SPES, and OSU experimental data. In this figure, the ordinate corresponds to the LHS of Equation (6.39) and the abscissa corresponds to the RHS of the equation. The integrals were computed over the range $-0.8 \leq t^* \leq 0$ where the lower limit corresponds to the start of ADS-4 blowdown and the upper limit to the start of IRWST injection. The reference line labeled y = x is included on the figure.

The results in Figure 6.7 indicate that a relatively good mass balance on the vessel has been achieved as the data are near the y = x line as expected. The figure shows remarkably good agreement given the experimental uncertainty associated with mass flow measurements. It was expected that the mass balance would likely be within about 10 - 20% at best. This result

Figure 6.7. ROSA, SPES, and OSU mass balances in nondimensional coordinates for the ADS-4 phase.

suggests that the major sinks and sources of mass have been properly accounted for. Note that in Figure 6.7 the two different time scales have been represented for the SPES result.

Figure 6.8 shows the integrals of the nondimensional mass flows used in Figure 6.7. In this figure, the integral of the CMT flow has been plotted against the integral of the ADS-4 flow. The deviation in the data from the y = x line is of course the inventory change in the vessel. This figure illustrates the significance of the CMT inventory in the overall mass balance on the vessel. Furthermore, the relationship among the facilities is similar in terms of magnitude and in that the CMT inventory supplies a fairly large fraction of the flow that is exiting the system through the ADS-4. Note that the significant slope change in the SPES curve is related to the actual opening of the ADS-4 valves.

The results presented in Figures 6.7 and 6.8 show that the process of scaling the experimental data with the nondimensional residence time of the vessel (Π_7) was successful and that the behavior of the nondimensional flows in the facilities is reasonably similar. The results shown indicate that a reasonable mass balance can be effected for each of the facilities using the equations developed. Furthermore, it appears that reasonable reference scales have been determined since, for all the facility data sets, the range of the left hand side of Equation (6.39) is between similar limits as is the range of the right hand side of the equation. This result suggests that a common basis has been developed so that in nondimensional coordinate space, the data collapse.

Figure 6.8. ROSA, SPES, and OSU nondimensional flow integrals for ADS-4 phase.

The reference scales developed in this analysis appear to be reasonable in light of the design of the individual facilities. For example, the reference time scales for the AP600 plant and for the ROSA facility are approximately equal as expected. Also, the OSU facility reference time scale is on the order of half the reference time scale for the AP600 and the ROSA facility. This is reasonable since the design philosophy of the OSU system was to approximate one-half time scale for the all of important transport processes. The SPES time scale results because the SPES ADS-4 valve area is oversized by a factor of approximately [ ]^{a,c}. This fact helps to explain the noticeable effect of the ADS-4 valve opening.

Vessel Outflow

We now proceed to examine the flows that influence the vessel mass balance, i.e., the terms appearing on the RHS of Equation (6.38). First, we examine the facility measured ADS-4 flow rates in light of the reference scales selected to show that the scale choices were reasonable and adequate.

A frozen flow assumption can be used to estimate a reference ADS-4 mass flow rate assuming no knowledge of the ADS-4 discharge quality. This assumption involves computing a critical mass flux by multiplying the vapor sound speed[23] and vapor density at the reference pressure conditions. Figure 6.9 shows a comparison of the measured integrated ADS-4 mass flux and the integrated mass flux computed with the HEM model for various qualities using the measured upper head pressure as input for the ROSA experiment. Both the HEM result and the measured result were divided by the frozen value for normalization.

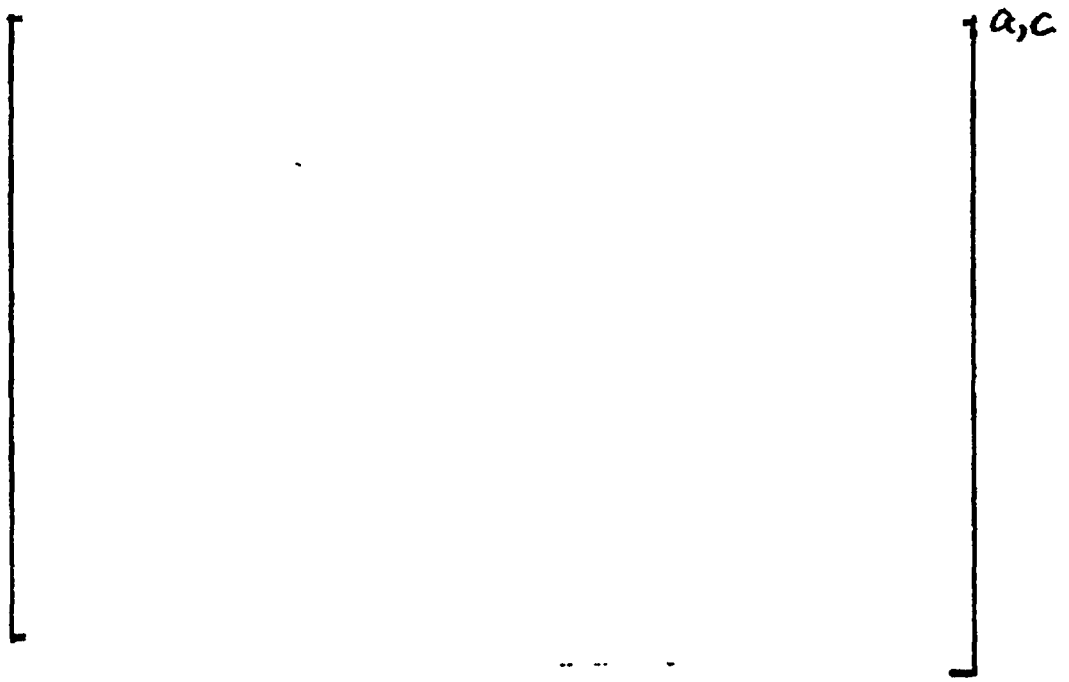

Figure 6.9. ROSA experiment AP-CL-03 ADS-4 mass flux.

The results shown in Figure 6.9 indicate that the integrated normalized ADS-4 mass flux for ROSA AP-CL-03 is approximately bounded on the high side by the HEM result for quality of 0.3 for a fair portion of the ADS-4 blowdown. By inspection, it is seen that the mass flux based on the frozen flow model approximates the average of the measured mass flux. For the ROSA experiment, the average measured mass flow was about [ ]a,c whereas the frozen model mass flux of [ ]a,c gives a reference flow of [ ]a,c The information in Figure 6.9 shows that the reference flow scale picked using HEM (without knowledge of the data) for the ROSA ADS-4 flow is reasonable as both the time and reference flow scales are of order unity as desired.

Figure 6.10 shows the SPES experiment data displayed on the same integrated ratio basis as the ROSA data on Figure 6.9. As shown, the frozen assumption is a reasonable representation of the upper bound of the measured integrated flow rate until t* ~0.2 when the data become larger. For reference, the average measured total ADS flow rate (including the ADS1-3 train and the ADS-4 train) was [ ]a,c for the SPES experiment. Using this average value with the combined ADS1-3 and ADS-4 flow area produces an average mass flux of [ ]a,c which is only about 7% higher than the reference mass flux value used. The measured integrated data in Figure 6.10 are reasonably bounded by the HEM 30% quality line indicating that the reference flow scale selected without knowledge of the data is reasonable.

Figure 6.11 indicates that the measured ADS-4 mass flux in OSU is considerably higher than predicted using the frozen flow assumption. This result is the reason that the measured average ADS-4 flow rate was used to establish the reference flow rate. The results in Figure 6.11 indicate that the HEM model evaluated at low quality (≤~0.05) bounds the measured APEX data and

Figure 6.10. SPES experiment S00401 ADS-4 mass flux for ADS-4 blowdown.

Figure 6.11. OSU experiment SB5 ADS-4 mass flux for ADS-4 blowdown.

that the friction dominated discharge flow rate can be approximated by HEM evaluated at low quality as was done above to establish a reference flowrate value.

The data shown in the previous figures indicate that reasonable flow scales have been determined for the ROSA and SPES facilities since the integrated outflow from the system is in reasonable agreement with the integrated reference mass flux. As indicated, the HEM model for a quality of 20-30% produces reasonable reference flow values for the ROSA and SPES experiments. The frozen flow assumption did not work for the OSU experiment as the data suggest that the ADS-4 flow was not choked. The data indicate the flow contains significant liquid and in this case, the ADS-4 flowrate is bounded by the HEM model at low (~1- 5%) quality.

Vessel Inflow

As shown in Equation (6.38), the CMT flows along with the hot leg flows influence the vessel mass balance. We now examine the CMT flows in light of the CMT tank and line equations with the goal of showing that the equations collapse the experimental data and hence the equations and the Π groups in them are correct. We note from the previous sections that the CMT equations contain Π groups that contain line resistance and line inertia parameters and the reference flow for the CMT along with the system time scale. Based on the order of magnitude analysis shown in Section 6.2.7, the $\Pi_{2\text{-cmt}}$ and $\Pi_{3\text{-cmt}}$ groups are quite large indicating that the transient term on the left hand side of the CMT line equation can be neglected so that Equation (6.34) applies.

Using Equations (6.25) and (6.34) gives the following

$$\dot{m}^*_{cmt} = \Pi_{16} Q^*_{cmt} = \Pi_{16}\left[\Pi_{18} L^*_{CMT} - \Pi_{17} L^* + \Delta Y^*\right]^{1/2} \tag{6.40}$$

Both sides of Equation (6.40) can be integrated and the resulting equation

$$\int \dot{m}^*_{cmt} dt^* = \int \Pi_{16} Q^*_{cmt} = \int \Pi_{16}\left[\Pi_{18} L^*_{CMT} - \Pi_{17} L^* + \Delta Y^*\right]^{1/2} dt^* \tag{6.41}$$

was used to examine the experimental data. Figures 6.12 - 6.14 show the results for the facility data where the integral of the nondimensional CMT flow rates are plotted versus the RHS of Equation (6.41). As is shown in these figures, all of the data are near the y = x line as expected.

Analytic Solution for Vessel Level

In Appendix F, an analytic solution for the vessel level equation is developed for the ADS-4 blowdown. Solutions for the vessel level greater than or equal to the DVI nozzle elevation and the vessel level less than the DVI nozzle are developed. For the vessel level greater than or equal to the DVI nozzle, the solution is

$$V_1^*(t^*) - V_1^*(0) = \left[\Pi_{16} Q^*_{cmt}(0) - 1\right] t^* + \frac{\Pi_{16}\hat{\Pi}_{19}}{2Q^*_{CMT}(0)}\left[Q^*_{CMT}(0) + \frac{\Pi_{17}}{\hat{\Pi}_{19}}\right]\frac{t^{*2}}{2} + \ldots \tag{6.42}$$

where
$\hat{\Pi}_{19} = (\Pi_{18}\Pi_{15} - \Pi_{17}\Pi_{16})$ for $L^*_V \geq L^*_{DVI}$ and it is assumed that the nondimensionalized ADS-4

[ ] a,c

Figure 6.12. ROSA AP-CL-03 CMT line equation.

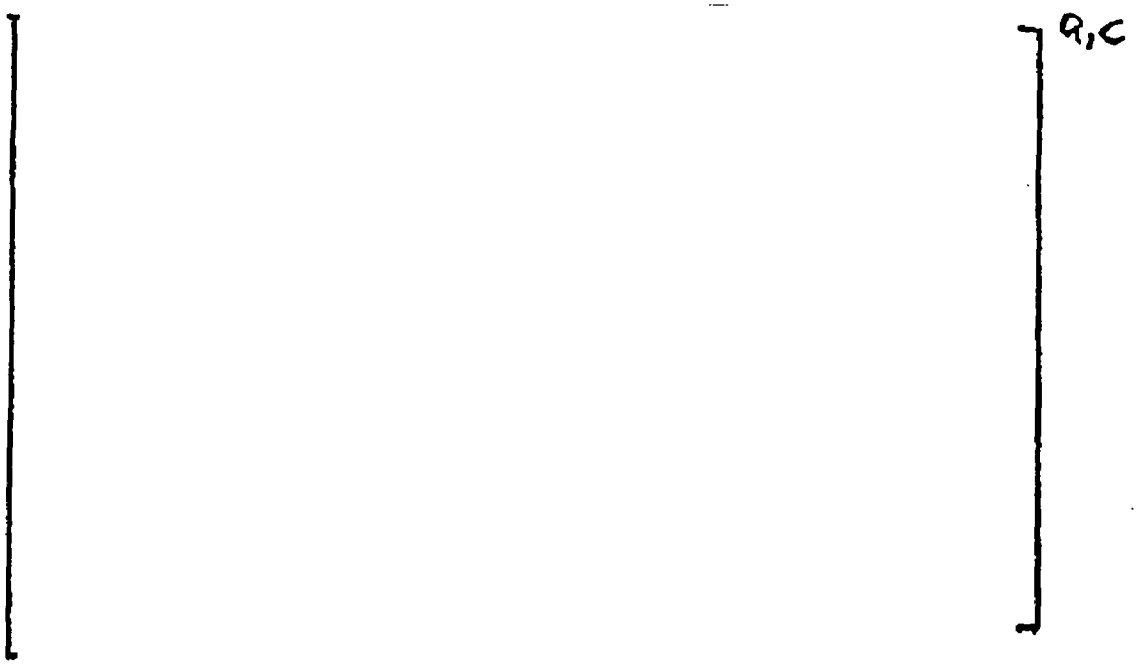

Figure 6.13. SPES S00401 CMT line equation.

Figure 6.14. OSU SB5 CMT line equation.

flowrate is 1 (see Appendix F). Note that Equation (6.42) applies mainly to the ROSA experiment because of the relationship between the vessel level and the DVI elevation.

For the case of the vessel level less than the DVI nozzle, the solution is

$$V_1^* - V_1^*(0) = \left[\Pi_{16} Q_{CMT}^*(0) - \dot{m}_{ADS4}^*\right] t^* + \frac{\Pi_{16}\Pi_{18}\Pi_{15}}{4} t^{*2} \text{ for } L_v^* < L_{DVI}^*. \quad (6.43)$$

Figure 6.15 shows a comparison of the experimental data for the one inch cold leg break experiments with Equations (6.42) and (6.43). The nature of the agreement provides additional evidence for the validity of the equations and scale assumptions.

Discussion of Reference Parameters - Selection With and Without Data Knowledge

If no experimental information is available, reference parameters must be selected in a blind fashion, that is without benefit of data knowledge. However, if experimental information is available, it can support or confirm reference parameter selection. In the present case, there is no plant data so reference parameters must be selected without data knowledge. Since experimental facility data is available, reference parameters can be first selected assuming no data knowledge for the facilities and then these selections can be examined/confirmed using the data. Such a process helps to verify that reasonable reference values for the plant have been chosen. Here we summarize observations regarding selection of reference parameters both with and without data

[a,c]

Figure 6.15. Analytic solution for vessel level during ADS-4 blowdown.

knowledge referred to hereafter as "with-data" and "without-data."

For both situations (without-data and with-data), the vessel time scale was determined in the same fashion via the Π_7 group and the same reference vessel volume was chosen by design. For the with-data view, the reference pressures were chosen based on the measured data. For the without-data view, the reference pressure was chosen to be the pressurizer steam dome pressure (as determined by the IRWST head and ADS lines connecting the sparger to the top of the pressurizer) plus the head of liquid in the pressurizer and surge line. The liquid level in the pressurizer was assumed to be at a position approximately midway between the top of the pressurizer and an elevation corresponding to the IRWST level. For the ROSA and SPES experiments, the view without-data was resulted in reference pressures that were somewhat lower (20 - 40 kPa) than those based on the data. For the OSU experiment, the two views yielded basically the same reference pressure. Part of the minor difference in reference pressure for the SPES experiment is due to the fact that part of the ADS 1-3 blowdown was considered as ADS-4 blowdown as discussed above. The reference pressure differences had little effect on the resulting selection of reference saturated liquid densities and temperatures for the facilities.

Reference ADS-4 outflow scales for the experimental facilities (and plant) without-data view were based on the HEM model as discussed above. The ADS-4 discharge quality was estimated from the core vapor generation rate and a reference CMT flow rate. This quality estimate was then used with the HEM model to compute a reference discharge rate. The quality so estimated was of the order of 20-30% for the plant and the ROSA experiment, approximately 14% for the SPES experiment, and about 7% for the OSU experiment. These reference flow rate scales, in conjunction with the reference volume and density, produced vessel time scales for ADS-4 blowdown consistent with the duration of the ADS-4 blowdown which was the desired result.

Reference ADS-4 outflow for the with-data view was evaluated with application of a simple frozen flow model for the ROSA and SPES facilities (and the plant) since the actual ADS-4 discharge quality is not known. The ADS-4 discharge was assumed to be saturated steam leaving the system at the vapor sound speed for a quality of unity. For the OSU experiment the measured average flow was used as the reference ADS-4 flow since the ADS-4 flow does not appear to be choked and the frozen assumption did not apply. Review of these results and the data indicated that the reference flow scales selected are reasonably consistent with the HEM model results discussed above for the without-data view although for the OSU experiment, the without-data procedure results in a reference flow rate that is slightly low relative to the data (most likely due to a quality estimate that is slightly large). The resulting effect is a vessel time scale slightly larger than the duration of ADS-4 blowdown in the OSU experiment. A better estimate would be made using a lower quality with the HEM model to estimate a reference ADS-4 scale for the OSU experiment.

From the without-data viewpoint, reference flow values selected using the approach described above produced vessel time scale estimates that were close to those estimated from the with-data view as might be expected based on the discussion of the data above. Based on evaluation of the data, both selections were shown to provide reasonable reference flow scales for the facilities.

Nominal geometric parameters for the plant and facilities such as hardware elevation changes, initial levels, etc. are used in the without-data approach. It is recognized that situations arise wherein the value of an experiment parameter may be different than the expected nominal value based on evaluation of experiment results data. Tank levels are an example in that levels may deviate from an expected value for a variety of reasons. Such differences could impact the results obtained from the with-data approach relative to the without-data approach if this initial level factors into the computation of a reference flow or a reference length in a dimensionless group. An example is the SPES experiment delayed ADS-4 activation as discussed above. In general, deviation from nominal values has not been a significant issue to date.

6.3.7 Concluding Remarks

The ADS-4 flow and the CMT flow were the two principal mass flow terms influencing the vessel mass balance for the ADS 4 blowdown phase. Reference parameters for the dimensionless transit time group controlling the vessel mass balance were determined and used to conduct mass balances for the facility data to show that the major sources and sinks were accounted for.

Based on comparison to data, the HEM model evaluated at a quality determined from a core energy balance provides an adequate reference ADS-4 flow rate value for the facilities that is close to the average of the measured ADS-4 discharge flow for the ROSA, SPES, and OSU facilities. This reference flow rate used with a reference volume and density provided reasonable time scales for the ADS-4 time scales. This same approach should therefore be applicable to the plant for specification of the reference flow rate and time scale.

CMT line flows and tanks were analyzed using the relevant equations developed for the system to demonstrate application of the methodology as one moves away from the vessel component. This effort demonstrated that the equations and the dimensionless groups that arise from the equations are correct. These groups were used with the dimensionless form of the equations to show that the data collapse relatively well and in the expected manner.

Based on review and evaluation of the dimensionless groups and equations, transient or line inertia effects were not expected to be of importance. Examination of the data indicates this expectation to be true.

Values of the dimensionless groups resulting from the ADS-4 phase indicate that the facility values bound the plant values. This result suggests that the plant performance is bounded by the experimental data and that the data are applicable for code adequacy evaluations.

6.4 IRWST Injection Phase

This phase, as defined here is a subphase of the PIRT phase with the same name, encompassing only the initial refill of the vessel. The application of steps 1 through 5 of the methodology for this phase is presented in Appendix E of this report.

6.4.1 Step 1: IRWST Injection Phase, Phase Description

The phase defined in the PIRT as the IRWST Injection begins with the injection of IRWST liquid and ends with the beginning of SUMP injection. Here the initial subphase is analyzed, which includes the interval from the beginning of IRWST injection and the establishment of a quasi-steady flow from the IRWST through the vessel and out the ADS-4 valves. In this initial period, the fluid is forced through the core by the hydrostatic head of the IRWST. Eventually, the head in the IRWST begins to decrease and with it the flow through the DVI line, leading to the next subphase of this process.

6.4.2 Step 2: IRWST Injection Phase, Relevant Subsystems and Components

As illustrated in Figure 6.16, the main components involved in this subphase are the IRWST, the DVI lines, the reactor vessel, the hot legs, the pressurizer, the ADS-4 lines and valves, and the ADS-123 discharge which acts as an extension of the gas space of the pressurizer. The rest of the system (the cold side) is mostly filled with steam. The CMTs have completed draining and the cold legs and steam generators are no longer participating paths for the main flows in the system, which enable us to neglect them in this phase.

When this phase begins, the system is depressurizing mostly through the ADS-4 valves which are the largest relief openings in the system. The pressurizer has some water and the ADS-123 flow has transitioned from choked to friction controlled flow. As the pressure in the upper head drops and equals the head of water in the IRWST (plus the containment pressure), the check valves in the IRWST injection lines open and allow the cold IRWST fluid to enter the vessel at the DVI connections. This cold water flows through the core, where it is heated and boils. Steam and saturated water flow into the hot legs and out the ADS-4 in the CMT loop side, and in the pressurizer side the ADS-4 is a tee in which the hot leg flow and the fluid draining from the pressurizer converge and go out the ADS-4.

6.4.3 Step 4: IRWST Injection Phase, Governing Equations

The dynamic equations for each component and connecting line are derived from basic conservation laws (Appendix E) and the nondimensionalized forms are summarized as follows

The vessel mass balance is given by

$$\frac{dV_l^*}{dt^*} = \frac{dL_v^*}{dt^*} = \Pi_{7-V-IRWST}\left(\dot{m}_{dvi}^* - \dot{m}_{hl}^*\right) \tag{6.44}$$

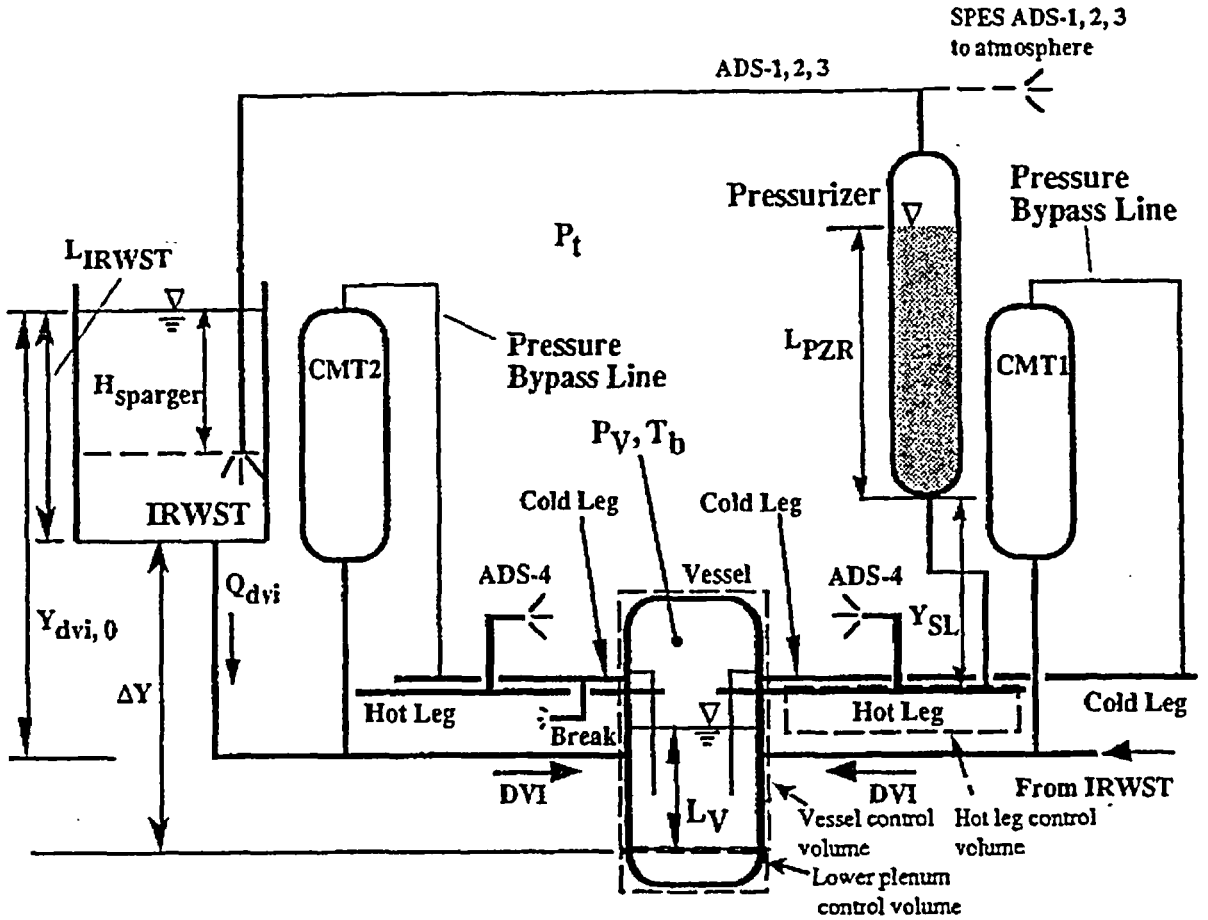

Figure 6.16. IRWST Injection schematic and important components.

where

$$\dot{m}^{*}_{dvi} = \Pi_{23} Q^{*}_{dvi} \tag{6.45}$$

$$\dot{m}^{*}_{ADS-4} = \dot{m}^{*}_{PZR} + \dot{m}^{*}_{sl} \tag{6.46}$$

$$\dot{m}^{*}_{ADS-4} = G_{crit}(HEM@x_{ADS-4}) A_{ADS-4} / \dot{m}_0 \tag{6.47}$$

$$x_{ADS-4} = \frac{\dot{q}_{core} - \rho_l Q_{dvi} C_p (T_{sat} - T_{LP})}{\rho_l Q_{dvi} h_{fg}} \tag{6.48}$$

The pressurizer mass balance is

$$\frac{dL^{*}_{PZR}}{dt^{*}} = -\Pi_{15-PZR} \dot{m}^{*}_{PZR} \tag{6.49}$$

where the rise velocity of cap bubbles is used to estimate the pressurizer flow rate

$$\dot{m}^{*}_{PZR} = 0.1 \rho_l A_{SL} \sqrt{g D_{SL}} / \dot{m}_0 \tag{6.50}$$

The DVI line flow is

$$Q^*_{dvi} = \left[(\Delta Y^* - \Pi_{19} L^*) + \Pi_{20}(1 - P^*_V)\right]^{1/2} \tag{6.51}$$

where the transient term dQ^*_{dvi}/dt^* is neglected as it is much smaller than the other terms in the equation, the containment back pressure P_t is assumed to be approximately constant, and L^* is the maximum of the vessel level and the elevation of the DVI nozzle or

$$L^* = \max(L^*_V, L^*_{DVI}). \tag{6.52}$$

The vessel pressure is estimated using the pressurizer pressure and the hydrostatic head in the surge line (Y_{SL} is the surge line height) and pressurizer tank

$$P^*_V = P^*_{PZR} + \Pi^{-1}_{20}(\Pi_{22} L^*_{PZR} + \rho^*_{SL} Y^*_{SL}) \tag{6.53}$$

Lower plenum mixing is described by the following energy balance

$$\frac{d(T_{dvi} - T_{lp})^*}{dt^*} = -\Pi_{21} Q^*_{dvi}(T_{dvi} - T_{lp})^* \tag{6.54}$$

We used the homogeneous equilibrium model to calculate a critical mass flow rate through ADS-4. The surge line density ρ_{SL} was assumed approximately constant. The dimensionless coefficients are described in Table 6.21.

Table 6.21. Dimensionless coefficients in IRWST Injection Phase.

Dimensionless Coefficient	Algebraic Description	Physical Interpretation
$\Pi_{7\text{-V-IRWST}}$	$\frac{\dot{m}_0 t_0}{\rho_l V_0}$	Vessel nondimensional residence time
$\Pi_{15\text{-PZR}}$	$\frac{\dot{m}_0 t_0}{\rho_l V_{PZR,0}}$	Ratio of vessel mass to pressurizer mass
Π_{19}	$\frac{V_0}{A_0 Y_{dvi,0}}$	Ratio of head in vessel to IRWST line head
Π_{20}	$\frac{P_t}{\rho_l g Y_{dvi,0}}$	Ratio of containment pressure to IRWST line head
Π_{21}	$\frac{Q_{dvi,0} t_0}{V_{lp+dc,0}}$	Lower plenum nondimensional mixing time
Π_{22}	$\frac{V_{PZR,0}}{A_{PZR,0} Y_{dvi,0}}$	Ratio of pressurizer head to IRWST line head
Π_{22}/Π_{20}	$\frac{\rho_l g V_{PZR,0}}{A_{PZR,0} P_t}$	Ratio of pressurizer head to containment pressure
Π_{23}	$\frac{\rho_l}{\dot{m}_0}\left(\frac{g Y_{dvi,0}}{R_{dvi,0}}\right)^{1/2}$	Ratio of DVI flow to reference flow

6.4.4 Step 6: IRWST Injection Phase, Selection Of Reference Parameters

The reference values were chosen such that the normalized variables and their derivatives in each equation are of Order one; and we selected the time scale of the system as the time of the mass inventory in the vessel. The details of reference parameter selection for the IRWST phase are presented in Appendix E. The reference parameters are presented in Table 6.22 and the resulting numerical values of the Π groups are given in Table 6.23. Ratios of the Π groups for the experiment facilities relative to AP600 are given in Table 6.24.

Table 6.22. Reference parameters for plant and facilities during the IRWST Injection Phase.

Reference Parameters[a]	AP600	ROSA	SPES	OSU
P_0 (kPa)				
A_{prr} (m^2)				
$\left(\frac{K}{2A^2}\right)_{dvi-both}$ (m^{-4})				
Y_{dvi-0} (m)				
$L_{irwst-0}$ (m)				
V_{v-0} (m^3)				
A_{adv-1} (m^2)				
$\dot{q}_{core}$ (MW)				
Q_{dvi} both (m^3/s)				
ρ_f (kg/m^3)				
x_{core}				
$G_{critical-hem}$ at $2x_{core}$ (kg/m^2-s)				
$G_{critical-hem}$ at x=1.0 (kg/m^2-s)				
$\dot{m}_{ADS4-c}$ (kg/s)				
$\dot{m}_{ADS4-nc}$ (kg/s)				
$\dot{m}_{v-net} = \dot{m}_0$ (kg/s)				
$\dot{m}_{v-net-mod}$ (kg/s)				
t_0 (s)				
$t_{0-osu-cpes}$ (s)				

a. Note that some of the reference parameters from facility to facility are different. This is due to the fact that the facilities are of significantly different scale size. See page 1 of this report.

Table 6.23. Π values for the IRWST Injection Phase.

Π s	AP600	ROSA	SPES	OSU
$\Pi_{7\text{-vessel}}$				
$\Pi_{15\text{-pzr}}$				
Π_{19}				
Π_{20}				
Π_{21}				
Π_{22}				
Π_{22}/Π_{20}				
Π_{23}				

a,c

Table 6.24. Π Ratios between facilities and AP600 for the IRWST Injection Phase.

Ratio	ROSA/AP600	SPES/AP600	OSU/AP600
$\Pi_{7\text{-vessel}}$			
$\Pi_{15\text{-pzr}}$			
Π_{19}			
Π_{20}			
Π_{21}			
Π_{22}			
Π_{22}/Π_{20}			
Π_{23}			

a,c

6.4.5 Step 7: IRWST Injection Phase, Order Of Magnitude Analysis

The equations for flows into and out of the vessel can be substituted into the vessel mass balance equation to provide the following expression

$$\frac{dV^*}{dt^*} = \sqrt{\frac{g_0 L_0 t_0^2}{V_0^2 R'_0}}\left[\frac{g^*}{R'^*}\left(L^*_{irwst} - L^*_{DC} + \Delta Y^* + Y^*_{sparger} - L^*_{PZR} - \frac{\rho^*_{SL}}{\rho^*} Y^*_{SL}\right)\right]^{1/2} - \frac{G_{crit_0} A_0 t_0}{\rho_0 V_0}\frac{G^*_{crit} A^*}{\rho^*} + \frac{0.1 t_0 A_0 \sqrt{g_0 D_0}}{V_0} A^* \sqrt{g^* D^*} \quad (6.55)$$

The dimensionless coefficients are summarized in Table 6.25. The values for the IRWST and ADS-4 flows agree fairly well in the full pressure facilities. In all the facilities the pressurizer

draining flows are lower than the IRWST and ADS-4 flows indicating that this flow is not as important. In all the facilities the relative ordering of the terms is the same.

Table 6.25. Dimensionless parameters for reactor vessel balance equation.

Dimensionless group	Physical meaning	AP600	ROSA	SPES	OSU
$\sqrt{\frac{g_0 L_0 t_0^2}{V_0^2 R'_0}}$	Ratio of IRWST flow to vessel volume				
$\frac{G_{crit_0} A_0 t_0}{\rho_0 V_0}$	Ratio of ADS-4 flow to vessel volume				
$\frac{0.1 t_0 A_0 \sqrt{g_0 D_0}}{V_0}$	Ratio of pressurizer surge line flow to vessel volume				

6.4.6 Step 8: IRWST Injection Phase, Verification with Data

As noted previously, experimental data and calculation results indicate that the minimum vessel inventory is reached during the ADS-4 blowdown phase just prior to the start of IRWST injection. The primary system is mostly saturated at this time, the CMTs are empty or nearly empty, and the break flow rate and ADS-1, -2, -3 flow rates are negligible. Experimental data show that the liquid remaining in the pressurizer begins to drain back into the hot legs during the early part of the IRWST phase. This pressurizer draining can interact with the core refilling process resulting in oscillatory behavior.

As indicated above, the primary consideration for this analysis is the liquid inventory in the vessel as this inventory is the controlling factor for core cooling.

Vessel Mass Balance

The nondimensional mass balance for the vessel (Equation (6.44)) can be rewritten by substituting Equation (6.46) and moving the ADS-4 term to the left-hand side. With the reference parameters selected so that Π_7 is 1 this equation becomes

$$\frac{dV_l^*}{dt^*} + \dot{m}_{ads4}^* = \dot{m}_{dvi}^* + \dot{m}_{pzr}^* \tag{6.56}$$

Equation (6.56) can be integrated with respect to t^* to give the dimensionless liquid volume as

$$\int_0^{t^*} \frac{dV_l^*}{dt^*}\, dt^* + \int_0^{t^*} \dot{m}_{ads4}^* dt^* = \int_0^{t^*} \dot{m}_{dvi}^* dt^* + \int_0^{t^*} \dot{m}_{pzr}^* dt^* \tag{6.57}$$

or

$$V_i^*(t^*) - V_i^*(0) + \int_0^{t^*} \dot{m}_{ads4}^* dt^* = \int_0^{t^*} \dot{m}_{dvi}^* dt^* + \int_0^{t^*} \dot{m}_{prz}^* dt^* \tag{6.58}$$

where the second term on the left-hand side is a constant of integration. Alternate forms of this equation can be written to accommodate the experimental data available. For example, in cases where a usable mass flow rate measurement was not available for the pressurizer a level measurement was substituted and the mass flow rate integral (in dimensional form) calculated as

$$\int_0^t \dot{m}_i dt = \int_0^t \frac{dM_i}{dt} dt = \int_0^t \rho_i A_i \frac{dL_i}{dt} dt = \rho_i A_i L_i(t)\Big|_0^t \tag{6.59}$$

where M is the total mass, A is the cross sectional area, and L is the measured level in the component under consideration (the i^{th} component - pressurizer, catch tank, etc. Most experimental measurements of mass flow consider flow into the pressurizer to be positive in sign and flow out of the pressurizer to be negative in sign so care must be exercised to ensure that the proper sign is associated with the pressurizer mass flows when utilized in Equation (6.58).

Equation (6.58) (or as modified using Equation (6.59)) can be used with experimental data to calculate the nondimensional vessel liquid volume change with dimensionless time for the IRWST phase. As in the ADS-4 blowdown phase, the equation will balance if the mass inflows and outflows have been accounted for. Also, the variables will be of O[1] if reasonable reference scales have been selected and the results of plotting the left hand side of the equation against the right hand side of the equation should have a slope near unity.

Figure 6.17. ROSA, SPES and OSU mass balances in nondimensional coordinates for the IRWST phase.

Figure 6.17 shows the result of computing Equation (6.58) for 1" CLB experiments in ROSA, SPES, and OSU. The integrals were computed over the range $0 \leq t^* \leq 1.5$. The agreement between the facilities is good and in general the data are close to the y = x line.

Figures 6.18, 6.19, and 6.20 show the integrals of the individual mass flow rate components used in Figure 6.17. In all three facilities the IRWST and ADS-4 flows are of similar magnitude and about a factor of 6 larger than the pressurizer draining flow.

The results presented above indicate that the process of scaling the facility data with the appropriate nondimensional residence time as determined by the Π_7 group was successful and that the basic behavior is similar. Differences noted in results are explicable in light of facility design differences and/or modeling assumptions. The reference scales developed in this analysis are reasonable given the design of the individual facilities in that the reference time scale for the AP600 plant calculation and the ROSA facility are roughly equal as expected. The OSU facility reference time scale is on the order of one-half the time scale for the ROSA facility and the plant calculation as expected.

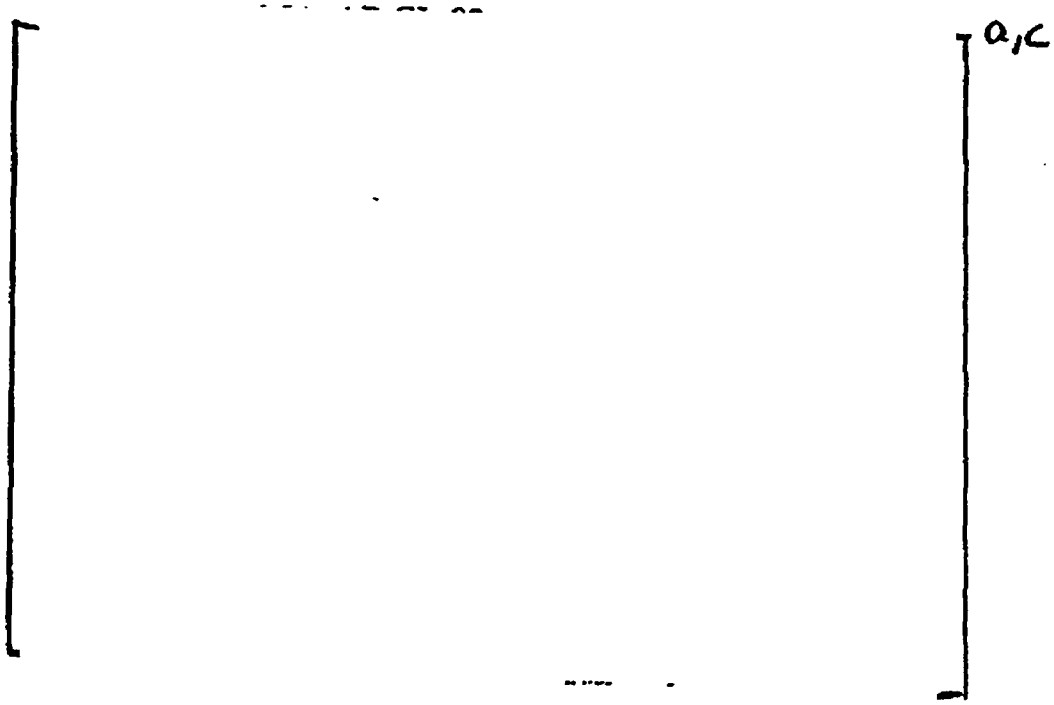

Figure 6.18. ROSA experiment AP-CL-03 mass balance component integrals versus nondimensional time for the IRWST phase.

Figure 6.19. SPES experiment S00401 mass balance component integrals versus nondimensional time for the IRWST phase.

Figure 6.20. OSU experiment SB 5 mass balance component integrals versus nondimensional time for the IRWST phase.

Vessel Outflow

Figure 6.21 shows a comparison of integrated ratios of the ROSA AP-CL-03 ADS-4 measured mass flux for the IRWST phase of the transient divided by the mass flux from the frozen flow assumption used to establish the reference ADS-4 mass flow rate. Also shown for reference are results from the HEM model also ratioed to the frozen flow assumption. The HEM model was evaluated using the vessel upper head pressure and a range of qualities as input. As discussed above for the ADS-4 blowdown phase, the frozen flow assumption produced a reference flow rate value that was quite close to the average of the measured data. This observation holds true for the IRWST phase as well. From Figure 6.21, it is observed that the integral of the measured data divided by the reference mass flux compares well to the reference which in this case is the line y = x. The average mass flux based on the data shown in Figure 6.21 is [ ]a,c whereas the frozen model value is [ ]a,c Note that the measured integrated mass flux ratio is bounded by the HEM model for the quality range $0.3 \le x \le 0.5$. The results in Figure 6.21 indicate that the HEM model as used above produces a reasonable ADS-4 reference flow scale for the ROSA experiment.

Figure 6.22 shows the ratio of the ADS-4 mass flux for the SPES experiment and the reference value integrated in dimensionless time along with HEM values also divided by the reference mass flux. The average of the measured mass flux was about [ ]a,c which is in good agreement

Figure 6.21. ROSA experiment AP-CL-03 ADS-4 integrated normalized mass flux ratio for IRWST phase and homogeneous equilibrium model.

Figure 6.22. SPES experiment S00401 ADS-4 integrated normalized mass flux ratio for IRWST phase and homogeneous equilibrium model.

with the reference frozen flow assumption and is close to the HEM value for quality of 0.1. The results in Figure 6.22 indicate that the HEM flow assumption as used above produces a reasonable reference flow scale for the SPES experiment.

As was the case for ADS-4 blowdown, the frozen flow assumption did not produce a usable reference flow rate value for the IRWST phase in the OSU SB5 experiment since the ADS-4 does not appear to be choked. Even though the ADS-4 valve is not choked in the SB5 experiment, the integrated measured mass flux ratio is compared to the HEM model in Figure 6.23 for reference. The results in Figure 6.23 suggest that the HEM model evaluated at low quality (5-10%) can be used to estimate a reference ADS-4 discharge flow for the OSU experiment.

Figure 6.23. OSU experiment SB5 ADS-4 integrated normalized mass flux ratio for IRWST phase and homogeneous equilibrium model.

Vessel Inflows

We now turn to the examination of the IRWST flow since this flow is one of the major components in the vessel mass balance. The IRWST line equation contains Π groups which contain line resistance, reference pressure, the reference IRWST flow, and reference elevation or head terms but not the line inertia since the order of magnitude analysis indicated that the inertial term in the line equation can be neglected. With the estimates of the IRWST/DVI line resistances given in Appendix B, the line equation can be used to show that the data collapse. From Equation (6.51), the DVI line normalized volumetric flow can be expressed as

$$Q^*_{dvi} = \left[\left(\Delta Y^* - \Pi_{19} L^*\right) + \Pi_{20}\left(1 - P^*_V\right)\right]^{1/2} \tag{6.60}$$

or in terms of nondimensional mass flow

$$\dot{m}^*_{dvi} = \Pi_{23} Q^*_{dvi} = \Pi_{23}\left[\left(\Delta Y^* - \Pi_{19} L^*\right) + \Pi_{20}\left(1 - P^*_V\right)\right]^{1/2} \tag{6.61}$$

where as previously, P_t and the IRWST level are assumed essentially constant and the definitions for P, L, and ΔY are the same as discussed in the context of Equation (6.51). Note that Equation (6.61) is written in terms of mass flow and the Π groups are thus defined as

$$\Pi_{19} = \frac{V_0}{A_0 Y_{dvi,0}}$$

$$\Pi_{20} = \frac{P_t}{\rho_l g Y_{dvi,0}} \tag{6.62}$$

$$\Pi_{23} = \frac{\rho_l}{\dot{m}_0}\left(\frac{g Y_{dvi,0}}{\dot{R}_{dvi,0}}\right)^{1/2}$$

As was done for the CMTs, the IRWST tank and DVI line equations could be combined to express the relationship between the various nondimensional groups. However, as mentioned above, the IRWST level was assumed to remain essentially constant for the IRWST refill phase due to the large size of the tank. As such, we can simply integrate both sides of Equation (6.61) to get the following expression

$$\int_0^{t^*} \dot{m}^*_{dvi} dt^* = \int_0^{t^*} \Pi_{23}\left[\left(\Delta Y^* - \Pi_{19} L^*\right) + \Pi_{20}\left(1 - P_V^*\right)\right]^{1/2} dt^* \tag{6.63}$$

that we can apply to the data. Figures 6.24 through 6.26 show the result of this where the measured dvi normalized mass flow rate is plotted on the ordinate and the right hand side of Equation (6.63) is plotted on the abscissa. As shown in the figures the data are close to the y = x line indicating that the Π groups and reference parameters are correct.

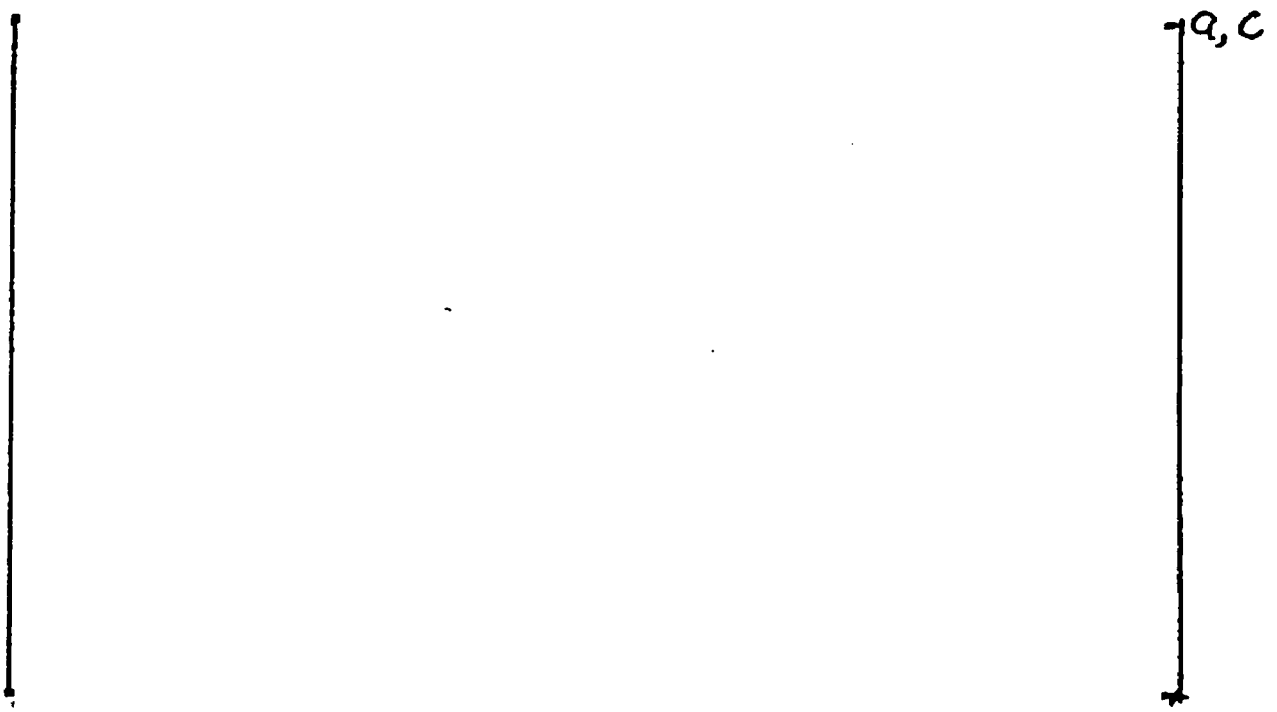

Figure 6.24. ROSA AP-CL-03 IRWST tank level - DVI line parameter relationship in nondimensional coordinates.

Figure 6.25. SPES S00401 IRWST tank level - DVI line parameter relationship in nondimensional coordinates.

Figure 6.26. OSU SB5 IRWST tank level - DVI line parameter relationship in nondimensional coordinates.

Analytic Solution for Vessel Level

As shown in Appendix F the vessel level equation can be simplified and solved analytically with asymptotic solutions for the cases of nondimensional time being large and small. The short time solution is

$$V_l^*(t^*) - V_l^*(0) = \frac{2}{3}\Pi_{23}\left[\left(\Pi_{22}\Pi_{15}\dot{m}_{pzr}^* - \Pi_{20}\frac{dP_{pzr}^*}{dt^*}\right)^{\frac{1}{2}}\right]t^{*3/2} - \left(\dot{m}_{ADS4}^* - \dot{m}_{pzr}^*\right)t^* \qquad (6.64)$$

which takes on the following coefficients for the experimental facilities.

ROSA: [ ]a,c

SPES:

OSU:

The solution for large values of t^* is

$$V_l^*(\infty) - V_l^*(t^*) = \left[V_l^*(\infty) - V_l^*(0)\right]\exp\left[-\Pi_{23}\Pi_{19}t^*/(2Q_{dvi}^*(\infty))\right] \qquad (6.65)$$

which takes on the following coefficients for the experimental facilities.

ROSA: [ ]a,c

SPES:

OSU:

These solutions are plotted with data from 1" CLB experiments in Figures 6.27, 6.28, and 6.29 for the experimental facilities. The agreement with data is generally good at early and late times. This quality of agreement provides additional credence for the scaling estimates of the dominant processes.

Discussion of Reference Parameters - Selection With and Without Data Knowledge

As discussed in Section 6.3, if no experimental information is available, reference parameters must be selected in a blind fashion, that is without benefit of data knowledge. Experimental information can, however, be used to support or confirm reference parameter selection if such is available. Thus values for reference parameters can be selected from a "without-data" view as though there is no experimental information and from a "with-data" view using knowledge about available experimental information. Comparisons between the parameters selected using the two

Figure 6.27. Analytic solution for vessel level with data from ROSA experiment AP-CL-03.

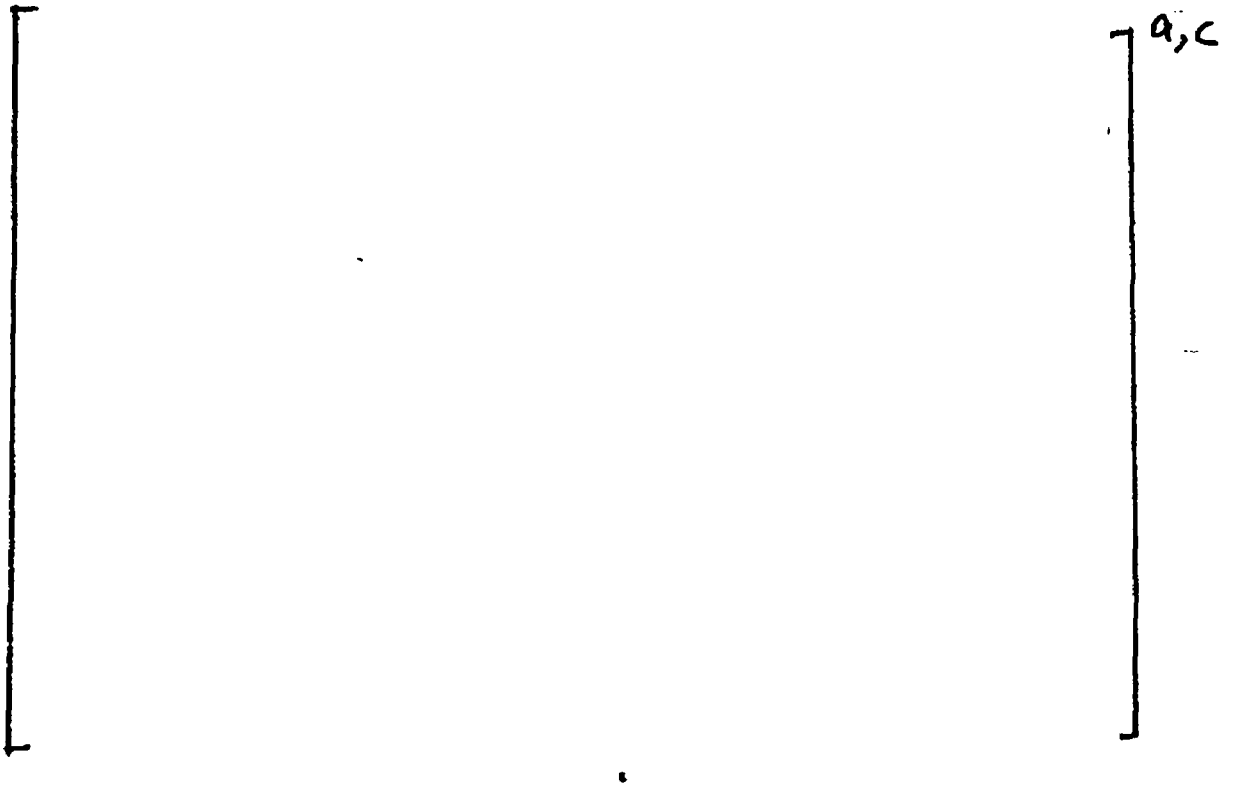

Figure 6.28. Analytic solution for vessel level with data from SPES experiment S00401.

Figure 6.29. Analytic solution for vessel level with data from OSU experiment SB5.

views helps assure that reasonable reference values have been selected. Here we summarize observations regarding selection of reference parameters using the two approaches.

In both cases (without-data and with-data), the vessel time scale was determined from the Π_7 group and the vessel volume above the bottom of the heated length was selected as the vessel reference volume. For both cases, the system reference pressure at the initiation of the IRWST injection phase was selected to be the hydrostatic head imposed on the vessel by the water level in the IRWST plus atmospheric pressure. Thus for each of the experiments, the without-data view and the with-data view arrived at the same reference pressure. Reference liquid and vapor properties and saturation temperature were selected based on this reference pressure and are thus consistent between the two views. The reference flow for the vessel was selected to be a net flow based on a reference inflow minus a reference outflow. In both cases, the inflow was the reference IRWST injection flow and the outflow was based on a reference ADS-4 flow.

As discussed above, the reference ADS-4 outflow for the without-data view was based on application of the HEM model evaluated at a quality of about 30% for the ROSA experiment and 10% for the SPES experiment. The HEM model at low quality (1-5%) was used to establish a reference ADS 4 flow for the OSU experiment. Review of the experimental data indicated these scale selections were reasonable and consistent with the with-data approach of using a simple frozen flow model for the ROSA and SPES facilities (and the plant) since the ADS-4 discharge quality is not known. In the frozen flow model, it was assumed that the ADS-4 discharge is

saturated steam leaving the system at the vapor sound speed for a quality of unity. For the OSU experiment the frozen flow assumption did not apply since the ADS 4 is not choked during IRWST injection and the measured data average was used in the with-data view.

The reference IRWST flow was computed for both the without-data and with-data views using line resistances and assumptions about the reference head driving the IRWST flow. The net flow scale was the difference between a reference IRWST flow and the reference ADS-4 discharge flow. This approach produced net reference flows for the two different views that were reasonably consistent for the ROSA and SPES experiments and thus produced vessel time scales that were of similar order (within 50%). In general the without-data approach produced time scales that were less than the time scales derived from the with-data approach. Part of the difference stems from the underestimation of the quality used in the HEM model and overestimation of the IRWST reference flow rate which in turn resulted in a net flow scale that was too large and hence a time scale that was smaller than estimated based on the data.

Nominal facility geometric parameters (such as hardware elevation changes) were used in the without-data and with-data viewpoints. Furthermore, both approaches independently evaluated line resistances for use in the computation of reference flow rates for the IRWST flow. Examination of the Π groups evaluated for the DVI lines indicate that the internal and external approaches are consistent and the major factor influencing the numeric values of the Π groups is related to the calculated time scale differences discussed above.

6.4.7 Concluding Remarks

The ADS-4, pressurizer, and IRWST flows were shown to be the major terms influencing the vessel mass balance. Reference parameters for the dimensionless residence time group controlling the vessel mass balance were determined and used to conduct mass balances for the facility data to show that the major sources and sinks were accounted for. The HEM model was used to estimate the reference ADS 4 flow and the IRWST reference flow was estimated using line resistance and a nominal driving head. For the OSU experiment reference ADS-4 flow, a value calculated using the HEM model with a quality of 1-5% was shown to agree reasonably well with the data although the ADS-4 flow was not believed to be choked. This result suggests that the friction dominated ADS 4 flowrate is close to the low quality HEM value and that the HEM value is useful for specifying the reference.

The DVI flows and IRWST tank level were examined using the equations developed for the system to demonstrate the application of the methodology for flows that influence the vessel mass balance. Average resistance values and other reference parameters were used to numerically evaluate Π groups for the IRWST tank and DVI line(s). The dimensionless form of the equations along with the Π groups were used to show that the DVI flows and parameters influencing the net head (vessel level and pressure) data collapse in the expected fashion. This result adds validity to the correctness of the equations and the dimensionless groups involved and provides a consistency check.

As expected, due the large cross sectional area of the IRWST tanks in the facilities, the Π group scaling the level change ($\Pi_{15\text{-}dvi}$) in the tank with the flow out of the tank is very small relative to the Π groups scaling the DVI line(s) flow ($\Pi_{1\text{-}dvi}$, $\Pi_{2\text{-}dvi}$, and $\Pi_{3\text{-}dvi}$) with the system levels and pressures. This result simply means that the IRWST is a large source and the level change is small for the flow rates involved during IRWST injection.

Based on review and evaluation of the dimensionless groups and equations, transient or line inertia effects were not expected to be of importance. Examination of the data indicates this expectation to be true.

Values of the dimensionless groups resulting from the IRWST phase indicate that the facility values bound the plant values. This result suggests that the plant behavior is bounded by the experimental data and that the data are applicable for code adequacy evaluations.

6.5 IRWST Drain (Long Term Cooling) Phase

The IRWST draining phase is a relatively long period at the beginning of the long term cooling phase. Of the three test facilities, only OSU is partially equipped to represent aspects of this phase. OSU has a sump tank, but it does not have a containment and there is not condensate return to the IRWST. In this section, we apply the scaling methodology using the OSU test results available. The steps, as listed earlier, are applied to this phase in the following fashion.

6.5.1 Step 1: IRWST Drain (Long Term Cooling) Phase Description

The IRWST draining phase begins when the IRWST starts to inject coolant into the primary system. The IRWST injection phase analyzed in the previous section is a small portion at the very beginning of the IRWST draining phase. During this initial period, the vessel refills and the pressurizer empties much faster than the IRWST drains and therefore, the IRWST level can be assumed constant. Right after the vessel has refilled, however, the next dominant process is the draining of the IRWST, with a much larger time scale. After the relatively short transient at the beginning of this phase, the vessel level adjusts to a declining IRWST level, and the phase ends when the IRWST reaches the elevation that triggers the opening of motor valves that connect the IRWST directly with the Sump. At this point, both tanks quickly reach a common level above the DVI line and the hydraulic behavior reaches a quasi-steady state. That event is what we have chosen to call the end of the IRWST draining phase and the beginning of the long term cooling phase.

6.5.2 Steps 2 and 3: IRWST Drain (Long Term Cooling) System Components and Topology

Figure 6.30 is a schematic description of the system configuration at the beginning of IRWST draining. The components involved are:

- The IRWST that supplies the head and the coolant for the primary system.
- The DVI lines through which the coolant gets into the system. Check valves in all these lines prevent backflow from the system into the IRWST.
- The vessel, which continues to be the focal point of our interest, but no longer dictates the time scale of the phase.
- The upper head steam volume, whose pressure opposes DVI flow and drives ADS-4 flow.
-
- The core that provides energy to boil the incoming flow and is a resistance to flow.
- The hot legs where fluid can accumulate and be held up by the steam outflow.

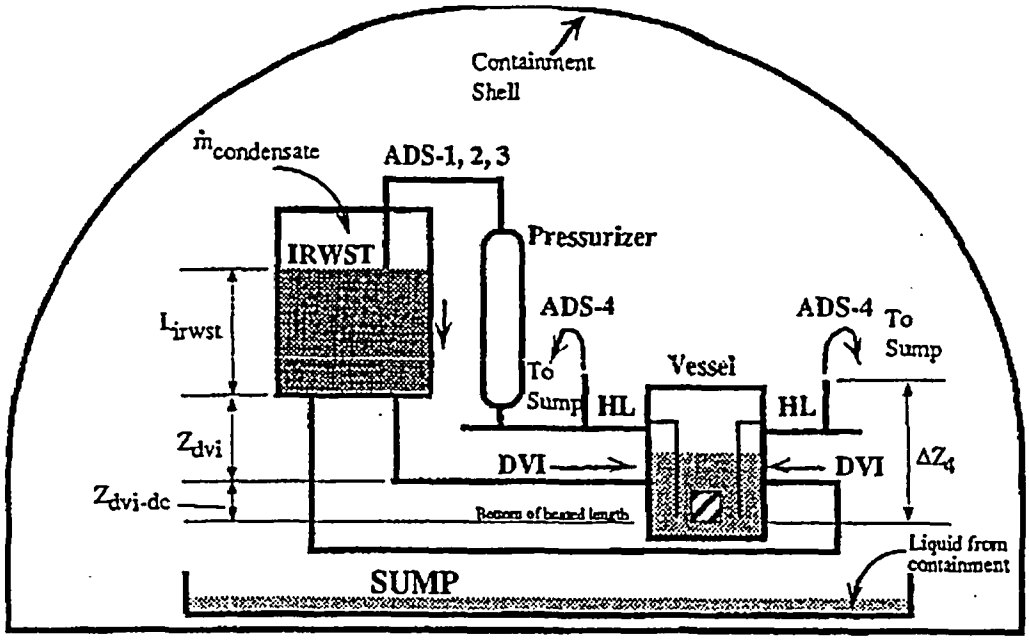

Figure 6.30. System configuration during IRWST draining (prior to sump injection).

- The ADS-4 valves and lines through which the primary dumps inventory into the containment.

- The containment that now interacts with the primary by affecting the exit pressure of ADS-4 and the energy level of the coolant in the IRWST.

6.5.3 Step 4: IRWST Drain (Long Term Cooling) Governing Equations

The development of the governing equations and corresponding assumptions is given in Appendix G. We begin this section with the nondimensional equations that resulted from that development.

$$\rho_f^* A_{it}^* \frac{dL_{it}^*}{dt^*} = \frac{\dot{m}_0 t_0}{\rho_0 A_0 L_0}\left(\dot{m}_{g-ads4}^* - \dot{m}_{dvi}^*\right) \tag{6.66}$$

$$\frac{dT_{it}^*}{dt^*} = \frac{\dot{m}_0 t_0}{\rho_0 L_0 A_0}\left(\dot{m}_{g-ads4}^* c_p^* T_{cont.}^* - \dot{m}_{dvi}^* c_p^* T_{it}^*\right) + \frac{U_0 A_{it-w0} \Delta T_0 t_0}{\rho_0 c_{p0} L_0 A_0 T_0} U_{it}^* A_{it-w}^* \left(T_{cc}^* - T_{it}^*\right) \tag{6.67}$$

$$\left(M_{it-cc}^* c_{p-cc}^*\right)\frac{dT_{it-cc}^*}{dt^*} = \left(\frac{U_0 A_{it-w0} \Delta T_0 t_0}{M_{it-cc} c_{pcc0} T_0}\right) U_{it}^* A_{it-w}^* \left(T_{it}^* - T_{it-cc}^*\right) \tag{6.68}$$

$$\left(\frac{L}{A}\right)^*_{dvi}\frac{d\dot{m}^*_{dvi}}{dt^*}=\left(\frac{\rho_0 g Y_0 t_0}{(L/A)_0\dot{m}_0}\right)\rho^*_f\left(L^*_{it}+Z^*_{dvi}+Z^*_{dc-dvi}\right)$$
$$-\left(\frac{\rho_{ads4-0}g\Delta Z_0 t_0}{(L/A)_0\dot{m}_0}\right)\rho^*_{ads4}\Delta Z^*_4$$
$$-\frac{\dot{m}_0 t_0}{2\rho_0(L/A)_0}(K/A^2)_{dvi-0}\frac{\dot{m}^{*2}_{dvi}}{\rho^*_f}(K/A^2)^*_{dvi} \qquad (6.69)$$
$$-\frac{\dot{m}_0 t_0}{2\rho_{ads4-0}(L/A)_0}(K/A^2)_{ads4-0}\frac{\dot{m}^{*2}_{ads4}}{\rho^*_{ads4}}(K/A^2)^*_{ads4}$$

$$\frac{dT^*_{lp}}{dt^*}=\left(\frac{\dot{m}_0 t_0}{\rho_0 V_0}\right)\frac{\dot{m}^*_{dvi}}{\rho^*_f V^*_{lp+dc}}\left(T^*_{it}-T^*_{lp}\right) \qquad (6.70)$$

The coefficients in these equations are the Π groups for this phase of the transient. Table 6.26 summarizes these groups. Most have been encountered and defined in the analysis of other phases. Two new groups appear, both related to heat transfer in the IRWST. Physical interpretation of the groups is given below.

Table 6.26. Nondimensional coefficients (Πs) for the IRWST draining phase.

Π group	Definition	Description
Π_2	$(\rho_0 g Y_0 t_0) / ((L/A)_0\dot{m}_0)$	Ratio of line head to line momentum
Π_3	$(\dot{m}_0 t_0(K/A^2)_0) / (2\rho_0(L/A)_0)$	Ratio of line friction to line momentum
Π_7	$(\dot{m}_0 t_0) / (M_{l0})$	Ratio of system time to vessel emptying time
Π_9	$(\dot{m}_0 t_0) / (\rho_0 V_0)$	Ratio of system time to transit time through lower vessel vols.
Π_{15}	$(\dot{m}_0 t_0) / (\rho_0 A_0 L_0)$	Ratio of system time to tank emptying time
$\Pi_{18\text{-}f}$	$(U_0 A_{w0}\Delta T_0 t_0) / (\rho_0 c_{p0} L_0 A_0 T_0$	Ratio of heat transferred to/from fluid to fluid internal energy
$\Pi_{18\text{-}w}$	$(U_0 A_{w0}\Delta T_0 t_0) / (c_{cc\text{-}p0} M_{cc0} T_0)$	Ratio of heat transferred to/from fluid to wall internal energy

6.5.4 Step 6: IRWST Drain (Long Term Cooling) Selection of Reference Parameters

The next step in the methodology is the selection of reference values that will enable conduct of the order of magnitude analysis and thus obtain a reduced set of equations and Πs. The parameters are the reference values that define the Π groups and, as before, they are chosen to make the asterisked terms in the equations O[1]. Several of the parameters listed in Table 6.26 are derived from more basic parameters such as pressure. The following list defines those needed for Order of Magnitude Analysis.

P_0 Reference system pressure, (upper head pressure) is taken as the sum of the containment pressure and the head of liquid above the hot legs.

$$P_0 = \rho_0 g(L_{ir-0} + Z_{dvi}) + P_{containment} \quad (6.71)$$

where $P_{containment}$ is assumed to be a fixed boundary condition equal to 101.34 kPa (1 atm).

ρ_0, h_{fg0}, c_{p0} The liquid and vapor properties are taken as saturation at P_0.

ρ_{ads4-0} In lieu of a bottom-up correlation for the phase separation in the hot-leg ADS-4 tee, we assume that all of the fluid is leaving the system through the ADS-4 and evaluate a reference density as follows:

$$\rho_{ads4-0} = \frac{\dot{m}_0^2 R_{ads4}}{P_b - P_{containment}} \quad (6.72)$$

x_{core} Core exit quality is needed to evaluate the fractions of liquid and gas leaving the system. The quality is based on a core energy balance as:

$$x_{core} = \frac{\dot{q}_0 - \dot{m}_{dvi-0} c_{p0} (T_{sat-0} - T_{ir-0})}{\dot{m}_{dvi-0} h_{fg0}} \quad (6.73)$$

$\dot{q}_0$ Core heat generation is taken to be the corresponding decay heat at 10,000 seconds.

$\left(\frac{K}{2A^2}\right)_0$ Reference line hydraulic resistance will be the line resistance for the line. Ratios of resistances between interacting lines will appear as nondimensional coefficients.

$(L/A)_0$ The inertia of a line will be its own reference. As with the resistances, ratios of inertia parameters between interacting lines will appear as nondimensional coefficients.

$\dot{m}_0$ The characteristic mass flow of the system is the mass flow through the DVI lines, assuming reference values of head, $\dot{q}_0$, and ρ_0. The equations are solved for steady-state to obtain a value for $\dot{m}_0$.

M_0 Each participating tank has a characteristic liquid mass. For example, for the vessel it is the mass of liquid that would occupy the core region and the upper plenum.

$$M_{tank-0} = \rho_0 L_0 A_0 = \rho_0 V_{tank} \quad (6.74)$$

M_{cc} The tank wall involved in the heat transfer is assumed to be the mass of the concrete wall and floor, about 0.3048 m deep (1 ft), in contact with the liquid. The result for AP600 is about 626,000 kg of concrete in contact with the IRWST water. Note that the IRWST and sump in OSU do not have concrete walls.

U_0 The reference heat transfer coefficient is evaluated in Appendix G. Using the values given there (w_{cc} of [redacted] a w_{steel} of [redacted] an estimated h_{tank} of about [redacted] (for natural convection on a vertical wall)), and the thermophysical properties of concrete and steel listed in Table G-2 of Appendix G.

$$U_{it-0} = \left[\right. \qquad \left.\right] \tag{6.75}$$

Note that the contributions of the steel and the convective heat transfer coefficient to the overall coefficient are very small.

t_0 If the IRWST is the only reservoir draining into the primary, this is the drain time up to the point of SUMP activation

$$t_0 = M_{tank} / \dot{m}_0 \tag{6.76}$$

6.5.5 Step 7: IRWST Drain (Long Term Cooling) Order Of Magnitude Analysis

Having chosen reference parameters, one can now evaluate the numerical values of the nondimensional coefficients and determine, from the governing equations, which processes are faster and slower than the main process (draining of the IRWST), and reduce the number of dynamic equations.

Starting in the same order as they are written before, we have the IRWST equation first. The selection of the characteristic time makes this nondimensional coefficient identical to one.

$$\rho_f^* A_{it}^* \frac{dL_{it}^*}{dt^*} = \left(\dot{m}_{g-ads4}^* - \dot{m}_{dvi}^*\right) \tag{6.77}$$

A cursory evaluation of quality at the ADS-4 (using P_0 and ρ_{ads4-0}) indicates that $\dot{m}_{g-ads4}^*$ is a small fraction, between [redacted] (OSU) and [redacted] (AP600) of the reference flow. Thus indicating that the $\dot{m}_{dvi}^*$ dominates the draining of this tank. A similar analysis of the energy balance equation indicates that the convective heat transfer (mixing of flows in and out) is dominating the thermal response of the tank.

$$\frac{dT_{it}^*}{dt^*} = \left(\dot{m}_{g-ads4}^* c_p^* T_{cont.}^* - \dot{m}_{dvi}^* c_p^* T_{it}^*\right) \tag{6.78}$$

Furthermore, the energy balance for the wall material indicates that given the values obtained for Π_{18-w}, this process is much to slow to actively participate in the dynamics of the tank. Therefore, the wall temperature maybe assumed constant for this phase.

$$\left(M_{it-cc}^* c_{p-cc}^*\right)\frac{dT_{it-cc}^*}{dt^*} = \Pi_{18-it-w} U_{it}^* A_{it-w}^* \left(T_{it}^* - T_{it-cc}^*\right) \tag{6.79}$$

The DVI line coefficients are large with respect to $\Pi_{15\text{-}it}$ (1.0) so the line can be assumed to respond rapidly. The momentum equation can be converted to an algebraic form neglecting the dynamic term in the left hand side or

$$0=\Pi_{2-dvi}\rho_f^*\left(L_{it}^*+Z_{dvi}^*+Z_{dc-dvi}^*\right)-\Pi_{2-ads4}\rho_{ads4}^*\Delta Z_4^* -\Pi_{3-dvi}\frac{\dot{m}_{dvi}^{*2}}{\rho_f^*}\left(K/A^2\right)_{dvi}^*-\Pi_{3-ads4}\frac{\dot{m}_{ads4}^{*2}}{\rho_{ads4}^*}\left(K/A^2\right)_{ads4}^* \tag{6.80}$$

which can be manipulated further to produce

$$\rho_f^*\left(L_{it}^*+Z_{dvi}^*+Z_{dc-dvi}^*\right)=\frac{\Pi_{3-dvi}}{\Pi_{2-dvi}}\frac{\dot{m}_{dvi}^{*2}}{\rho_f^*}\left(K/A^2\right)_{dvi}^* +\frac{\Pi_{3-ads4}}{\Pi_{2-dvi}}\frac{\dot{m}_{ads4}^{*2}}{\rho_{ads4}^*}\left(K/A^2\right)_{ads4}^*+\frac{\Pi_{2-ads4}}{\Pi_{2-dvi}}\rho_{ads4}^*\Delta Z_4^* \tag{6.81}$$

Since $\dot{m}_{dvi}\approx\dot{m}_{ads4}$, the above equation can be re-written as

$$\dot{m}_{dvi}^{*2}\left(\frac{\Pi_{3-dvi}}{\Pi_{2-dvi}}\frac{\left(K/A^2\right)_{dvi}^*}{\rho_f^*}+\frac{\Pi_{3-ads4}}{\Pi_{2-dvi}}\frac{\left(K/A^2\right)_{ads4}^*}{\rho_{ads4}^*}\right)=\rho_f^*\left(L_{it}^*+Z_{dvi}^*+Z_{dc-dvi}^*\right)-\frac{\Pi_{2-ads4}}{\Pi_{2-dvi}}\rho_{ads4}^*\Delta Z_4^* \tag{6.82}$$

Note in Equation (6.82) that ratios of nondimensional groups multiply the asterisked variables. Table 6.27 lists these ratios for the plant and the OSU facility.

Table 6.27. Summary of relevant Π groups, Π ratios, and nondimensional reference quantities during the IRWST draining phase.

Group or ratio	AP600	OSU	AP600/OSU
$Z_{dvi}^*+Z_{dc-dvi}^*$			
Π_{2-ads4}/Π_{2-dvi}			
$(\Pi_{3-dvi}+\Pi_{3-ads4})/\Pi_{2-dvi}$			

Based on the order of magnitude analysis, using the values listed in Table 6.27, and on the system configuration, the main features of the system performance during this phase are described by a set of two dynamic and two algebraic equations.

The DVI line mass flow is

$$\dot{m}_{dvi}^{*2}=\frac{L_{it}^*+Z_{dvi}^*+Z_{dc-dvi}^*-\dfrac{\Pi_{2-ads4}}{\Pi_{2-dvi}}}{\dfrac{\Pi_{3-dvi}}{\Pi_{2-dvi}}+\dfrac{\Pi_{3-ads4}}{\Pi_{2-dvi}}} \tag{6.83}$$

The core exit quality is

$$x_{core}=\frac{\dot{q}_0-\dot{m}_{dvi-0}c_{p0}\left(T_{sat-0}-T_{ir-0}\right)}{\dot{m}_{dvi-0}h_{fg0}} \tag{6.84}$$

where we assume that $x_{ads4} \approx x_{core}$.

The IRWST tank level is

$$\frac{dL_{ir}^{*}}{dt^{*}} = (x_{ads4} - 1)\dot{m}_{dvi}^{*} \tag{6.85}$$

and the IRWST liquid temperature is

$$\frac{dT_{ir}^{*}}{dt^{*}} = \dot{m}_{dvi}^{*}\left(x_{ads4}T_{cont.}^{*} - T_{ir}^{*}\right) \tag{6.86}$$

6.5.6 Step 8: IRWST Drain (Long Term Cooling) Verification with Data

Verification with data is the final step in the methodology, and the one in which the assumptions are tested. In this particular case, there is no data available that encompasses all of the processes. OSU tests have a sump tank, which is intended to simulate the sump and the sump injection later on; but it does not have a containment or condensate return ($\dot{m}_{condensate}$) to the IRWST. According to the reference values, the condensate return, $\dot{m}_{condensate}$, is a small fraction of $\dot{m}_{dvi}$ and can be neglected.

For the application of the methodology, the order of magnitude analysis points to the following processes:

The DVI line mass flow

$$\dot{m}_{dvi}^{*2} = \frac{L_{ir}^{*} + Z_{dvi}^{*} + Z_{dc-dvi}^{*} - \dfrac{\Pi_{2-ads4}}{\Pi_{2-dvi}}}{\dfrac{\Pi_{3-dvi}}{\Pi_{2-dvi}} + \dfrac{\Pi_{3-ads4}}{\Pi_{2-dvi}}} \tag{6.87}$$

and the IRWST tank draining

$$L_{ir}^{*} = -\int \dot{m}_{dvi}^{*} dt^{*} \tag{6.88}$$

Figure 6.31 shows the data from several OSU SBLOCA tests plotted according to Equation (6.87). The data basically fall on a straight line as expected. During the startup transient (when the IRWST flow is just starting) shown on the right hand side of Figure 6.31, the DVI flow rapidly reaches a steady value given by Equation (6.87). It is seen that the IRWST drain is essentially a series of steady-state points wherein the flow rate is given by Equation (6.87). Clearly, the data indicate a linear relationship between the square of the DVI flow rate and the head and resistance terms as expected.

Figure 6.31. Left and right sides of Equation (6.87) SBLOCA scenarios in the OSU facility.

6.5.7 Concluding Remarks

For the IRWST Drain Phase, the scaling analysis indicates that the IRWST drain time determines the time scale of the system and this time scale is much larger than the vessel residence time. As such, the drain down is basically a series of steady-state points wherein the flow rate through the DVI, core, and out the ADS-4 valves depends primarily on the IRWST water level and, to a lesser extent, the ratio of the hydraulic resistances in the DVI and ADS-4 trains. The head parameters and resistance ratios that determine the DVI flow rate for the drain down are well preserved in the OSU facility relative to the AP600. As shown in Table 6.27, the ratios of the nondimensional groups between the OSU facility and the AP600 are very close to unity suggesting that the behavior shown in Figure 6.31 should be representative of the plant.

6.6 IRWST/Sump Injection (Long Term Cooling) Phase

The Sump Injection phase is defined to begin after the IRWST Draining phase has proceeded to a point where the Sump level has increased to a height near or at the so-called curb level which causes activation of check valves and motor-operated valves that allow communication between the IRWST and Sump. The Sump level thereafter remains at this constant value and the system is near steady-state.

6.6.1 Step 1: IRWST/Sump Injection (Long Term Cooling) Phase Description

The Sump level continues to increase during the IRWST draining period due to the influx of primary fluid from the break and ADS-4 discharge. When the Sump level exceeds the IRWST level, check valves connecting the Sump to the DVI lines open allowing Sump injection to commence. Motor operated recirculation valves in the Sump lines open when the IRWST low level set point (1.37 m above the IRWST bottom in the AP600) is reached allowing the levels in the Sump and IRWST to equilibrate. During the Sump Injection phase, the system operates in a quasi steady-state with liquid flowing from the Sump and IRWST into the IRWST and DVI lines and finally into the primary by virtue of the gravity head. The core decay energy heats and evaporates a portion of this fluid producing steam which flows along with entrained water from the vessel into the hot legs and out the ADS-4 valves. The core decay power and the steaming rate are slowly decreasing and the primary system pressure is near atmospheric pressure. The core inlet temperature will be near saturation temperature.

This phase corresponds to the time after Sump injection has been initiated, all hydraulic transients have died out and the only parameter that changes slightly with time is the core decay heat. The Sump and IRWST constitute a large reservoir of water that remains at a constant fixed level. Water enters the vessel through the DVI lines and leaves through the ADS-4 lines. The ADS-4 valves discharge at an elevation above the Sump liquid level and the circulation through the vessel is caused by the density difference between the cold incoming fluid and the warmer outgoing two-phase mixture. The steam discharged from the primary condenses on the containment walls and returns to the IRWST while the liquid discharged flows into the sump.

From a top-down perspective, the distribution of void in the hot-side (above the core, upper plenum, hot legs, and ADS-4 discharge) of the system is unknown. However, since the major analysis focus is on the vessel inventory, simplifying assumptions about void distribution in the vessel are made to achieve closure.

6.6.2 Steps 2 and 3: IRWST/Sump Injection (Long Term Cooling) System Components and Topology

The system configuration and components involved during the Sump Injection phase are depicted schematically in Figure 6.32. This figure shows the basic level relationships and important system components during this phase. The sump is connected to the primary system DVI lines through two separate piping trains each consisting of check valves and motor operated valves.

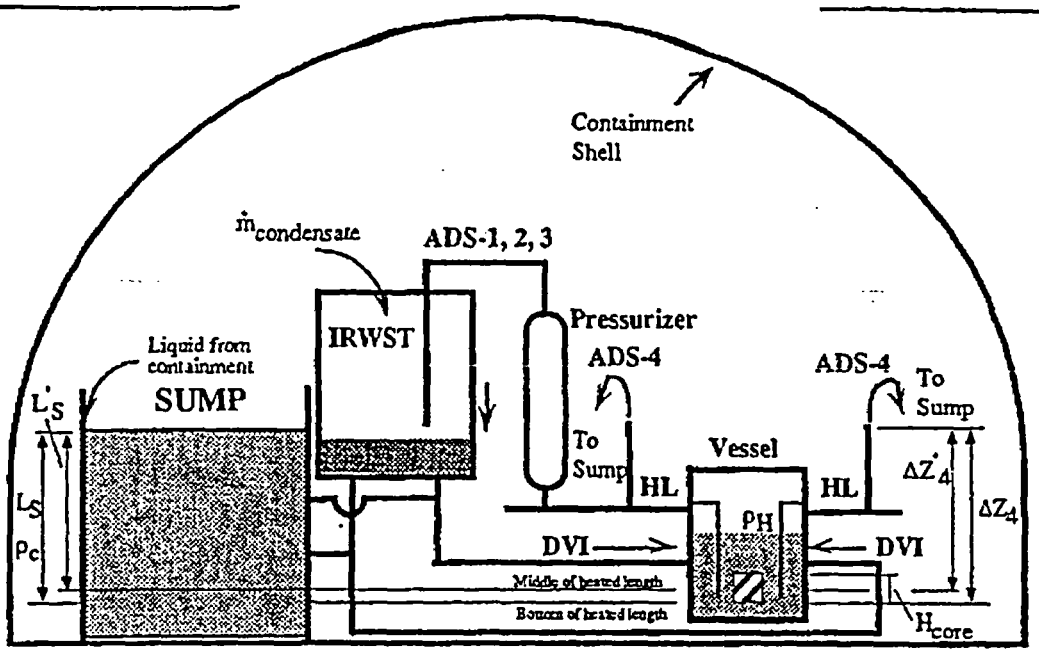

Figure 6.32. Schematic for Long Term Cooling Phase (after Sump injection) showing components involved.

Figure 6.32 depicts the time at which the sump level has exceeded the IRWST level, the check valves have opened, and the recirculation valves have opened allowing the sump and IRWST levels to equilibrate at a level above the DVI line elevation.

As shown in Figure 6.32, during the Sump Injection Phase, the IRWST and sump are effectively connected together and constitute a single large reservoir of inventory that supplies fluid at constant head to the primary system via the DVI lines. In addition to the Sump, the components that participate during the IRWST Drain Phase are also active during the sump injection phase and include the IRWST, Sump, the DVI lines, the ADS-4 valves and lines, the vessel, the core, and the containment.

As indicated in Figure 6.32, the cold side fluid density is assumed to be ρ_C, the hot side fluid density is ρ_H, the fluid density through the core is assumed to vary linearly from ρ_C to ρ_H, and the fluid mixture is homogeneous from the top of the core (heated length) to the ADS-4/hot leg tee connection. Furthermore, the subcooling length in the core will be neglected as it is small. Also, the flow through the ADS-1,-2,-3 train is assumed to be negligible relative to the flow through the ADS-4 train.

6.6.3 Step 4: IRWST/Sump Injection (Long Term Cooling) Governing Equations

The equations in this phase consist of algebraic equations since the system is assumed to be in steady-state operation. The goal is to determine the vessel inventory M_V as a function of other known and measurable parameters.

The momentum equation is written between the surface of the liquid level in the IRWST/Sump through the ADS-4 valves. As stated above, a linear density variation is assumed along the

heated length of the core so that the effective cold and hot side liquid heights (relative to those shown in Figure 6.32) are reduced by one-half of the core height. In other words, the cold side height (liquid height at density ρ_C) extends from the surface of the Sump level to core mid-plane and the hot side height (liquid height at density ρ_H) extends from the core mid plane to the elevation of the ADS-4 discharge. The momentum equation thus becomes

$$\rho_c g L_s' - \rho_c g \Delta Z_4' - \dot{m}^2 \left(\frac{1}{\rho_c} R_{dvi}' + \frac{1}{\rho_H} R_{ADS}'\right) = 0 \tag{6.89}$$

where $\Delta Z_4'$ is ΔZ_4 - $H_{core}/2$ and L_S' is L_S - $H_{core}/2$.

In terms of mass flow, Equation (6.89) can be rewritten as:

$$\dot{m}^2 = \frac{\rho_c g L_s' - \rho_H g \Delta Z_4'}{\left(\frac{R_{dvi}'}{\rho_c} + \frac{R_{ads}'}{\rho_H}\right)} \tag{6.90}$$

The hot side density, ρ_H, can be determined from the quality which can be determined from an energy balance across the core as

$$x = \frac{\dot{q}_{core} - \dot{m} C_p \Delta T}{h_{fg} \dot{m}}. \tag{6.91}$$

Thus

$$\rho_H = \frac{1}{(1-x)v_f + x v_g} \tag{6.92}$$

where v_f is $1/\rho_C$ and ρ_C is the liquid density (saturated) at containment pressure and ΔT is the subcooling at the core entrance. A small amount of subcooling exists at the core inlet due to the fact that the fluid in the lower plenum "sees" a pressure equal to the hydrostatic head of the column of liquid above it plus the containment pressure. Thus, we have three equations and three unknowns x, ρ_H and $\dot{m}$. The core and upper plenum region inventory is

$$M_v = \frac{1}{2}\rho_c V_{core} + \frac{1}{2}\rho_H \left(V_{core} + V_{up}\right) \tag{6.93}$$

Equations (6.90), (6.91) and (6.92) can be used to get an expression for ρ_H as a function of all known parameters. Substituting Equation (6.91) into (6.92) gives

$$\rho_H = \frac{1}{\left(1 - \frac{\dot{q} - \dot{m} C_p \Delta T}{h_{fg} \dot{m}}\right)\frac{1}{\rho_c} + \frac{q - \dot{m} C_p \Delta T}{h_{fg} \dot{m}} v_g} \tag{6.94}$$

Multiplying the numerator and denominator of Equation (6.94) by $\rho_C h_{fg} \dot{m}$ and collecting terms gives

$$\rho_H = \frac{\rho_c h_{fg} \dot{m}}{\dot{m}\left(h_{fg} + C_p \Delta T - C_p \Delta T \rho_c v_g\right) + \dot{q}\left(\rho_c v_g - 1\right)} \tag{6.95}$$

Substituting Equation (6.90) into Equation (6.95) gives then

$$\rho_H = \frac{\rho_c h_{fg} \left[\dfrac{\rho_c g L_s^{\cdot} - \rho_H g \Delta Z_4^{\cdot}}{\left(R_{dvi}^{\cdot}/\rho_c\right) + \left(R_{ads}^{\cdot}/\rho_H\right)}\right]^{\frac{1}{2}}}{\left[\dfrac{\rho_c g L_s^{\cdot} - \rho_H g \Delta Z_4^{\cdot}}{\left(R_{dvi}^{\cdot}/\rho_c\right) + \left(R_{ads}^{\cdot}/\rho_H\right)}\right]^{\frac{1}{2}} \left(h_{fg} + C_p \Delta T\left(1 - \rho_c v_g\right)\right) + \dot{q}\left(\rho_c v_g - 1\right)} \tag{6.96}$$

Equation (6.96) can be used in Equation (6.93) to provide an expression for the vessel core and upper plenum region mass.

6.6.4 Step 5: IRWST/Sump Injection (Long Term Cooling) Nondimensionalization

We now proceed to nondimensionalize the equations given in the previous section. In the standard manner, such is accomplished by dividing variables by their reference values and denoting the result with an asterisk to indicate a dimensionless quantity. Nondimensionalization of Equation (6.93) yields

$$M_V^* = \frac{\rho_0 V_0}{2M_0} \rho_c^* V_{core}^* + \frac{V_0}{2M_0} \rho_{H0} \rho_H^* \left(V_{core}^* + V_{up}^*\right) \tag{6.97}$$

where quantities with an asterisk are nondimensional and subscript 0 implies a reference quantity. An expression for the nondimensional hot side density can be developed from Equation (6.96) and substituted into Equation (6.97). After algebra, the expression for the nondimensional density is

$$\rho_{H0} \rho_H^* = \rho_0 h_{fg_0} \rho_c^* h_{fg}^* A \Big/ \left[A h_{fg_0} h_{fg}^* + \left(A C_{P_0} \Delta T_0 C_p^* \Delta T^* - \dot{q}_0 \dot{q}^*\right)\left(1 - \frac{v_{g_0}}{v_{f_0}} \frac{v_g^*}{v_f^*}\right)\right] \tag{6.98}$$

where

$$A = \left(\frac{\rho_0^2 g L_0}{R_{dvi_0}^{\cdot}}\right)^{1/2} \left[\frac{\rho_c^* L_s^{\cdot *} - \dfrac{\rho_{H0}}{\rho_0} \dfrac{\Delta Z_{4_0}}{L_0} \rho_H^* \Delta Z_4^{\cdot *}}{\left(\dfrac{R_{dvi}^*}{\rho_c^*}\right) + \dfrac{\rho_0}{\rho_{H0}} \left(\dfrac{R_{ads_0}^{\cdot}}{R_{dvi_0}^{\cdot}}\right) \dfrac{R_{ads}^*}{\rho_H^*}}\right]^{1/2} \tag{6.99}$$

Note that the first term in Equation (6.99) is a reference flow rate which can be defined as

$$\dot{m}_{S_0} = \left(\frac{\rho_0^2 g L_0}{R_{dvi_0}^{\cdot}}\right)^{1/2} \tag{6.100}$$

Other collections of reference values in Equations (6.98) and (6.99) are defined as

$$\Pi_{\rho_{dvi}} = \frac{v_{g_0}}{v_{f_0}} \tag{6.101}$$

$$\Pi_{Z_{dvi}} = \frac{\rho_{H0}}{\rho_0}\frac{\Delta Z_{4_0}}{L_0} \tag{6.102}$$

$$\Pi_{\dot{R}_{dvi}} = \frac{\rho_0}{\rho_{H0}}\left(\frac{\dot{R}_{ads_0}}{\dot{R}_{dvi_0}}\right) \tag{6.103}$$

With these definitions, Equation (6.99) becomes

$$A = \dot{m}_{S_0}\left[\frac{\rho_c^* L_S^{**} - \Pi_{Z_{dvi}}\rho_H^* \Delta Z_4^{**}}{\left(\frac{\dot{R}_{dvi}^*}{\rho_c^*}\right) + \Pi_{\dot{R}_{dvi}}\frac{\dot{R}_{ads}^*}{\rho_H^*}}\right]^{1/2} = \dot{m}_{S_0} A^* \tag{6.104}$$

where A^* is the bracketed term in Equation (6.104). Substituting this result along with Equation (6.101) into Equation (6.98) gives

$$\rho_{H0}\rho_H^* = \rho_0 h_{fg_0}\rho_c^* h_{fg}^* \dot{m}_{S_0} A^* \Big/ \left[\dot{m}_{S_0} A^* h_{fg_0} h_{fg}^* + \left(\dot{m}_{S_0} A^* C_{P_0}\Delta T_0 C_p^*\Delta T^* - \dot{q}_0\dot{q}^*\right)\left(1 - \Pi_{\rho_{dvi}}\frac{v_g^*}{v_f^*}\right)\right] \tag{6.105}$$

Dividing the numerator and denominator of the RHS of Equation (6.105) by $\dot{m}_{S0}h_{fg_0}$ results in

$$\begin{aligned}\rho_{H0}\rho_H^* &= \frac{\rho_0\rho_c^* h_{fg}^* A^*}{A^* h_{fg}^* + \left(A^*\frac{C_{P_0}\Delta T_0}{h_{fg_0}}C_p^*\Delta T^* - \frac{\dot{q}_0}{\dot{m}_{S_0}h_{fg_0}}\dot{q}^*\right)\left(1 - \Pi_{\rho_{dvi}}\frac{v_g^*}{v_f^*}\right)} \\ &= \frac{\rho_0\rho_c^* h_{fg}^* A^*}{A^* h_{fg}^* + \left(A^*\Pi_{SUB}C_p^*\Delta T^* - \Pi_{\dot{q}}\dot{q}^*\right)\left(1 - \Pi_{\rho_{dvi}}\frac{v_g^*}{v_f^*}\right)}\end{aligned} \tag{6.106}$$

where

$$\Pi_{SUB} = \frac{C_{P_0}\Delta T_0}{h_{fg_0}} \tag{6.107}$$

$$\Pi_{\dot{q}} = \frac{\dot{q}_0}{\dot{m}_{S_0}h_{fg_0}} \tag{6.108}$$

Finally, substituting Equation (6.106) in to Equation (6.97) gives

$$M_V^* = \frac{\rho_0 V_0}{2M_0}\rho_c^* V_{core}^* + \frac{V_0}{2M_0}\left(V_{core}^* + V_{up}^*\right)\rho_{H0}\rho_H^*$$

$$= \frac{\rho_0 V_0}{2M_0}\rho_c^* V_{core}^* + \frac{\rho_0 V_0}{2M_0}\left(V_{core}^* + V_{up}^*\right)\frac{\rho_c^* h_{fg}^* A^*}{A^* h_{fg}^* + \left(A^*\Pi_{SUB}C_p^*\Delta T^* - \Pi_{\dot{q}}\dot{q}^*\right)\left(1 - \Pi_{\rho_{on}}\frac{v_g^*}{v_f^*}\right)} \qquad (6.109)$$

If we define Π_{LTC} as

$$\Pi_{LTC} = \frac{\rho_c^* h_{fg}^* A^*}{A^* h_{fg}^* + \left(A^*\Pi_{SUB}C_p^*\Delta T^* - \Pi_{\dot{q}}\dot{q}^*\right)\left(1 - \Pi_{\rho_{on}}\frac{v_g^*}{v_f^*}\right)} \qquad (6.110)$$

and note that $\rho_0 V_0/M_0$ is unity, then Equation (6.109) simplifies to

$$M_V^* = \frac{1}{2}\rho_c^* V_{core}^* + \frac{1}{2}\left(V_{core}^* + V_{up}^*\right)\Pi_{LTC} \qquad (6.111)$$

Table 6.28 summarizes the nondimensional groups listed above.

Table 6.28. Nondimensional coefficients for the IRWST/Sump Injection Phase.

Π Group	Definition	Description
$\Pi_{\rho_{on}}$	$\frac{v_{g_0}}{v_{f_0}}$	Vapor to liquid specific volume ratio
$\Pi_{Z_{on}}$	$\frac{\rho_{H0}}{\rho_0}\frac{\Delta Z_{4_2}}{L_0}$	Ratio of head on the ADS side to the head on the IRWST side
$\Pi_{R_{on}}$	$\frac{\rho_0}{\rho_{H0}}\left(\frac{R_{ads_0}}{R_{dvi_0}}\right)$	Density weighted ratio of ADS-4 and DVI line resistances
Π_{SUB}	$\frac{C_{p_0}\Delta T_0}{h_{fg_0}}$	Subcooling number
$\Pi_{\dot{q}}$	$\frac{\dot{q}_0}{\dot{m}_{s_0}h_{fg_0}}$	Phase change number

6.6.5 Step 6: IRWST/Sump Injection (Long Term Cooling) Selection of Reference Parameters

Reference parameters are chosen to make the asterisked variables in the above equations of O[1]. Table 6.29 describes the reference parameters and Table 6.30 lists the numerical values.

Table 6.29. Reference parameters for IRWST/Sump Injection Phase.

Reference Parameter	Description
V_0	Volume of core plus volume of upper plenum to top of hot legs
ρ_0	Saturation density at $P_0 = P_{cont} + \rho_{sat} g L_s$
ΔT_0	Subcooling due to hydrostatic head in lower plenum
M_0	$\rho_o V_o$
C_{P0}	Saturated liquid specific heat at P_0
h_{fg0}	Heat of vaporization at P_0
v_{fg0}	Vapor-liquid specific volume change at P_0
L_0	Maximum sump level (determined by the curb height) minus one-half the core height $\left(L_s'\right)$
q_0	Core decay heat
$R'_{dvi,0}$	R'_{dvi} - the Sump/DVI line combined resistance
$R'_{ads\text{-}4,0}$	$R'_{ads\text{-}4}$ - the ADS-4 train combined resistance
ρ_{H0}	Hot side reference fluid density
ΔZ_0	$\Delta Z_4'$ - distance from core mid-plane to the ADS-4 discharge elevation

Table 6.30. Reference parameter values for IRWST/Sump Injection Phase.

Reference Parameter	AP600	OSU
V_0 (m^3)		
P_0 (kPa)		
ρ_0 (kg/m^3)		
ΔT_0 (K)		
M_0 (kg)		
C_{P0} (kJ/kg-K)		
h_{fg0} (kJ/kg)		
v_{g0} (m^3/kg)		
v_{fg0} (m^3/kg)		
L_0 (m)		
q_0 (kW)		
$R'_{dvi,0}$ (m^{-4})		
$R'_{ads\text{-}4,0}$ (m^{-4})		
ρ_{H0} (kg/m^3)		
ΔZ_0 (m)		
L_S (m)		
ΔZ_4 (m)		

a, c

6.6.6 Step 7: IRWST/Sump Injection (Long Term Cooling) Order of Magnitude Analysis

Table 6.31 lists the nondimensional groups that derive from use of the reference conditions listed above. Also listed is the predicted nondimensional vessel mass. The values in this table indicate relatively good agreement between the plant values and the OSU values.

Table 6.31. Nondimensional coefficients for the IRWST/Sump Injection Phase.

Π Group	AP600	OSU
$\Pi_{\rho_{ori}}$		
$\Pi_{Z_{ori}}$		
$\Pi_{R'_{ori}}$		
Π_{SUB}		
$\Pi_{\dot{q}}$		
Π_{LTC}		
M^*_V		

a, c

6.6.7 Step 8: IRWST/Sump Injection (Long Term Cooling) Verification with Data

OSU experiments support the observation that the collapsed liquid level in the vessel reaches a constant value shortly after Sump injection commences. This implies a relatively constant vessel mass since other experiment parameters are not changing. The collapsed vessel level remains at an elevation near the DVI nozzle for the duration of the phase. Based on the experiment values, the nondimensional mass is approximately [ ]^{a,c} in contrast to the estimates shown in Table 6.29. This was to be expected due to the assumptions made in the analysis. In particular, the assumption of a homogeneous density in the upper regions of the core and above the core is not adequate. Experimental data suggests that significant phase separation occurs in the upper core region and upper plenum. In effect, a significant fraction of the liquid in the mixture flowing out the top of the heated region separates and/or de-entrains in the upper plenum. Attempts to supplement the above analysis using a drift flux approach were not successful in that unreasonable drift flux parameter values were required. The basic issue is that the flow regime in the upper core and plenum is geometry dependent and likely annular - not bubbly flow. The essence of the problem is that a more detailed, local effects description of the phase distribution is needed for the particular geometry in the upper plenum and various tee connections leading to the ADS-4 valves.

7. CONCLUSIONS

An analysis technique was developed and applied to three scaled experimental facilities to assess scaling aspects related to key system response and evaluate the applicability of the data for assessing computer programs used in the licensing process. In this analysis the methodology was applied to data from 1 inch cold leg break accident simulations. The analyses helped to identify and quantify dominant nondimensional groups and hence processes, geometric features, and operational parameters in each phase of the transient. Based on the analysis the following observations were drawn.

Simplified lumped parameter descriptions of system components and interconnections, based on conservation equations, were used to identify and describe dominant features of reactor system thermal-hydraulic response during a 1 inch cold leg break scenario.

General Observations

Based on the dimensionless forms of the equations the dominant nondimensional groups and important facility parameters were identified for each phase of the break scenario. The equations were applied to data from three scaled facilities and captured the main phenomena seen in the experiments.

Data Applicability

When applying the technique to the experimental facilities the equations were normalized with sets of reference parameters developed with and without knowledge of the experimental results. The differences in the resulting nondimensionalized equations were generally small. The differences did not indicate any substantive changes in the system response. The insensitivity of the analysis results to small changes in the reference parameters used lends confidence in the technique for evaluating the applicability of the experimental data for assessment of codes for AP600 system analysis.

Several specific conclusions were drawn based on application of the technique to a one inch cold leg break scenario.

In the initial portion of the subcooled blowdown phase, the system mass and pressure responses are primarily controlled by the break flow rate. (In some accident scenarios it may be necessary to consider the balance of core, steam generator, and PRHR heat flows.) Following pressurizer draining and core scram, the balance of core, steam generator, and PRHR heat flows along with the break flow play an important role in the pressure response. System mass loss continues to be dominated by the break flow.

During the initial intermediate (passive cooling) phase the mass inventory is controlled by the break flow until the accumulator draining and CMT draining begin. In this interval the

depressurization rate is influenced by the balance of core and PRHR heat flows as well as the break volumetric flow. Following the initiation of accumulator injection and CMT draining, these flows dominate the mass balance until ADS flow begins. The low temperature of these flows influences the depressurization process primarily by decreasing the average specific volume of the system. Beginning at this point the important processes in the transient are controlled by the actions of the engineered safety systems.

After the ADS-1,-2,-3 flows begin they, in addition to the accumulator and CMT flows, influence the mass balance and the depressurization rate. The ADS influence on the depressurization rate is accentuated by the discharge being high quality.

Order of magnitude analysis of the Intermediate Phase suggests that the nondimensional pressure and inventory are relatively independent of break size provided the break is small (for example if the break flowrate is much less than the ADS-1,-2,-3 flowrate). These nondimensional parameters depend on accumulator and CMT mass and, to a lesser extent, on the details of the net heating from core decay heat and steam generator and PRHR heat transfer. Analysis suggests that the overall normalized change in PCS mass during this phase should approximately 0.6. The experimental data tend to support this conclusion.

During the pre-IRWST portion of the ADS-4 blowdown the vessel mass inventory is determined by the balance between CMT and ADS-4 flow rates. The CMT head relative to the vessel liquid level, CMT line resistance, and ADS-4 quality are important parameters during this phase. Temperature of the CMT liquid and mixing in the lower plenum affect the ADS-4 quality.

In the initial vessel refill during the IRWST phase the vessel mass inventory is determined by the balance between IRWST, pressurizer surge line, and ADS-4 flow rates. The pressurizer draining (surge line flow) is an important contributor to vessel refill. The IRWST and pressurizer head relative to the vessel level, IRWST line resistance, and ADS-4 quality are important parameters during this phase. Temperature of the IRWST liquid and mixing in the lower plenum affect the ADS-4 quality. The effects of oscillatory pressurizer draining were observed but did not significantly affect the vessel refill process.

During the IRWST Draining Phase, the flow rate through the DVI, core, and out the ADS-4 valves depends primarily on the IRWST water level and, to a lesser extent, the ratio of the hydraulic resistances in the DVI and ADS-4 trains. IRWST drain time is the relevant time scale and is much larger than the vessel time scale. Since the relevant head and resistance ratios are well preserved in the OSU facility, similarity to plant response is expected.

During the IRWST/Sump Injection Phase, the collapsed liquid level in the vessel reaches a constant value at approximately the DVI nozzle elevation shortly after Sump injection commences. Thereafter, the vessel mass inventory is relatively constant. Attempts to accurately predict the equilibrium inventory using a homogeneous approach were not totally successful. The actual inventory is significantly larger than predicted. A detailed definition of the phase distribution and separation in the upper core, upper plenum, and path to the ADS-4 valves is

needed to better address this aspect of Sump injection. However, based on the homogeneous approximations used, the dimensionless groups that describe this process are of similar magnitude for AP600 and OSU.

Adequacy of Data

The magnitudes of the nondimensional coefficients in the reduced conservation equations were similar for the experimental facilities and the AP600 system. More specifically, the same processes were indicated to be dominant in the experimental facilities as in the AP600. This similarity indicates that the experimental results are useful for understanding the expected response of the AP600 system. Although no single facility provides a complete representation of the AP600 response for all phases of the transient, the facilities as a collective whole encompass the expected performance of plant. Based on the magnitudes of the nondimensional groups, the data from the experimental facilities are believed to be in the correct parameter range to adequately test and validate computer codes used for auditing vendor's AP600 analysis.

Facility Distortions

Based on this analysis, known facility distortions do not adversely impact the experimental data applicability for code assessment purposes. For example, in the ROSA facility, the DVI nozzles are located on the vessel at a distance below the hot leg elevation that is somewhat lower than the scaled value. Even so, the scaled response of the ROSA experiment during the ADS-4 blowdown phase and the IRWST injection phase was similar to the other facilities. The SPES facility has several known distortions including oversized ADS 4 area, ADS-1,-2,-3 valves that discharge to atmosphere rather than to the IRWST, and excess heat loss that is offset by increasing core power. The oversized ADS-4 area influences the time scale during ADS-4 blowdown (the time scale is shorter relative to the plant). This effect was accounted for and the scaled response of the vessel inventory during ADS-4 blowdown was similar to the other facilities. While the SPES ADS-1,-2,-3 train discharges to atmosphere instead of to the IRWST, and therefore does not influence the IRWST fluid temperature, the similarity in the scaled SPES vessel inventory to the other facilities, suggests no major effect of this distortion. Excess heat loss in SPES is compensated by increasing core power above scaled decay heat values. During the intermediate phase, it is expected that this excess core power will effect the balance between core power and PRHR heat removal. This will effect the SPES depressurization rate as it is primarily controlled by this imbalance during Subphases I and II. While this distortion may exist in the SPES experiment, the effects should be readily accounted for in code analysis and, therefore, should not adversely impact the applicability of the data.

Based on the reference parameters selected for the experimental facilities, there are distortions in the PRHR heat transfer rates relative to the AP600. Based on the nondimensional group characterizing the PRHR, PRHR heat transfer rate in ROSA is larger than the plant while both the SPES and OSU rates are smaller than the plant. Examination of the one-inch cold leg break experiment data supports this conclusion. These distortions, however, appeared to have limited impact on the transient response or the conditions at ADS-4 actuation.

Evaluation of the nondimensional groups indicates that some minor distortions stemming from reduced pressure operating conditions exist in the OSU facility for the intermediate phase. The source of the distortions is due primarily to thermodynamic property derivative values. Even so, the major factors influencing depressurization in the OSU experiment are the same as those in the other facilities. Analysis and review of data also showed a potential difference between the OSU experiment and the other facilities related to the ADS-4 flow. Due to the reduced pressure operation (and reduced height) in OSU, the ADS-4 flow does not appear to be choked during ADS-4 blowdown and IRWST injection for the experiment analyzed. However, the friction dominated flowrate was close to values obtained from the HEM model and HEM could be used to establish reference flow values. As such, this difference does not appear to be a major distortion and, furthermore, should be adequately handled by analysis codes.

Relation to PIRT

The important phenomena identified for the one inch cold leg break were generally in agreement with those identified in the PIRT. Several phenomena were noted to play a significant role in the accident sequence that were not listed as high priority in the PIRT. These phenomena were:

- The CMT level and line resistance during the ADS-4 Blowdown and IRWST Phases
- The IRWST/DVI flow resistance during the IRWST Phase
- The initial pressurizer inventory at the start of the IRWST Phase

The ranking of these phenomena has been adjusted in the current PIRT.

8. REFERENCES

1. "AP600 Standard Safety Analysis Report," Simplified Passive Advanced Light Water Reactor Plant Program, Westinghouse Electric Company (Proprietary), June 26, 1992 and revisions.

2. C. D. Fletcher, et al. "Adequacy Evaluation of RELAP5/MOD3, Version 3.2.1.2 for Simulating AP600 Small Break Loss-of-coolant Accidents," Idaho National Engineering Laboratory, INEL-96/0400, draft report published November 1996.

3. K. E. Carlson, et al., "RELAP5/MOD3 Code Manual (Draft)," Idaho National Engineering Laboratory, NUREG/CR-5535, INEL-95/0174, 7 Volumes, August 1995.

4. M. Rigamonti, "SPES-2 Facility Description," Sezione Reattori Innovativi (SIET), 00183RI92, Revision 0 (Proprietary), April 1994.

5. Westinghouse Electric Company, "Westinghouse AP600 Long Term Cooling Test at Oregon State University, Facility Drawings, Piping and Instrumentation Diagrams," LTCT-T3-300 (Proprietary), December 1994.

6. Japan Atomic Energy Research Institute, "Large Scale Test Facility; System Description for the ROSA/AP600 and ROSA-V Configurations (for the Third Installed Core)," Revision A, Draft, February, 1995 March 1996.

7. R. R. Schultz, "International Code Assessment and Applications Program: Summary of Code Assessment Studies Concerning RELAP5/MOD2, RELAP5/MOD3, and TRAC-B," Idaho National Engineering Laboratory, NUREG/IA-0128, EGG-EAST-8719, December 1993.

8. "Adequacy Evaluation of RELAP5/MOD3 for Simulating AP600 Small Break Loss-of-Coolant Accidents," Idaho National Engineering Laboratory, INEL-96/0380, (Proprietary), October 1996.

9. D. Bessette, M. DiMarzo, and P. Griffith, "Phenomenology Observed in the AP600 Integral Systems Test Programs Conducted in the ROSA-AP600, APEX, and SPES-2 Facilities," U. S. Nuclear Regulatory Commission Report (draft report to be published), August 1996.

10. Technical Program Group, "An Integrated Structure and Scaling Methodology for Severe Accident Technical Issue Resolution," Idaho National Engineering Laboratory, Draft Report for Comment, NUREG/CR-5809, EGG-2659, November 1991.

11. Westinghouse Electric Corporation, "Quick Look Report for OSU Matrix Test SB5," LTCT-T2R-02S, AP600 Test Program, August 1994, Revision 0.

12. J. T. Groome, "CL#3, 1" Bottom of Pipe Break with Modified ADS 1, 2, and 3 Logic and ROSA ADS Setpoints, NRC-22," Oregon State University, OSU-APEX-96007, Revision 0, June 19, 1996.

13. R. A. Shaw, et al., "Quick Look Report for ROSA/AP600 Experiment AP-CL-03," JAERI-memo 06-249, October 1994.

14. Westinghouse Electric Corporation, "AP600 Design Certification Program SPES-2 Tests Final Data Report," WCAP-14309, Vol. 1, March 1995 (Westinghouse Proprietary Class 2).

15. Westinghouse Electric Corporation, "Quick Look Report for SPES-2 Matrix Test S00401," PXS-T2R-020 (Proprietary), Preliminary, July 1994.

16. C. D. Fletcher, et al., "Interim Phenomena Identification and Ranking Tables for Westinghouse AP600 Small Break Loss-of-Coolant Accident, Main Steam Line Break, and Steam Generator Tube Rupture Scenarios, Appendix H - Summary of Plant Systems and Automatic Actions (Proprietary)," Idaho National Engineering Laboratory, INEL-94/0061, Revision 1, July, 1995.

17. J. D. Burtt, et al., "Interim Phenomena Identification and Ranking Tables for Westinghouse AP600 Small Break Loss-of-Coolant Accident, Main Steam Line Break, and Steam Generator Tube Rupture Scenarios," Idaho National Engineering Laboratory, INEL-94/0061, Revision 2, draft report to be published November 1996.

18. M. G. Ortiz, et al., "Application of the Global Scaling Analysis Tools to the AP600 Integration Study," Idaho National Engineering Laboratory, INEL-94/0117, (Proprietary), report to be published December 1996.

19. W. Wulff, "Scaling of thermohydraulic systems," Nuc. Eng. Des., 163, March 1996, 355-395.

20. J. N. Reyes, et al., "Low-Pressure Integral Systems Test Facility Scaling Report," Westinghouse Electric Company (Proprietary), WCAP-14270, January 1995.

21. R. E. Henry, H. K. Fauske, "The Two-Phase Critical Flow of One-component Mixtures in Nozzles, Orifices, and Short Tubes," Journal of Heat Transfer, May 1971.

22. D. G. Hall and Linda S. Czapary, "Tables of Homogeneous Equilibrium Critical Flow Parameters for Water in SI Units," Idaho National Engineering Laboratory, EGG-2056, September 1980.

23. H. B. Karplus, "Propagation of Pressure Waves in a Mixture of Steam and Water," ARF, 4132 12, pp. 39, January 1961.

APPENDIX A

PRESSURE RATE EQUATION AND TANK LEVEL DERIVATION

APPENDIX A

PRESSURE RATE EQUATION AND TANK LEVEL DERIVATION

This Appendix details the development of a simple pressure rate equation and a level equation useful for the analysis of the blowdown of a saturated fluid from a component contained in a system. The development is done for a simple control volume and follows that given in Ref. A-1. After the equations are developed, the set is nondimensionalized. While the development is general, various assumptions are implemented during the course of the development. The assumptions are summarized here for clarity:

- fixed control volume
- thermodynamic equilibrium is assumed
- no work is done on or by the system
- kinetic and potential energy changes are assumed negligible
- the subcomponent of interest (e.g. the pressurizer) contains saturated fluid
- no energy generation in the control volume but net heat flow (e.g. heaters) occurs
- outflows have average volume properties; inflows do not (necessarily)

Equation Development

Consider the control volume shown in Figure A-1. Work is done on (ΣW_{in}) and by (ΣW_{out}) this system, energy (e) is convected across the boundaries of the system ($\Sigma \dot{m}e)_{in}$ and $\Sigma \dot{m}e)_{out}$), and heat is transferred across the boundaries of the system (Σq_{in} and Σq_{out}). E, the total energy stored in the system is the sum of the kinetic, potential, and internal energy or

$$E = \varepsilon M \qquad \text{(A-1)}$$

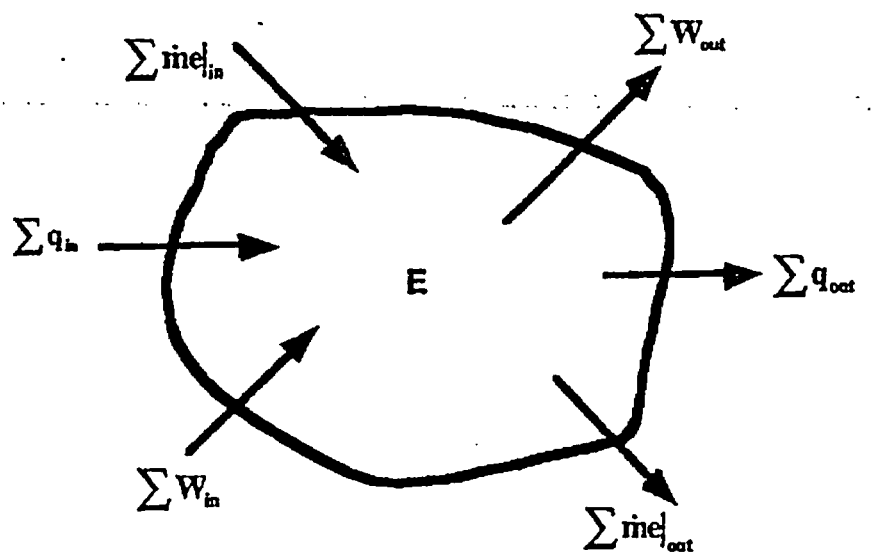

Figure A-1. Simple control volume.

where

ε - stored energy per unit mass

M - total mass

It follows that

$$\varepsilon \equiv \frac{u^2}{2} + gZ + \mu \tag{A-2}$$

where

u - velocity

g - acceleration of gravity

Z - gravitational potential

μ - specific internal energy

Mass flows across system boundaries carry stored energy and transfer energy by flow work. The energy transfer due to mass flow across a boundary is then

$$\dot{m}(\varepsilon + pv) = \dot{m}\left(\frac{u^2}{2} + gZ + \mu + pv\right) \tag{A-3}$$

where

$\dot{m}$ - mass flow rate

p - pressure

v - specific volume

By definition, the enthalpy h is

$$h = \mu + pv \tag{A-4}$$

Substituting Equation (A-4) into Equation (A-3) gives an expression for e, the energy convected per unit mass

$$e = h + \frac{u^2}{2} + gZ \tag{A-5}$$

With the definitions above, a statement of the first law of thermodynamics (out - in + stored = generated) for the control volume in Figure A-1 with no energy generation is

$$\Sigma \dot{W}_{out} + \Sigma \dot{m}e]_{out} + \Sigma q_{out} - \Sigma \dot{W}_{in} - \Sigma \dot{m}e]_{in} - \Sigma q_{in} + \frac{dE}{dt} = 0 \tag{A-6}$$

where

ΣW_{out} - rate of work done by the system

ΣW_{in} - rate of work done on the system.

Mass is conserved for the control volume and the continuity equation states

$$\Sigma \dot{m}_{out} - \Sigma \dot{m}_{in} + \frac{dM}{dt} = 0 \tag{A-7}$$

An equation of state for the control volume wherein the pressure is a function of the specific internal energy and the specific volume can be written as

$$p = p(\mu, v) \equiv p\left(\frac{U}{M}, \frac{V}{M}\right) \tag{A-8}$$

Equation (A-8) can be differentiated with time to get

$$\frac{dp}{dt} = \frac{\partial p}{\partial \mu}\Big|_v \frac{du}{dt} + \frac{\partial p}{\partial v}\Big|_\mu \frac{dv}{dt} = \frac{\partial p}{\partial\left(\frac{U}{M}\right)\Big|_{\frac{V}{M}}} \frac{d\left(\frac{U}{M}\right)}{dt} + \frac{\partial p}{\partial\left(\frac{V}{M}\right)\Big|_{\frac{U}{M}}} \frac{d\left(\frac{V}{M}\right)}{dt} \tag{A-9}$$

where

U - total internal energy

V - control volume total volume.

If the kinetic and potential energy contributions to the total stored energy in the control volume are ignored, Equations (A-1) and (A-2) lead to

$$E \approx U \approx \varepsilon M = \mu M \tag{A-10}$$

Equation (A-10) can be differentiated with time to get

$$\frac{dE}{dt} = \frac{d(\mu M)}{dt} = \mu \frac{dM}{dt} + M \frac{d\mu}{dt} \tag{A-11}$$

Substituting Equation (A-7) into Equation (A-11) yields

$$\frac{dE}{dt} = \mu(\Sigma \dot{m}_{in} - \Sigma \dot{m}_{out}) + M \frac{d\mu}{dt} \tag{A-12}$$

Substituting Equation (A-12) into the energy balance Equation (A-6), assuming that the work terms are zero, and collecting terms gives

$$\Sigma \dot{m}_{out}(e_{out} - \mu) - \Sigma \dot{m}_{in}(e_{in} - \mu) + \Sigma q_{out} - \Sigma q_{in} + M \frac{d\mu}{dt} = 0 \tag{A-13}$$

Equation (A-9) can be rearranged to obtain an expression for the last term in Equation (A-13)

$$\frac{du}{dt} = \left[\frac{dp}{dt} - \frac{\partial p}{\partial v}\Big|_\mu \frac{dv}{dt}\right] \frac{1}{\frac{\partial p}{\partial \mu}\Big|_v} \tag{A-14}$$

Substituting Equation (A-14) into Equation (A-13) and multiplying through by the term $1/M\,(dp/d\mu)_v$ gives the following

$$\frac{1}{M}\frac{\partial p}{\partial \mu}\Big|_v [\Sigma \dot{m}_{out}(e_{out} - \mu) - \Sigma \dot{m}_{in}(e_{in} - \mu) + \Sigma q_{out} - \Sigma q_{in}] + \frac{dp}{dt} - \frac{\partial p}{\partial v}\Big|_\mu \frac{dv}{dt} = 0 \tag{A-15}$$

Solving Equation (A-15) for dp/dt yields

$$\frac{dp}{dt} = \frac{1}{M}\frac{\partial p}{\partial \mu}\Big|_v \left[\Sigma \dot{m}_{in}(e_{in} - \mu) - \Sigma \dot{m}_{out}(e_{out} - \mu) + \Sigma q_{in} - \Sigma q_{out}\right] + \frac{\partial p}{\partial v}\Big|_\mu \frac{dv}{dt} \tag{A-16}$$

The specific volume by definition is $v = V/M$. Differentiating this expression with time gives

$$\frac{dv}{dt} = \frac{d\left(\frac{V}{M}\right)}{dt} = \frac{1}{M}\frac{dV}{dt} - \frac{v}{M}\frac{dM}{dt} = \frac{1}{M}\left(\frac{dV}{dt} - v\left(\Sigma \dot{m}_{in} - \Sigma \dot{m}_{out}\right)\right) \tag{A-17}$$

where Equation (A-7) was substituted for dM/dt. Noting that for a fixed control volume, dV/dt is zero and substituting (A-17) into Equation (A-16) gives

$$\frac{dp}{dt} = \frac{1}{M}\frac{\partial p}{\partial \mu}\Big|_v \left[\Sigma \dot{m}_{in}(e_{in} - \mu) - \Sigma \dot{m}_{out}(e_{out} - \mu) + q_{net}\right] + \frac{1}{M}\frac{\partial p}{\partial v}\Big|_\mu \left[v\left(\Sigma \dot{m}_{out} - \Sigma \dot{m}_{in}\right)\right] \tag{A-18}$$

where for convenience, q_{net} is defined as

$$q_{net} = \Sigma q_{in} - \Sigma q_{out} \tag{A-19}$$

If kinetic and potential energy changes are assumed negligible, then from Equation (A-5), it is apparent that $e = h$ and Equation (A-18) becomes

$$\frac{dp}{dt} = \frac{1}{M}\frac{\partial p}{\partial \mu}\Big|_v \left[\Sigma \dot{m}_{in}(h_{in} - \mu) - \Sigma \dot{m}_{out}(h_{out} - \mu) + q_{net}\right] + \frac{1}{M}\frac{\partial p}{\partial v}\Big|_\mu \left[v\left(\Sigma \dot{m}_{out} - \Sigma \dot{m}_{in}\right)\right] \tag{A-20}$$

Equation (A-20) contains the derivative of pressure with specific internal energy at constant specific volume and the derivative of pressure with specific volume at constant specific internal energy. Since we are most interested in a saturated fluid system it is convenient to write the derivative of pressure with specific volume at constant specific internal energy in terms of the derivative of pressure with specific internal energy at constant specific volume using the triple product relation or

$$\frac{\partial p}{\partial v}\Big|_\mu = \frac{-\frac{\partial p}{\partial \mu}\Big|_v}{\frac{\partial v}{\partial \mu}\Big|_p} \tag{A-21}$$

μ and v an be defined in terms of the equilibrium quality as

$$\mu = \mu_f + x\,\mu_{fg} \tag{A-22}$$

and

$$v = v_f + x\,v_{fg} \tag{A-23}$$

where

x - equilibrium quality
v_f - specific volume of saturated liquid
μ_f - specific internal energy of saturated liquid

$v_{fg} = v_g - v_f$
$\mu_{fg} = \mu_g - \mu_f$
v_g - specific volume of saturated vapor
μ_g - specific internal energy of saturated vapor

Using Equations (A-22) and (A-23), the specific internal energy can be written as

$$\mu = \mu_f + (v - v_f)\frac{u_{fg}}{v_{fg}} \tag{A-24}$$

Along the saturation line, μ_f, v_f, μ_{fg}, and v_{fg} are functions of pressure only so that the derivative of Equation (A-24) with respect to specific volume at constant pressure yields

$$\frac{\partial \mu}{\partial v}\Big|_p = \frac{\partial \mu_f}{\partial v}\Big|_p + \frac{\partial\left(v\frac{\mu_{fg}}{v_{fg}}\right)}{\partial v}\Big|_p - \frac{\partial\left(v_f\frac{\mu_{fg}}{v_{fg}}\right)}{\partial v}\Big|_p = \frac{\mu_{fg}}{v_{fg}}\frac{\partial v}{\partial v}\Big|_p = \frac{\mu_{fg}}{v_{fg}} \tag{A-25}$$

Substituting Equation (A-21) into Equation (A-20), using (A-25), and collecting terms gives

$$\frac{dp}{dt} = \frac{1}{M}\frac{1}{\frac{\partial \mu}{\partial p}\Big|_v}\left[\Sigma \dot{m}_{in}\left(h_{in} - \mu + v\frac{\mu_{fg}}{v_{fg}}\right) - \Sigma \dot{m}_{out}\left(h_{out} - \mu + v\frac{\mu_{fg}}{v_{fg}}\right) + q_{net}\right] \tag{A-26}$$

An expression for the thermodynamic property derivative term in the numerator is needed. This expression can be developed from the thermodynamic relations

$$d\mu = T\,ds - p\,dv \tag{A-27}$$

and

$$h = T\,ds + v\,dp \tag{A-28}$$

where
T - temperature
s - specific entropy

Taking the partial derivatives of Equations (A-27) and (A-28) with respect to pressure at constant specific volume gives

$$\frac{\partial \mu}{\partial p}\Big|_v = T\frac{\partial s}{\partial p}\Big|_v \tag{A-29}$$

and

$$\frac{\partial h}{\partial p}\Big|_v = T\frac{\partial s}{\partial p}\Big|_v + v\frac{\partial p}{\partial p}\Big|_v = T\frac{\partial s}{\partial p}\Big|_v + v \tag{A-30}$$

Solving Equation (A-30) for the derivative of entropy with pressure yields

$$\frac{\partial s}{\partial p}\Big|_v = \frac{1}{T}\left[\frac{dh}{dp}\Big|_v - v\right] \tag{A-31}$$

Defining the enthalpy in terms of equilibrium quality and using Equation (A-23) to define the quality gives

$$h = h_f + x\,h_{fg} = h_f + \frac{(v - v_f)}{v_{fg}}\,h_{fg} = h_f - \frac{v_f\,h_{fg}}{v_{fg}} + v\,\frac{h_{fg}}{v_{fg}} \tag{A-32}$$

Taking the partial derivative of Equation (A-32) with respect to pressure at constant specific volume yields

$$\frac{\partial h}{\partial p}\Big|_v = \frac{dh_f}{dp} - \frac{d}{dp}\left(\frac{v_f\,h_{fg}}{v_{fg}}\right) + v\,\frac{d}{dp}\left(\frac{h_{fg}}{v_{fg}}\right) + \frac{h_{fg}}{v_{fg}}\frac{\partial v}{\partial p}\Big|_v \tag{A-33}$$

where the first three terms are total derivatives since along the saturation line h_f, v_f, h_{fg}, and v_{fg} are functions of pressure only and the last term is zero.

Substituting Equation (A-33) into Equation (A-31) gives

$$\frac{\partial s}{\partial p}\Big|_v = \frac{1}{T}\left[\frac{dh}{dp}\Big|_v - v\right] = \frac{1}{T}\left[\frac{dh_f}{dp} - \frac{d}{dp}\left(\frac{v_f\,h_{fg}}{v_{fg}}\right) + v\,\frac{d}{dp}\left(\frac{h_{fg}}{v_{fg}}\right) - v\right] \tag{A-34}$$

Substituting this latter expression into Equation (A-29) gives the desired expression for the partial derivative of specific internal energy with pressure at constant specific volume

$$\frac{\partial \mu}{dp}\Big|_v = T\frac{\partial s}{\partial p}\Big|_v = \left[\frac{dh}{dp}\Big|_v - v\right] = \left\{\frac{dh_f}{dp} - \frac{d}{dp}\left(\frac{v_f\,h_{fg}}{v_{fg}}\right) + v\left[\frac{d}{dp}\left(\frac{h_{fg}}{v_{fg}}\right) - 1\right]\right\} \tag{A-35}$$

Consider a control volume representing a tank as shown in Figure A-2 with total volume V_0, height H_0, cross-sectional area A_0, and liquid height L. The tank void fraction is defined as

$$\alpha = 1 - \frac{L}{H_0} \tag{A-36}$$

and from Equation (A-36), the liquid fraction is

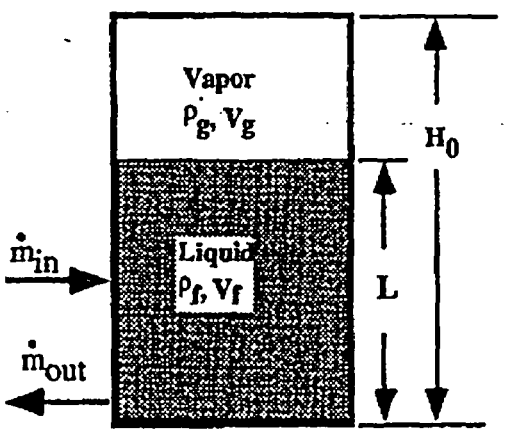

V_0 - volume of tank
A - cross sectional area of tank

Figure A-2. Control volume representing a tank.

$$1-\alpha=\frac{L}{H_0} \tag{A-37}$$

where

α - void fraction

The mass in the tank is

$$M=V_o\rho=V_0[\alpha\rho_g+(1-\alpha)\rho_f] \tag{A-38}$$

where

ρ - some average density

ρ_g - saturated vapor density

ρ_f - saturated liquid density

Differentiating Equation (A-38) with time gives

$$\frac{dM}{dt}=V_0\frac{d[\alpha\rho_g+(1-\alpha)\rho_f]}{dt}+[\alpha\rho_g+(1-\alpha)\rho_f]\frac{dV_0}{dt} \tag{A-39}$$

Expanding the first term, noting that dV_0/dt is zero, and using Equation (A-7) yields

$$\frac{dM}{dt}=V_0\left[\alpha\frac{d\rho_g}{dt}+\rho_g\frac{d\alpha}{dt}+(1-\alpha)\frac{d\rho_f}{dt}-\rho_f\frac{d\alpha}{dt}\right]=\dot{m}_{in}-\dot{m}_{out} \tag{A-40}$$

Substituting Equations (A-36) and (A-37) into (A-40) gives

$$\frac{dM}{dt}=V_0\left[\left(1-\frac{L}{H_0}\right)\frac{d\rho_g}{dt}+\rho_g\frac{d\left(1-\frac{L}{H_0}\right)}{dt}+\frac{L}{H_0}\frac{d\rho_f}{dt}-\rho_f\frac{d\left(1-\frac{L}{H_0}\right)}{dt}\right]=\dot{m}_{in}-\dot{m}_{out} \tag{A-41}$$

Expanding the derivative terms, assuming that the saturated liquid density is constant, and collecting dL/dt terms gives

$$\frac{V_0}{H_0}(\rho_f-\rho_g)\frac{dL}{dt}=\dot{m}_{in}-\dot{m}_{out}-V_0\left(1-\frac{L}{H_0}\right)\frac{d\rho_g}{dt} \tag{A-42}$$

Along the saturation line, ρ_g is a function of pressure only so we can write

$$\frac{d\rho_g}{dt}=\frac{d\rho_g}{dp}\Big|_{sat}\frac{dp}{dt} \tag{A-43}$$

and Equation (A-42) becomes

$$\frac{V_0}{H_0}(\rho_f-\rho_g)\frac{dL}{dt}=\dot{m}_{in}-\dot{m}_{out}-V_0\left(1-\frac{L}{H_0}\right)\frac{d\rho_g}{dp}\Big|_{sat}\frac{dp}{dt} \tag{A-44}$$

For equilibrium conditions, the quality can be written in terms of void fraction and density as

$$x = \alpha\frac{\rho_g}{\rho} = \left(1 - \frac{L}{H_0}\right)\frac{v}{v_g} = \frac{\left(1 - \frac{L}{H_0}\right)}{v_g}\frac{V_0}{M} \tag{A-45}$$

Defining L^* to be L/H_0, substituting into Equation (A-38), and collecting terms gives

$$M = V_0\left[\frac{1}{v_g} - L^*\left(\frac{1}{v_g} - \frac{1}{v_f}\right)\right] = V_0\left[\frac{1-L^*}{v_g} + \frac{L^*}{v_f}\right] \tag{A-46}$$

Using the definition of L^* and substituting into Equation (A-45) yields the following expression for quality in terms of liquid height and specific volumes

$$x = \frac{1-L^*}{1+L^*\left(\frac{v_g}{v_f} - 1\right)} \tag{A-47}$$

The specific enthalpy, specific volume, and specific internal energy terms in Equation (A-26) can be written in terms of quality using Equations (A-22), (A-23), and (A-32). The result in turn can be written in terms of L^* using Equation (A-47). Likewise, Equation (A-35), the derivative of specific internal energy with respect to pressure at constant specific volume, can be written in terms of L^*. Performing these substitutions and using Equation (A-46) for M gives after algebra and simplification the following pressure rate equation

$$\frac{dP}{dt} = \frac{1}{V_0\rho}\frac{1}{\left.\frac{\partial\mu}{\partial P}\right|_v}\left[\sum \dot{m}_{in}\left\{h_{in} - \mu_f - \frac{(1-L^*)}{1+L^*\left(\frac{v_g}{v_f}-1\right)}\mu_{fg} + \left(v_f + \frac{(1-L^*)}{1+L^*\left(\frac{v_g}{v_f}-1\right)}v_{fg}\right)\frac{\mu_{fg}}{v_{fg}}\right\}\right.$$

$$-\sum \dot{m}_{out}\left\{h_f + \frac{(1-L^*)}{1+L^*\left(\frac{v_g}{v_f}-1\right)}h_{fg} - \mu_f - \frac{(1-L^*)}{1+L^*\left(\frac{v_g}{v_f}-1\right)}\mu_{fg}\right. \tag{A-48}$$

$$\left.\left.+\left(v_f + \frac{(1-L^*)}{1+L^*\left(\frac{v_g}{v_f}-1\right)}v_{fg}\right)\frac{\mu_{fg}}{v_{fg}}\right\} + q_{net}\right]$$

Note that it is assumed that the outflows have volume average properties whereas inflows do not.

Using Equations (A-23) and (A-47) in (A-35) and performing similar operations gives the following expression for the thermodynamic property derivative in terms of L^*.

$$\left.\frac{\partial\mu}{dp}\right|_v = \left\{\frac{dh_f}{dp} - \frac{d}{dp}\left(\frac{v_f h_{fg}}{v_{fg}}\right)\right\} + \left\{v_f + \frac{(1-L^*)v_{fg}}{1+L^*\left(\frac{v_g}{v_f}-1\right)}\left[\frac{d}{dp}\left(\frac{h_{fg}}{v_{fg}}\right)-1\right]\right\} \tag{A-49}$$

Equations (A-48) and (A-49) along with the tank level equation ((A-44)) repeated below

$$\frac{V_0}{H_0}(\rho_f-\rho_g)\frac{dL}{dt} = \dot{m}_{in} - \dot{m}_{out} - V_0\left(1-\frac{L}{H_0}\right)\left.\frac{d\rho_g}{dp}\right|_{sat}\frac{dp}{dt} \tag{A-50}$$

form a set that can be used to analyze the depressurization of a component control volume. The unknowns in these equations are the level L (or L^*) and the pressure p. Boundary and initial conditions for the flow rates and thermodynamic states must be provided.

Nondimensionalization of Equations

It is useful to nondimensionalize the equations developed in the previous section so that an order of magnitude analysis can be conducted using experimental facility data to provide boundary conditions.

First we will nondimensionalize Equation (A-48). The following variables are defined where the subscript 0 denotes some as yet unspecified reference state

$$v = \frac{V_0}{M} \Rightarrow v^* = \frac{v}{V_0/M_0};\rho^* = \frac{\rho}{\rho_0};h^* = \frac{h}{h_0};p^* = \frac{p}{p_0};\mu^* = \frac{\mu}{\mu_0};\dot{m}^* = \frac{\dot{m}}{\dot{m}_0};$$
$$q^*_{net} = \frac{q_{net}}{q_{net_0}};t^* = \frac{t}{t_0};\left.\frac{\partial\mu}{\partial p}\right|_v^* = \frac{\partial\mu/\partial p|_v}{\partial\mu/\partial p|_{v_0}} \tag{A-51}$$

Nondimensionalizing each term in Equation (A-48) using (A-51) gives the following:

$$\frac{dp}{dt} = \frac{d(p_0p^*)}{d(t_0t^*)} = \frac{p_0}{t_0}\frac{dp^*}{dt^*} \tag{A-52}$$

$$V_0\left[\frac{1-L^*}{v_g}+\frac{L^*}{v_f}\right]\left.\frac{\partial\mu}{\partial p}\right|_v = V_0\left[\frac{1-L^*}{v_g^*\frac{V_0}{M_0}}+\frac{L^*}{v_f^*\frac{V_0}{M_0}}\right]\left.\frac{\partial\mu}{\partial p}\right|_{v_0}\left.\frac{\partial\mu^*}{\partial p^*}\right|_{v^*}$$
$$= M_0\left.\frac{\partial\mu}{\partial p}\right|_{v_0}\left[\frac{1-L^*}{v_g^*}+\frac{L^*}{v_f^*}\right]\left.\frac{\partial\mu^*}{\partial p^*}\right|_{v^*} = M_0\left.\frac{\partial\mu}{\partial p}\right|_{v_0}\varphi\left.\frac{\partial\mu^*}{\partial p^*}\right|_{v^*} \tag{A-53}$$

where φ is defined as

$$\varphi = \left[\frac{1-L^*}{v_g^*} + \frac{L^*}{v_f^*}\right]. \tag{A-54}$$

$$\sum \dot{m}_{in}\left(h_{in} - \left(\mu_f + x\mu_{fg}\right) + \left(v_f + xv_{fg}\right)\frac{\mu_{fg}}{v_{fg}}\right) = \sum \dot{m}_{in}^* \dot{m}_0 (h-\mu)_0 \left(h_{in} - \left(\mu_f + x\mu_{fg}\right)\right)^* +$$

$$\sum \dot{m}_{in}^* \dot{m}_0 \frac{v_0 \mu_{fg_0}}{v_{fg_0}} \left(v_f^* + xv_{fg}^*\right)\frac{\mu_{fg}^*}{v_{fg}^*} \tag{A-55}$$

$$= \dot{m}_0 (h_{in} - \mu)_0 \sum \dot{m}_{in}^* \left(h_{in} - \left(\mu_f + x\mu_{fg}\right)\right)^* + \dot{m}_0 v_0 \frac{\mu_{fg_0}}{v_{fg_0}} \sum \dot{m}_{in}^* \left(v_f + xv_{fg}\right)^* \frac{\mu_{fg}^*}{v_{fg}^*}$$

$$\sum \dot{m}_{out}\left(h_f + xh_{fg} - \left(\mu_f + x\mu_{fg}\right) + \left(v_f + xv_{fg}\right)\frac{\mu_{fg}}{v_{fg}}\right) =$$

$$\sum \dot{m}_{out}^* \dot{m}_0 (h-\mu)_0 \left(h_f + xh_{fg} - \left(\mu_f + x\mu_{fg}\right)\right)^* + \sum \dot{m}_{out}^* \dot{m}_0 \frac{v_0 \mu_{fg_0}}{v_{fg_0}} \left(v_f + xv_{fg}\right)^* \frac{\mu_{fg}^*}{v_{fg}^*} \tag{A-56}$$

$$= \dot{m}_0 (h-\mu)_0 \sum \dot{m}_{out}^* \left(h_f + xh_{fg} - \left(\mu_f + x\mu_{fg}\right)\right)^* + \dot{m}_0 v_0 \frac{\mu_{fg_0}}{v_{fg_0}} \sum \dot{m}_{out}^* \left(v_f + xv_{fg}\right)^* \frac{\mu_{fg}^*}{v_{fg}^*}$$

Putting Equations (A-52) through (A-56) into (A-48), multiplying the result by t_0 / p_0, and simplifying gives

$$\frac{dp^*}{dt^*} = \frac{t_0 \dot{m}_0 (h_{in} - \mu)_0}{p_0 M_0} \frac{\partial p}{\partial \mu}\bigg|_{v_0} \sum \dot{m}_{in}^* \left(h_{in} - \left(\mu_f + x\mu_{fg}\right)\right)^* \frac{\partial p}{\partial \mu}\bigg|_v^* \frac{1}{M^*}$$

$$+ \frac{t_0 \dot{m}_0 v_0}{p_0 M_0} \frac{\mu_{fg_0}}{v_{fg_0}} \frac{\partial p}{\partial \mu}\bigg|_{v_0} \sum \dot{m}_{in}^* \left(v_f + xv_{fg}\right)^* \frac{\mu_{fg}^*}{v_{fg}^*} \frac{\partial p}{\partial \mu}\bigg|_v^* \frac{1}{M^*}$$

$$- \frac{t_0 \dot{m}_0 (h-\mu)_0}{p_0 M_0} \frac{\partial p}{\partial \mu}\bigg|_{v_0} \sum \dot{m}_{out}^* \left(h_f + xh_{fg} - \left(\mu_f + x\mu_{fg}\right)\right)^* \frac{\partial p}{\partial \mu}\bigg|_v^* \frac{1}{M^*} \tag{A-57}$$

$$- \frac{t_0 \dot{m}_0 v_0}{p_0 M_0} \frac{\mu_{fg_0}}{v_{fg_0}} \frac{\partial p}{\partial \mu}\bigg|_{v_0} \sum \dot{m}_{out}^* \left(v_f + xv_{fg}\right)^* \frac{\mu_{fg}^*}{v_{fg}^*} \frac{\partial p}{\partial \mu}\bigg|_v^* \frac{1}{M^*}$$

$$+ \frac{t_0 q_0}{p_0 M_0} \frac{\partial p}{\partial \mu}\bigg|_{v_0} q_{net}^* \frac{\partial p}{\partial \mu}\bigg|_v^* \frac{1}{M^*}$$

If the collection of reference parameters multiplying the nondimensional terms in Equation (A-57) is defined as

$$\Phi_1 = \frac{t_0 \dot{m}_0 (h_{in} - \mu)_0}{p_0 M_0} \left.\frac{\partial p}{\partial \mu}\right|_{v_0}$$

$$\Phi_2 = \frac{t_0 \dot{m}_0 v_0}{p_0 M_0} \frac{\mu_{fg_0}}{v_{fg_0}} \left.\frac{\partial p}{\partial \mu}\right|_{v_0}$$

$$\Phi_3 = \frac{t_0 \dot{m}_0 (h - \mu)_0}{p_0 M_0} \left.\frac{\partial p}{\partial \mu}\right|_{v_0} \qquad \text{(A-58)}$$

$$\Phi_4 = \frac{t_0 \dot{m}_0 v_0}{p_0 M_0} \frac{\mu_{fg_0}}{v_{fg_0}} \left.\frac{\partial p}{\partial \mu}\right|_{v_0}$$

$$\Phi_5 = \frac{t_0 q_0}{p_0 M_0} \left.\frac{\partial p}{\partial \mu}\right|_{v_0}$$

Equation (A-57) becomes

$$\begin{aligned}
\frac{dp^*}{dt^*} = {} & \Phi_1 \sum \dot{m}^*_{in} \left(h_{in} - \left(\mu_f + x\mu_{fg}\right)\right)^* \left.\frac{\partial p}{\partial \mu}\right|^*_v \frac{1}{M^*} \\
& + \Phi_2 \sum \dot{m}^*_{in} \left(v_f + x v_{fg}\right)^* \frac{\mu^*_{fg}}{v^*_{fg}} \left.\frac{\partial p}{\partial \mu}\right|^*_v \frac{1}{M^*} \\
& - \Phi_3 \sum \dot{m}^*_{out} \left(h_f + x h_{fg} - \left(\mu_f + x\mu_{fg}\right)\right)^* \left.\frac{\partial p}{\partial \mu}\right|^*_v \frac{1}{M^*} \qquad \text{(A-59)} \\
& - \Phi_4 \sum \dot{m}^*_{out} \left(v_f + x v_{fg}\right)^* \frac{\mu^*_{fg}}{v^*_{fg}} \left.\frac{\partial p}{\partial \mu}\right|^*_v \frac{1}{M^*} \\
& + \Phi_5 q^*_{net} \left.\frac{\partial p}{\partial \mu}\right|^*_v \frac{1}{M^*}
\end{aligned}$$

Equation (A-50), the expression for the tank level can be nondimensionalized in a similar fashion. Each term is as follows:

$$\frac{V_0}{H_0} (\rho_f - \rho_g) \frac{dL}{dt} = \frac{V_0 \rho_0}{H_0} (\rho^*_f - \rho^*_g) \frac{H_0}{t_0} \frac{dL^*}{dt^*} = \frac{V_0 \rho_0}{t_0} (\rho^*_f - \rho^*_g) \frac{dL^*}{dt^*} \qquad \text{(A-60)}$$

$$(\dot{m}_{in} - \dot{m}_{out}) = \dot{m}_0 (\dot{m}^*_{in} - \dot{m}^*_{out}) \qquad \text{(A-61)}$$

$$V_0 \left(1 - \frac{L}{H_0}\right) \frac{d\rho_g}{dp} \frac{dp}{dt} = V_0 \frac{\rho_0}{t_0} (1 - L^*) \frac{d\rho^*_g}{dp^*} \frac{dp^*}{dt^*} \qquad \text{(A-62)}$$

Substituting the above three expressions into Equation (A-50) gives after some simplification

$$\frac{dL^*}{dt^*} = \frac{\dot{m}_0 t_0}{\rho_0 V_0}\frac{\left(\dot{m}_{in}^* - \dot{m}_{out}^*\right)}{\left(\rho_g^* - \rho_f^*\right)} - \frac{\left(1-L^*\right)}{\left(\rho_g^* - \rho_f^*\right)}\frac{d\rho_g^*}{dp^*}\frac{dp^*}{dt^*}$$

$$= \Phi_6\frac{\left(\dot{m}_{in}^* - \dot{m}_{out}^*\right)}{\left(\rho_g^* - \rho_f^*\right)} - \frac{\left(1-L^*\right)}{\left(\rho_g^* - \rho_f^*\right)}\frac{d\rho_g^*}{dp^*}\frac{dp^*}{dt^*} \qquad \text{(A-63)}$$

where Φ_6 is defined as $\dot{m}_0 t_0/M_0$.

Summary

Nondimensional forms of the pressure rate equation, the level equation, definitions, and nondimensional groups are

Pressure rate equation

$$\frac{dp^*}{dt^*} = \Phi_1\sum \dot{m}_{in}^*\left(h_{in} - \left(\mu_f + x\mu_{fg}\right)\right)^*\frac{\partial p}{\partial \mu}\bigg|_v^*\frac{1}{M^*} + \Phi_2\sum \dot{m}_{in}^*\left(v_f + xv_{fg}\right)^*\frac{\mu_{fg}^*}{v_{fg}^*}\frac{\partial p}{\partial \mu}\bigg|_v^*\frac{1}{M^*}$$

$$-\Phi_3\sum \dot{m}_{out}^*\left(h_f + xh_{fg} - \left(\mu_f + x\mu_{fg}\right)\right)^*\frac{\partial p}{\partial \mu}\bigg|_v^*\frac{1}{M^*} - \Phi_4\sum \dot{m}_{out}^*\left(v_f + xv_{fg}\right)^*\frac{\mu_{fg}^*}{v_{fg}^*}\frac{\partial p}{\partial \mu}\bigg|_v^*\frac{1}{M^*} \qquad \text{(A-64)}$$

$$+\Phi_5 q_{net}^*\frac{\partial p}{\partial \mu}\bigg|_v^*\frac{1}{M^*}$$

Level equation

$$\frac{dL^*}{dt^*} = \Phi_6\frac{\left(\dot{m}_{in}^* - \dot{m}_{out}^*\right)}{\left(\rho_g^* - \rho_f^*\right)} - \frac{\left(1-L^*\right)}{\left(\rho_g^* - \rho_f^*\right)}\frac{d\rho_g^*}{dp^*}\frac{dp^*}{dt^*} \qquad \text{(A-65)}$$

where the nondimensional groups are

$$\Phi_1 = \frac{t_0\dot{m}_0\left(h_{in} - \mu\right)_0}{p_0 M_0}\frac{\partial p}{\partial \mu}\bigg|_{v_0} \qquad \text{(A-66)}$$

$$\Phi_2 = \frac{t_0\dot{m}_0 v_0}{p_0 M_0}\frac{\mu_{fg_0}}{v_{fg_0}}\frac{\partial p}{\partial \mu}\bigg|_{v_0} \qquad \text{(A-67)}$$

$$\Phi_3 = \frac{t_0\dot{m}_0\left(h - \mu\right)_0}{p_0 M_0}\frac{\partial p}{\partial \mu}\bigg|_{v_0} \qquad \text{(A-68)}$$

$$\Phi_4 = \frac{t_0\dot{m}_0 v_0}{p_0 M_0}\frac{\mu_{fg_0}}{v_{fg_0}}\frac{\partial p}{\partial \mu}\bigg|_{v_0} \qquad \text{(A-69)}$$

$$\Phi_5 = \frac{t_0 q_0}{p_0 M_0} \left.\frac{\partial p}{\partial \mu}\right|_{v_0} \tag{A-70}$$

$$\Phi_6 = \frac{t_0 \dot{m}_0}{M_0} \tag{A-71}$$

Reference

A-1. R. T. Lahey and F. J. Moody, "The Thermal-Hydraulics of a Boiling Water Nuclear Reactor," American Nuclear Society, Chicago, IL, 1977.

APPENDIX B

TABLES OF USEFUL AP600 FACILITY PARAMETERS

APPENDIX B

TABLES OF USEFUL AP600 FACILITY PARAMETERS

Tables of geometric and operational parameters for the AP600 design and the AP600 test facilities are included in this appendix. Table B-1 includes a cross section of parameters for various components in the systems. Tables B-2 and B-3 include additional detail on the ADS1-3 and ADS-4 diameters and areas. Table B-4 is a compendium of component elevations relative to the hot leg centerlines of the various facilities. Component volumes are given in Table B-5. Hydraulic resistance distribution is listed in Table B-6. Tables B-7 through B-14 provide useful information pursuant to the ADS-4 blowdown phase and the IRWST refill phase.

Table B-1. Useful facility parameters.

Facility	AP600	ROSA	SPES	APEX
Parameter/Component				
Distance from core bottom to midpoint of ADS1-3 valves (m)				
Primary volume (m^3)				
Initial pressure (MPa)				
Initial hot leg temp (K)				
Initial cold leg temp (K)				
Initial core flowrate (kg/s)				
Initial core power (MW)				
Vessel				
Inside diameter (m)				
Wall thickness (m)				
Core height (m)				
Lower plenum height (m)				
Upper plenum height (m)				
Upper head height (m)				
Downcomer gap (m)				
Hot legs				
Inner diameter (m)				
Average length (m)				
Wall thickness (mm)				
Steam generators (1/2)				
Total plena volume (m^3)				
Plena height (m)				
Tubesheet thickness (m)				
Tube ID (mm)				
Tube wall thickness (mm)				
Number of tubes				
Height tallest tube bend above tubesheet (m)				
Height of shortest tube bend above tubesheet (m)				
Tube and plena volume (m^3)				
Cold legs				
Number				
Inner diameter (m)				
Average length (m)				
Wall thickness (mm)				

a,c

Table B-1. Useful facility parameters (continued).

Facility / Parameter/Component	AP600	ROSA	SPES	APEX
Pressurizer				
Tank ID (m)				
Volume (m^3)				
Height (m)				
Surge line ID (mm)				
Surge line length (m)				
Surge line volume (m^3)				
PRHR				
Inlet line ID (mm)				
Inlet line length (m)				
Average tube length (m)				
Tube ID (mm)				
Tube thickness (mm)				
Number				
Outlet line length (m)				
CMT (1/2)				
Tank height (m)				
Tank ID (m)				
Tank volume (m^3)				
PBL ID (mm)				
PBL length (m)				
Discharge line length (m)				
ADS1-3				
Inlet line ID (mm)				
Average inlet line length (m)				
Average outlet line length (m)				
Total flow area (m^2)				
Sparger to bottom IRWST (m)				
ADS4				
Inlet line ID (mm)				
Elevation of discharge above hot leg (m)				
Total flow area (m^2)				
Valves represented				
IRWST				
Tank height (m)				
Tank ID (m)				
Elevation of bottom tank above hot leg (m)				
Tank volume (m^3)				

9,c

Table B-1. Useful facility parameters (continued).

Facility	AP600	ROSA	SPES	APEX
Parameter/Component				
Accumulator (1/2)				
Tank volume (m^3)				
Discharge line ID (mm)				
Discharge line length (m)				
Break (1-inch)				
Diameter (mm)				

a,c

Table B-2. ADS and break diameters.

Facility	AP600		ROSA		SPES		APEX
Component	dia.[a] (mm)	dia.[b] (mm)	dia.[c] (mm)	dia.[d] (mm)	dia.[e] (mm)	dia.[f] (mm)	dia.[g] (mm)
ADS-1							
ADS-2							
ADS-1+2							
ADS-3							
ADS-1+2+3							
ADS4-1							
ADS4-2							
ADS4-total							
Break(1 inch)							

a,c

a. Scaled plant value for SPES configuration (second ROSA column * sqrt(30.5))
b. Nominal expected plant value (from RELAP5 input deck)
c. SPES configuration values (ROSA Test AP-CL-03)
d. Nominal scaled AP600 values for ROSA
e. SPES scaled values (first ROSA column*sqrt(30.5/395))
f. Actual SPES values (Note that ADS-4 is 1.6 oversized on diameter)
g. Actuals for OSU APEX Test NRC22

Table B-3. ADS and break areas.

Facility	AP600		ROSA		SPES		APEX
Component	area[a] (mm^2)	area[b] (mm^2)	area[c] (mm^2)	area[d] (mm^2)	area[e] (mm^2)	area[f] (mm^2)	area[g] (mm^2)
ADS-1							
ADS-2							
ADS-1+2							
ADS-3							
ADS-1+2+3							
ADS4-1							
ADS4-2							
ADS4-total							
Break(1 inch							

a. Scaled plant value for SPES configuration (second ROSA column * 30.5)
b. Nominal expected plant value (from RELAP5 input deck)
c. SPES configuration values (ROSA Test AP-CL-03)
d. Nominal scaled AP600 values for ROSA
e. SPES scaled values (first ROSA column*(30.5/395))
f. Actual SPES values (Note that ADS-4 is 1.6 oversized on diameter)
g. Actuals for OSU APEX Test NRC22

Table B-4. AP600 and facility component elevations in meters relative to hot leg center line.

Component	AP600 (m)	ROSA (m)	SPES (m)	APEX (m)
Bottom lower plenum				
Downcomer bottom				
Downcomer top				
Bottom of heated length				
Top of heated length				
Bottom of upper head				
DVI nozzle centerline				
Hot leg centerline				
Cold leg centerline				
Pressurizer bottom				
Pressurizer top				
Top of SG tube sheet				
Secondary level				
Top of U-tubes (tall)				
Top of U-tubes (short)				
Bottom of CMT				
Top of CMT				
Bottom of accumulator				
Top of accumulator				
Bottom of PRHR heat exchanger (average)				
Top of PRHR heat exchanger (average)				
Bottom of IRWST (Z_1)				
IRWST water level				
Top of vessel				
Bottom of vessel				
Sump elevation (top)				
Sump elevation (bottom)				
Sparger elevation (Z_2)				
Sparger to bottom of IRWST (Z_2-Z_1)				
Curb elevation				
ADS-4				

a, c

Table B-5. Component volume distributions for AP600 and facilities.

Component	AP600 (m^3)	ROSA (m^3)	SPES (m^3)	APEX (m^3)
Downcomer				
Lower plenum				
Core				
Upper plenum				
Upper head				
Hot leg #1				
Steam generator #1				
Cold leg #1				
Cold leg #3				
Hot leg #2				
Steam generator #2				
Cold leg #2				
Cold leg #4				
Pressurizer				
Pressurizer surge line				
DVI line #1				
CMT #1				
PBL #1				
Accumulator #1				
Accumulator #1(liquid)				
DVI line #2				
CMT #2				
PBL #2				
Accumulator #2				
Accumulator #2(liquid)				
Total (include ACC tank) (m^3)				
Total (include ACC liquid) (m^3)				
Total (no ACC) (m^3)				
Total (no CMT, no ACC) (m^3)				

a,c

Table B-6. Hydraulic resistance for AP600 and facilities.

Component Hydraulic resistance	AP600 (m^{-4})	ROSA (m^{-4})	SPES (m^{-4})	APEX (m^{-4})	SPES (flow test) (m^{-4})
Annular DC and CL nozzles (avg)					
Downcomer					
Lower plenum					
Core inlet					
Core					
Core outlet					
Upper plenum and HL nozzles (avg)					
Vessel total					
Hot leg A nozzle					
Hot leg A					
SG A					
Cold leg A					
Cold leg A nozzle					
Two CLs in parallel					
Loop A total (CLs in parallel)					
Hot leg B nozzle					
Hot leg B					
SG B					
Cold leg B					
Cold leg B nozzle					
Two CLs in parallel					
Loop B total (CLs in parallel)					
Pressurizer surge line					
Common PBL					
PBL-A					
Common+PBL-A					
PBL-B					
Common+PBL-B					
CMT-A discharge line					
CMT-B discharge line					
IRWST common					
IRWST-A line					
IRWST-B line					
DVI-A line					
DVI-B line					
Sump-A					
Sump-B					

9, C

Table B-6. Hydraulic resistance for AP600 and facilities (continued).

Component Hydraulic resistance	AP600 (m^{-4})	ROSA (m^{-4})	SPES (m^{-4})	APEX (m^{-4})	SPES (flow test) (m^{-4})
IRWST/DVI-A combined					
IRWST/DVI-B combined					
Sump/IRWST/DVI-A combined					
Sump/IRWST/DVI-B combined					
ACC-A discharge line					
ACC-B (or H) discharge line					
PRHR lines and heat exchanger					
ADS1-3 common inlet					
ADS-1 valve/orifice					
ADS-2 valve/orifice					
ADS-3 valve/orifice					
ADS1-3 common outlet					
Common inlet+ADS-1+ common outlet					
Common inlet+ADS-2+ common outlet					
Common inlet+ADS-3+ common outlet					
ADS-4 (1 failure)					
ADS-4 (0 failure)					

a, c

Note: SPES accumulator data are without any orificing.

Table B-7. CMT and vessel areas.

Facility	ROSA	SPES	APEX
CMT Area (m^2)[1]			
Vessel area (m^2)[2]			

a, c

1. Area of one CMT.
2. Represents downcomer plus core area

Table B-8. Levels at initiation of ADS-4 blowdown.

Facility	ROSA[3]	SPES[4,5]	APEX[6]
CMT-A (m)[1]			
CMT-B (m)[1]			
Downcomer (m)[2]			

a, c

1. Level relative to bottom of CMT tank (based on data).
2. Collapsed level relative to bottom tap used in the measurement.
3. Data for Test AP-CL-03.
4. Levels at 5300 s (time at which "A" tank reached 20% level) [ADS-4 fired at 5653 s].
5. Data for Test S00401.
6. Data for Test SB05.

Table B-9. Levels from Table B-8 put on a common basis (bottom of core heated length).

Facility	ROSA	SPES	APEX
Downcomer level bottom tap elevation with respect to hot leg centerline (m)			
Bottom of heated length with respect to hot leg centerline (m)			
DVI nozzle centerline with respect to hot leg centerline (m)			

a,c

Table B-10. Elevation of bottom of CMT tank relative to hot leg centerline.

Facility	ROSA	SPES	APEX
Elevation of CMT tank bottom relative to hot leg centerline (m)			

a,c

Table B-11. Conditions at start of ADS-4 blowdown.

Facility	ROSA	SPES	APEX
Downcomer level relative to bottom of heated length (m)[1]			
Elevation of CMT level relative to bottom of heated length (m)[2]			
Elevation of DVI nozzle relative to bottom of heated length (m)[3]			

a,c

1. Equation (a) below.
2. Equation (b) below.
3. Equation (c) below.

Table B-12. Equations for Table B-11.

Equation (a): $L_{DC} = L_{DC,m} + (Z_{bottom\ tap\ DC} - Z_{bottom\ heated\ length})$

L_{DC} - downcomer level relative to bottom of heated length

$L_{DC,m}$ - measured downcomer level

$Z_{bottom\ tap,DC}$ - elevation of bottom tap used for downcomer level measurement

$Z_{bottom\ heated\ length}$ - elevation of bottom of heated length with respect to hot leg centerline

Equation (b): $Z_{CMT\ level} = L_{CMT\ level} + Z_{CMT\ tank} + |Z_{bottom\ heated\ length}|$

$Z_{CMT\ level}$ - CMT level relative to bottom of heated length

$L_{CMT\ level}$ - measured CMT tank level

$Z_{CMT\ tank}$ - elevation of bottom of CMT relative to hot leg centerline

$Z_{bottom\ heated\ length}$ - elevation of bottom of heated length relative to hot leg centerline

Equation (c): $Z_{DVI\ nozzle} = Z_{DVI\ nozzle\ rel\ HLCL} - Z_{bottom\ heated\ length}$

$Z_{DVI\ nozzle}$ - DVI nozzle centerline relative to bottom of heated length

$Z_{DVI\ nozzle\ rel\ HLCL}$ - DVI nozzle centerline relative to hot leg centerline

$Z_{bottom\ heated\ length}$ - elevation of bottom of heated length relative to hot leg centerline

Table B-13. ADS-4 offtake diameters and ratios.

Facility	AP600	ROSA	SPES	APEX
Hot leg diamter (m)				
A-side[1] diameter (m)				
B-side[2] diameter (m)				
Offtake diameter/hot leg diameter				
A-side				
B-side				
Offtake area/hot leg area				
A-side				
B-side				

a, c

1. Loop containing PRHR and pressurizer.
2. Loop without pressurizer.

Table B-14. IRWST parameters.

Facility	AP600	ROSA[4]	SPES[5]	APEX[6]
ΔY (m)[1]				
$Y_{DVI,0}$ (m)[2]				
L_{IRWST} (m)[3]				

a, c

1. Bottom of IRWST - bottom of heated length.
2. $L_{IRWST,0} - Y_{DVI}$
3. IRWST level relative to bottom of IRWST tank.
4. Data from Test AP-CL-03.
5. Data from Test S00401.
6. Data from Test SB05.

APPENDIX C

MULTIFIELD PRESSURE RATE EQUATION DEVELOPMENT FOR THE INTERMEDIATE PHASE

APPENDIX C

MULTIFIELD PRESSURE RATE EQUATION DEVELOPMENT FOR THE INTERMEDIATE PHASE

This Appendix details the development of a simple multi-field pressure rate equation useful for the analysis of the depressurization of a system containing subcooled liquid, saturated fluid, and noncondensible gases. The development is done for a control volume of fixed size. The equations are cast in nondimensional form after development.

Equation Development

Consider the volume shown in Figure C-1 containing fluid fields i, j,...etc. (only two of them being shown). Using subscript k to denote either field, conservation of mass can be written for each control volume as

$$\frac{\partial \rho_k V_k}{\partial t} = \sum \dot{m}_{in,k} - \sum \dot{m}_{out,k} \tag{C-1}$$

and conservation of energy can be written as

$$\frac{\partial \rho_k V_k \varepsilon_k}{\partial t} = \sum \dot{m}_{in,k} e_{in,k} - \sum \dot{m}_{out,k} e_{out,k} + \dot{q}_{net,k} \tag{C-2}$$

where

ε - total specific energy of field k (internal + kinetic + potential)
e_k - convected specific energy of field k (enthalpy + kinetic + potential)
$\dot{m}_k$ - mass flow into or out of field k

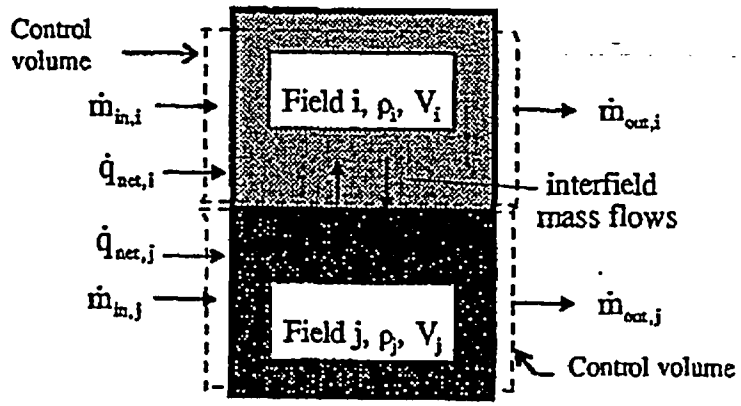

Figure C-1. Example of a volume containing two fields; the development is for a multifield system.

$\dot{q}_{net,k}$ - net energy transferred into or out of field k

ρ_k - density of phase k

V_k - volume occupied by field k

Note that the interfield transfer terms have not been written explicitly. As we will see later, they cancel, to a first approximation, in the dP/dt equation and special identification is not necessary. For the time being, consider them to be part of the inflows and outflows belonging to a field, k.

Neglecting kinetic and potential energies we note that for the conditions of interest here

$$e_k = h_k = u_k + P_k v_k. \tag{C-3}$$

where h_k is enthalpy, u_k is internal energy, and v_k is specific volume.

The pressure in each field is assumed to be equal and can be represented as a function of two intensive variables. If we let the pressure be a function of internal energy and specific volume then

$$P_k = P(u_k, v_k) \tag{C-4}$$

Equation (C-4) can be differentiated with respect to time to get a pressure rate equation as

$$\frac{dP_k}{dt} = \left.\frac{\partial P_k}{\partial e_k}\right|_{v_k} \frac{\partial e_k}{\partial t} + \left.\frac{\partial P_k}{\partial v_k}\right|_{e_k} \frac{\partial v_k}{\partial t} \tag{C-5}$$

Expanding the LHS of Equation (C-2) and substituting Equations (C-1) and (C-3) gives

$$\frac{\partial \rho_k V_k u_k}{\partial t} = \rho_k V_k \frac{\partial u_k}{\partial t} + u_k \frac{\partial \rho_k V_k}{\partial t} = \rho_k V_k \frac{\partial u_k}{\partial t} + u_k \left(\sum \dot{m}_{in,k} - \sum \dot{m}_{out,k}\right) \tag{C-6}$$

Combining this result with the RHS of Equation (C-2) and combining terms yields

$$\rho_k V_k \frac{\partial u_k}{\partial t} = \sum \dot{m}_{in,k}(h_{in,k} - u_k) - \sum \dot{m}_{out,k}(h_{out,k} - u_k) + \dot{q}_{net,k} \tag{C-7}$$

The LHS of the continuity equation can be written using specific volume rather than density and expanded to get

$$\frac{\partial V_k}{\partial t} - v_k\left(\sum \dot{m}_{in,k} - \sum \dot{m}_{out,k}\right) = \rho_k V_k \frac{\partial v_k}{\partial t} \tag{C-8}$$

Since the total volume of the control volume shown in Figure C-1 is constant, Equation (C-8) can be summed over the fields of interest noting that

$$\sum_k \frac{\partial V_k}{\partial t} = 0 \tag{C-9}$$

to get

$$\sum_k \rho_k V_k \frac{\partial v_k}{\partial t} = -\sum_k v_k \left[\sum \dot{m}_{in,k} - \sum \dot{m}_{out,k}\right] \tag{C-10}$$

A mass balance for each field can be written as

$$\frac{dM_k}{dt} = \sum \dot{m}_{in,k} - \sum \dot{m}_{out,k} \tag{C-11}$$

where M is the total mass. Summing Equation (C-11) over the fields, gives

$$\frac{dM}{dt} = \sum_k \frac{dM_k}{dt} = \sum_k \left[\sum \dot{m}_{in,k} - \sum \dot{m}_{out,k}\right] \tag{C-12}$$

where the inner sums denote the sums over in- and out flows.

Equation (C-12) can be nondimensionalized using reference values for M, t, and the flow rate to get

$$\frac{dM^*}{dt^*} = \Psi_{13} \sum_k \left[\sum \dot{m}^*_{in,k} - \sum \dot{m}^*_{out,k}\right] \tag{C-13}$$

where

$$\begin{aligned} M^* &= M/M_0 \\ t^* &= t/t_0 \\ \dot{m}^* &= \dot{m}/\dot{m}_0 \\ \Psi_{13} &= \frac{\dot{m}_0 t_0}{M_0} \end{aligned} \tag{C-14}$$

Multiplying Equation (C-5) by $\rho_k V_k$ and substituting Equations (C-7) and (C-8) for the time derivatives of internal energy and specific volume yields for the pressure rate equation

$$\begin{aligned} \rho_k V_k \frac{dP_k}{dt} = {} & \left.\frac{\partial P_k}{\partial u_k}\right|_{v_k} \left(\sum \dot{m}_{in,k}(h_{in,k} - u_k) - \sum \dot{m}_{out,k}(h_{out,k} - u_k) + \dot{q}_{net,k}\right) \\ & + \left.\frac{\partial P_k}{\partial v_k}\right|_{u_k} \left(\frac{\partial V_k}{\partial t} - v_k\left(\sum \dot{m}_{in,k} - \sum \dot{m}_{out,k}\right)\right) \end{aligned} \tag{C-15}$$

Using Equation (C-9) and summing Equation (C-15) over the fields noting that the pressure is the same in each field gives

$$\begin{aligned} \frac{dP}{dt} = {} & \frac{1}{\sum\left((\rho_k V_k)/\left(\partial P/\partial v|_u\right)_k\right)} \left\{\sum_k \frac{\partial P/\partial u|_v)_k}{\partial P/\partial v|_u)_k} \left[\sum \dot{m}_{in,k}\left(h_{in,k} - u_k\right) - \sum \dot{m}_{out,k}\left(h_{out,k} - u_k\right)\right.\right. \\ & \left.\left. + \dot{q}_{net,k}\right] - \sum_k v_k\left(\sum \dot{m}_{in,k} - \sum \dot{m}_{out,k}\right)\right\} \end{aligned} \tag{C-16}$$

For the three fields considered subscript l denotes subcooled liquid, m denotes a homogenous steam-water mixture, and N denotes nitrogen or steam.

For these fields, the interfield transfers are the result of inflows and outflows related to the mixture, where all the vaporization/condensation processes occur as intrafield transfers within the mixture field. By virtue of ΣV_k = constant, the effect of the interfield transfers in the last summation in Equation (C-16) vanish, i.e. the volumes removed or added to the mixture field by transfer of steam to the steam/nitrogen field or transfer of liquid to the subcooled field are exactly compensated for by changes in volume of these other fields. There is a small volume effect due to heating or cooling of these interfield flows once they enter a field at a different temperature, but the effect is small and is neglected here.

Expanding Equation (C-16) for the three fields considered gives

$$\frac{dP}{dt}=\frac{1}{\left(\frac{\rho_l V_l}{\partial P/\partial v_l|_{u_l}}+\frac{\rho_m V_m}{\partial P/\partial v_m|_{u_m}}+\frac{\rho_N V_N}{\partial P/\partial v_N|_{u_N}}\right)}\left\{\frac{\partial P/\partial u_l|_{v_l}}{\partial P/\partial v_l|_{u_l}}I_l+\frac{\partial P/\partial u_m|_{v_m}}{\partial P/\partial v_m|_{u_m}}I_m+\frac{\partial P/\partial u_N|_{v_N}}{\partial P/\partial v_N|_{u_N}}I_N\right.$$
$$\left.-II_l-II_m-II_N\right\} \qquad \text{(C-17)}$$

I_l, I_m, I_N, II_l, II_m, and II_N are defined as

$$I_l=\sum\dot{m}_{in,l}\left(h_{in,l}-u_l\right)-\sum\dot{m}_{out,l}\left(h_{out,l}-u_l\right)+\dot{q}_{net,l}$$
$$I_m=\sum\dot{m}_{in,m}\left(h_{in,m}-u_m\right)-\sum\dot{m}_{out,m}\left(h_{out,m}-u_m\right)+\dot{q}_{net,m}$$
$$I_N=\sum\dot{m}_{in,N}\left(h_{in,N}-u_N\right)-\sum\dot{m}_{out,N}\left(h_{out,N}-u_N\right)+\dot{q}_{net,N}$$
$$II_l=v_l\left(\sum\dot{m}_{in,l}-\sum\dot{m}_{out,l}\right) \qquad \text{(C-18)}$$
$$II_m=v_m\left(\sum\dot{m}_{in,m}-\sum\dot{m}_{out,m}\right)$$
$$II_N=v_N\left(\sum\dot{m}_{in,N}-\sum\dot{m}_{out,N}\right)$$

For convenience, the I_l, I_m, and I_N terms in Equation (C-18) can be written as

$$I_k=I_{a,k}+I_{b,k}+I_{c,k}$$

where

$$I_{a,l}=\sum\dot{m}_{in,l}\left(h_{in,l}-u_l\right)$$
$$I_{b,l}=\sum\dot{m}_{out,l}\left(h_{out,l}-u_l\right) \qquad \text{(C-19)}$$
$$I_{c,l}=\dot{q}_{net,l}$$

$$
\begin{aligned}
I_{a,m} &= \sum \dot{m}_{in,m}\left(h_{in,m} - u_m\right) \\
I_{b,m} &= \sum \dot{m}_{out,m}\left(h_{out,m} - u_m\right) \\
I_{c,m} &= \dot{q}_{net,m} \\
I_{a,N} &= \sum \dot{m}_{in,N}\left(h_{in,N} - u_N\right) \\
I_{b,N} &= \sum \dot{m}_{in,N}\left(h_{in,N} - u_N\right) \\
I_{c,N} &= \dot{q}_{net,N}
\end{aligned}
\qquad \text{(C-19)}
$$

Equation (C-17) can then be written in the following form

$$
\begin{aligned}
\frac{dP}{dt} &= C_{1,1}I_{a,1} + C_{1,1}I_{b,1} + C_{1,1}I_{c,1} + C_{1,m}I_{a,m} + C_{1,m}I_{b,m} + C_{1,m}I_{c,m} \\
&\quad + C_{1,N}I_{a,N} + C_{1,N}I_{b,N} + C_{1,N}I_{c,N} + C_2\Pi_1 + C_2\Pi_m + C_2\Pi_N
\end{aligned}
\qquad \text{(C-20)}
$$

where the C coefficients are defined as

$$
C_{1,k} = \frac{\partial P/\partial u\big|_{v_k} / \partial P/\partial v_k\big|_{u_k}}{\sum_k \rho_k V_k / \partial P/\partial v_k\big|_{u_k}}
\qquad \text{(C-21)}
$$

$$
C_2 = \frac{1}{\sum_k \rho_k V_k / \left(\partial P/\partial v_k\right)\big|_{u_k}}
\qquad \text{(C-22)}
$$

The C_1 coefficients for each field represent the partial derivative of pressure with specific energy at constant specific volume for the field adjusted by the mass fraction weighted ratio of partial derivatives of pressure with specific volume at constant specific energy for all the fields. The C_2 coefficient is the inverse of the sum of the mass fraction weighted partial derivatives of pressure with specific volume at constant specific energy for the fields.

Equation (C-20) can be nondimensionalized using the following definitions

$$
\begin{aligned}
&P^* = \frac{P}{P_0}; t^* = \frac{t}{t_0}; \dot{m}^* = \frac{\dot{m}}{\dot{m}_0}; \dot{q}^*_{net,i} = \frac{\dot{q}_{net,i}}{\dot{q}_0}; \rho^* = \frac{\rho}{\rho_0}; \\
&\rho^* V_i^* = \frac{\rho_i V_i}{M_0}; V_i^* = \frac{V_i}{V_0}; (h_i - u)^* = \frac{Pv}{(Pv)_0}; \\
&\left.\frac{\partial P}{\partial u_i}\right|^*_{v_i} = \left.\frac{\partial P}{\partial u_i}\right|_{v_i} \left.\frac{\partial u_i}{\partial P}\right|_{v_0}; \left.\frac{\partial P}{\partial v_i}\right|^*_{u_i} = \left.\frac{\partial P}{\partial v_i}\right|_{u_i} \left.\frac{\partial v_i}{\partial P}\right|_{u_0}
\end{aligned}
\qquad \text{(C-23)}
$$

to get

$$\frac{dP^*}{dt^*} = \Psi_1 C^*_{1,1} I^*_{a,1} + \Psi_2 C^*_{1,1} I^*_{b,1} + \Psi_3 C^*_{1,1} I^*_{c,1} + \Psi_4 C^*_{1,m} I^*_{a,m}$$
$$+\Psi_5 C^*_{1,m} I^*_{b,m} + \Psi_6 C^*_{1,m} I^*_{c,m} + \Psi_7 C^*_{1,N} I^*_{a,N} + \Psi_8 C^*_{1,N} I^*_{b,N} \quad \text{(C-24)}$$
$$+\Psi_9 C^*_{1,N} I^*_{c,N} + \Psi_{10} C^*_2 \Pi^*_1 + \Psi_{11} C^*_2 \Pi^*_m + \Psi_{12} C^*_2 \Pi^*_N$$

where the terms are defined as follows

$$\Psi_1 = C_{1,1,0}\dot{m}_0\left(h_{in,1} - u_1\right)_0 t_0 / P_0 = \frac{C_{1,1,0}\left(h_{in,1} - u_1\right)_0 M_0 \Psi_{13}}{P_0} \quad \text{(C-25)}$$

$$\Psi_2 = C_{1,1,0}\dot{m}_0\left(h_{out,1} - u_1\right)_0 t_0 / P_0 = \frac{C_{1,1,0}\left(h_{out,1} - u_1\right)_0 M_0 \Psi_{13}}{P_0} \quad \text{(C-26)}$$

$$\Psi_3 = C_{1,1,0}\dot{q}_0 t_0 / P_0 = \frac{C_{1,1,0}\dot{q}_0 M_0 \Psi_{13}}{P_0 \dot{m}_0} \quad \text{(C-27)}$$

$$\Psi_4 = C_{1,m,0}\dot{m}_0\left(h_{in,m} - u_m\right)_0 t_0 / P_0 = \frac{C_{1,m,0}\left(h_{in,m} - u_m\right)_0 M_0 \Psi_{13}}{P_0} \quad \text{(C-28)}$$

$$\Psi_5 = C_{1,m,0}\dot{m}_0\left(h_{out,m} - u_m\right)_0 t_0 / P_0 = \frac{C_{1,m,0}\left(h_{out,m} - u_m\right)_0 M_0 \Psi_{13}}{P_0} \quad \text{(C-29)}$$

$$\Psi_6 = C_{1,m,0}\dot{q}_0 t_0 / P_0 = \frac{C_{1,m,0}\dot{q}_0 M_0 \Psi_{13}}{P_0 \dot{m}_0} \quad \text{(C-30)}$$

$$\Psi_7 = C_{1,N,0}\dot{m}_0\left(h_{in,N} - u_N\right)_0 t_0 / P_0 = \frac{C_{1,N,0}\left(h_{in,N} - u_N\right)_0 M_0 \Psi_{13}}{P_0} \quad \text{(C-31)}$$

$$\Psi_8 = C_{1,N,0}\dot{m}_0\left(h_{out,N} - u_N\right)_0 t_0 / P_0 = \frac{C_{1,N,0}\left(h_{out,N} - u_N\right)_0 M_0 \Psi_{13}}{P_0} \quad \text{(C-32)}$$

$$\Psi_9 = C_{1,N,0}\dot{q}_0 t_0 / P_0 = \frac{C_{1,N,0}\dot{q}_0 M_0 \Psi_{13}}{P_0 \dot{m}_0} \quad \text{(C-33)}$$

$$\Psi_{10} = C_{2,0} v_{1,0}\dot{m}_0 t_0 / P_0 = \frac{C_{2,0} v_{1,0} M_0 \Psi_{13}}{P_0} \quad \text{(C-34)}$$

$$\Psi_{11} = C_{2,0} v_{m,0}\dot{m}_0 t_0 / P_0 = \frac{C_{2,0} v_{m,0} M_0 \Psi_{13}}{P_0} \quad \text{(C-35)}$$

$$\Psi_{12} = C_{2,0} v_{N,0} \dot{m}_0 t_0 / P_0 = \frac{C_{2,0} v_{N,0} M_0 \Psi_{13}}{P_0} \tag{C-36}$$

$$C^*_{1,l} = C_{1,l} / C_{1,l,0};\ C^*_{1,m} = C_{1,m} / C_{1,m,0};\ C^*_{1,N} = C_{1,N} / C_{1,N,0} \tag{C-37}$$

$$C^*_2 = C_2 / C_{2,0} \tag{C-38}$$

$$I^*_{a,l} = I_{a,l} / \left(\dot{m}_0 \left(h_{in,l} - u_l\right)_0\right);\ I^*_{a,m} = I_{a,m} / \left(\dot{m}_0 \left(h_{in,m} - u_m\right)_0\right);\ I^*_{a,N} = I_{a,N} / \left(\dot{m}_0 \left(h_{in,N} - u_N\right)_0\right) \tag{C-39}$$

$$I^*_{b,l} = I_{b,l} / \left(\dot{m}_0 \left(h_{out,l} - u_l\right)_0\right);\ I^*_{b,m} = I_{b,m} / \left(\dot{m}_0 \left(h_{out,m} - u_m\right)_0\right);\ I^*_{b,N} = I_{b,N} / \left(\dot{m}_0 \left(h_{out,N} - u_N\right)_0\right) \tag{C-40}$$

$$I^*_{c,l} = I_{c,l} / \dot{q}_0;\ I^*_{c,m} = I_{c,m} / \dot{q}_0;\ I^*_{c,N} = I_{c,N} / \dot{q}_0 \tag{C-41}$$

and Ψ_{13} is defined in Equation (C-14).

Equations (C-13), (C-14), and (C-24)-(C-41) represent the nondimensionalized mass balance and pressure rate equation for fields in a control volume of constant total volume. Table C-1 provides a description and physical interpretation of the dimensionless Ψ groups defined in Equation (C-14) and Equations (C-25)-(C-36).

Table C-1. Physical interpretation of Ψ groups for intermediate phase.

Dimensionless Coefficient	Physical Interpretation
Ψ_1	Ratio of pressure change, due to change in specific energy of the subcooled field from mass inflows, to the reference pressure
Ψ_2	Ratio of pressure change, due to change in specific energy of the subcooled field from mass outflows, to the reference pressure
Ψ_3	Ratio of pressure change, due to change in specific energy of the subcooled field from heat transfer, to the reference pressure
Ψ_4	Ratio of pressure change, due to change in specific energy of the saturated field from mass inflows, to the reference pressure
Ψ_5	Ratio of pressure change, due to change in specific energy of the saturated field from mass outflows, to the reference pressure
Ψ_6	Ratio of pressure change, due to change in specific energy of the saturated field from heat transfer, to the reference pressure
Ψ_7	Ratio of pressure change, due to change in specific energy of the Nitrogen/steam field from mass inflows, to the reference pressure
Ψ_8	Ratio of pressure change, due to change in specific energy of the Nitrogen/steam field from mass outflows, to the reference pressure
Ψ_9	Ratio of pressure change, due to change in specific energy of the Nitrogen/steam field from heat transfer, to the reference pressure

Table-C-1. Physical interpretation of Ψ groups for intermediate phase (cont'd).

Dimensionless Coefficient	Physical Interpretation
Ψ_{10}	Ratio of pressure change, due to change in specific volume of the subcooled field from heat transfer, to reference pressure
Ψ_{11}	Ratio of pressure change, due to change in specific volume of the saturated field from heat transfer, to reference pressure
Ψ_{12}	Ratio of pressure change, due to change in specific volume of the Nitrogen/steam field from heat transfer, to reference pressure
Ψ_{13}	Ratio of integrated mass flow to reference mass

Property Derivative Evaluation for Mixture Field

In the above development of the pressure rate equation thermodynamic property derivatives need to be evaluated. In particular, the following derivatives are required

$$\left.\frac{\partial P}{\partial u_k}\right|_{v_k} ; \left.\frac{\partial P}{\partial v_k}\right|_{u_k} \tag{C-42}$$

For the saturated mixture field we can write the following expressions for the internal energy and specific volume

$$\begin{aligned} u_k &= u_f + x u_{fg} \quad \text{and} \\ v_k &= v_f + x v_{fg} \end{aligned} \tag{C-43}$$

where

u_f - saturated liquid internal energy
u_g - saturated vapor internal energy
u_{fg} - internal energy change on vaporization ($u_g - u_f$)
v_f - saturated liquid specific volume
v_g - saturated vapor specific volume
v_{fg} - specific volume change on vaporization ($v_g - v_f$)
x - quality

Noting that

$$\left.\frac{\partial P}{\partial u_k}\right|_{v_k} = \frac{1}{\partial u_k / \partial P|_{v_k}}$$

we can write in general terms the derivative of internal energy with pressure using Equation (C-43) as

$$\left.\frac{\partial u}{\partial P}\right|_v = \frac{du_f}{dP} + x\frac{du_{fg}}{dP} + u_{fg}\left.\frac{\partial x}{\partial P}\right|_v \tag{C-44}$$

where the derivatives of subscripted variables such as u_f and u_{fg} are written as total derivatives since u_f and u_{fg} are only functions of pressure and the derivatives are assumed to be taken along the saturation line. Quality can be written in terms of specific volume or internal energy using Equation (C-43) as

$$x = \frac{v - v_f}{v_{fg}} \text{ or } x = \frac{u - u_f}{u_{fg}} \tag{C-45}$$

The first form of Equation (C-45) can be differentiated with respect to pressure at constant specific volume to get an expression for the quality derivative as

$$\left.\frac{\partial x}{\partial P}\right|_v = \left[\left.\frac{v_{fg}\partial(v - v_f)}{\partial P}\right|_v - (v - v_f)\Big|_v \frac{dv_{fg}}{dP}\right]\frac{1}{v_{fg}^2} = \frac{-1}{v_{fg}}\left[\frac{dv_f}{dP} + x\frac{dv_{fg}}{dP}\right] \tag{C-46}$$

Substituting Equation (C-46) into (C-44), using Equation (C-45), and noting that v is held constant then yields

$$\left.\frac{\partial u}{\partial P}\right|_v = \frac{du_f}{dP} + x\frac{du_{fg}}{dP} + \left(\frac{-u_{fg}}{v_{fg}}\right)\left[\frac{dv_f}{dP} + x\frac{dv_{fg}}{dP}\right] \tag{C-47}$$

In the same fashion, an expression for the derivative of specific volume with pressure at constant internal energy can be written as

$$\left.\frac{\partial v}{\partial P}\right|_u = \frac{dv_f}{dP} + x\frac{dv_{fg}}{dP} + \left(\frac{-v_{fg}}{u_{fg}}\right)\left[\frac{du_f}{dP} + x\frac{du_{fg}}{dP}\right] \tag{C-48}$$

C Coefficients for Multifield Depressurization Rate with One Field being an Ideal Gas

The C coefficients that arise in the multifield depressurization rate equation (Equation (C-16)) are defined by Equations (C-21) and (C-22). Consider that one of the fields is an ideal gas of molecular weight M. For example, this field could be near-atmospheric pressure steam, in which case M is 18, or near-atmospheric pressure nitrogen, in which case M is 28. We are interested in the impact of the ideal gas molecular weight and hence, gas composition in the field, on the C coefficients.

To proceed, we write the ideal gas equation of state as

$$Pv = \frac{P}{\rho} = \frac{RT}{M} \tag{C-49}$$

where R is the ideal gas constant, T is absolute temperature, and M is the molecular weight. We also note that for an ideal gas the internal energy is

$$u = C_v T \tag{C-50}$$

where the specific heat at constant volume is

$$C_V = \frac{C_{VM}}{M} \tag{C-51}$$

with C_{VM} being the molar specific heat at constant volume, which is a constant.

We can then write the property derivatives involved in the C coefficients as

$$\left.\frac{\partial P}{\partial u}\right|_v = \frac{1}{C_V}\left.\frac{\partial P}{\partial T}\right|_v = \frac{R}{C_V M v} \tag{C-52}$$

$$\left.\frac{\partial P}{\partial v}\right|_u = \left.\frac{\partial P}{\partial v}\right|_T = -\frac{1}{v^2}\frac{RT}{M} \tag{C-53}$$

Consider first the terms in the denominators of the C coefficients, i.e.

$$\sum_k \rho_k V_k \Big/ \left(\partial P/\partial v_k\right)\Big|_{u_k}$$

If field k is an ideal gas, then using Equations (C-49) and (C-53) we have

$$\rho_k V_k \Big/ \left(\partial P/\partial v_k\right)\Big|_{u_k} = \frac{V_k}{\left(-\frac{RT}{vM}\right)_k} = \frac{V_k}{-P}. \tag{C-54}$$

Clearly, Equation (C-54) indicates that the denominator of the C coefficients is independent of molecular weight M of the ideal gas field – if one exists.

Consider now the numerators of the C coefficients. For $C_{1,k}$ the numerator is

$$\left.\frac{\partial P}{\partial u_k}\right|_{v_k} \Big/ \left.\frac{\partial P}{\partial v_k}\right|_{u_k}$$

If field k is an ideal gas, then from Equations (C-49), (C-52), and (C-53) the numerator would be

$$\left.\frac{\partial P}{\partial u_k}\right|_{v_k} \Big/ \left.\frac{\partial P}{\partial v_k}\right|_{u_k} = \frac{R}{C_V M v} \Big/ \left(-\frac{1}{v^2}\frac{RT}{M}\right) = \frac{R}{C_{VM}} \Big/ (-P). \tag{C-55}$$

Recalling that C_{VM} is a constant independent of molecular weight, we come to the conclusion that, the numerators in the C coefficient expressions (Equations (C-21) and (C-22)) are also independent of molecular weight. Note that the numerator in Equation (C-22) is unity.

In view of both the numerators and denominators being independent of molecular weight of the ideal gas field, we conclude that the C coefficients will be independent of the composition of the ideal gas when it is one of the fields involved in the depressurization rate calculation. This means that the values of the C coefficients that may be involved in various scaling studies will not depend on whether the fields is steam, nitrogen, or some mixture.

APPENDIX D

PRHR REFERENCE HEAT TRANSFER AND FLOW RATE

APPENDIX D

PRHR REFERENCE HEAT TRANSFER AND FLOW RATE

In this appendix, we develop simple expressions for the natural circulation heat transfer rate in the passive residual heat removal system (PRHR). The resulting expressions are used to establish reference heat transfer values for the PRHR.

Consider the simple closed loop shown in Figure D-1. A heat addition section is contained in the lower portion of the loop and a heat removal section situated at a higher elevation. With respect to the AP600, the heat addition section represents the core and the heat removal section represents the PRHR heat exchanger tubes located in the IRWST tank.

For the purposes of this development we assume that the fluid in the region above the midpoint of the heat addition section to the midpoint of the heat removal section is at density ρ_h and that the fluid in the region below the midpoint of the heat removal section to the midpoint of the heat addition section is at density ρ_c where $\rho_c > \rho_h$.

For steady state conditions, the momentum equation for this loop implies a balance between the frictional pressure losses and the driving head due to the fluid density change or

$$\Delta P_f = \Delta P_H \qquad \text{(D-1)}$$

where ΔP_f and ΔP_H are the frictional losses and driving head, respectively. For the elevations shown on the loop in Figure D-1 along with the density distribution assumption discussed above, the driving head is

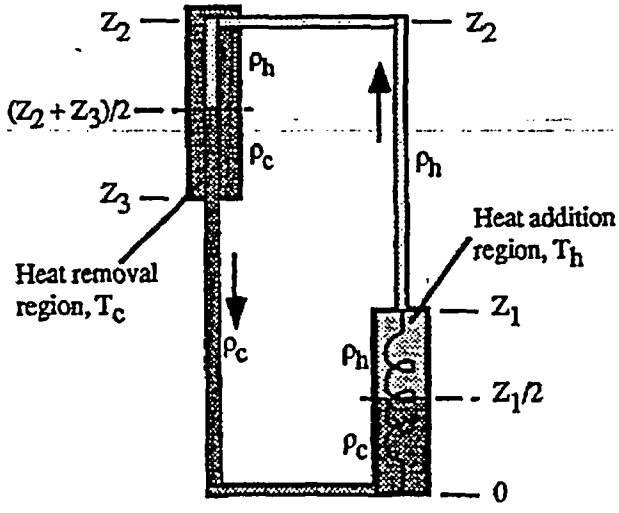

Figure D-1. Closed loop with heat addition and heat removal.

$$\Delta P_H = \rho_h g(Z_2 - \frac{Z_2 + Z_3}{2}) + \rho_c g(\frac{Z_2 + Z_3}{2}) - \rho_c g\frac{Z_1}{2} - \rho_h g(Z_1 - \frac{Z_1}{2}) - \rho_h g(Z_2 - Z_1) \quad \text{(D-2)}$$

which reduces to

$$\Delta P_H = (\rho_c - \rho_h) g(\frac{Z_2 + Z_3}{2} - \frac{Z_1}{2}) = \Delta\rho g \Delta Z \quad \text{(D-3)}$$

where g is the acceleration due to gravity, $\Delta\rho$ is ρ_c - ρ_h, and ΔZ is the difference in thermal center elevations in the heat removal section and the heat addition section. The density difference can be written in terms of the coefficient of thermal expansion as

$$\Delta\rho = \beta\rho_f(T_h - T_c) = \beta\rho_f \Delta T \quad \text{(D-4)}$$

where ρ_f is the saturated liquid density at the average temperature and β is defined as

$$\beta = \frac{-1}{\rho}\frac{\partial\rho}{\partial T}\Big|_P \quad \text{(D-5)}$$

The frictional pressure drop around the loop can be written in terms of the hydraulic resistance, R', the mass flow rate, and the saturated liquid density as

$$\Delta P_f = \frac{R' \dot{m}^2}{\rho_f} \quad \text{(D-6)}$$

The hydraulic resistance is defined as

$$R' = \sum_i \left[\left(\left(\frac{fl}{d_h}\right)_i + K_i\right)\frac{1}{2A_i^2}\right] \quad \text{(D-7)}$$

where f is the friction factor, l is component length, d_h is the hydraulic diameter, A_i is the cross section flow area, and K represents a loss coefficient.

Equations (D-1), (D-3), (D-4), and (D-6) can be combined to get the following expression for the mass flow rate

$$\dot{m} = \left[\frac{\rho_f^2 g\beta\Delta T\Delta Z}{R'}\right]^{1/2} \quad \text{(D-8)}$$

The heat removal rate can be expressed as

$$\dot{q} = \dot{m}c_p(T_h - T_c) = \dot{m}c_p\Delta T \quad \text{(D-9)}$$

where c_p is the specific heat. Substituting Equation (D-8) into (D-9) gives the final expression for the heat transfer rate

$$\dot{q} = \left[\frac{c_p^2\rho_f^2 g\beta(\Delta T)^3\Delta Z}{R'}\right]^{1/2} \quad \text{(D-10)}$$

With ΔZ, hydraulic resistance, thermal property values, and a temperature difference, Equation (D-10) can be used to estimate a reference PRHR heat transfer rate. PRHR hydraulic

resistance and ΔZ (using Equation (D-3)) are known from facility design information. The temperature difference (maximum) between the PRHR inlet and outlet can be estimated as the difference between the saturation temperature at primary system pressure minus IRWST fluid temperature.

APPENDIX E

DERIVATION OF GOVERNING EQUATIONS AND NONDIMENSIONAL GROUPS (Πs) FOR THE ADS-4 BLOWDOWN AND IRWST INJECTION PHASE

APPENDIX E

DERIVATION OF GOVERNING EQUATIONS AND NONDIMENSIONAL GROUPS (Πs) FOR THE ADS-4 BLOWDOWN AND IRWST INJECTION PHASE

The conservation equations for mass and energy are developed for the ADS-4 Blowdown and IRWST injection phases. The development focuses on the reactor vessel mass balance and the flows that affect this mass balance. Energy flows are considered when they contribute to important mechanisms in the mass balance. The equations are developed separately for each phase.

ADS-4 Blowdown Phase

For the ADS-4 Blowdown Phase the following assumptions were made.

- The accumulators are empty
- The CMTs are 20% full and draining through the DVI lines into the downcomer
- No IRWST flow
- ADS-1;-2,-3 choking ends very soon after ADS-4 opening effectively ending ADS-1,-2,-3 flow
- The much larger area of the ADS-4 relative to the break area allows break flow to be ignored
- The ADS-4 flow can be modeled using the HEM assumptions
- No pressurizer draining occurs hence there is no pressurizer flow
- The CMT temperature can be considered constant
- There is no flow from the hot legs into the steam generators
- There is no flow from the downcomer into the cold legs.

Using these assumptions the vessel mass balance for the control volume shown in Figure E-1 can be written as

$$\rho_l \frac{dV_l}{dt} = \rho_l Q_{CMT} - \dot{m}_{bl} \equiv \rho_l A_v \frac{dL_v}{dt} \qquad \text{(E-1)}$$

and the CMT mass (or drain rate) can be written as

$$\rho_l \frac{dV_{CMT}}{dt} = \rho_l(-Q_{CMT}). \qquad \text{(E-2)}$$

The flow rate in the CMT/DVI line based on a momentum balance between the CMT and the DVI nozzle can be written as

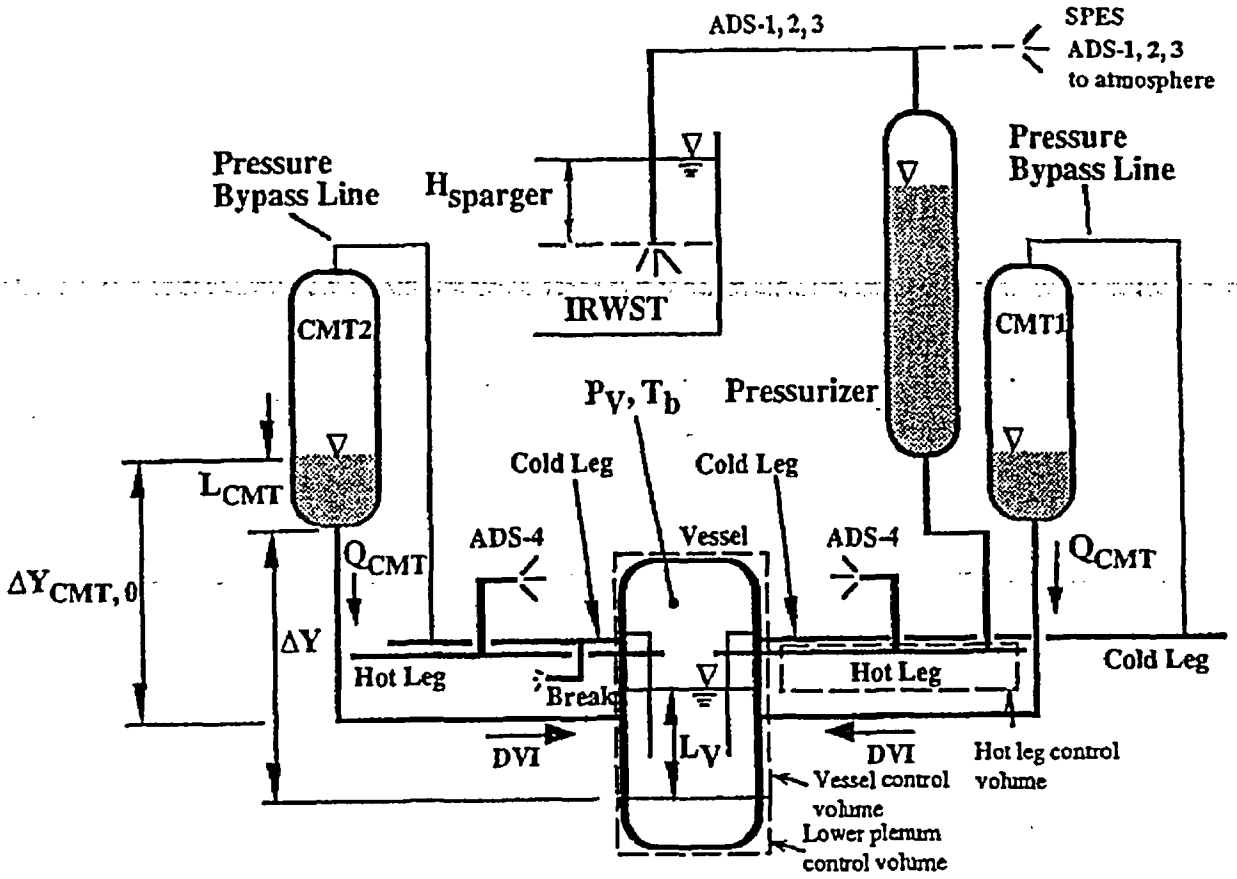

Figure E-1. Schematic for ADS-4 blowdown.

$$\rho_l\left(\frac{L}{A}\right)_{CMT}\frac{dQ_{CMT}}{dt} = \rho_l g(L_{CMT} - L_{DC}) - \rho_l R'_{CMT} Q^2_{CMT} + \rho_l g\Delta Y \qquad \text{(E-3)}$$

where L_{DC} is the maximum of the actual vessel level or the DVI nozzle elevation, i.e.

$$L_{DC} = \max(L_{DVI}, L_V)$$

and ΔY is the datum difference for the CMT level and the vessel/downcomer level.

As stated above, it is assumed that CMT liquid injected does not reach the cold legs and flow out the break so that all the flow from the CMTs is assumed to enter the vessel lower plenum. This assumption is justified because the downcomer level is lower than the cold leg nozzle elevation.

Based on the hot leg control volume shown in Figure E-1 and with the assumptions stated above (hot leg to steam generator flows are zero and no pressurizer flow), the hot leg flow consists only of the ADS-4 flow which can be represented as HEM critical flow. The quality at the ADS-4

discharge is based on an energy balance for the core and is estimated as shown based on core power and lower plenum subcooling.

$$\dot{m}_{hl} = \dot{m}_{ADS-4} = HEM(x_{ADS-4})$$

$$x_{ADS-4} = \frac{\dot{q}_f - Q_{CMT}\rho_l C_p(T_{sat} - T_{lp})}{\rho_l Q_{CMT} h_{fg}} \tag{E-4}$$

The lower plenum temperature is estimated using an energy balance based on residence time of CMT flow in the lower plenum.

$$\frac{dT_{lp}}{dt} = \frac{Q_{CMT}}{V_{lp+dc}}(T_{CMT} - T_{lp}). \tag{E-5}$$

These equations constitute a closed set that can be used to estimate the vessel mass inventory. Reference values were selected to nondimensionalize the equations and make the dependent variables and their derivatives of O[1].

The reference mass flow, time, and CMT volumetric flowrate are

$$\dot{m}_0 = \dot{m}_{ADS-4}(x_{ADS-4})$$

where $\dot{m}_{ADS-4}$ is from the HEM model evaluated at x_{ADS-4} and is assumed approximately constant,

$$t_0 = \frac{V_0\rho_l}{\dot{m}_0}$$

where V_0 is the vessel volume above the bottom of the heated length, and

$$Q_{CMT,0} = \left[\frac{g\Delta Y_{CMT,0}}{R_{CMT,0}}\right]^{1/2} \tag{E-6}$$

where $\Delta Y_{CMT,0}$ is the distance from the CMT water level to the DVI nozzle (e.g., $L_{CMT} + \Delta Y - L_V$ when L_V is at the elevation of the DVI nozzle).

The variables were nondimensionalized using reference parameters as shown below.

$$V_l^* = \frac{V_l}{V_0}; t^* = \frac{t}{t_0}; L_V^* = \frac{L_V}{V_0/A_0}; \dot{m}_{ADS-4}^* = \frac{\dot{m}_{ADS-4}}{\dot{m}_0}; Q_{CMT}^* = \frac{Q_{CMT}}{Q_{CMT,0}}; L_{CMT}^* = \frac{L_{CMT}}{L_{CMT,0}}$$

$$\Delta Y^* = \frac{\Delta Y}{\Delta Y_{CMT,0}}; (T_{CMT} - T_{lp})^* = \frac{(T_{CMT} - T_{lp})}{\Delta T_0} \tag{E-7}$$

The resulting dimensionless equations are presented here. For the vessel inventory

$$\frac{dV_l^*}{dt^*} = \frac{dL_V^*}{dt^*} = \Pi_{7-V}(\Pi_{16}Q_{CMT}^* - \dot{m}_{ADS-4}^*). \tag{E-8}$$

The CMT flowrate is given by

$$\frac{dQ^*_{CMT}}{dt^*} = -\Pi_{2-CMT}\left[\Pi_{17}L_{DC}^{*} - \Pi_{18}L^*_{CMT} - \Delta Y^*\right] - \Pi_{3-CMT}Q^{*2}_{CMT} \tag{E-9}$$

where

$$L^*_{DC} = L^*_V \text{ for } L^*_V \geq L^*_{DVI} \text{ and} \tag{E-10}$$

$$= L^*_{DVI} \text{ for } L^*_V < L^*_{DVI}$$

and the CMT level is given by

$$\frac{dL^*_{CMT}}{dt^*} = -\Pi_{15-CMT}Q^*_{CMT}. \tag{E-11}$$

Using the definition for Q_{CMT_0} given in Equation (E-6) makes $\Pi_{2\text{-}CMT}$ and $\Pi_{3\text{-}CMT}$ equal in value and much larger than unity. With these coefficients much larger than the time dependent term, the CMT flow equation can be rearranged as

$$Q^*_{CMT} = \left(\Pi_{18}L^*_{CMT} - \Pi_{17}L^* + \Delta Y^*\right)^{1/2}. \tag{E-12}$$

This equation can be written in terms of mass flow by using Π_{16} to produce

$$\dot{m}^*_{CMT} = \Pi_{16}Q^*_{CMT} = \Pi_{16}(\Pi_{18}L^*_{CMT} - \Pi_{17}L^*_{DC} + \Delta Y^*)^{1/2}. \tag{E-13}$$

With these expressions and the selection of reference parameters making $\Pi_{7\text{-}V} \equiv 1.0$ the vessel mass balance can be written as

$$\frac{dV^*_l}{dt^*} = \Pi_{7-V}\left(\dot{m}^*_{CMT} - \dot{m}^*_{ADS-4}\right). \tag{E-14}$$

The lower plenum temperature is estimated as

$$\frac{d(T_{CMT} - T_{lp})^*}{dt^*} = -\Pi_{9-lp}Q^*_{CMT}(T_{CMT} - T_{lp})^*. \tag{E-15}$$

where the CMT temperature is taken to be approximately constant.

The dimensionless coefficients are given below.

$$\Pi_{2-CMT} = \frac{g\Delta Y_{CMT,0}t_0}{Q_{CMT,0}L/A)_{CMT,0}} \tag{E-16}$$

$$\Pi_{3-CMT} = \frac{Q_{CMT,0}t_0R^*_{CMT,0}}{L/A)_{CMT,0}} \tag{E-17}$$

$$\Pi_{7-V} = \frac{\dot{m}_0t_0}{\rho_1V_0} \tag{E-18}$$

$$\Pi_{9-lp} = \frac{Q_{CMT,0} t_0}{V_{lp+dc,0}} \quad \text{(E-19)}$$

$$\Pi_{15-CMT} = \frac{Q_{CMT,0} t_0}{A_{CMT,0} L_{CMT,0}} \quad \text{(E-20)}$$

$$\Pi_{16} = \frac{\rho_l}{\dot{m}_0} \left(\frac{g \Delta Y_{CMT,0}}{R_{CMT,0}} \right)^{1/2} \quad \text{(E-21)}$$

$$\Pi_{17} = \frac{V_0}{A_0 \Delta Y_{CMT,0}} \quad \text{(E-22)}$$

$$\Pi_{18} = \frac{L_{CMT,0}}{\Delta Y_{CMT,0}} \quad \text{(E-23)}$$

IRWST Initial Refill Phase

In the IRWST phase the following assumptions were made.

- The CMTs and accumulators are empty
- The ADS-1,-2,-3 flow has transitioned from choked to friction dominated
- The ADS-4 flow is relatively low quality choked flow that can be modeled using the HEM assumptions
- The pressurizer draining can be modeled using a surge line velocity based on the rise of cap bubbles
- Because the ADS-4 area is much larger than the break area and there is very little pressure drop between the pressurizer and hot leg, only the ADS-4 flow needs to be considered as an outflow
- The IRWST level and temperature can be considered constant.
- The containment pressure can be considered constant
- There is no flow from the hot legs to the steam generators
- There is no flow from the downcomer into the cold legs
- Vessel pressure is determined by the head of liquid in the pressurizer and surge line.

Using these assumptions, the vessel mass balance for the vessel control volume shown in the schematic in Figure E-2 can be written as

$$\rho_l \frac{dV_l}{dt} = \rho_l Q_{dvi} - \dot{m}_{hl} \equiv \rho_l A_v \frac{dL_v}{dt} \quad \text{(E-24)}$$

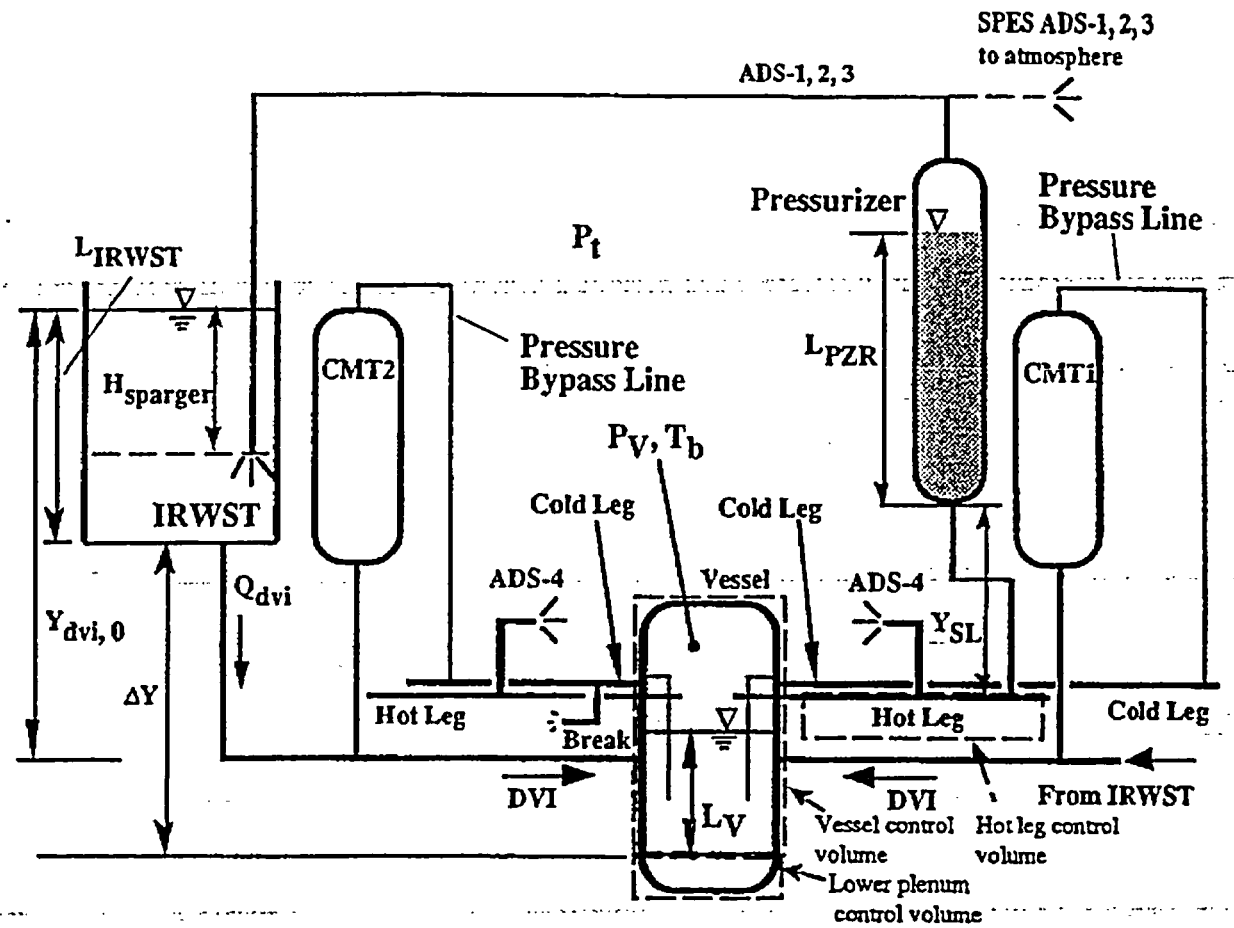

Figure E-2. Schematic for IRWST refill.

assuming that there is no flow from the DVI line to the cold leg and out the break. This is justified as the downcomer level is beneath the cold leg nozzle at least until refill is complete. The hot leg flow can be written in terms of the ADS-4 and pressurizer surge line flows as

$$\dot{m}_{ADS-4} = \dot{m}_{hl} + \dot{m}_{PZR} \tag{E-25}$$

assuming, as indicated above, that there is no flow from the hot legs into the steam generators. The ADS-4 flow can be written as

$$\dot{m}_{ADS-4} = HEM(x_{ADS-4}) \tag{E-26}$$

where based on a core energy balance, the outlet quality is

$$x_{ADS-4} = \frac{\dot{q}_f - Q_{dvi}\rho_i C_p (T_{sat} - T_{lp})}{\rho_f Q_{dvi} h_{fg}} \tag{E-27}$$

and the lower plenum fluid temperature is

$$\frac{dT_{lp}}{dt} = \frac{Q_{dvi}}{V_{lp+dc}}(T_{dvi} - T_{lp}). \tag{E-28}$$

The pressurizer surge line flow is based on the rise velocity of cap bubbles as

$$\dot{m}_{PZR} = 0.1\rho_l\sqrt{gD_{SL}}A_{SL}. \tag{E-29}$$

The DVI flow is written in terms of the IRWST flow since the CMTs and accumulators are assumed to be empty during this phase. As mentioned above, all of the IRWST flow is assumed to enter the vessel as the downcomer level is beneath the cold leg nozzles and therefore no spillover into the cold legs can occur

$$\rho_l\left(\frac{L}{A}\right)_{dvi}\frac{dQ_{dvi}}{dt} = \rho_l g(L_{IRWST} - L_{DC} + \Delta Y) - \rho_l R_{dvi}^{'}Q_{dvi}^2 + (P_t - P_V). \tag{E-30}$$

In Equation (E-30), L_{DC} is the maximum of the actual vessel level and the DVI nozzle elevation or

$$L_{DC} = \max(L_V, L_{DVI}) \tag{E-31}$$

and ΔY is the elevation difference in datums between the bottom of the IRWST and the vessel level.

The vessel pressure is greater than the pressurizer pressure due to the static head of liquid in the pressurizer and surge line or

$$P_V - P_{PZR} = \rho_l g(L_{PZR} + \frac{\rho_{SL}}{\rho_l}Y_{SL}). \tag{E-32}$$

In Equation (E-32), ρ_{SL} is the surge line density and Y_{SL} is the distance from the bottom of the pressurizer to the surge line-hot leg connection. The containment pressure is assumed to be higher than the pressurizer pressure because of the static head of liquid in the IRWST above the ADS-1,-2,-3 sparger outlet. It is assumed that choking in the ADS-1,-2,-3 lines has ended prior to this phase beginning.

Reference conditions for the mass flow, time, and DVI volumetric flow were chosen as follows. $\dot{m}_0 = \rho_l Q_{dvi} - \dot{m}_{ADS-4}(x_{ADS-4})$ which is assumed to be approximately constant, $Q_{dvi,0}$ is evaluated assuming the vessel level is at the DVI nozzle elevation and P_t - P_V is zero (i.e. no back pressure), and $\dot{m}_{ADS-4}(x_{ADS-4})$ is based on HEM evaluated at core outlet quality based on an energy balance across the core at the start of the phase. The reference time is selected as

$$t_0 = \frac{V_0\rho_l}{\dot{m}_0} \tag{E-33}$$

where V_0 is the vessel volume above the bottom of the heated length. The reference DVI flow is

$$Q_{dvi,0} = \left[\frac{gY_{dvi,0}}{R_{dvi,0}^{\cdot}}\right]^{1/2} \tag{E-34}$$

where $Y_{dvi,0}$ is the distance from the initial IRWST water level to the DVI nozzle.

Initial pressure, $P_{t,0}$, is assumed to be containment pressure (~1 atmosphere) plus initial IRWST head.

Using these reference conditions the following dimensionless variables were defined.

$$\begin{gathered} V_l^* = \frac{V_l}{V_0};t^* = \frac{t}{t_0};L_V^* = \frac{L_V}{V_0/A_0};\dot{m}_{ADS-4}^* = \frac{\dot{m}_{ADS-4}}{\dot{m}_0};\dot{m}_{dvi}^* = \frac{\dot{m}_{dvi}}{m_0}; \\ \dot{m}_{PZR}^* = \frac{\dot{m}_{PZR}^*}{\dot{m}_0};\dot{m}_{hl}^* = \frac{\dot{m}_{hl}^*}{\dot{m}_0};L_{PZR}^* = \frac{L_{PZR}A_{PZR,0}}{V_{PZR,0}};Q_{dvi}^* = \frac{Q_{dvi}}{Q_{dvi,0}};P_{PZR}^* = \frac{P_{PZR}}{P_{t,0}} \end{gathered} \tag{E-35}$$

$$P_V^* = \frac{P_V}{P_{t,0}};\Delta Y^* = \frac{L_{IRWST} + \Delta Y}{Y_{dvi,0}};(T_{dvi} - T_{lp})^* = \frac{(T_{dvi} - T_{lp})}{\Delta T_0} \tag{E-36}$$

$$\rho_{SL}^* = \frac{\rho_{SL}}{\rho_l};Y_{SL}^* = \frac{Y_{SL}}{Y_{dvi,0}};Q_{dvi,0} = \left[\frac{gY_{dvi,0}}{R_{dvi,0}^{\cdot}}\right]^{1/2} \tag{E-37}$$

Substituting these variables into the dimensional equations gives the following set of dimensionless equations. For the vessel mass

$$\frac{dV_l^*}{dt^*} = \frac{dL_V^*}{dt^*} = \Pi_{7-V-IRWST}\left(\dot{m}_{dvi}^* - \dot{m}_{hl}^*\right) \tag{E-38}$$

where

$$\dot{m}_{dvi}^* = \Pi_{23}Q_{dvi}^* \tag{E-39}$$

and

$$\dot{m}_{ADS-4}^* = \dot{m}_{PZR}^* + \dot{m}_{hl}^* \tag{E-40}$$

Noting that in Equation (E-30) the dQ^*_{dvi}/dt^* term is much less than the other terms, and rearranging gives

$$Q_{dvi}^* = \left[(\Delta Y^* - \Pi_{19}L^*) + \Pi_{20}(1 - P_V^*)\right]^{1/2}. \tag{E-41}$$

The pressure difference between the vessel and pressurizer becomes

$$P_{PZR}^* - P_V^* = -\Pi_{20}^{-1}(\Pi_{22}L_{PZR}^* + \rho_{SL}^*Y_{SL}^*). \tag{E-42}$$

Writing the hot leg flow in terms of the ADS-4 and surge line flow allows the vessel mass balance to be written as

$$\frac{dV_l^*}{dt^*} = \frac{dL_V^*}{dt^*} = \Pi_{7-V-IRWST}\left(\Pi_{23}\left[\Delta Y^* - \Pi_{19}L_{DC}^* + \Pi_{20}\left(1-P_V^*\right)\right]^{1/2} - \dot{m}_{ADS-4}^* + \dot{m}_{PZR}^*\right). \quad \text{(E-43)}$$

The dimensionless groups are described below.

$$\Pi_{7-V-IRWST} = \frac{\dot{m}_0 t_0}{\rho_l V_0} \quad \text{(E-44)}$$

$$\Pi_{15-PZR} = \frac{\dot{m}_0 t_0}{\rho_l V_{PZR,0}} \quad \text{(E-45)}$$

$$\Pi_{19} = \frac{V_0}{A_0 Y_{dvi,0}} \quad \text{(E-46)}$$

$$\Pi_{20} = \frac{P_t}{\rho_l g Y_{dvi,0}} \quad \text{(E-47)}$$

$$\Pi_{21} = \frac{Q_{dvi,0} t_0}{V_{lp+dc,0}} \quad \text{(E-48)}$$

$$\Pi_{22} = \frac{V_{PZR,0}}{A_{PZR,0} Y_{dvi,0}} \quad \text{(E-49)}$$

$$\Pi_{23} = \frac{\rho_l}{\dot{m}_0}\left(\frac{g Y_{dvi,0}}{R_{dvi,0}^{\cdot}}\right)^{1/2} \quad \text{(E-50)}$$

APPENDIX F

DERIVATIONS OF ANALYTICAL EXPRESSIONS FOR VESSEL INVENTORY (ADS-4 AND IRWST INJECTION PHASES)

APPENDIX F

DERIVATIONS OF ANALYTICAL EXPRESSIONS FOR VESSEL INVENTORY (ADS-4 AND IRWST INJECTION PHASES)

This Appendix details the development of analytical expressions for vessel inventory for the ADS-4 and early IRWST injection phases. The ADS-4 development is presented first for the two cases of the vessel level above or below the DVI nozzle elevation. The IRWST development is presented for the two cases of short time (as the vessel starts to refill) and long time (as the vessel level approaches the hot leg elevation).

ADS-4 Discharge Phase

The derivation for the analytical expression for the vessel inventory during ADS-4 discharge for the case of the vessel level above the elevation of the DVI nozzle is given below. The expression is

$$V_1^*(t^*) - V_1^*(0) = \left[\Pi_{16} Q_{CMT}^*(0) - 1\right] t^* + \frac{\Pi_{16}\hat{\Pi}_{19}}{2Q_{CMT}^*(0)}\left[Q_{CMT}^*(0) + \frac{\Pi_{17}}{\hat{\Pi}_{19}}\right]\frac{t^{*2}}{2} + \ldots \qquad \text{(F-1)}$$

where

$\hat{\Pi}_{19} = (\Pi_{18}\Pi_{15} - \Pi_{17}\Pi_{16})$ for $L_V^* \geq L_{DVI}^*$.

Case 1 - $L_V^* \geq L_{DVI}^*$

In the subsequent derivation we drop the superscript asterisk and understand that all quantities are nondimensional.

The nondimensionalized governing equations are

$$\frac{dV_1}{dt} = \frac{dL_V}{dt} = \Pi_{7-V}\left[\Pi_{16} Q_{CMT} - \dot{m}_{ADS4}\right] \qquad \text{(F-2)}$$

$$\frac{dL_{CMT}}{dt} = -\Pi_{15-CMT} Q_{CMT} \qquad \text{(F-3)}$$

$$\frac{dQ_{CMT}}{dt} = -\Pi_{2-CMT}\left[\Pi_{17} L_V - \Pi_{18} L_{CMT} - \Delta Y\right] - \Pi_{3-CMT} Q_{CMT}^2 \quad \text{for } L_V \geq L_{DVI} \qquad \text{(F-4)}$$

We assume (though it is not necessary) that:

- $\dot{m}_{ADS4} = 1$ (i.e. it is constant at $\dot{m}_0$)

- $\Pi_{2-CMT} = \Pi_{3-CMT}$ = large (follows from definitions of Π_{2-CMT} and Π_{3-CMT})
- $\Pi_{7-V} = 1$ (by definition of t_o as the vessel residence time)
- $dQ_{CMT}/dt \cong 0$

Furthermore, multiplying Equation (F-2) by Π_{17} and Equation (F-3) by Π_{18} we can write (after making the assumptions)

$$\frac{d}{dt}\left[\Pi_{18}L_{CMT}-\Pi_{17}L_V-\Delta Y\right]=\left(\Pi_{18}\Pi_{15}-\Pi_{17}\Pi_{16}\right)Q_{CMT}-\Pi_{17} \qquad \text{(F-5)}$$

where ΔY can be included in the derivative since it is a constant.

Taking the derivative of Equation (F-4) after making the assumptions (which are justified for the AP600 and the various facility geometries and resistances) and substituting in Equation (F-5), we have

$$\frac{dQ_{CMT}^2}{dt} = \hat{\Pi}_{19}Q_{CMT} - \Pi_{17} \qquad \text{(F-6)}$$

where

$$\hat{\Pi}_{19} = \Pi_{18}\Pi_{15} - \Pi_{17}\Pi_{16}.$$

Eliminating Q_{CMT} between Equation (F-2) and Equation (F-6) and integrating gives

$$\frac{V_1}{\Pi_{16}}-\frac{Q^2}{\hat{\Pi}_{19}}=-\left[\frac{1}{\Pi_{16}}+\frac{\Pi_{17}}{\hat{\Pi}_{19}}\right]t + C \qquad \text{(F-7)}$$

When $t = 0$, $V_I = V_I(0)$ and $Q_{CMT}^2 = Q_{CMT}^2(0)$ and Equation (F-7) along with the above condition results in

$$\frac{V_I - V_I(0)}{\Pi_{16}} - \frac{Q_{CMT}^2 - Q_{CMT}^2(0)}{\hat{\Pi}_{19}} = -\left[\frac{1}{\Pi_{16}}+\frac{\Pi_{17}}{\hat{\Pi}_{19}}\right]t. \qquad \text{(F-8)}$$

To proceed, we need an approximation for $\left[Q_{CMT}^2 - Q_{CMT}^2(0)\right]$ in terms of t. This can be done in many ways, but we proceed in the simplest way at present.

At first sight it appears straightforward to integrate Equation (F-6) and substitute the exact solution in Equation (F-8). However, one obtains a complex transcendental equation for Q_{CMT} that cannot be solved explicitly for Q_{CMT} and then substituted in Equation (F-8). Therefore we follow the alternate path of expanding Q_{CMT} in a power series in t. To a first approximation

$$\frac{1}{\hat{\Pi}_{19}}\frac{dQ_{CMT}^2}{dt} = Q_{CMT}(0)+\frac{\Pi_{17}}{\hat{\Pi}_{19}} \qquad \text{(F-9)}$$

or using at $t = 0$, $Q_{CMT}^2 - Q_{CMT}^2(0)$ we have

$$\frac{1}{\hat{\Pi}_{19}}\left[Q_{CMT}^2 - Q_{CMT}^2(0)\right] = \left[Q_{CMT}(0) + \frac{\Pi_{17}}{\hat{\Pi}_{19}}\right]t \qquad \text{(F-10)}$$

To a second approximation

$$\frac{1}{\hat{\Pi}_{19}}\frac{dQ_{CMT}^2}{dt} = Q_{CMT}(0) + \frac{\hat{\Pi}_{19}}{2Q_{CMT}(0)}\left[Q_{CMT}(0) + \frac{\Pi_{17}}{\hat{\Pi}_{19}}\right]t + \frac{\Pi_{17}}{\hat{\Pi}_{19}} \qquad \text{(F-11)}$$

From the above expressions,

$$\frac{1}{\hat{\Pi}_{19}}\left[Q_{CMT}^2 - Q_{CMT}^2(0)\right] = Q_{CMT}(0)t + \frac{\hat{\Pi}_{19}}{2Q_{CMT}(0)}\left[Q_{CMT}(0) + \frac{\Pi_{17}}{\hat{\Pi}_{19}}\right]t^2 + \frac{\Pi_{17}}{\hat{\Pi}_{19}}t \qquad \text{(F-12)}$$

Substituting in Equation (F-8) gives

$$V_1 - V_1(0) = \left[Q_{CMT}(0)\Pi_{16} - 1\right]t + \frac{\Pi_{16}\hat{\Pi}_{19}}{2Q_{CMT}(0)}\left[Q_{CMT}(0) + \frac{\Pi_{17}}{\hat{\Pi}_{19}}\right]\frac{t^2}{2} + ... \qquad \text{(F-13)}$$

which is the final result for $L_V \geq L_{DVI}$. Note that it is entirely straightforward to put $\dot{m}_{ADS4} \neq 1$ in the derivation as long as it is constant. Note that once $L_V < L_{DVI}$, then this derivation does not apply. The derivation is most useful for ROSA. It does not apply in most cases to SPES and OSU (only for a short time). While Equation (F-13) is an approximation it converges rapidly for ROSA, i.e., the t^3 term is negligible.

Case 2 - $L^*_V < L^*_{DVI}$

The derivation for the analytical expression for the vessel inventory during ADS-4 discharge for the case of the vessel level below the elevation of the DVI nozzle is given below. The expression is

$$V_1^* - V_1^*(0) = \left[\Pi_{16}Q_{CMT}^*(0) - \dot{m}_{ADS4}^*\right]t^* + \frac{\Pi_{16}\Pi_{18}\Pi_{15}}{4}t^{*2} \text{ for } L_V^* < L_{DVI}^*. \qquad \text{(F-14)}$$

In the subsequent derivation we again drop the superscript asterisk and understand that all quantities are nondimensional.

Equations (F-2) and (F-3) are the same as given above but we don't assume $\dot{m}_{ADS4} = 1$. This is done to accommodate the SPES experiment in which $\dot{m}_{ADS4}$ is constant, but the constant changes at some point in time.

Equation (F-4) becomes

$$Q_{CMT} = \left[\Pi_{18}L_{CMT} - \Pi_{17}L_{DVI} - \Delta Y\right]^{1/2} \text{ for } L_V < L_{DVI}. \qquad \text{(F-15)}$$

This leads to the following modified version of Equation (F-6)

$$\frac{dQ_{CMT}^2}{dt} = \Pi_{18}\Pi_{15}Q_{CMT}. \qquad \text{(F-16)}$$

Integrating Equation (F-16) yields

$$Q_{CMT} - Q_{CMT}(0) = \frac{\Pi_{18}\Pi_{15}}{2}t. \qquad \text{(F-17)}$$

Substituting this result into Equation (F-2) and integrating gives

$$V_l = \frac{\Pi_{16}\Pi_{18}\Pi_{15}}{4}t^2 + \Pi_{16}Q_{CMT}(0)t - \dot{m}_{ADS4}t + C. \qquad \text{(F-18)}$$

For $V_l = V_l(0)$ at $t = 0$, the following results

$$V_l - V_l(0) = \left[\Pi_{16}\, Q_{CMT}(0) - \dot{m}_{ADS4}\right]t + \frac{\Pi_{16}\Pi_{18}\Pi_{15}}{4}t^2 \qquad \text{(F-19)}$$

where $\dot{m}_{ADS4}$ is a known constant.

Equation (F-19) is the final result for $L_V < L_{DVI}$ and is an exact solution.

IRWST Injection Phase

The derivations for the analytical expression for the vessel inventory during IRWST injection for the cases of short times and long times are given below.

Case 1 - Short Times

The solution for short times is

$$V_l^* - V_l^*(0) = \tfrac{2}{3}\Pi_{23}\left[\left(\Pi_{22}\Pi_{15}\dot{m}_{PZR}^* - \Pi_{20}\frac{dP_{PZR}^*}{dt^*}\right)^{\frac{1}{2}}t^*\right]^{\frac{3}{2}} - (\dot{m}_{ADS4}^* - \dot{m}_{PZR}^*)t^* \qquad \text{(F-20)}$$

In the subsequent derivation we drop the superscript asterisk and understand all quantities are nondimensional.

The governing equations are

$$\frac{dV_l}{dt} = \frac{dL_V}{dt} = \Pi_{23}Q_{DVI} - \dot{m}_{IRL} \qquad \text{(F-21)}$$

$$\frac{dL_{PZR}}{dt} = -\Pi_{15}\dot{m}_{PZR} \qquad \text{(F-22)}$$

$$Q_{dvi}=\left[(\Delta Y-\Pi_{19}L)+\Pi_{20}(1-P_v)\right]^{1/2} \text{ (assuming inertial term negligible)} \quad \text{(F-23)}$$

where $L = L_V$ for $L_V \geq L_{DVI}$
$L = L_{DVI}$ for $L_V < L_{DVI}$

$$P_{PZR}-P_V=-\frac{1}{\Pi_{20}}\left[\Pi_{22}L_{PZR}+\rho_{SL}Y_{SL}\right] \quad \text{(F-24)}$$

$$\dot{m}_{HL}=\dot{m}_{ASD4}-\dot{m}_{PZR}. \quad \text{(F-25)}$$

We assume $\dot{m}_{PZR}$ and $\dot{m}_{ASD4}$ are constants and dP_{PZR}/dt = constant. Note that Π_{19} in Equation (F-23) is unrelated to Π_{19} in the previous section.

Squaring and differentiating Equation (F-23) gives

$$\frac{dQ_{DVI}^2}{dt}=-\Pi_{20}\frac{dP_V}{dt}=\Pi_{22}\Pi_{15}\dot{m}_{PZR}-\Pi_{20}\frac{dP_{PZR}}{dt} \quad \text{(F-26)}$$

where Equations (F-22) and (F-24) have been used to expand dP_V/dt and $L = L_{DVI}$. Integrating this expression gives

$$Q_{DVI}=\left[\Pi_{22}\Pi_{15}\dot{m}_{PZR}t-\Pi_{20}\frac{dP_{PZR}}{dt}t\right]^{1/2}. \quad \text{(F-27)}$$

From Equation (F-21) after substituting Equations (F-25) and (F-27) we have

$$\frac{dV_1}{dt}=\Pi_{23}\left[\left(\Pi_{22}\Pi_{15}\dot{m}_{PZR}t-\Pi_{20}\frac{dP_{PZR}}{dt}t\right)^{\frac{1}{2}}\right]-(\dot{m}_{ADS4}-\dot{m}_{PZR}). \quad \text{(F-28)}$$

Integrating and setting $V_1 = V_1(0)$ at $t = 0$ gives

$$V_1-V_1(0)=\frac{2}{3}\Pi_{23}\left[\left(\Pi_{22}\Pi_{15}\dot{m}_{PZR}-\Pi_{20}\frac{dP_{PZR}}{dt}\right)^{\frac{1}{2}}\right]t^{\frac{3}{2}}-(\dot{m}_{ADS4}-\dot{m}_{PZR})t \quad \text{(F-29)}$$

which is the required expression for short times.

Case 2 - Long Times

For long times, e.g. $t \rightarrow \infty$ we make the following assumptions

- $L_V \rightarrow L_V(\infty)$ hot leg level
- $\dot{m}_{HL} \rightarrow \dot{m}_{ADS4} = \dot{m}_{DVI} \rightarrow \Pi_{23}Q_{DVI}(\infty)$
- $\dot{m}_{PZR} \rightarrow 0$
- $P_V \rightarrow$ Constant

From Equation (F-23) we have

$$\frac{dQ_{DVI}^2}{dt} = -\Pi_{19}\frac{dL_V}{dt}. \qquad \text{(F-30)}$$

Define $Q_{DVI}(t)$ and L_V as

$$Q_{DVI}(t) = Q_{DVI}(\infty) + \Delta Q_{DVI}(t) \qquad \text{(F-31)}$$

$$L_V = L_V(\infty) - \Delta L_V(t). \qquad \text{(F-32)}$$

Substituting these definitions into Equation (F-30) and linearizing gives

$$-\frac{d\Delta Q_{DVI}}{dt} = -\frac{\Pi_{19}}{2Q_{DVI}(\infty)}\frac{d\Delta L_V}{dt} \qquad \text{(F-33)}$$

or

$$-\Delta Q_{DVI} = -\frac{\Pi_{19}\Delta L_V}{2Q_{DVI}(\infty)}. \qquad \text{(F-34)}$$

Substituting for Q_{DVI} in Equation (F-21) we have

$$\frac{d\Delta L_V}{dt} = \frac{dV_1}{dt} = \Pi_{23}\left[Q_{DVI}(\infty) + \frac{\Pi_{19}\Delta L_V}{2Q_{DVI}(\infty)}\right] - \dot{m}_{HL}. \qquad \text{(F-35)}$$

Noting that $\dot{m}_{HL}$ is $\Pi_{23}Q_{DVI}(\infty)$ and simplifying Equation (F-35) gives

$$\Delta L_V = (\Delta L_V)_0 \exp[-\Pi_{23}\Pi_{19}t/(2Q_{DVI}(\infty))] \qquad \text{(F-36)}$$

where ΔL_V is proportional to $\Delta V_1 = V_1(\infty) - V_1(t)$.

Thus

$$\Delta V_1 = (\Delta V_1)_0 \exp[-\Pi_{23}\Pi_{19}t/(2Q_{DVI}(\infty))]. \qquad \text{(F-37)}$$

To obtain $(\Delta V_1)_0$ we can only use the condition at t = 0 (not a very good initial condition for this case). Nonetheless this gives the following result for long times

$$V_1(\infty) - V_1(t) = [V_1(\infty) - V_1(0)]\exp[-\Pi_{23}\Pi_{19}t/(2Q_{DVI}(\infty))]. \qquad \text{(F-38)}$$

APPENDIX G

EQUATION DEVELOPMENT FOR IRWST DRAIN PHASE

APPENDIX G

EQUATION DEVELOPMENT FOR IRWST DRAIN PHASE

This Appendix deals with the development of simplified equations useful for the analysis of the IRWST drain phase. The equations are cast in nondimensional form after development.

Equation Development

Based on the phase definition, the identified processes, components, and the schematic shown in Figure G-1, the system of governing equations can be formulated. Mass conservation and fluid energy conservation will be written for the tanks and connecting pipes will require a momentum equation.

A mass balance on the IRWST gives

$$\rho_f A_{irwst} \frac{dL_{irwst}}{dt} = \dot{m}_{condensate} - \dot{m}_{dvi} \qquad \text{(G-1)}$$

where $\dot{m}_{condensate}$ is the condensed steam that flows back from the containment walls into the IRWST, A_{IRWST} is the IRWST cross sectional area, ρ_f is fluid density, L_{IRWST} is the tank liquid level, and $\dot{m}_{dvi}$ is the flow rate out of the IRWST into the DVI lines. Note that there could be a delay period between the time at which the steam is released at the ADS-4 valves and the time it

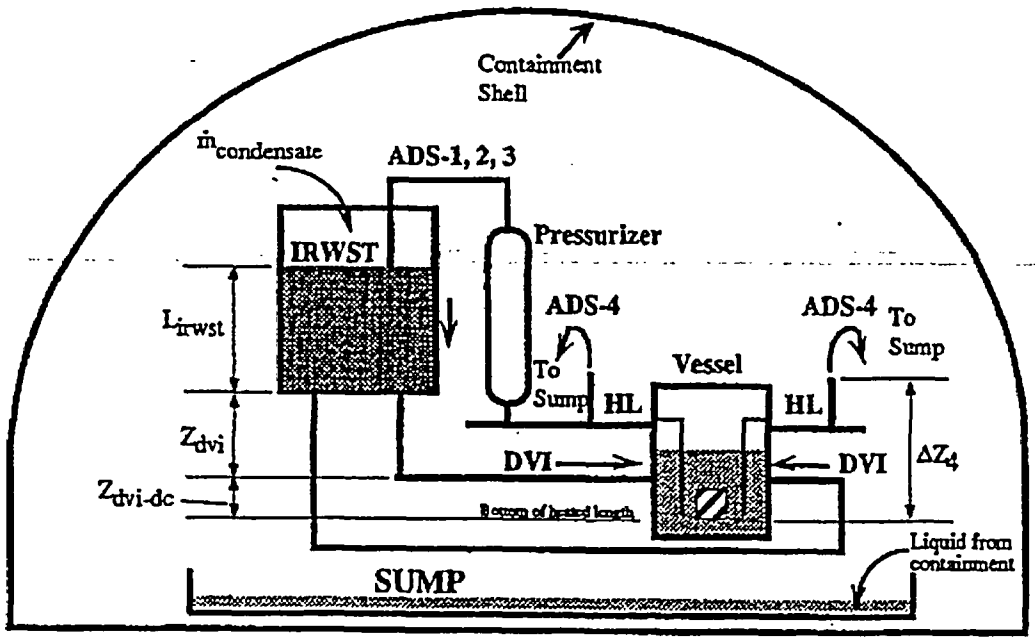

Figure G-1. System configuration during IRWST drain phase (prior to sump injection).

returns to the IRWST as condensate. Based on a film thickness of 0.001 m, it is estimated that if every metal structure in the AP600 containment were to collect a film of condensate, the total amount of water held up in such a film would be about 24 m^3. This volume is only 1.3% of the IRWST inventory (1,880 m^3). Furthermore, such a film would form during the early stages of the transient, and would not be building up during this stage. Therefore, no significant delay associated with the return of condensate to the IRWST is expected and the condensate flow rate is assumed equal to the rate of steam released into the containment through the ADS valves or

$$\dot{m}_{condensate} = x_{ads4}\dot{m}_{ads4} + \dot{m}_{ads123} = \dot{m}_{g-ads4} + \dot{m}_{ads123} \qquad \text{(G-2)}$$

where x_{ads4} is the ADS-4 quality, $\dot{m}_{ads4}$ is the ADS-4 flow rate, and $\dot{m}_{ads123}$ is the flow rate through the ADS-1,-2,-3 valves (assumed to be steam).

The temperature of the IRWST water depends on the IRWST mass inflows and outflows and the fluid interaction with the tank walls. The schematic in Figure G-2 illustrates the concrete structure of the IRWST, the steel lining, and the water level. To model the concrete as a lumped

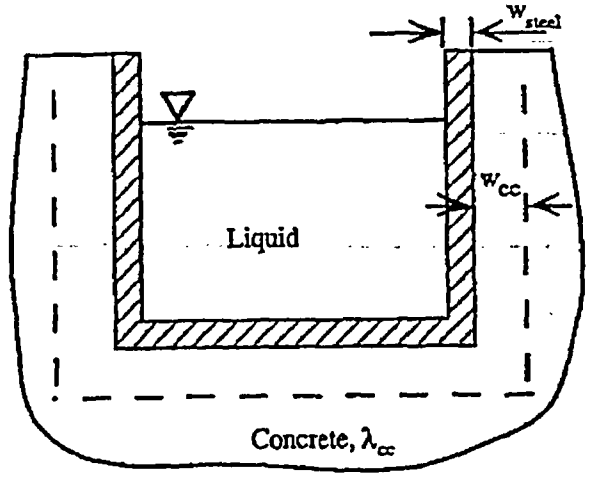

Figure G-2. Schematic of concrete penetration depth (thickness) to be determined according to duration of heating process.

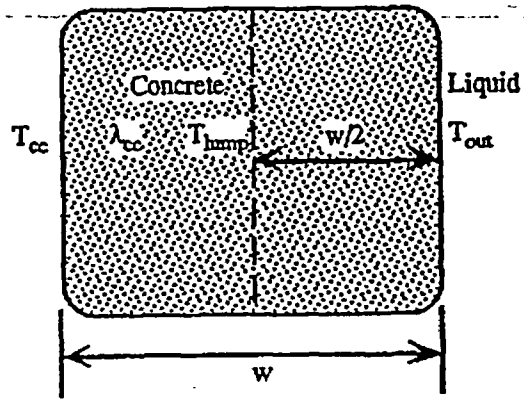

Figure G-3. Portion of concrete wall showing penetration depth (thickness) and variable definitions.

structure, a penetration depth in the concrete (w_{cc}) that defines the mass of concrete involved in the process will be defined. To do this, consider a portion of the concrete wall, as shown in Figure G-3, with thermal conductivity λ_{cc}, and thickness w, which depends on how long the wall is exposed to a temperature difference. An energy balance, in lumped parameter form, for this system is

$$\rho_{cc}c_{p-cc}w\frac{dT_{lump}}{dt}=\frac{\lambda_{cc}}{w/2}\left(T_{out}-T_{cc}\right) \tag{G-3}$$

If T_{lump} is approximated at time τ to be the average of the maximum and minimum temperatures in the problem, the Equation (G-3) can be rewritten as:

$$w^2\equiv\frac{4\lambda_{cc}\tau}{\rho_{cc}c_{p-cc}} \tag{G-4}$$

Equation (G-4) can be used to evaluate w_{cc} for the time duration of the phase. With this information, the overall heat transfer coefficient between the IRWST wall and the fluid is defined as

$$U_{irwst}=\left(\frac{1}{\frac{w_{it-cc}}{\lambda_{cc}}+\frac{w_{steel}}{\lambda_{steel}}+\frac{1}{h_{irwst}}}\right) \tag{G-5}$$

where w_{it-cc} is the penetration depth for the IRWST concrete, w_{steel} is the steel liner thickness, and h_{irwst} is the heat transfer coefficient between the IRWST liquid and the tank inside wall, and λ_{cc} and λ_{steel} are the thermal conductivity of the concrete and steel liner, respectively. In the same fashion, the overall heat transfer coefficient for the Sump is

$$U_{sump}=\left(\frac{1}{\frac{w_{s-cc}}{\lambda_{cc}}+\frac{w_{steel}}{\lambda_{steel}}+\frac{1}{h_{sump}}}\right) \tag{G-6}$$

The IRWST fluid energy balance is given by

$$\frac{dT_{irwst}}{dt}=\frac{\dot{m}_{condensate}c_pT_{cont.}-\dot{m}_{dvi}c_pT_{irwst}+U_{irwst}A_{irwst-w}\left(T_{irwst-concrete}-T_{irwst}\right)}{\rho_fc_pL_{irwst}A_{irwst}} \tag{G-7}$$

and the energy balance for the concrete structure around the IRWST tank assuming only energy transfer to the fluid is

$$\left(M_{irwst-concrete}c_{p-concrete}\right)\frac{dT_{irwst-concrete}}{dt}=U_{irwst}A_{irwst-w}\left(T_{irwst}-T_{irwst-concrete}\right) \tag{G-8}$$

Note that while the Sump is not an active participant during this phase, equations equivalent to (G-7) and (G-8) could be written for the sump fluid and walls. During the IRWST drain, the Sump acts only as a reservoir where the break and ADS-4 liquid flows accumulate.

A force balance written from the surface of the IRWST, through the DVI injection line, and through the ADS-4 valves to the containment provides a momentum equation in which pressure is eliminated and yields the following

$$\left(\frac{L}{A}\right)_{dvi}\frac{d\dot{m}_{dvi}}{dt}=\rho_f g\left(L_{irwst}+Z_{dvi}+Z_{dc-dvi}\right)$$

$$-\frac{1}{\rho_f\left(\frac{K}{2A^2}\right)_{dvi}}\dot{m}_{dvi}^2 \qquad \text{(G-9)}$$

$$-\frac{1}{\rho_{ads4}}\dot{m}_{ads4}^2\left(\frac{K}{2A^2}\right)_{ads4}-\rho_{ads4}g\Delta Z_4$$

In Equation (G-9), $Z_{dc\text{-}dvi}$ and ΔZ_4 are the elevation of the DVI nozzle and the ADS-4 valves, respectively with respect to the bottom of the heated length. In reality, and for the evaluation of reference parameters, these two elevations need a small correction to account for the fact that the fluid density in the core side is not ρ_{ads4} from the bottom of the heated length.

As stated in the phase description, assumptions are made with respect to the system behavior during this period of time. It is assumed that the sum of the ADS-1,-2,-3 and ADS-4 mass flows is equal to the DVI mass flow or

$$\dot{m}_{dvi}=\dot{m}_{ads4}+\dot{m}_{ads123} \qquad \text{(G-10)}$$

However, $\dot{m}_{ads4} >> \dot{m}_{ads1,2,3}$, so that Equation-(G-10) becomes

$$\dot{m}_{dvi}\equiv\dot{m}_{ads4} \qquad \text{(G-11)}$$

The mass in the vessel is given as

$$M_{vessel}=\int_{V_v}\rho dV \qquad \text{(G-12)}$$

An energy balance across the core yields

$$x_{core}=\left(\frac{\dot{q}_{core}-\dot{m}_{dvi}c_p\left(T_{sat}(P_b)-T_{lp}\right)}{h_{fg}\dot{m}_{dvi}}\right) \qquad \text{(G-13)}$$

where Tsat is assumed to be based on vessel pressure or

$$T_{sat}=T_{sat}(P_b) \qquad \text{(G-14)}$$

and T_{lp} is the lower plenum (core inlet) fluid temperature.

The density of the flow through the ADS-4 valves depends on parameters including the core vapor generation rate, the phase separation in the hot leg and associated tee connections to the

ADS-4 and PRHR off-takes, the flow rate through the ADS-4 system, and so forth. A bottom-up or local relationship or correlation is required to define this density, e.g.,

$$\rho_{ads4} \equiv f(\text{entrainment}, Q_{ads4}, q_{core}, x_{ads4}, ...) \tag{G-15}$$

In lieu of an appropriate correlation, we assume that the density is that needed to match the flow into the system through the DVI line. This is not precisely true since there is likely some flow through the ADS-1,2,3 valves.

Lower Plenum Temperature

$$\frac{dT_{lp}}{dt} = \frac{\dot{m}_{dvi}}{\rho_f V_{lp+dc}}\left(T_{irwst} - T_{lp}\right) \tag{G-16}$$

We have now a closed system of equations that we can normalize and nondimensionalize to obtain the participating nondimensional groups.

Normalization and Nondimensionalization

We now re-write the governing equations, normalizing all variables. For clarity, we redefine the subscripts so that concrete is now cc, containment is ct, irwst is it, and sump is s.

$$\frac{\rho_0 A_0 L_0}{t_0}\rho_f^* A_{it}^* \frac{dL_{it}^*}{dt^*} = \dot{m}_0\left(\dot{m}_{g-ads4}^* - \dot{m}_{dvi}^*\right) \tag{G-17}$$

$$\frac{T_0}{t_0}\frac{dT_{it}^*}{dt^*} = \frac{\dot{m}_0 c_{p0} T_0\left(\dot{m}_{g-ads4}^* c_p^* T_{cont.}^* - \dot{m}_{dvi}^* c_p^* T_{it}^*\right) + U_0 A_{w0}\Delta T_0 U_{it}^* A_{it-w}^*\left(T_{cc}^* - T_{it}^*\right)}{\rho_0 c_{p0} L_0 A_0 \rho_f^* c_p^* L_{it}^* A_{it}^*} \tag{G-18}$$

$$\frac{M_{it-cc0} c_{pcc0} T_0}{t_0}\left(M_{it-cc}^* c_{p-cc}^*\right)\frac{dT_{it-cc}^*}{dt^*} = U_0 A_{it-w0}\Delta T_0 U_{it}^* A_{it-w}^*\left(T_{it}^* - T_{it-cc}^*\right) \tag{G-19}$$

$$\left(\frac{L}{A}\right)_0 \frac{\dot{m}_0}{t_0}\left(\frac{L}{A}\right)_{dvi}^* \frac{d\dot{m}_{dvi}^*}{dt^*} = (\rho_0 g Y_0)\rho_f^*\left(L_{it}^* + Z_{dvi}^* + Z_{dc-dvi}^*\right) - \rho_{ads4-0}\Delta Z_0 g \rho_{ads4}^*\Delta Z_4^*$$

$$-\frac{\dot{m}_0^2}{2\rho_0}\left(\frac{K}{A^2}\right)_{dvi-0}\frac{\dot{m}_{dvi}^{*2}}{\rho_f^*}\left(\frac{K}{A^2}\right)_{dvi}^* \tag{G-20}$$

$$-\frac{\dot{m}_0^2}{2\rho_{ads4-0}}\left(\frac{K}{A^2}\right)_{ads4-0}\frac{\dot{m}_{ads4}^2}{\rho_{ads4}^*}\left(\frac{K}{A^2}\right)_{ads4}^*$$

The reference pressure P_0 is defined by the hydrostatic pressure due to the head of liquid in the IRWST plus containment pressure as

$$P_0 = \rho_0 g(L_0 + Z_{dvi}) + 1 \text{ atm} \tag{G-21}$$

$$\frac{T_0}{t_0}\frac{dT_{lp}^*}{dt^*}=\frac{\dot{m}_0 T_0}{\rho_0 V_0}\frac{\dot{m}_{dvi}^*}{\rho_f^* V_{lp+dc}^*}\left(T_{it}^*-T_{lp}^*\right) \tag{G-22}$$

The equations above can now be written in nondimensional form, thus identifying the nondimensional coefficients that dominate this phase. Table G-1 lists the groups and their physical description.

$$\rho_f^* A_{it}^* \frac{dL_{it}^*}{dt^*}=\frac{\dot{m}_0 t_0}{\rho_0 A_0 L_0}\left(\dot{m}_{g-ads4}^*-\dot{m}_{dvi}^*\right)=\Pi_{15-it}\left(\dot{m}_{g-ads4}^*-\dot{m}_{dvi}^*\right) \tag{G-23}$$

$$\begin{aligned}\frac{dT_{it}^*}{dt^*}&=\frac{\dot{m}_0 t_0}{\rho_0 L_0 A_0}\left(\dot{m}_{g-ads4}^* c_p^* T_{cont.}^*-\dot{m}_{dvi}^* c_p^* T_{it}^*\right)+\frac{U_0 A_{it-w0}\Delta T_0 t_0}{\rho_0 c_{p0} L_0 A_0 T_0}U_{it}^* A_{it-w}^*\left(T_{cc}^*-T_{it}^*\right)\\&=\Pi_{15-it}\left(\dot{m}_{g-ads4}^* c_p^* T_{cont.}^*-\dot{m}_{dvi}^* c_p^* T_{it}^*\right)+\Pi_{18-f-it}U_{it}^* A_{it-w}^*\left(T_{cc}^*-T_{it}^*\right)\end{aligned} \tag{G-24}$$

$$\begin{aligned}\left(M_{it-cc}^* c_{p-cc}^*\right)\frac{dT_{it-cc}^*}{dt^*}&=\left(\frac{U_0 A_{it-w0}\Delta T_0 t_0}{M_{it-cc}c_{pcc0}T_0}\right)U_{it}^* A_{it-w}^*\left(T_{it}^*-T_{it-cc}^*\right)\\&=\Pi_{18-w-it}U_{it}^* A_{it-w}^*\left(T_{it}^*-T_{it-cc}^*\right)\end{aligned} \tag{G-25}$$

$$\begin{aligned}\left(\frac{L}{A}\right)_{dvi}^*\frac{d\dot{m}_{dvi}^*}{dt^*}&=\left(\frac{\rho_0 g Y_0 t_0}{(L/A)_0\dot{m}_0}\right)\rho_f^*\left(L_{it}^*+Z_{dvi}^*+Z_{dc-dvi}^*\right)-\left(\frac{\rho_{ads4-0}g\Delta Z_0 t_0}{(L/A)_0\dot{m}_0}\right)\rho_{ads4}^*\Delta Z_4^*\\&-\frac{\dot{m}_0 t_0}{2\rho_0(L/A)_0}\left(K/A^2\right)_{dvi-0}\frac{\dot{m}_{dvi}^{*2}}{\rho_f^*}\left(K/A^2\right)_{dvi}^*\\&-\frac{\dot{m}_0 t_0}{2\rho_{ads4-0}(L/A)_0}\left(K/A^2\right)_{ads4-0}\frac{\dot{m}_{ads4}^{*2}}{\rho_{ads4}^*}\left(K/A^2\right)_{ads4}^*\\&=\Pi_{2-dvi}\rho_f^*\left(L_{it}^*+Z_{dvi}^*+Z_{dc-dvi}^*\right)-\Pi_{2-ads4}\rho_{ads4}^*\Delta Z_4^*\\&-\Pi_{3-dvi}\frac{\dot{m}_{dvi}^{*2}}{\rho_f^*}\left(K/A^2\right)_{dvi}^*-\Pi_{3-ads4}\frac{\dot{m}_{ads4}^{*2}}{\rho_{ads4}^*}\left(K/A^2\right)_{ads4}^*\end{aligned} \tag{G-26}$$

$$\frac{dT_{lp}^*}{dt^*}=\left(\frac{\dot{m}_0 t_0}{\rho_0 V_0}\right)\frac{\dot{m}_{dvi}^*}{\rho_f^* V_{lp+dc}^*}\left(T_{it}^*-T_{lp}^*\right)=\Pi_{9-lp}\frac{\dot{m}_{dvi}^*}{\rho_f^* V_{lp+dc}^*}\left(T_{it}^*-T_{lp}^*\right) \tag{G-27}$$

Table G-1. Nondimensional groups and description for IRWST drain phase.

Group	Definition	Description
Π_2	$(\rho_0 g Y_0 t_0)/((L/A)_0 \dot{m}_0$	Ratio of hydrostatic force to inertial force
Π_3	$(\dot{m}_0 t_0 (K/A^2)_0)/(2\rho_0 (L/A)_0)$	Ratio of line frictional force to inertial force
Π_7	$(\dot{m}_0 t_0)/(M_{10})$	Nondimensional residence time
Π_9	$(\dot{m}_0 t_0)/(\rho_0 V_0)$	Nondimensional residence time
Π_{15}	$(\dot{m}_0 t_0)/(\rho_0 A_0 L_0)$	Nondimensional residence time
$\Pi_{18\text{-}f}$	$(U_0 A_{w0} \Delta T_0 t_0)/(\rho_0 c_{p0} L_0 A_0 T_0)$	Ratio of heat transferred from fluid to the heat capacity of the fluid
$\Pi_{18\text{-}w}$	$(U_0 A_{w0} \Delta T_0 t_0)/(c_{cc\text{-}p0} M_{cc0} T_0)$	Ratio of heat transferred from fluid to the heat capacity of the wall

Overall Heat Transfer Coefficient Evaluation

To establish a reference condition, the overall heat transfer coefficient for the IRWST wall is evaluated assuming natural circulation heat transfer between the fluid and a vertical concrete wall along with Equations (G-4) and (G-5). For this evaluation, a correlation for free convection on a cold vertical wall given in Ref. G-1 is used. This correlation gives expressions for the Nusselt number as a function of the Grahsof and Prandtl numbers for the laminar and turbulent regimes as follows:

Laminar regime	Transition	Turbulent regime
$Nu_x = 0.508 \dfrac{Gr_x^{1/4} Pr^{1/2}}{(0.952+Pr)^{1/4}}$	$Gr_x \approx 1.E8$	$Nu_x = 0.149(Pr^{0.175} - 0.55) Gr_x^{0.36}$
$Nu_L = 4/3 Nu_x\|_{x=L}$		$Nu_L = \dfrac{4}{3}(0.508) \dfrac{Gr_{trans}^{1/4} Pr^{1/2}}{(0.952+Pr)^{1/4}} + \dfrac{1}{1.08}\left[1 - \left(\dfrac{Gr_{trans}}{Gr_L}\right)^{0.92}\right] \times (0.149)(Pr^{0.175} - 0.55) Gr_L^{0.36}$

where

C_p - specific heat
L - wall height
Gr_x - Grashof number ($\Delta\rho/\rho g x^3/\nu^2 = \beta\Delta T\, g x^3/\nu^2$)
Gr_L - Grashof number ($\Delta\rho/\rho g L^3/\nu^2 = \beta\Delta T\, g L^3/\nu^2$)
Nu_x - Nusselt number (hx/k)
Pr - Prandtl number ($\mu C_p/k$)
h - heat transfer coefficient
k - thermal conductivity
x - axial distance along the wall
β - volume thermal expansion coefficient ($-1/\rho\ \partial\rho / \partial T|_P$)
μ - dynamic viscosity
ν - kinematic viscosity (μ/ρ)
ρ - fluid density

Fluid properties in this correlation are evaluated at a reference temperature that is the average of the highest and lowest temperatures in the problem. For the present case, the highest temperature is saturation temperature at containment pressure (assumed to be 1 atm) and the coldest temperature is that of the IRWST water at initial conditions (assumed to be ~290 K). The pressure is assumed to be the average of the pressure at the bottom of the IRWST tank and the pressure at the IRWST liquid surface where the IRWST tank is assumed to be a a level of ~9m. With these assumptions, the conditions and values shown in Table G-2 result.

Table G-2. Fluid properties for evaluation of overall heat transfer coefficient.

Property or condition	Value
T_{wall} (K)	
T_{sat} (K) (at 1 atm)	
T_{cold} (K)	
T_{ref} (K) [= Tcold + 0.5 (Tsat - Tcold)]	
L (m)	
ρ (kg/m^3)	
P_{ref} (kPa) [= 0.5(1 atm + (ρgL + 1 atm)]	
β (1/K)	
μ (Pa-s)	
ν (m^2/s)	
C_p (kJ/kg-K)	
k (W/m-K)	
Pr	
Gr_L	

The value of the Grashof number given in Table G-2 indicates that the turbulent flow form of the correlation should be used. Evaluating the correlation gives a value of [ ]a,c for Nu_L. Solving for the heat transfer coefficient yields

$$h_{irwst} = \frac{Nu_L k}{L} = [\quad]^{a,c} \tag{G-28}$$

As mentioned above, the IRWST wall consists of concrete with a carbon steel liner. Dimensions and thermal properties for this geometry are given in Table G-3.

Table G-3. IRWST wall thermal properties.

Material	Carbon Steel	Concrete
thickness (m)[a]	[	]a,c
k (w/m-K)[b]		
ρ (kg/m^3)[b,c]		
c_p (kJ/kg-K)[b,c]		
ρc_p (kJ/m^3-K)[b]		

a. Values from Reference G-2.
b. Values from Reference G-3.
c. Values from Reference G-4.

Using the property values in Table G-3 along with Equation (G-4) allows the approximate conduction depth of the concrete wall to be calculated as

$$w \equiv \sqrt{\frac{4\lambda_{cc}\tau}{\rho_{cc}c_{p-cc}}} = [\quad]^{a,c} \tag{G-29}$$

where τ of 15E3 s is the approximate drain time of the IRWST from the initial level to a level where sump injection commences. This is a conservative calculation since as the liquid level drains, the surface area of the tank wall interacting with the IRWST liquid is decreasing. Using the results of Equations (G-28) and (G-29) in Equation (G-5) then allows estimation of U_0 for the IRWST wall as

$$U_{irwst} = \left(\frac{1}{\frac{w_{it-cc}}{\lambda_{cc}} + \frac{w_{steel}}{\lambda_{steel}} + \frac{1}{h_{irwst}}} \right) = [\quad]^{a,c} \tag{G-30}$$

References

G-1. D. K. Edwards, V. E. Denny, and A. F. Mills, "Transfer Processes: An Introduction to Diffusion, Convection, and Radiation,", Hemisphere Publishing Corporation, Washington, Second Edition, 1979, pp. 166.

G-2. D. R. Spencer, "Scaling Analysis for AP600 Passive Containment Cooling System," Westinghouse Electric Corporation, WCAP-14190 (proprietary report), October 1994.

G-3. K. E. Carlson, et al., "RELAP5/MOD3 Code Manual (Draft)," Idaho National Engineering Laboratory, NUREG/CR-5535, INEL-95/0174, 7 Volumes, August 1995.

G-4. J. G. Collier, "Convective Boiling and Condensation," McGraw Hill, London, 1972, pp. 411.